Horacio J.Antúnez

BULK-METAL FORMING PROCESSES FROM COMPUTATIONAL MODELLING VIA SENSITIVITY ANALYSIS TO TOOL SHAPE OPTIMIZATION

(PRACA HABILITACYJNA)

1/2001

WARSZAWA 2001

ISSN 0208-5658

Praca wpłynęła do Redakcji dnia 21 listopada 2000 r.

recenzent - Prof.dr hab.inż. prof.zw. Maciej Pietrzyk

Praca habilitacyjna

Instytut Podstawowych Problemów Techniki PAN
Nakład 100 egz. Ark. wyd.10,5 Ark. druk.13,0
Oddano do drukarni w maju 2001 r.

ATOS - Poligrafia-Reklama, W-wa, ul. Jana Kazimierza 35/37

Contents

Introduction

Towards the end of the sixties and the beginning of the seventies, electronic computers started to be developed in a larger scale than up to then, and thus became available to researchers. And quite quickly a number of already available methods to solve engineering problems began to be applied.

Until then such methods had required, even to obtain at least a roughly meaningful result, a prohibitively heavy calculation work as they had to be applied by hand. Basically this involved the solution of relatively large systems of equations or the repetitive solution of rather simple problems.

By that time a good amount of theoretical knowledge, which allowed the successful solution of many linear problems, was available. Mechanics, material science, algebra and numerical analysis provided the necessary background for these methods to be applied.

The first applications of numerical methods concerned those linear problems. Among them, static problems of civil engineering were on top of the list. And this to the extent that many concepts and names taken from this field have remained in the new developing computer methods even when applied to other problems. Typical examples of problems solved in this period are linear elasticity and heat conduction.

Shortly afterwards, it became clear that nonlinear problems should also be addressed, and this to satisfy countless practical requirements. Hence, the development of a number of disciplines started. In material science, an outstanding step was performed by including more complex constitutive equations, which involved more state and history variables. On the other hand, more powerful mathematical tools were developed to describe large displacements and deformations. Boundary conditions of ongoing processes were more precisely described including, among others, contact conditions and friction.

It would be hard to summarize all the developments of computational mechanics in the recent decades. Just to mention the subjects they concerned, effort was concentrated in material modelling, geometry and boundary conditions description, numerical methods for discretization and for efficient solution of the equation systems, and operations involving the mesh of finite elements including optimization of the bandwidth, remeshing, mesh refinement and coarsening, all

aiming at minimizing an appropriate error norm. Practically all the engineering problems of interest have been addressed, many of them involving coupled problems.

Still further elaborations included the use of the solved system of equations to perform sensitivity analysis by the so-called analytical methods. These resulted to provide the sensitivity coefficients, and did that at a residual cost as compared to the cost of solving the overall problem. The inclusion of sensitivity analysis with respect to shape parameters finally prepared the way to shape optimization, since not only a given design functional, but also its gradient in the design space were available to be used by an optimization algorithm.

In this historical context, one of the fields which has attracted more interest is that of metal forming simulations, probably for its interest for industrial applications. Practically all the subjects quoted above for computational mechanics in general are dealt with in this field.

A series of options are available for building a computational model for metal forming simulation. Most frequently, each choice implies to reject other possibilities, and some goals are obtained but some drawbacks arise. Hints about the proper choice may be given by the type of process being simulated. This, confirmed by the experience of many researchers, supports the position that it is more convenient to have several specialized programs, each of which effectively analyzes a given class of problems, than to have a complex, much larger general purpose program which, to a given extent, is adapted to the characteristic features of (almost?) every practical problem.

Within the preceding framework, the present work is a collection of developments performed at the Institute of Fundamental Technological Research of the Polish Academy of Sciences. All of them are concerning one specific way of modelling metal forming processes; this is especially suited for hot forming conditions, and has been conceived for steady-state processes, although it can be applied in transient ones as well.

The naturally suited application of this model is extrusion; however, it can be used also in free forging, cutting and rolling (including seamless tube rolling), for which results are shown as well.

Stationary and transient processes are separately presented here; not only for the sake of clarity of the exposition and for historical reasons, but to show the analysis problem, sensitivity analysis and shape optimization as successive steps within a logical line of thinking. Essentially this process was followed in the computer simulation of metal forming, feeding into each step all the results obtained in the preceding ones.

In this work, the steady state is presented first, starting by the flow approach. Following, the discretization by finite elements is given. Here the different features accounted for in the model are explained. Once the analysis model is

complete, the sensitivity is ready to be introduced. First, parametric sensitivity is discussed, what is incidentally useful to show the available methods for sensitivity analysis. Shape sensitivity is considered next, followed by the optimization algorithm which finds, according to given criteria and design restrictions, the optimum design.

Afterwards transient processes are considered. A full transient formulation is considered and used to obtain an incremental method that makes use of linear elements due to a proper time-step splitting. Attention is focused on the full explicit version. Further, sensitivity analysis within such model and discretization is shown. In addition, the pseudo-concentration method is briefly revisited and used in connection to Fourier series expansion of the problem of seamless tube rolling.

Some additional –but significant– topics are discussed in the course of the main presentation. The simulation of almost perfect plasticity poses the problem of uniqueness (or its lack), and this is discussed in the context of cutting simulation. Pressure stabilization is necessary to apply a friction model based on a Coulomb-type law. In this context a bilinear interpolation is introduced, which takes advantage of a method for similar pressure stabilization used in fluid mechanics. Sensitivity analysis suggests that its results can have an additional application in evaluating the effect on the solution of numerical parameters needed in some models. This is the case of the upwind parameters in coupled thermo-mechanical problems and the time step in time integration of transient processes. The introduction of shape sensitivity analysis of forming processes gives the occasion to consider the extension to large displacements of the two available methods. In the shape optimization part, the problem of shape parameterization requires special attention. Two different techniques of interpolating points in the discretized domain in terms of the design parameters are proposed.

Chapter 1

Flow approach – foundations

1.1 Introductory comments

For several centuries, since man left the stone age and entered the metal age, he made thorough use of ductility as an essential property of metals under appropriate conditions. Thanks to it man was able to make his own tools and weapons. The final product was frequently very different in shape from the initial one. It was also observed that by heating up to a certain point, metals were more workable, and also that cold deformed metals were certainly more stiff but also more brittle. This initially rudimentary knowledge about metal properties was gradually developed, quantified and with time became more precise. Different theories and models on the micro and macro level arose to explain the metal behaviour under different conditions. Their application in practice has, however, been limited to simple geometries and tensile states due to difficulties connected with the evaluation of the parameters entering the models and with the usage of these models to real situations. Roughly speaking, until the computer age, their application was limited to academic examples and some civil engineering problems.

Only then applications to metal forming processes were attempted, once the available computational tools allowed to handle complex tensile states and large displacements. In fact, these two are first range features of metal forming operations. The hypothesis of small displacements makes no sense here, and usually a fundamental choice on the motion description must be done: material (Lagrangian) or spatial (Eulerian) approach. The preferred approach may result from the consideration of the particular process to be modelled. Indeed, of more generality seems the Lagrangian approach, but since some processes impose similar —and very long— trajectories to many particles, and the piece being formed behaves as a *flowing* material, an Eulerian approach has been considered more efficient for their description. This means that the equilibrium equations must be written in rate form. Additionally, from considering the large displacements and deformations that take place, it comes out that elastic ones can well be neglected.

Eventually, the final configuration of the formed piece once the loads are removed may be obtained if we know the actual stresses in the material.

The above argumentation states the bases of the flow approach, in which, by a similar conception as in some analytical methods for analyzing plasticity (e.g. the slip-line and the upper-bound theories) the velocity field at a given time is searched for. This may be the solution we are looking for in steady state problems, or one picture of the time evolution, with which we should proceed to the following time step according to some defined time integration rule, in transient processes.

1.2 Some history

The flow approach has been widely applied by researchers and it has been incorporated into many commercial computational codes. Already in the late sixties Goon et al. [51] realized that metal forming processes are amenable to be treated as flow problems of a non-Newtonian fluid. The first application to the flow of metals with viscosity calculated as a function of the effective strain rate was made by Cornfield and Johnson [35]. Almost simultaneously Lee and Kobayashi [79] and Zienkiewicz and Godbole [114] generalized the procedures to the solution of plastic and viscoplastic problems.

Short after these first applications, it was also observed that the same formalism could be applied to many other problems as well, such as polymer forming and creep. Thus the flow approach was applied (frequently in the same paper [113, 111, 114, 116]) to different problems. In all of them the equilibrium equation in rate form is solved with an additional constraint to impose incompressibility. Essentially, the different models are characterized by the assumed law for the viscosity.

Many developments on the flow approach followed these first works, once its core was established. They concerned a great variety of issues about physical, mathematical and computational aspects of the model. Just to name a few, frictional contact [27, 87, 116] and free surface conditions [116], thermal coupling [6, 41, 119], microstructure evolution [105], damage [86] were accounted for in the model; attention was also paid to the way the incompressibility constraint is imposed and to its consequences in the discretization. Many alternative methods became thus available (e.g. Lagrange multipliers, penalty [116], augmented Lagrangian). Thermally-coupled problems made apparent the need of upwind techniques [6, 56, 57, 69, 110, 119] connected with the problem discretization. Later on, rezoning, remeshing, and mesh refining techniques [52, 117, 122, 115] became necessary in processes involving large deformations or where the error norm was to be kept below a prefixed value. All the time, mixed, velocity-pressure formulations were conditioned regarding the admissible type of interpolation for both variables by the so-called Brezzi-Babuska condition [50], typically the approximation functions for the velocity had to be of one order higher than those of the

pressure. Afterwards this limitation has been removed by the introduction of stabilization [10, 63] methods which "filter out" spurious pressure modes and allow to more comfortable formulations. Schemes for transient processes which make use of linear triangles and tetrahedra have been recently introduced [4, 14, 120].

The standard analysis problem for metal forming processes has been also extended to sensitivity analysis. Having started in the eighties, the references on this matter in the nineties is quite abundant. Again, metal forming applications followed the path of other areas: sensitivity to material [10, 72] and to shape parameters [12]. With such information available, shape optimization has been the next step expected and the task has been undertaken in [13, 44, 66].

Some of these issues will be discussed in the following chapters. In any case, it can be stated that the flow approach, while keeping its conceptional simplicity, has incorporated a number of features which make it competitive with the elasto-plastic –displacement based approach, which, roughly speaking, can be considered as "the other" possibility to deal with metal forming problems.

As it frequently happens, however, the separation between both approaches has not remained untouched and clear. Elastic effects have been accounted for in the flow approach in [37], followed by other formulations [26]. Besides, some "hybrid" formulations have been proposed in addition to the intuitive pairings: flow approach–spatial (Eulerian) description, and elasto-plastic approach–material (Lagrangian) description. Probably the most popular among them are the so-called ALE (Arbitrary Lagrangian-Eulerian) formulations, where the reference frame has its own (arbitrary) velocity [19, 42, 62, 97]. On the other hand, an Eulerian description has been used in a full elasto-plastic formulation [48]. Moreover, upon proceeding from the stationary to the transient solution, the natural extension of the flow approach has ended in a material description, as in [111], for instance. However, the Eulerian philosophy has been conserved even in transient processes e.g. by the pseudo-concentration method [7, 104]. In addition, still some other formulations have been proposed that try to avoid or to minimize the inherent drawbacks of material formulations at large deformations: excessive mesh distortion and the need of remeshing.

It can be seen that just *metal forming* as a keyword is far too comprehensive for it alone to be a subject of discussion. Several topics will be covered in the following chapters. In the sequel we will consider the continuum mechanics foundations for the flow approach and the hypotheses involved in the derivation will be accordingly highlighted.

1.3 Continuum mechanics background

1.3.1 Rigid-viscoplastic material model

We have mentioned that, within the flow approach, metal under forming conditions is modelled as an incompressible non-Newtonian fluid, and the balance

equation is that of a (non-linear, thus) Stokes flow. The set of equations is formally analogous to that of incompressible non-linear elasticity, where we have velocities instead of (small) displacements, and strain rates instead of strains. This analogy has been used to emphasize how simple may be to implement the flow approach, as long as one has a program that can handle incompressible elasticity, obviously.

In what follows the model for a rigid-viscoplastic material —the rigid-plastic one being a particular case of it— which constitutes the core of the flow approach, will be presented.

We start putting forward the basic variables we are dealing with: velocities v_i and pressure p (which will appear later on). The symmetric part of the velocity gradient defines the Eulerian deformation rate tensor (also called the stretching tensor)

$$d_{ij} \equiv \dot{\varepsilon}_{ij} = \frac{1}{2}(v_{i,j} + v_{j,i}) \tag{1.1}$$

To neglect the elastic part of the deformation means to assume that the whole strain rate tensor is of plastic nature

$$\dot{\varepsilon}_{ij} \cong \dot{\varepsilon}^{\mathrm{p}}_{ij} \tag{1.2}$$

Therefore, the index 'p' will be omitted from now on for simplicity of notation. (However, it will be kept as a reminder in the symbol for the accumulated strain, Eq. (1.5) below). It also means that the material is rigid for any combination of stresses not satisfying the *yield condition*. This assumption has consequences when not all the analyzed domain is loaded up to the yield surface, and it will be discussed later on in Section 2.3.2.

Scalar quantities derived from the plastic strain rate and stress deviator tensors are, respectively, the effective strain rate and the effective (or reduced) stress. They are defined as proportional to the respective second invariant

$$\dot{\bar{\varepsilon}} = \left(\frac{2}{3}\dot{\varepsilon}_{ij}\dot{\varepsilon}_{ij}\right)^{\frac{1}{2}} \tag{1.3}$$

$$\bar{\sigma} = \left(\frac{3}{2}\sigma^{D}_{ij}\sigma^{D}_{ij}\right)^{\frac{1}{2}} \quad ; \qquad \sigma^{D}_{ij} = \sigma_{ij} - \frac{1}{3}\delta_{ij}\sigma_{kk} \tag{1.4}$$

The effective strain rate gives us, by time integration, the effective plastic strain

$$\bar{\varepsilon}^{\mathrm{p}} = \int_0^t \dot{\bar{\varepsilon}}\, \mathrm{d}\tau \tag{1.5}$$

According to the *flow theory of plasticity*, the response of a strain hardening material is specified by: (i) an initial yield condition, (ii) a hardening rule and (iii) a flow rule. We first consider the *yield condition*. Experience teaches that to a first approximation the yielding of a metal is unaffected by a moderate hydrostatic pressure superposed on a combined-stress state [58, 81]. Metal plasticity theories

accordingly assume that the yield condition is independent of the spherical part of the stress. We can write

$$f(\sigma_{ij}, \bar{\varepsilon}^{\mathrm{p}}) = F(\sigma_{ij}^{D}) - \sigma_{Y}(\bar{\varepsilon}^{\mathrm{p}}) = 0 \tag{1.6}$$

where F is the *yield function* and $\sigma_{Y}(\bar{\varepsilon}^{\mathrm{p}})$ is the current yield stress obtained from the uniaxial test data. This form corresponds to an isotropic strain hardening material. Other models for hardening may be included in this point, in which case the yield stress will be a more complicated function of the strain tensor and/or, as in the case of viscoplastic materials, of the strain rate tensor. For ductile materials the Huber-Mises yield condition is most frequently used

$$F = \bar{\sigma} \tag{1.7}$$

The yield condition represents a surface in the stress space, and it gives us a reference frame to define the *flow rule* relating strain and stress rates, $\dot{\varepsilon}_{ij}$ *vs* $\dot{\sigma}_{kl}$. The rate form of Eq. (1.6) reads

$$\dot{f}(\sigma_{ij}, \bar{\varepsilon}^{\mathrm{p}}) = \frac{\partial F}{\partial \sigma_{ij}}\dot{\sigma}_{ij} - \frac{\partial \sigma_{Y}}{\partial \bar{\varepsilon}^{\mathrm{p}}}\dot{\bar{\varepsilon}} = 0 \tag{1.8}$$

and it is known as the *consistency condition*. It states that any stress point remains on the yield surface during plastic flow. We notice that the quantity

$$h_1 = \frac{\partial \sigma_{Y}}{\partial \bar{\varepsilon}^{\mathrm{p}}} \tag{1.9}$$

is a measure of the strain hardening.

Making use of Eqs. (1.7) and (1.9), the consistency condition Eq. (1.8) takes, for the case of Huber-Mises condition, the form

$$\frac{3}{2}\frac{\sigma_{ij}^{D}}{\bar{\sigma}}\dot{\sigma}_{ij} - h_1\dot{\bar{\varepsilon}} = 0 \tag{1.10}$$

since, using Eq. (1.4),

$$\frac{\partial \bar{\sigma}}{\partial \sigma_{ij}} = \frac{3}{2\bar{\sigma}}\sigma_{kl}^{D}\left(\delta_{ik}\delta_{jl} - \frac{1}{3}\delta_{kl}\delta_{ij}\right) = \frac{3}{2\bar{\sigma}}\left(\sigma_{ij}^{D} - \frac{1}{3}\underbrace{\sigma_{kk}^{D}}_{=0}\delta_{ij}\right) = \frac{3\sigma_{ij}^{D}}{2\bar{\sigma}} \tag{1.11}$$

The unit normal to the yield surface is given by

$$n_{ij} = \frac{\partial \bar{\sigma}}{\partial \sigma_{ij}^{D}}\left(\frac{\partial \bar{\sigma}}{\partial \sigma_{kl}^{D}}\frac{\partial \bar{\sigma}}{\partial \sigma_{kl}^{D}}\right)^{\frac{1}{2}} = \frac{\sigma_{ij}^{D}}{\|\sigma_{kl}^{D}\|} = \sqrt{\frac{3}{2}}\frac{\sigma_{ij}^{D}}{\bar{\sigma}} \tag{1.12}$$

hence replacing Eq. (1.12) into Eq. (1.10) we may obtain

$$\dot{\bar{\varepsilon}} = \frac{1}{h_1}\sqrt{\frac{3}{2}}n_{ij}\dot{\sigma}_{ij} \tag{1.13}$$

Besides, we postulate the existence of a plastic potential $g = g(\bar{\sigma}, \bar{\varepsilon}^p)$, from which the strain rate tensor is obtained as its gradient in the stress space

$$\dot{\varepsilon}_{ij} = \dot{\lambda} \frac{\partial g}{\partial \sigma_{ij}} \tag{1.14}$$

By squaring both sides and summing on i, j we get, using Eqs. (1.3) and (1.4)

$$\dot{\bar{\varepsilon}} = \sqrt{\frac{2}{3}} \dot{\lambda} \underbrace{\left(\frac{\partial g}{\partial \sigma_{kl}} \frac{\partial g}{\partial \sigma_{kl}} \right)^{\frac{1}{2}}}_{\left\| \frac{\partial g}{\partial \sigma_{kl}} \right\|} \tag{1.15}$$

Replacing $\dot{\lambda}$ from Eq. (1.15) into Eq. (1.14) yields

$$\dot{\varepsilon}_{ij} = \sqrt{\frac{3}{2}} \dot{\bar{\varepsilon}} \frac{\partial g}{\partial \sigma_{ij}} \left\| \frac{\partial g}{\partial \sigma_{kl}} \right\|^{-1} = \sqrt{\frac{3}{2}} \dot{\bar{\varepsilon}} n_{ij}^g \tag{1.16}$$

where n_{ij}^g is the unit normal to the plastic potential g. Finally, replacing $\dot{\bar{\varepsilon}}$ from Eq. (1.13) into Eq. (1.16) we obtain

$$\dot{\varepsilon}_{ij} = \frac{1}{h} n_{kl} \dot{\sigma}_{kl} n_{ij}^g \tag{1.17}$$

with

$$h = \frac{2}{3} h_1 \tag{1.18}$$

as the hardening modulus.

For associative flow, making use of Drucker's definition of a stable plastic material, the plastic potential g is identical to the yield condition — a convex surface in the stress space. Then it will be, in Eq. (1.17), $n_{ij}^g = n_{ij}$.

If we now consider the viscous effects during plastic deformation, an additional term should appear in Eq. (1.8), since now $\sigma_Y = \sigma_Y(\bar{\varepsilon}^p, \dot{\bar{\varepsilon}})$. However, we are interested in the relation between strain rates and stresses (instead of stress rates). We postulate that the flow rule in the form of Eq. (1.16) with the assumption of associative flow holds, i.e.

$$\dot{\varepsilon}_{ij}(\sigma_{kl}, \bar{\varepsilon}^p) = \sqrt{\frac{3}{2}} \dot{\bar{\varepsilon}} n_{ij}(\sigma_{kl}) \tag{1.19}$$

with the effective inelastic strain rate expressed by

$$\dot{\bar{\varepsilon}} = \dot{\bar{\varepsilon}}(\bar{\sigma}, \bar{\varepsilon}^p) \tag{1.20}$$

1.3.2 Overstress (Prager-Perzyna) model

In some way the problem has been now transferred to that of specifying the concrete form of Eq. (1.20). The expressions are derived from the yield condition Eq. (1.6) rather than from the consistency condition Eq. (1.8). Among different proposed functions, the *overstress* or Prager-Perzyna model [88, 89] has shown to work very well and it has been widely applied. It reads

$$\dot{\bar{\varepsilon}}(\bar{\sigma}, \bar{\varepsilon}^{\mathrm{p}}) = \zeta \left\langle \phi\left(\frac{F}{\sigma_Y} - 1\right)\right\rangle \tag{1.21}$$

where the notation

$$< a >= \begin{cases} a & \text{if} \quad a > 0 \\ 0 & \text{if} \quad a \leq 0 \end{cases} \tag{1.22}$$

has been used, and ζ is a material parameter.

The model postulates that because of the strain-rate effect, an actual stress higher than the (static) yield stress σ_Y develops. Indeed, if both $\dot{\bar{\varepsilon}}$ and ζ are greater than zero, we can write from Eq. (1.21)

$$F - \sigma_Y(\bar{\varepsilon}^{\mathrm{p}})\left(1 + \phi^{-1}(\dot{\bar{\varepsilon}}/\zeta)\right) = 0 \tag{1.23}$$

where ϕ^{-1} is the inverse function of ϕ (provided it exists). Eq. (1.23) may be read as the 'viscous' (i.e. rate sensitive) counterpart to the static yield condition, Eq. (1.6). For vanishing rate sensitivity Eq. (1.23) reduces to Eq. (1.6), while non-zero rate sensitivity assures that the stresses in the dynamic inelastic process will generally exceed the static yield surface. Moreover, the bigger the overstress, the higher the inelastic effective strain rate developing in the process. In passing, these are conditions to be fulfilled by the function ϕ. The expression

$$\sigma_Y^{(d)} = \sigma_Y(\bar{\varepsilon}^{\mathrm{p}})\left(1 + \phi^{-1}(\dot{\bar{\varepsilon}}/\zeta)\right) \tag{1.24}$$

is sometimes referred to as the *dynamic yield stress*

$$\sigma_Y^{(d)} = \sigma_Y^{(d)}(\bar{\varepsilon}^{\mathrm{p}}, \dot{\bar{\varepsilon}}) \tag{1.25}$$

This *overstress*, scaled by the 'static' yield stress σ_Y is the argument of the overstress function ϕ.

Replacing Eq. (1.21) into Eq. (1.19) we obtain a constitutive equation similar to that of a fluid

$$\dot{\varepsilon}_{ij} = \frac{1}{2\mu}\sigma_{ij}^{D} \tag{1.26}$$

from which

$$\frac{1}{2\mu} = \frac{3\zeta}{2\bar{\sigma}}\left\langle \phi\left(\frac{F}{\sigma_Y} - 1\right)\right\rangle \tag{1.27}$$

In other words, we are looking for the expression for the viscosity μ which will allow us to treat the viscoplastic material as a fluid.

Squaring both sides of Eq. (1.26) and using Eqs. (1.3) and (1.4) results

$$\dot{\bar{\varepsilon}} = \frac{1}{2\mu}\frac{2}{3}\bar{\sigma} \tag{1.28}$$

Now we can replace the yield function F in Eq. (1.21) by the Huber-Mises yield condition, Eq. (1.7), and make use of Eq. (1.28)

$$\dot{\varepsilon} = \zeta \left\langle \phi\left(\frac{3}{2}\frac{2\mu\dot{\bar{\varepsilon}}}{\sigma_Y} - 1\right)\right\rangle \tag{1.29}$$

A quite general form of the overstress function may be given by a power-type law

$$\phi(x) = x^n \tag{1.30}$$

where n will be an additional material constant. Replacing into Eq. (1.29) yields

$$\dot{\bar{\varepsilon}} = \zeta\left(\frac{3\mu\dot{\bar{\varepsilon}}}{\sigma_Y} - 1\right)^n \tag{1.31}$$

from which we can obtain an explicit expression for the viscosity

$$\mu = \frac{1}{3\dot{\bar{\varepsilon}}}\sigma_Y(\bar{\varepsilon}^p)\left[1 + \left(\frac{\dot{\bar{\varepsilon}}}{\zeta}\right)^{\frac{1}{n}}\right] \tag{1.32}$$

or

$$\mu = \frac{1}{3\dot{\bar{\varepsilon}}}\left[\sigma_Y(\bar{\varepsilon}^p) + \left(\frac{\dot{\bar{\varepsilon}}}{\gamma}\right)^{\frac{1}{n}}\right] \tag{1.33}$$

with $\gamma = \frac{\zeta}{(\sigma_Y)^n}$ sometimes referred to as fluidity.

The viscoplastic flow rule Eq. (1.26), where the viscosity is given by an expression of the type of Eq. (1.33) implies the assumption that the whole material is entirely plastic during the whole deformation history. Hence $\dot{\bar{\varepsilon}} > 0$ everywhere in the material thus avoiding formal complications related to the existence of rigid zones.

1.3.3 Power-law (Norton-Hoff) model

A slightly different model results by assuming in Eq. (1.6) a vanishing yield stress, that is, plastic flow develops at any stress level, although for small stresses the plastic flow can be very small. The equivalent viscosity for such model is given by [60, 28]

$$\mu = 2K(\bar{\varepsilon}^p)\,(\dot{\bar{\varepsilon}})^{(m-1)} \tag{1.34}$$

By introducing the condition $\sigma_Y = 0$ we can write Eq. (1.21) as

$$\dot{\varepsilon} = \xi\,\langle\varphi(F)\rangle \tag{1.35}$$

with $\xi = \xi(\bar{\varepsilon}^p)$, which, together with the Huber-Mises condition and assuming a power-type form for φ yields

$$\dot{\bar{\varepsilon}} = \xi \bar{\sigma}^{\frac{1}{m}} \tag{1.36}$$

which, using Eq. (1.28) results in

$$\mu = \frac{\bar{\sigma}^{(1-\frac{1}{m})}}{3\xi} \tag{1.37}$$

or

$$\mu = \frac{(\dot{\bar{\varepsilon}}/\xi)^m}{3\dot{\bar{\varepsilon}}} \tag{1.38}$$

which is equivalent to the cited expression provided

$$2K(\bar{\varepsilon}^p) = \frac{1}{3(\xi(\bar{\varepsilon}^p))^m} \tag{1.39}$$

and it can be read as a particular case of Eq. (1.33) (with $m = \frac{1}{n}$, $\gamma = \xi$ and $\varphi = \phi\sigma_Y^n$), for $\sigma_Y = 0$. In fact, for highly rate sensitive materials the overstress due to viscous effects is much bigger than the static yield stress σ_Y, which may be then neglected. For this reason the model has been sometimes applied, e.g. [28, 36, 44].

In [28] a more detailed description of the model and its implementation into finite elements can be found. However, in the present work, only the Prager-Perzyna model has been used.

1.3.4 Analogy with incompressible elasticity

We can summarize the complete set of equations representing the flow or rigid-viscoplastic material rewriting Eqs. (1.1) and (1.26) together with the equilibrium equation. It reads

$$\begin{aligned} \sigma_{ij,j} &= 0 && \text{– equilibrium} \\ \dot{\varepsilon}_{ij} &= \frac{1}{2}(v_{i,j} + v_{j,i}) && \text{– compatibility} \\ \dot{\varepsilon}_{ij} &= \frac{1}{2\mu}(\sigma_{ij} - \frac{1}{3}\sigma_{kk}\delta_{ij}) && \text{– flow rule} \end{aligned} \tag{1.40}$$

where the viscosity μ is given by Eq. (1.33) or Eq. (1.34) and includes the perfectly plastic material behaviour by assigning appropriate values to the model parameters (e.g. $\gamma \to \infty$ and/or $n \to \infty$ in Eq. (1.33)). The above set of equations can be confronted with those for incompressible linear elasticity (static case, no body forces), which read

$$\begin{aligned} \sigma_{ij,j} &= 0 \\ \varepsilon_{ij} &= \frac{1}{2}(u_{i,j} + u_{j,i}) \\ \varepsilon_{ij} &= \frac{1}{2\mu_s}(\sigma_{ij} - \frac{1}{3}\sigma_{kk}\delta_{ij}) \end{aligned} \tag{1.41}$$

with u_i and ε_{ij} standing for the components of the displacement vector and deformation tensor, respectively, and μ_s denoting the shear modulus. By confronting Eqs. (1.40) and (1.41) it is straightforward to observe that both sets of equations exhibit a remarkable formal similarity, with the following quantities corresponding to each other

$$v_i \leftrightarrow u_i, \quad \dot{\varepsilon}_{ij} \leftrightarrow \varepsilon_{ij}, \quad \mu \leftrightarrow \mu_s \tag{1.42}$$

σ_{ij} having the same meaning in both cases. The analogy has a great computational potential since it allows us to treat advanced plastic flow problems by using computer software developed for linear incompressible elasticity. To do so, one simply has to allow the shear modulus μ to be a given function of the current state variables and their rates; this last feature necessitates the use of an iterative loop since the 'parameter' of the theory μ depends on velocities that are the basic unknowns in the problem.

Chapter 2

Modelling of metal forming using the flow approach

2.1 Introductory comments

Having reviewed in the previous chapter the foundations of the flow approach, we will now face the task of its computer implementation. In doing so, a number of issues arise that quite clearly show the potentials and the limitations of this approach. The former encourage us to overcome the latter. Indeed, an effective way to develop computational models for the problem of large deformation of metals is to treat the material as an incompressible viscous fluid of a non-Newtonian kind. This approach, formally identical to that typical of the theory of rigid–viscoplasticity and known as the flow approach, has been used extensively in recent years in conjunction with the finite element method to solve a variety of bulk and sheet metal forming problems, [6, 74, 86, 114, 116].

Much of the success of the flow approach is due to its simplicity. In particular, if inertia terms are neglected, then the flow equations for the von Mises material are analogous to those of classical non-linear incompressible elasticity with velocities, strain rates and non-linear viscosity playing the role of displacements, strains and shear modulus of the corresponding elasticity model, respectively, as it has been shown in the previous chapter. This allows finite element computer programs for metal forming analysis to be directly obtained by a simple modification of standard finite element codes written for 2D and 3D elasticity applications.

This chapter is devoted to the discretized formulation of the flow approach, accounting also for different physical aspects of the model aiming at its application to situations of practical importance. Following, the sensitivity analysis of different metal forming processes described in the framework of the finite element flow approach is addressed. The literature on the subject appears to be very scarce, [10, 11, 12, 18, 44, 72, 73, 76, 99].

We shall begin this chapter with a discussion of the finite element model to

be used for the analysis of flow problems, Section 2.2. The formulation of metal forming sensitivity with respect to material parameters entering the constitutive model considered, such as the yield limit σ_0, fluidity γ, exponent of the viscoplastic flow law n, etc. follows in Section 2.3. Some specific computational studies presented therein concern a direct extrusion process and a cutting problem. Next, the problem of shape sensitivity analysis for a class of metal forming processes is discussed, Section 2.4. The procedure is illustrated by calculating the sensitivities of some independent and dependent variables with respect to the die angle in an extrusion problem and to the roller radius in a plane rolling process. Finally, shape optimization based on the previous results of shape sensitivity will be presented, Section 2.5. Attention will be placed on the way the possible design variables are related to the overall shape of the domain. The numerical illustrations should emphasize the practical usefulness of the proposed approach.

2.2 The discretized formulation

2.2.1 Equations of flow approach

In the following sections we shall consider the problem of evaluating the sensitivities of primary and secondary variables describing metal forming problems. In view of the practical aspects pointed out in the previous section and outlined earlier in Chapter 1, we shall develop sensitivity equations in the framework of the flow approach. Keeping in mind the main objective of computing sensitivities as a byproduct of the equilibrium solution, we shall first discuss a discretized formulation describing the latter problem.

Metal forming processes typically involve very large deformations. This allows us to neglect the elasticity of the material and to adopt the rigid–viscoplastic (or rigid–plastic) material model. If necessary, the elastic recovery can be approximately calculated in the final step of the analysis by removing the loads. In some situations this may result in relatively large displacements, significantly affecting the final shape of the workpiece being manufactured. This happens especially in sheet forming and is much less noticeable in bulk forming; the effect is referred to in the literature as elastic spring-back.

Additional features of metal forming processes are that (i) in many processes material particles follow similar paths along streamlines so that we can basically speak of stationarity conditions prevailing during the process, and (ii) dynamic terms are rarely significant. The first observation suggests that the Eulerian approach is more naturally suited to describe the material motion than the Lagrangian one, and that velocities give more useful information about the material state than displacements, which if needed can be calculated by integration of the velocities for given material points. Furthermore, as has been pointed out in Section 2.1 the material is considered to be a non-Newtonian fluid for which inertia terms can be neglected, since for a typical process the Reynolds number is of the order 10^{-9}. This justifies the second observation above and leads

to a formal analogy between the viscoplastic flow and nonlinear incompressible elasticity referred to in Section 1.3.4. On the basis of these facts the flow approach seems best suited for an analysis of steady-state processes. Nevertheless, non-stationary problems can also be solved using velocity-based updating of the configuration, or by some other alternative techniques (for example, by considering a fixed mesh in which the metal flows together with a fictitious material, the interface between them being tracked by solving an advective transport equation [7, 104]). Transient solutions can be obtained in most cases by using either an explicit or implicit time integration scheme.

To solve the 3D equilibrium problem describing a stationary metal forming operation the equilibrium equation in absolute notation [70] is taken in the weak form as,

$$\int_{\Omega} \boldsymbol{\sigma} \cdot \delta\dot{\boldsymbol{\epsilon}} \, \mathrm{d}\Omega = \int_{\Omega} \mathbf{f} \, \delta\mathbf{v} \, \mathrm{d}\Omega + \int_{\partial\Omega_\sigma} \mathbf{t} \, \delta\mathbf{v} \, \mathrm{d}(\partial\Omega) \tag{2.1}$$

where $\delta\dot{\boldsymbol{\epsilon}}$ is the virtual plastic deformation rate compatible with the virtual velocity field $\delta\mathbf{v}$ that fulfill the kinematic boundary conditions, while $\mathbf{f}$ and $\mathbf{t}$ stand for prescribed distributed volumetric loads in the domain Ω and prescribed surface traction on the boundary $\partial\Omega_\sigma$, respectively.

Stresses and strain rates are related by the constitutive equation for the rigid-viscoplastic material as presented in Section 1.3, which reads, in index notation

$$\sigma_{ij} = \sigma^{\mathrm{D}}_{ij} - p\,\delta_{ij} = 2\mu\,\dot{\varepsilon}_{ij} - p\,\delta_{ij} \tag{2.2}$$

where, cf. Eq. (1.33)[1]

$$\mu = \frac{1}{3\dot{\bar{\varepsilon}}}\left[\sigma_0 + \left(\frac{\dot{\bar{\varepsilon}}}{\gamma}\right)^{\frac{1}{n}}\right] \tag{2.3}$$

is the equivalent viscosity, which is a function of the equivalent strain rate, defined in terms of the strain rate tensor $\dot{\varepsilon}_{ij}$ as

$$\dot{\bar{\varepsilon}} = \sqrt{\tfrac{2}{3}\dot{\varepsilon}_{ij}\dot{\varepsilon}_{ij}} \tag{2.4}$$

$\dot{\varepsilon}_{ij}$ is computed in terms of velocities v_i as

$$\dot{\varepsilon}_{ij} = \frac{1}{2}\left(\frac{\partial v_i}{\partial x_j} + \frac{\partial v_j}{\partial x_i}\right) \tag{2.5}$$

and $p = -\frac{1}{3}\sigma_{ii}$ is the pressure (assumed positive in compression). No strain hardening material is assumed for simplicity.

We should point out that because of the nonlinearity entering in a complex manner through the viscosity μ, there is no known functional yielding the solution by making its first variation vanish. Instead, either the principle of virtual

[1]The symbol for the static yield stress σ_Y, used in Chapter 1, which stressed the *yielding* of the material will be replaced by σ_o, which stresses the static meaning of this quantity.

velocities or the weighted residual method must be used to obtain the set of equations suitable for discretization.

Another important feature of the problem, which has to be accounted for is that the flow is incompressible. The condition is expressed by requiring the rate of work generated during material compression/expansion to vanish

$$\int_{\Omega} \dot{\varepsilon}_{ii}\, \delta p \, d\Omega = 0 \tag{2.6}$$

Among other possible ways of imposing this condition (such as penalty or augmented Lagrangian formulations), the one using the pressure p as a discretized variable leads to a set of Lagrange multipliers, one for each discrete pressure.

The problem of imposing incompressibility has been extensively studied and is known to produce very serious difficulties in the numerical solution if certain conditions are not fulfilled. We will come back to this point in Section 2.2.4. However, let us notice in passing that conditions that assure a stable (i.e. 'wiggle-free') pressure solution are usually fulfilled for the known and widely applied discretization models for Newtonian fluids, since research on this subject was classically concentrated in this field. However, a non-Newtonian fluid may locally not fulfill the stability condition even if those well tested discretization models are applied. This is why additional work is necessary here, and it will be the subject of Section 2.2.4.

The system consisting of Eqs. (2.1) and (2.6) can be used to derive the finite element equations. We assume the velocity $\mathbf{v}$ and pressure p to be functions of their nodal values by using their respective expansions

$$\mathbf{v} = \boldsymbol{\phi}\, \dot{\mathbf{q}}, \qquad p = \hat{\boldsymbol{\phi}}\, \bar{\mathbf{p}} \tag{2.7}$$

The fact that we are dealing with a mixed formulation, which implies the use of variables of different nature (vector and scalar) somewhat complicates the notation, especially upon discretization. According to the expressions for $\boldsymbol{\phi}$ and $\hat{\boldsymbol{\phi}}$ given in Eqs. (2.8), (2.9) and (2.12) below, while $\bar{\mathbf{p}}$ is an array of scalar elements, $\dot{\mathbf{q}}$ is an array of vectors, cf. Eqs. (2.10) and (2.11) below. We can define the address of its elements twofold: using a global numbering throughout the array; or addressing to a particular node and, inside it, to the referred velocity component. Furthermore, even if for clarity we place $\dot{\mathbf{q}}$ and $\bar{\mathbf{p}}$ as two separated vectors, in fact their components are node-wise grouped in only one vector.

In mixed formulations it is much more likely than in so-called irreducible ones to have different approximations for different variables. Therefore a different notation for the shape functions of different variables is advisable. For this reason a "hat" is used to distinguish the pressure shape functions from those of each of the velocity components. A similar argumentation may be used in any problem ruled by more than one equation, where variables of different type are involved, like e.g. mechanical problems with thermal coupling, as it will come out in Section 2.2.6.

The $(3 \times N)$ matrix $\boldsymbol{\phi}$ collects shape functions interpolating the velocity field in the whole region considered in terms of the $(N \times 1)$ nodal velocity vector $\dot{\mathbf{q}}$,

N being the overall number of kinematic degrees of freedom in the discretized system. Specification of the equations to the plane strain case considered in the examples is straightforward.

For S nodes in the system and no kinematic boundary conditions accounted for so far we clearly have $N = 3S$. The components in the vector $\dot{\mathbf{q}}$ are ordered by the node numbers and, for each node, by the component numbers. The shape function matrix $\boldsymbol{\phi}$ consists of S matrices $\boldsymbol{\phi}^{(s)}$, $s = 1, 2, \ldots, S$, of dimension 3×3 each

$$\boldsymbol{\phi}_{3\times N} = \left[\boldsymbol{\phi}^{(1)}\ \boldsymbol{\phi}^{(2)} \ldots\ \boldsymbol{\phi}^{(S)}\right] \tag{2.8}$$

with

$$\boldsymbol{\phi}^{(s)}_{3\times 3} = \begin{bmatrix} \phi_1^{(s)} & 0 & 0 \\ 0 & \phi_2^{(s)} & 0 \\ 0 & 0 & \phi_3^{(s)} \end{bmatrix}, \qquad s = 1, 2, \ldots, S \tag{2.9}$$

The buildup of the vector $\dot{\mathbf{q}}$ is of the form

$$\dot{\mathbf{q}}_{N\times 1} = \{\dot{\mathbf{q}}^{(1)}\ \dot{\mathbf{q}}^{(2)} \ldots\ \dot{\mathbf{q}}^{(S)}\} \tag{2.10}$$

with

$$\dot{\mathbf{q}}^{(s)}_{3\times 1} = \{\dot{q}_1^{(s)}\ \dot{q}_2^{(s)}\ \dot{q}_3^{(s)}\}, \qquad s = 1, 2, \ldots, S \tag{2.11}$$

being the vector of the sth node velocities.

Most frequently the diagonal elements $\phi_i^{(s)}$ will be the same for $i = 1, 2, 3$; generally, different components may have different shape functions. Since the pressure p is a scalar quantity and $\bar{p}_1, \bar{p}_2, \ldots$ are assumed to be defined at the system nodes, the matrix $\hat{\boldsymbol{\phi}}$ is of dimension $1 \times S$ (i.e. it is a row vector) with the $\hat{\phi}^{(s)}$'s possibly different from the $\phi_i^{(s)}$'s

$$\hat{\boldsymbol{\phi}}_{1\times S} = \left[\hat{\phi}^{(1)}\ \hat{\phi}^{(2)} \ldots\ \hat{\phi}^{(S)}\right] \tag{2.12}$$

By differentiating the shape functions with respect to the space coordinates we obtain (cf. Eq. $(2.7)_1$) the strain rate vector $\dot{\boldsymbol{\varepsilon}}$ expressed in terms of the nodal velocities $\dot{\mathbf{q}}$ as

$$\dot{\boldsymbol{\varepsilon}}_{6\times 1} = \mathbf{B}_{6\times N}\, \dot{\mathbf{q}}_{N\times 1} \tag{2.13}$$

$\mathbf{B}$ being the $(6 \times N)$ matrix

$$\mathbf{B}_{6\times N} = \left[\mathbf{B}^{(1)}\, \mathbf{B}^{(2)} \ldots\ \mathbf{B}^{(S)}\right] \tag{2.14}$$

defined in terms of the components of the matrix $\boldsymbol{\phi}$ as

$$\mathbf{B}^{(s)}_{6\times 3} = \frac{1}{2}\begin{bmatrix} 2\phi^{(s)}_{1,1} & 0 & 0 \\ 0 & 2\phi^{(s)}_{2,2} & 0 \\ 0 & 0 & 2\phi^{(s)}_{3,3} \\ \phi^{(s)}_{1,2} & \phi^{(s)}_{2,1} & 0 \\ 0 & \phi^{(s)}_{2,3} & \phi^{(s)}_{3,2} \\ \phi^{(s)}_{1,3} & 0 & \phi^{(s)}_{3,1} \end{bmatrix} \tag{2.15}$$

where the notation $a_{,i} = \dfrac{\partial a}{\partial x_i}$ has been used.

Quite similarly the virtual velocities, rate of deformation and pressures are expressed in the form

$$\begin{aligned} \delta \mathbf{v} &= \boldsymbol{\phi}\, \delta \dot{\mathbf{q}} \\ \delta \dot{\boldsymbol{\varepsilon}} &= \mathbf{B}\, \delta \dot{\mathbf{q}} \\ \delta p &= \hat{\mathbf{B}}\, \delta \bar{\mathbf{p}} \end{aligned} \tag{2.16}$$

where the row vector $\hat{\boldsymbol{\phi}}$ was renamed for notational consistency as

$$\hat{\boldsymbol{\phi}} = \hat{\mathbf{B}} \tag{2.17}$$

By substituting Eqs. (2.7), (2.13) and (2.16) into Eq. (2.1) and observing that the last one holds for any virtual velocity, we obtain

$$\int_\Omega \mathbf{B}^{\mathrm{T}} \boldsymbol{\sigma}\, \mathrm{d}\Omega = \mathbf{Q} \tag{2.18}$$

with

$$\mathbf{Q} = \int_\Omega \boldsymbol{\phi} \hat{\mathbf{f}}\, \mathrm{d}\Omega + \int_{\partial\Omega_t} \boldsymbol{\phi} \hat{\mathbf{t}}\, \mathrm{d}\,(\partial\Omega) + \mathbf{P} \tag{2.19}$$

Here, $\mathbf{Q}$, $\hat{\mathbf{f}}$, $\hat{\mathbf{t}}$ and $\mathbf{P}$ are vectors with the same component ordering as employed in defining the vector $\mathbf{q}$, and $\mathbf{P}$ is the vector of concentrated loads applied at the nodes.

Replacing Eqs. (2.2) and (2.3) into Eq. (2.18) we get

$$\left(\int_\Omega 2\mu \mathbf{B}^{\mathrm{T}} \mathbf{B}\, \mathrm{d}\Omega\right) \dot{\mathbf{q}} - \left(\int_\Omega \mathbf{B}^{\mathrm{T}} \boldsymbol{\Gamma}\, \hat{\mathbf{B}}\, \mathrm{d}\Omega\right) \bar{\mathbf{p}} = \mathbf{Q} \tag{2.20}$$

i.e.

$$\mathbf{K}_{(\mu)}\, \dot{\mathbf{q}} + \mathbf{K}^{\mathrm{T}}_{(p)}\, \bar{\mathbf{p}} = \mathbf{Q} \tag{2.21}$$

where

$$\begin{aligned} \mathbf{K}_{(\mu)} &= \int_\Omega \mu\, \mathbf{k}_0\, \mathrm{d}\Omega = \int_\Omega 2\mu\, \mathbf{B}^{\mathrm{T}}\, \mathbf{B}\, \mathrm{d}\Omega \\ \mathbf{K}^{\mathrm{T}}_{(p)} &= -\int_\Omega \mathbf{k}^{\mathrm{T}}_{(p)}\, \mathrm{d}\Omega = -\int_\Omega \mathbf{B}^{\mathrm{T}} \boldsymbol{\Gamma}\, \hat{\mathbf{B}}\, \mathrm{d}\Omega \end{aligned} \tag{2.22}$$

the column vector $\boldsymbol{\Gamma}_{6\times 1} = \{1,1,1,0,0,0\}$ converting the total strain into its volumetric components.

The equilibrium equation (2.1) has to be solved together with the incompressibility condition (2.6) written in the weak form as

$$\int_\Omega \hat{\mathbf{B}}^{\mathrm{T}} \dot{\varepsilon}_{ii}\, \mathrm{d}\Omega = \mathbf{0} \tag{2.23}$$

which, after discretization, reads

$$\left(\int_\Omega \hat{\mathbf{B}}^{\mathrm{T}}\, \boldsymbol{\Gamma}^{\mathrm{T}} \mathbf{B}\, \mathrm{d}\Omega\right) \dot{\mathbf{q}} = \mathbf{0} \tag{2.24}$$

or, more compactly

$$\mathbf{K}_{(p)}\dot{\mathbf{q}} = \mathbf{0} \tag{2.25}$$

The fundamental set of equations for the $(N+S)$ unknowns $\dot{\mathbf{q}}$ and $\bar{\mathbf{p}}$ thus becomes

$$\begin{bmatrix} \mathbf{K}_{(\mu)} & \mathbf{K}_{(p)}^{\mathrm{T}} \\ \mathbf{K}_{(p)} & \mathbf{0} \end{bmatrix} \begin{bmatrix} \dot{\mathbf{q}} \\ \bar{\mathbf{p}} \end{bmatrix} = \begin{bmatrix} \mathbf{Q} \\ \mathbf{0} \end{bmatrix} \tag{2.26}$$

which can be written in a residual form as

$$\mathbf{R} = \mathbf{K}^{(S)}\bar{\mathbf{q}} - \bar{\mathbf{Q}} = \mathbf{0} \tag{2.27}$$

where

$$\bar{\mathbf{q}} = \begin{bmatrix} \dot{\mathbf{q}} \\ \bar{\mathbf{p}} \end{bmatrix}, \qquad \mathbf{K}^{(S)} = \begin{bmatrix} \mathbf{K}_{(\mu)} & \mathbf{K}_{(p)}^{\mathrm{T}} \\ \mathbf{K}_{(p)} & \mathbf{0} \end{bmatrix}, \qquad \bar{\mathbf{Q}} = \begin{bmatrix} \mathbf{Q} \\ \mathbf{0} \end{bmatrix} \tag{2.28}$$

It can be easily recognized that Eq. (2.26) corresponds to the equations describing the nonlinear Stokes flow.

The solution to Eq. (2.27) can be found by either direct iterations, for which only a quasi-linear rate of convergence can be achieved, or by the quadratically convergent Newton–Raphson method, for which a certain minimum level of strain rate hardening is required to converge [6]. In the latter case, by defining the residual after the ωth iteration as

$$\mathbf{R}^{(\omega)} = \mathbf{K}^{(S)(\omega)}\,\bar{\mathbf{q}}^{(\omega)} - \bar{\mathbf{Q}}^{(\omega)}, \qquad \omega = 0, 1, \ldots \tag{2.29}$$

we obtain the solution correction $\gamma\bar{\mathbf{q}}^{(\omega)}$ by setting the residual after the ωth iteration equal to $\mathbf{0}$. Employing the first-order Taylor expansion around $\bar{\mathbf{q}}^{(\omega)}$, this condition reads

$$\mathbf{R}^{(\omega+1)} \cong \mathbf{R}^{(\omega)} + \frac{\partial \mathbf{R}^{(\omega)}}{\partial \bar{\mathbf{q}}}\gamma\bar{\mathbf{q}}^{(\omega+1)} = \mathbf{0} \tag{2.30}$$

where γ stands here for the variation of the solution vector with the meaning of an iterative correction. The solution correction is computed as

$$\gamma\bar{\mathbf{q}}^{(\omega+1)} = -\left(\frac{\partial \mathbf{R}^{(\omega)}}{\partial \bar{\mathbf{q}}}\right)^{-1} \mathbf{R}^{(\omega)} \tag{2.31}$$

so that the $(\omega+1)$th approximation to the solution vector $\bar{\mathbf{q}}$ reads

$$\bar{\mathbf{q}}^{(\omega+1)} = \bar{\mathbf{q}}^{(\omega)} + \gamma\bar{\mathbf{q}}^{(\omega+1)} \tag{2.32}$$

where

$$\frac{\partial \mathbf{R}}{\partial \bar{\mathbf{q}}} = \mathbf{K}^{(S)} + \int_{\Omega} \left(\bar{\mathbf{k}}_0\bar{\mathbf{q}}\right) \frac{\partial \mu}{\partial \bar{\mathbf{q}}}\, \mathrm{d}\Omega - \frac{\partial \bar{\mathbf{Q}}}{\partial \bar{\mathbf{q}}} = \mathbf{K}^{(T)} \tag{2.33}$$

is the tangent stiffness matrix, the term $\partial\mu/\partial\bar{\mathbf{q}}$ is computed using the relations

$$\begin{aligned} \frac{\partial\mu}{\partial\dot{q}_\alpha} &= \frac{\partial\mu}{\partial\dot{\bar{\varepsilon}}}\frac{\partial\dot{\bar{\varepsilon}}}{\partial\dot{\varepsilon}_{ij}}\frac{\partial\dot{\varepsilon}_{ij}}{\partial\dot{q}_\alpha} = -\frac{2}{9}\left[\sigma_0 + \left(1-\frac{1}{n}\right)\left(\frac{\dot{\bar{\varepsilon}}}{\gamma}\right)^{\frac{1}{n}}\right]\frac{\dot{\varepsilon}_{ij}}{\dot{\bar{\varepsilon}}^3}B_{ij\alpha} \\ \frac{\partial\mu}{\partial\bar{p}_\beta} &= 0 \end{aligned} \tag{2.34}$$

with the definition of matrix $\mathbf{B}$ accordingly modified to allow the use of the tensor (instead of vector) notation of the strain rate vector, and

$$\bar{\mathbf{k}}_0 = \begin{bmatrix} \mathbf{k}_0 & \mathbf{0} \\ \mathbf{0} & \mathbf{0} \end{bmatrix} \tag{2.35}$$

The matrix $\mathbf{k}_0$ depends only on the problem geometry; in order to obtain $\mathbf{K}_{(\mu)}$, $\mathbf{k}_0$ is multiplied by the viscosity μ and integrated element-wise (Eq. $(2.22)_1$).

The formulation of the boundary value problem is completed by a suitable specification of the boundary conditions, which can be either of the sticking or the no-friction slipping-type, or of an intermediate type defined by the tangential force applied to the material boundary and computed according to a given friction law.

The basic flow formulation can be extended to better account for real situations encountered in metal forming practice: effects such as heat generation, material damage, free surfaces, boundary friction and contact can then be included, [2, 6, 10, 86].

In fact, complexity of most real metal forming problems exceeds the modelling possibilities of the flow approach in its standard version. Moreover, particular features requiring special attention, or at least a careful numerical treatment, are different for different processes. A very general and instructive example of metal forming processes is offered by considering the cutting problem. Similar, but typically much simpler situations may be found in the simulation of other forming processes. Moreover, a specialized analysis of cutting problems lays beyond the scope of the flow approach, at least in its present state. In a Lagrangian context this problem has been solved accounting for discontinuous chip formation with propagation of fractures through the deforming chip [82, 98, 100]. Nevertheless, a typical cutting process can be modelled in a simplified way by the movement of a rigid tool parallel to the surface of a semi-infinite domain representing the metal matrix at a given cutting depth d. Equivalently the tool may be fixed with the metal moving in the opposite direction; incidentally, such a situation is more convenient for numerical calculations. A metal chip is separated from the workpiece after it has been in contact with the tool. The metal chip has two free surfaces: one is the continuation, after a sharp change in direction at the shear deformation band, of the original free surface of the workpiece. The other side of the chip, beginning at the tool edge, is first in contact with the tool but after a certain distance it separates, generating the second free surface. Both of them must be found from the condition that for plane strain idealization they should coincide with streamlines. In addition, the former free surface representation

must allow for the occurrence of sharp angles corresponding to the discontinuity in the velocity field for the perfectly plastic case. The latter free surface involves a contact problem because the point of the chip separation from the tool is unknown a priori. Finally, for the parts of the boundary in contact with the solid surfaces friction forces should be calculated.

We note again in passing that once we know the way to model the cutting problem nearly all other metal forming problems can also be reliably addressed.

2.2.2 Boundary friction

A simple way to model the boundary friction, suggested in [111], is to insert a thin layer of elements connecting the fixed boundary with the material. According to the *Coulomb friction law*, a yield stress proportional to the pressure is assigned to the elements so that the material is acted upon by a tangential force proportional to the force normal to the boundary and directed opposite to the material movement. If the pressure happens to be zero, then a residual viscosity is imposed in order to avoid numerical singularity of the matrices. The viscosity is given by

$$\mu = \frac{\sigma_f}{3\dot{\bar{\varepsilon}}} \tag{2.36}$$

with σ_f defined as

$$\sigma_f = \begin{cases} \sigma_{vp} = \sigma_0 + (\dot{\bar{\varepsilon}}/\gamma)^{\frac{1}{n}} & \text{if} \quad p\nu > \sigma_{vp} \\ p\nu & \text{if} \quad 0 < p\nu < \sigma_{vp} \\ \kappa & \text{if} \quad p \leq 0 \end{cases} \tag{2.37}$$

where ν is the *friction coefficient* in the Coulomb friction law and κ is a small positive number such chosen as to avoid matrix singularity. In this way the more compressed the material against the surface, the bigger the shear stress between the friction layer and the rest of the material. For the friction elements the derivatives (2.34) take the form

$$\frac{\partial \mu}{\partial \dot{q}_\alpha} = \begin{cases} -\dfrac{2p\nu}{9\dot{\bar{\varepsilon}}^3}\dot{\varepsilon}_{ij}B_{ij\alpha} & \text{if} \quad 0 < p\nu < \sigma_{vp} \\ -\dfrac{2\delta}{9\dot{\bar{\varepsilon}}^3}\dot{\varepsilon}_{ij}B_{ij\alpha} & \text{if} \quad p \leq 0 \end{cases} \tag{2.38}$$

and

$$\frac{\partial \mu}{\partial p} = \begin{cases} \dfrac{\nu}{3\dot{\bar{\varepsilon}}} & \text{if} \quad 0 < p\nu < \sigma_{vp} \\ 0 & \text{if} \quad p < 0 \end{cases} \tag{2.39}$$

This method for handling frictional conditions has its obvious strength in its simplicity of implementation. However it increases the number of unknowns, introduces a geometrical inaccuracy of the size of the layer width, and numerical errors due to the high aspect-ratio of the friction elements. For these reasons this solution was abandoned for a better suited friction model, such as the one presented in Section 2.2.3, which also handles certain cases of contact.

2.2.3 Contact and friction

A more effective and rational alternative is to handle boundary friction by using friction–contact elements, in which both effects (contact and, if required, friction) are treated at the same time. Before discussing such a formulation another issue requires additional comments.

The contact description for steady-state flow differs somewhat from that known in transient, displacement-based situations. The difference comes from the way the free surfaces are handled. A non-steady process may (and usually will) have free surfaces with non-zero normal velocities. New locations of the surface are found by node updating in terms of their velocities and further corrections for the nodes which come in contact with a solid surface (representing the tool). Then they remain in contact (with the velocity component normal to the boundary set to zero) until there is a traction force between the solid boundary and the workpiece. On the other hand, in a steady-state process the problem consists in finding a stationary surface (or a stationary line, in 2D problems), to which the velocity is always tangent. If some parts of the surface are likely to interact with a solid boundary, then the two conditions must be satisfied simultaneously: no penetration of the flow into the solid boundary (i.e. the imposed zero normal velocity) and no traction forces between the workpiece and the tool. These conditions allow for specification of a criterion for determining the point at which the material separates from (or comes into contact with) the solid boundary. According to the flow direction with respect to the solid boundary two similar problems may be considered in the form of looking for either the so-called separation point or the point where the free surface comes into contact with the solid boundary. Although in our analysis we shall only consider the former case, the latter one can be treated similarly.

Along the surface, which may be either free or in contact with the solid boundary, normal velocities are constrained to zero if the material tries to cross the solid boundary, and they are set free if any traction exerted on the flow by the wall is found. In other words, a fixed node of the contact surface is released if the pressure is negative, and a free node is fixed if it has a penetrating normal velocity. The changes are performed one node at a time in the neighbourhood of the present limit of the contact zone, keeping the remaining nodes in the previous state. In this way, the separation point is adjusted until the free boundary originating from it becomes a streamline. It is worth pointing out that nodes on the free part of the surface may have a normal component of the velocity directed towards the solid boundary. However, this does not necessarily mean that the flow gets through the wall.

The imposition of conditional restrictions on the velocity component normal to the wall is achieved by four node contact elements which connect two nodes of the material with two auxiliary nodes fixed to the solid boundary (velocities and pressure are constrained to zero). At the beginning both sides are coincident. If the element is on the free surface, then its stiffness matrix is assumed as the null

matrix and no restriction is imposed on the degrees of freedom corresponding to the normal-to-boundary velocity. However, whenever the contact condition is satisfied, the normal velocities are constrained at the nodes in the fluid by equating them to their counterparts on the solid boundary (which are equal to zero) by means of a penalty parameter. According to the element numbering given in Fig. 2.1, the constraints

$$\alpha(v_1 - v_4) = 0\,, \qquad \alpha(v_2 - v_3) = 0 \tag{2.40}$$

are added to the global system in the respective equations for v_3 and v_4 through the element matrix, α being the penalty parameter. Since v_1 and v_2 are set to zero, the fluid normal velocities v_3 and v_4 will also be zero. In Fig. 2.1 the nodal velocities are given in the local coordinate system. If the local axes are not coincident with the global ones, Eqs. (2.40) are appropriately transformed so that the penalty parameter will then affect the two equations of the global system corresponding to both the velocity components at each node in contact with the solid boundary, thus ensuring the zero velocity across it.

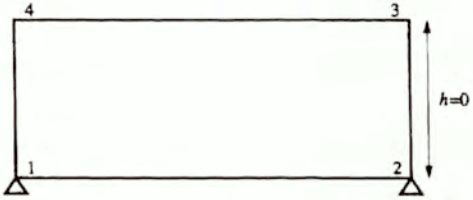

$$k_{44} = k_{11} = -k_{41} = -k_{14} = \begin{cases} \alpha & \text{if pressure at } 4 > 0 \\ 0 & \text{otherwise} \end{cases}$$

$$k_{33} = k_{22} = -k_{32} = -k_{23} = \begin{cases} \alpha & \text{if pressure at } 3 > 0 \\ 0 & \text{otherwise} \end{cases}$$

Figure 2.1 Contact element

Upon updating the free surface (see Section 2.2.5) no change will result in the nodes defining the surface whenever the normal velocity is zero. This may happen either because the free surface is already a streamline, or because it is in contact with the solid boundary. On the other hand, a different updated configuration will be obtained if there is a non-zero normal velocity component.

The friction conditions can be imposed in terms of the force vector using the same contact elements. According to the Coulomb friction law, the part of the boundary with the active contact condition is assumed to be acted upon by a distributed tangential friction force proportional to the pressure and opposite in direction to the velocity. (Other friction laws may also be considered and easily implemented since all the necessary information is available at the element level.)

If p_3 and p_4 are pressure values at nodes 3 and 4, respectively, cf. Fig. 2.1, then the distributed friction force along the element side $\overline{34}$ will be

$$\mathbf{f} = -\frac{\mathbf{v}}{||\mathbf{v}||}[p_3\psi + p_4(1-\psi)]\nu \tag{2.41}$$

where $\psi = (x - x_4)/(x_3 - x_4)$ and $x_4 \leq x \leq x_3$ is the local coordinate along the side $\overline{34}$, $0 \leq \psi \leq 1$ and ν is again the Coulomb friction coefficient. The equivalent nodal friction forces become

$$\begin{aligned} \mathbf{f}_3 &= -\frac{\mathbf{v}}{||\mathbf{v}||}\left(\frac{p_3}{3} + \frac{p_4}{6}\right)h\nu = -\frac{\mathbf{v}}{||\mathbf{v}||}\hat{f}_3 \\ \mathbf{f}_4 &= -\frac{\mathbf{v}}{||\mathbf{v}||}\left(\frac{p_3}{6} + \frac{p_4}{3}\right)h\nu = -\frac{\mathbf{v}}{||\mathbf{v}||}\hat{f}_4 \end{aligned} \tag{2.42}$$

where h is the contact element length. The friction forces calculated in this way may lead to unrealistic situations during the solution process and even cause the algorithm to diverge: a high pressure value may produce a non-physical opposite-to-the-flow friction force so large that it will produce a boundary flow moving against the main flow. In the iteration process the friction force may be changing sign from one iteration to another; if additionally its absolute value grows, then the solution algorithm will clearly not converge. For these practical reasons it has been found convenient to bound the friction force derived from Eq. (2.42) by two extreme values: one corresponding to the 'traction' case (the contact pressure less than, or equal to zero), in which the friction force vanishes, and another corresponding to the 'sticking' case, in which the tangent velocity is constrained and a maximum in the allowed friction force absolute value, say $\mathbf{f}_i^s$, is obtained. Hence, the actual module of the friction force for use in the model is

$$||\mathbf{f}_i|| = \begin{cases} ||\mathbf{f}_i^s|| & \text{for} \quad \hat{f}_i > ||\mathbf{f}_i^s|| \\ ||\mathbf{f}_i|| & \text{for} \quad 0 < \hat{f}_i < ||\mathbf{f}_i^s|| \\ 0 & \text{for} \quad \hat{f}_i < 0 \end{cases} \tag{2.43}$$

In comparison with the previous friction element (cf. Section 2.2.2), this one is more effective computationally since: (i) it needs no numerical integration and has fewer degrees of freedom, and (ii) it is more accurate as it does not require a 'thin' layer of elements (which in addition may introduce numerical errors because of their high length–width ratio) instead of just a contact surface. On the other hand, the friction force must be bounded either by imposing a no-counter-flow condition or the previously calculated tangential reactions for the sticking type.

2.2.4 Pressure stabilization

The application of any algorithm based on the pressure values at the boundary requires an accurate enough pressure field. It is a known fact that for nonlinear problems (unlike the linear case, [50]) the so-called *Brezzi–Babuska condition*

(often referred to as BB) is not satisfied even by the Q2/Q1 elements[1]. As a consequence, (generally moderate) spurious pressure modes appear. These pressure peaks, ranging alternately from negative to positive values, seriously disturb the solution and, consequently, any further procedure based on the values of the pressure field as well. This effect is sometimes called 'checkerboard', and it cannot be avoided nor reduced by simply refining the mesh.

A few methods (most of them, in fact, similar to each other) for pressure stabilization have been proposed in the context of linear Stokes and Navier-Stokes problems, i.e., for constant viscosity [63, 121]. They basically aim at generating the so-called stabilization matrix in the pressure-pressure entries of the global system of equations thus replacing the null submatrix $\mathbf{0}$ in Eq. (2.26). In the quoted works, the goal was only to achieve a solution free of spurious pressure modes using arbitrarily chosen shape functions, because approximations which satisfied the BB condition already gave good pressure solutions. Here, as it came out, by application of such technique the two goals were achieved.

We will consider one such method for pressure stabilization circumventing the Brezzi–Babuska condition, which has been proposed in [63]. According to it, the equilibrium equation suitably weighted by the gradient of the shape functions is added to the pressure equation in order to obtain the negative Laplacian in the diagonal block for the pressure, which is responsible for the stabilizing effect. The additional equation should vanish when the converged solution is reached. By applying this technique to the flow formulation for metal forming problems we add to the incompressibility condition (the second row of Eq. (2.26)) the equation

$$\int_\Omega \frac{\alpha h^2}{2\mu} \left[\nabla \hat{\boldsymbol{\phi}} \cdot (-\nabla \cdot \boldsymbol{\sigma}^{\mathrm{D}} + \nabla p - \mathbf{f}) \right] \, \mathrm{d}\Omega = 0 \tag{2.44}$$

where α is a stabilization coefficient, $0 \leq \alpha \leq 1$, h is a geometric characteristic (the element size parameter) and $\boldsymbol{\sigma}^{\mathrm{D}}$ is, as before, the stress deviator. For $\alpha = 0$ the system of equations reduces to the standard formulation for which the solution does not converge unless the Brezzi–Babuska condition is fulfilled.

The pressure equations assume the form

$$(\mathbf{K}_{(\mathrm{p})} + \mathbf{L})\dot{\mathbf{q}} + \mathbf{M}\mathbf{p} = \mathbf{H} \tag{2.45}$$

[1]The term 'Q2/Q1 element' refers to the Lagrangian isoparametric quadrilateral element with biquadratic and bilinear shape functions for velocity and pressure interpolation, respectively, and with nine nodes for the velocity and four for the pressure.

where

$$
\begin{aligned}
\mathbf{L} &= [\mathbf{L}_1 \;\; \mathbf{L}_2] \\
\mathbf{L}_1 &= -\int_\Omega \frac{\alpha h^2 k_p}{2\mu} \left\{ \hat{\boldsymbol{\phi}}_{,1} \frac{\partial}{\partial x_1} \left[\mu (2\boldsymbol{\phi}^{\mathrm{T}}_{1,1} + \boldsymbol{\phi}^{\mathrm{T}}_{1,2}) \right] + \hat{\boldsymbol{\phi}}_{,2} \frac{\partial}{\partial x_2} (\mu \boldsymbol{\phi}^{\mathrm{T}}_{1,2}) \right\} \mathrm{d}\Omega \\
\mathbf{L}_2 &= -\int_\Omega \frac{\alpha h^2 k_p}{2\mu} \left\{ \hat{\boldsymbol{\phi}}_{,1} \frac{\partial}{\partial x_1} (\mu \boldsymbol{\phi}^{\mathrm{T}}_{2,1}) + \hat{\boldsymbol{\phi}}_{,2} \frac{\partial}{\partial x_2} \left[\mu (\boldsymbol{\phi}^{\mathrm{T}}_{2,1} + 2\boldsymbol{\phi}^{\mathrm{T}}_{2,2}) \right] \right\} \mathrm{d}\Omega \\
\mathbf{M} &= \int_\Omega \frac{\alpha h^2 k_p^2}{2\mu} \hat{\boldsymbol{\phi}}_{,i} \hat{\boldsymbol{\phi}}^{\mathrm{T}}_{,i} \, \mathrm{d}\Omega \\
\mathbf{H} &= \int_\Omega \frac{\alpha h^2 k_p^2}{2\mu} \hat{\boldsymbol{\phi}}_{,i} \, f_i \, \mathrm{d}\Omega
\end{aligned}
\tag{2.46}
$$

and k_p is a pressure scaling factor [6] assumed proportional to the largest value of the equivalent viscosity μ while $\boldsymbol{\phi}_{i\,1\times S} = \left[\phi_i^{(1)} \; \phi_i^{(2)} \ldots \; \phi_i^{(S)} \right]$, cf. Eq. (2.9). The element matrices will in general be unsymmetric except for linear interpolations, in which case the second derivatives of the shape functions vanish. The sub-matrix $\mathbf{M}$ connecting pressures at different points is the negative discrete Laplacian, which is responsible for the stabilizing effect. The formulation has been implemented for Q1/Q1 shape functions (hence $\hat{\boldsymbol{\phi}} = \boldsymbol{\phi}_i$) within the developed finite element code for metal forming analysis and is used for the present calculations [1].

2.2.5 Free surfaces

A particularly important feature of the formulation at hand is the capability to handle free surfaces. The final configuration is searched for as part of the solution. To every velocity correction as obtained in each iteration, a mesh rearrangement must follow to update the free surfaces, recovering thus the zero-normal velocity-condition for them (which in steady-state 2D means they are streamlines). Integration from a fixed point plus the fulfillment of an additional condition to fully determine component-wise each nodal correction, provides a method for free surface updating. The most straightforward way of performing the integration, cf. [116], is by updating one of the coordinate components while leaving the other unchanged for each point defining the free surface, starting from a known point (x_0, y_0)

$$
y(x) = y_0 + \int_{x_0}^{x} \frac{\mathrm{d}y}{\mathrm{d}\bar{x}} \, \mathrm{d}\bar{x} = y_0 + \int_{x_0}^{x} \frac{v_y(\bar{x})}{v_x(\bar{x})} \, \mathrm{d}\bar{x} \tag{2.47}
$$

where v_x and v_y are the velocity components in the global coordinates. According to Eq. (2.47), the nodal coordinates in one direction (i.e. x) are kept fixed and the free surface is followed by changing the coordinates in the other direction (i.e. y). This scheme is convenient for its simplicity provided the free surfaces are roughly parallel to the coordinate axes and it is known in advance that the variations from an initial, estimated configuration will not be very large. However, in cases where

the free surfaces are expected to have more significant variations or even change the orientation with respect to the global coordinate system, a more general algorithm is required. For such cases we impose the free surface condition in the form

$$\int_{\partial\Omega_F} ||v_n||\, \mathrm{d}(\partial\Omega_F) = 0 \tag{2.48}$$

where $\partial\Omega_F$ is the unknown free surface, and v_n is the velocity component normal to the surface.

By calculating this integral in the discretized model we find the configuration at the $(\omega+1)$th iteration on the basis of the velocities and configuration at the iteration ω. The fulfillment of Eq. (2.48) will require the rotation of each segment $(a, a+1)$, to ensure that the velocity is tangent to it, Fig. 2.2. The condition of constancy of length of each segment must be included because Eq. (2.48) leaves this magnitude undetermined.

Figure 2.2 Free surface updating by curvilinear integration

As the next step a node rearrangement within the whole domain is performed in order to reduce the mesh distortion. From Eq. (2.48) we get the corrections to the boundary nodal coordinates which define the free surface for the new solution. Taking these corrections, denoted by w_i for each coordinate direction $(i = 1, 2)$, as imposed values in separate auxiliary problems in which the boundaries not belonging to any free surface are assumed fixed, we solve for each w_i the Laplace (pure diffusion) equation

$$\nabla^2 w_i = 0 \tag{2.49}$$

to obtain the desired field of nodal boundary corrections. These two linear problems can also be solved by the finite element method, making use of the same discretization as for the main problem. It is assumed that each such free surface update is small enough to justify dealing with the particular components as separate and independent problems. In any case the present discussion aims only at obtaining a more regular mesh resulting from the free surface updating. Even if the updating values were significant the mesh obtained would still be acceptable.

2.2.6 Thermo-mechanical problems

The model as described so far assumes, for clarity, isothermal or non-temperature dependent conditions. This may be acceptable in a number of situations but, of course, accounting for the thermo-mechanical coupling is a crucial point in metal forming simulation. The big amounts of energy which are involved in these operations are mainly transformed into heat, with the subsequent temperature increase and the further variation of material properties affecting the mechanical problem. For this reason, both problems —mechanical and thermal— should be jointly solved.

The thermal convection-diffusion problem introduces to the overall metal forming simulation its own features. From the mathematical point of view, the convective term introduces a parabolic nature to the elliptic operator given by the diffusive term. It is well known that the "classical", Galerkin approximation used in the finite element method consisting in weighting functions equal to the approximating (shape) functions, is the optimal solution for elliptic problems. In other cases, the weighting functions must include a corrective term, whose interpretation is that of compensating the artificial numerical diffusivity introduced by straightforward use of Galerkin approximations. Indeed, equal shape and weighting functions result in an under-diffused solution even for small Peclet numbers (which is a measure of the relative importance of the diffusive and the convective effects, and is defined as $Pe = v\, d\, \rho c_p / k$, where v is the fluid velocity, ρ, c_p and k are its density, specific heat and diffusivity coefficients, respectively, and d is a characteristic size measure). Moreover, for higher values of Pe another, more dramatic effect appears: the numerical solution for temperature becomes unstable with alternative maximum and minimum peaks on the mesh.

This observations have given place to the so-called upwind techniques, in which the direction of the incoming flow is weighted preferentially. The different available upwind schemes give specific forms of the weighting functions and the actual values of their parameters in order to eliminate the numerical (artificial) diffusitivity.

They all start from the one-dimensional case at steady state and without source term, where the solution may be analytically predicted. From then, they follow different ways of generalizing these results to multidimensional cases and non-stationary solutions including source terms. It is not the aim of these considerations to discuss which one is better, but just to make use of an upwind scheme which would satisfactorily work for metal forming problems. In what follows the thermal problem is formulated together with its discretization, which includes the use of the upwind scheme. In particular, the so-called anisotropic balancing dissipation [69] has been chosen for its simplicity and effectiveness. It should be noticed that the convection-diffusion problem in metal forming processes is not especially demanding since flows of at most only moderate Peclet numbers develop. Therefore different schemes could be equally chosen. Instead, in other fields like fluid dynamics the proper choice of the upwind scheme becomes a

crucial point to obtain good results.

For our problem, we start writing the energy balance in steady-state

$$k\nabla^2\theta - \rho c_p \mathbf{v}\cdot\nabla\theta = h_v \tag{2.50}$$

where θ is the temperature, k the heat conductivity, ρc_p the heat capacity per unit volume, and h_v stands for the heat generation rate which can be presented as, cf. [6, 116]

$$h_v = \eta\dot{\varepsilon}_{ij}\sigma_{ij} \tag{2.51}$$

with η indicating the fraction of plastic deformation energy transformed into heat.

The weak form of Eq. (2.50) reads after discretization

$$\mathbf{K}_{(\mathrm{T})}\mathbf{T} = \mathbf{F}_{(\Omega)} + \mathbf{F}_{(\partial\Omega)} \tag{2.52}$$

The two terms on the right-hand side of Eq. (2.52) result respectively from (i) bulk heat generation and (ii) boundary imposed heat flow h_s and/or heat transfer induced by the temperature difference between the material and the environment, coolant or tool (this temperature will be called T_m below). $\mathbf{T}$ is the vector of nodal temperatures and the system matrix and force vectors read

$$\begin{aligned}
\mathbf{K}_{(\mathrm{T})} &= \int_\Omega \left\{ \rho c_p \mathbf{W}\mathbf{v}\cdot\nabla\tilde{\boldsymbol{\phi}}^{\mathrm{T}} + k\nabla\mathbf{W}\,\nabla\tilde{\boldsymbol{\phi}}^{\mathrm{T}} \right\} \mathrm{d}\Omega \\
&\quad + \int_{\partial\Omega_q} \bar{h}\mathbf{W}\tilde{\boldsymbol{\phi}}^{\mathrm{T}}\,\mathrm{d}(\partial\Omega) \\
\mathbf{F}_{(\Omega)} &= \int_\Omega \mathbf{W}h_v\,\mathrm{d}\Omega \\
\mathbf{F}_{(\partial\Omega)} &= \int_{\partial\Omega_q} \mathbf{W}\left(h_s + \bar{h}T_\mathrm{m}\right)\,\mathrm{d}(\partial\Omega)
\end{aligned} \tag{2.53}$$

The symbol $\bar{h}$ stands for the heat transfer coefficient of the interface. In Eqs. (2.53) the weighting functions $\mathbf{W}$ may be different from the shape functions for temperature $\tilde{\boldsymbol{\phi}}$, possibly different from $\boldsymbol{\phi}_i$, cf. Eq. (2.9), and/or $\hat{\boldsymbol{\phi}}$, cf. Eq. (2.12). While the Galerkin approximation ($\mathbf{W} = \tilde{\boldsymbol{\phi}}$) is the best choice for elliptic functionals, here an anisotropic weighting is required in which the flow direction is preferred. The specific character of these functions depends on the upwind scheme considered (cf. e.g. [41, 57, 69, 110]). This generally means that the weighting functions and their gradients have to be calculated separately from the shape functions and their gradients. Here, however, the adopted upwind scheme is the one proposed in [69], which allows for the use of weighting functions equal to the shape functions by adding the so-called anisotropic balancing dissipation. Thus the equilibrium problem is still solved with the Galerkin approximation.

To recall this upwind technique let us go back to the energy balance equation. A more general form of Eq. (2.50) accounting for the anisotropic conductivity reads

$$\nabla\cdot(\mathbf{k}\cdot\nabla\theta) - \rho c_p \mathbf{v}\cdot\nabla\theta = h_v \tag{2.54}$$

and yields to a weak form which, after discretization reads similarly to Eq. (2.52), with a system matrix of the form

$$K_{(T)\alpha\beta} = \int_\Omega \left(\rho c_p W_\alpha \tilde{\phi}^{(\beta)}_{,i} v_i + W_{\alpha,i} k_{ij} \tilde{\phi}^{(\beta)}_{,j} \right) \mathrm{d}\Omega + \int_{\partial\Omega_q} \bar{h} W_\alpha \tilde{\phi}^{(\beta)} \, \mathrm{d}(\partial\Omega) \quad (2.55)$$

It can be shown [24, 69] that centered numerical schemes add a negative diffusitivity, which in the one-dimensional case amounts

$$k' = \frac{1}{2} \alpha ||\mathbf{v}|| d \, \rho c_p \quad (2.56)$$

where $\alpha = \coth\frac{\gamma}{2} - \frac{2}{\gamma}$ is the upwind coefficient and $\gamma = ||\mathbf{v}|| d \, \rho c_p / k$ is the local Peclet number, with d standing for the element size. Therefore, an equivalent but positive amount of diffusivity should be added in order to balance the effect of the numerical scheme. When dealing with two- and three-dimensional problems, a (rather pragmatic) generalization of the one-dimensional case is carried out by applying the diffusivity compensation in the flow direction. Equivalent formulations arise by using weighting functions calculated on the basis of the flow direction and the Peclet number, cf. [41, 57, 110], on the one hand, or by adding the artificial diffusitivity in the flow direction via its tensorial form, Eq. (2.54) within a Galerkin approximation.

The so-called anisotropic balancing dissipation tensor reads, for the two-dimensional case

$$\mathbf{k}' = \boldsymbol{\Theta}^{\mathrm{T}} \mathbf{k}'_o \boldsymbol{\Theta} \qquad \mathbf{k}'_o = \begin{bmatrix} k' & 0 \\ 0 & 0 \end{bmatrix} \quad (2.57)$$

where $\boldsymbol{\Theta}$ is the rotation matrix to transform the balancing tensor from the local to global basis, with the local basis defined by the flow direction and its in-plane normal. Taking the preceding facts into account, we see clearly that it is equivalent to discretize Eq. (2.54), or a "corrected" equation resulting from substituting in Eq. (2.54) $\mathbf{k}$ by $\mathbf{k} + \mathbf{k}'$ using a Galerkin approximation. Then the system matrix and the load vectors now, thus, read (cf. Eqs. (2.53) and (2.55))

$$\begin{aligned} K_{(T)\alpha\beta} &= \int_\Omega \left(\rho c_p \tilde{\phi}^\alpha \tilde{\phi}^\beta_{,i} v_i + \tilde{\phi}^\alpha_{,i} (k_{ij} + k'_{ij}) \tilde{\phi}^\beta_{,j} \right) \mathrm{d}\Omega \\ &\quad + \int_{\partial\Omega_q} \bar{h} \tilde{\phi}^\alpha \tilde{\phi}^\beta \, \mathrm{d}(\partial\Omega) \\ F_{(\Omega)\alpha} &= \int_\Omega \tilde{\phi}^\alpha h_v \, \mathrm{d}\Omega \\ F_{(\partial\Omega)\alpha} &= \int_{\partial\Omega_q} \tilde{\phi}^\alpha (h_s + \bar{h} T_\mathrm{m}) \, \mathrm{d}(\partial\Omega) \end{aligned} \quad (2.58)$$

Now we return to the coupled thermo-mechanical problem. Once we have formulated and discretized both problems, we consider their simultaneous solution. Assembling the equations system (2.26),(2.52) we arrive at the coupled form

$$\begin{bmatrix} \mathbf{K}_{(\mu)} & \mathbf{K}^{\mathrm{T}}_{(p)} & \mathbf{0} \\ \mathbf{K}_{(p)} & \mathbf{0} & \mathbf{0} \\ \mathbf{0} & \mathbf{0} & \mathbf{K}_{(T)} \end{bmatrix} \begin{bmatrix} \dot{\mathbf{q}} \\ \bar{\mathbf{p}} \\ \mathbf{T} \end{bmatrix} = \begin{bmatrix} \mathbf{Q} \\ \mathbf{0} \\ \mathbf{F}_{(\Omega)} + \mathbf{F}_{(\partial\Omega)} \end{bmatrix} \quad (2.59)$$

or, more compactly and in residual form

$$\tilde{\mathbf{R}} = \tilde{\mathbf{K}}^{(S)}\tilde{\mathbf{q}} - \tilde{\mathbf{Q}} = 0 \tag{2.60}$$

from which we follow a similar solution procedure as the one used for Eq. (2.27). The tangent stiffness matrix

$$\frac{\partial \tilde{R}_\alpha^{(\omega)}}{\partial \tilde{q}_\beta} = \tilde{K}_{\alpha\beta}^{(S)} + \frac{\partial \tilde{K}_{\alpha\gamma}^{(S)}}{\partial \tilde{q}_\beta}\tilde{q}_\gamma - \frac{\partial \tilde{Q}_\alpha}{\partial \tilde{q}_\beta} = \tilde{K}_{\alpha\beta}^{(T)} \tag{2.61}$$

will be (at the element level) a full matrix instead of block diagonal —as the secant stiffness matrix is— due to the thermo-mechanical coupling.

Splitting the residual vector similarly as we did with the vector of unknowns,

$$\tilde{\mathbf{R}} = \begin{bmatrix} \mathbf{R}_{\dot{q}} \\ \mathbf{R}_{\bar{p}} \\ \mathbf{R}_T \end{bmatrix} \tag{2.62}$$

we obtain the following sub-matrices of the tangent stiffness matrix

$$\begin{aligned}
\frac{\partial R_{\dot{q}\alpha}}{\partial \dot{q}_\beta} &= K_{(\mu)\alpha\beta} + \frac{\partial K_{(\mu)\alpha\gamma}}{\partial \mu}\dot{q}_\gamma \frac{\partial \mu}{\partial \dot{\bar{\varepsilon}}}\frac{\partial \dot{\bar{\varepsilon}}}{\partial \dot{q}_\beta} \\
\frac{\partial R_{\dot{q}\alpha}}{\partial \bar{p}_\beta} &= K^{\mathrm{T}}_{(\mathrm{p})\alpha\beta} \\
\frac{\partial R_{\dot{q}\alpha}}{\partial T_\beta} &= \frac{\partial K_{(\mu)\alpha\gamma}}{\partial \mu}\dot{q}_\gamma \frac{\partial \mu}{\partial T_\beta} \\
\frac{\partial R_{\bar{p}\alpha}}{\partial \dot{q}_\beta} &= K_{(\mathrm{p})\alpha\beta} \\
\frac{\partial R_{T\alpha}}{\partial \dot{q}_\beta} &= \frac{\partial K_{(T)\alpha\gamma}}{\partial \dot{q}_\beta}T_\gamma - \frac{\partial F_{(\Omega)\alpha}}{\partial \dot{q}_\beta} \\
\frac{\partial R_{T\alpha}}{\partial T_\beta} &= K_{(T)\alpha\beta} - \frac{\partial F_{(\Omega)\alpha}}{\partial \mu}\frac{\partial \mu}{\partial T_\beta} \\
\frac{\partial R_{\bar{p}\alpha}}{\partial \bar{p}_\beta} &= 0 \qquad \frac{\partial R_{\bar{p}\alpha}}{\partial T_\beta} = 0 \qquad \frac{\partial R_{T\alpha}}{\partial \bar{p}_\beta} = 0
\end{aligned} \tag{2.63}$$

In the above equations the material parameters used to calculate the equivalent viscosity μ may be a function of the temperature. For example if we have

$$\sigma_0 = \sigma_0(T), \qquad n = n(T) \tag{2.64}$$

it will be

$$\frac{\partial \mu}{\partial T_\beta} = \tilde{\phi}_\beta\left(\frac{\partial \mu}{\partial \sigma_0}\frac{\partial \sigma_0}{\partial T} + \frac{\partial \mu}{\partial n}\frac{\partial n}{\partial T}\right) \tag{2.65}$$

In addition, the heat generated by plastic deformation is both temperature and velocity (or rather its gradient) dependent, from which the corresponding terms of the coupling arise. Finally, the velocity also acts on the temperature field

by the derivative of the convective term and —through the added balancing dissipation— of the Peclet number.

Although the exact tangent matrix may not be necessary for the solution of the equilibrium problem, it turns out to be necessary to calculate it for the sensitivity stage.

2.3 Material parameter sensitivity

2.3.1 Formulation

In this section we shall derive equations for the sensitivity analysis of metal forming processes with respect to parameters defining the process through the constitutive equation (2.2) and other parameters such as the friction coefficient or an imposed velocity. The information resulting from this analysis can be very useful for deciding how to modify an already existing technology in order to improve its performance according to a given set of criteria. For example, we may want to know to what extent an increase in the ram velocity in an extrusion matrix will affect the dissipation energy rate of plastic deformation.

In order to simplify the presentation we will come back to the purely mechanical problem, leaving to Section 2.3.3 the sensitivity formulation of the thermally coupled problem as given in Section 2.2.6.

2.3.1.1 Direct differentiation method

Let us consider the general form of the sensitivity function as

$$\mathcal{G}(h) = G(\boldsymbol{\sigma}^{\mathrm{D}}(h), \bar{\mathbf{q}}(h); h) \tag{2.66}$$

We wish to calculate the sensitivity of G with respect to a material parameter h entering the theory, i.e. n, γ or σ_0, cf. Eq. (2.3). By following the direct differentiation approach (DDM) we calculate the design gradient

$$\frac{\mathrm{d}G}{\mathrm{d}h} = \frac{\partial G}{\partial h} + \frac{\partial G}{\partial \boldsymbol{\sigma}^{\mathrm{D}}}\frac{\mathrm{d}\boldsymbol{\sigma}^{\mathrm{D}}}{\mathrm{d}h} + \frac{\partial G}{\partial \bar{\mathbf{q}}}\frac{\mathrm{d}\bar{\mathbf{q}}}{\mathrm{d}h} \tag{2.67}$$

in which, given the solution to the equilibrium problem, $\partial G/\partial h$, $\partial G/\partial \bar{\mathbf{q}}$ and $\partial G/\partial \boldsymbol{\sigma}^{\mathrm{D}}$ are known (or can be routinely obtained) while $\mathrm{d}\boldsymbol{\sigma}^{\mathrm{D}}/\mathrm{d}h$ can be written as

$$\frac{\mathrm{d}\boldsymbol{\sigma}^{\mathrm{D}}}{\mathrm{d}h} = \frac{\mathrm{d}\boldsymbol{\sigma}^{\mathrm{D}}}{\mathrm{d}\bar{\mathbf{q}}}\frac{\mathrm{d}\bar{\mathbf{q}}}{\mathrm{d}h} \tag{2.68}$$

where

$$\frac{\mathrm{d}\boldsymbol{\sigma}^{\mathrm{D}}}{\mathrm{d}\bar{\mathbf{q}}} = \left[\frac{\mathrm{d}\boldsymbol{\sigma}^{\mathrm{D}}}{\mathrm{d}\dot{\mathbf{q}}} \quad \frac{\mathrm{d}\boldsymbol{\sigma}^{\mathrm{D}}}{\mathrm{d}\bar{\mathbf{p}}}\right]$$

According to Eqs. (2.18), (2.20) and (2.2)

$$\begin{aligned}\left[\frac{\mathrm{d}\boldsymbol{\sigma}^{\mathrm{D}}}{\mathrm{d}\dot{\mathbf{q}}}\right]_{6\times N} &= 2\left(\mathbf{B}\mu + \mathbf{B}\dot{\mathbf{q}}\frac{\partial\mu}{\partial\dot{\mathbf{q}}}\right)\\ \left[\frac{\mathrm{d}\boldsymbol{\sigma}^{\mathrm{D}}}{\mathrm{d}\bar{\mathbf{p}}}\right]_{6\times S} &= \mathbf{0}\end{aligned} \tag{2.69}$$

By substituting Eq. (2.68) into Eq. (2.67) we arrive at

$$\frac{\mathrm{d}G}{\mathrm{d}h} = \frac{\partial G}{\partial h} + \left(\frac{\partial G}{\partial\boldsymbol{\sigma}^{\mathrm{D}}}\frac{\mathrm{d}\boldsymbol{\sigma}^{\mathrm{D}}}{\mathrm{d}\bar{\mathbf{q}}} + \frac{\partial G}{\partial\bar{\mathbf{q}}}\right)\frac{\mathrm{d}\bar{\mathbf{q}}}{\mathrm{d}h} \tag{2.70}$$

It is seen that in order to effectively compute $\mathrm{d}G/\mathrm{d}h$ only $\mathrm{d}\mathbf{q}/\mathrm{d}h$ has to be obtained from additional calculations. By differentiating the equilibrium equation (2.27) with respect to h we have

$$\frac{\mathrm{d}}{\mathrm{d}h}\left(\mathbf{K}^{(S)}\bar{\mathbf{q}} - \bar{\mathbf{Q}}\right) = \frac{\mathrm{d}\mathbf{K}^{(S)}}{\mathrm{d}h}\bar{\mathbf{q}} + \mathbf{K}^{(S)}\frac{\mathrm{d}\bar{\mathbf{q}}}{\mathrm{d}h} - \frac{\mathrm{d}\bar{\mathbf{Q}}}{\mathrm{d}h} = \mathbf{0} \tag{2.71}$$

where

$$\frac{\mathrm{d}\mathbf{K}^{(S)}}{\mathrm{d}h} = \int_\Omega \frac{\partial\mu}{\partial h}\bar{\mathbf{k}}_0\,\mathrm{d}\Omega + \int_\Omega \frac{\partial\mu}{\partial\bar{\mathbf{q}}}\frac{\mathrm{d}\bar{\mathbf{q}}}{\mathrm{d}h}\bar{\mathbf{k}}_0\,\mathrm{d}\Omega \tag{2.72}$$

By combining Eqs. (2.71) and (2.72) we arrive at

$$\left(\mathbf{K}^{(S)} + \int_\Omega \bar{\mathbf{k}}_0\bar{\mathbf{q}}\frac{\partial\mu}{\partial\bar{\mathbf{q}}}\,\mathrm{d}\Omega - \frac{\partial\bar{\mathbf{Q}}}{\partial\bar{\mathbf{q}}}\right)\frac{\mathrm{d}\bar{\mathbf{q}}}{\mathrm{d}h} = -\left(\int_\Omega \frac{\partial\mu}{\partial h}\bar{\mathbf{k}}_0\,\mathrm{d}\Omega\right)\bar{\mathbf{q}} + \frac{\partial\bar{\mathbf{Q}}}{\partial h} \tag{2.73}$$

i.e. at, cf. Eq. (2.33)

$$\mathbf{K}^{(T)}\frac{\mathrm{d}\bar{\mathbf{q}}}{\mathrm{d}h} = -\left(\int_\Omega \frac{\partial\mu}{\partial h}\bar{\mathbf{k}}_0\,\mathrm{d}\Omega\right)\bar{\mathbf{q}} + \frac{\partial\bar{\mathbf{Q}}}{\partial h} \tag{2.74}$$

This equation can be used to find the nodal velocity and pressure design gradients $\mathrm{d}\bar{\mathbf{q}}/\mathrm{d}h$ provided the vector $\bar{\mathbf{q}}$ has been solved for from the equilibrium problem and substituted in the right-hand side of Eq. (2.74).

2.3.1.2 Adjoint system method

We can equivalently solve the sensitivity problem by the adjoint system method (ASM), for which we construct an extended function $G^* = G^*(\boldsymbol{\sigma}^{\mathrm{D}}(h), \bar{\mathbf{q}}(h); \boldsymbol{\lambda}(h); h)$ as

$$G^* = G + \boldsymbol{\lambda}^{\mathrm{T}}\mathbf{R} \tag{2.75}$$

in which the state equation $\mathbf{R} = \mathbf{0}$ is the same as before, cf. Eq. (2.27), and $\boldsymbol{\lambda}(h)$ is a $(N+S)$-dimensional kinematically admissible adjoint vector (cf. Eq. (2.7)), such that G^* is stationary with respect to $\bar{\mathbf{q}}$, i.e.

$$\frac{\mathrm{d}G^*}{\mathrm{d}\bar{\mathbf{q}}} = \mathbf{0} \tag{2.76}$$

We have

$$\frac{\mathrm{d}G^*}{\mathrm{d}h} = \frac{\mathrm{d}G}{\mathrm{d}h} + \frac{\mathrm{d}\boldsymbol{\lambda}^{\mathrm{T}}}{\mathrm{d}h}\mathbf{R} + \boldsymbol{\lambda}^{\mathrm{T}}\frac{\mathrm{d}\mathbf{R}}{\mathrm{d}h} \tag{2.77}$$

which simplifies to

$$\frac{\mathrm{d}G^*}{\mathrm{d}h} = \frac{\mathrm{d}G}{\mathrm{d}h} \tag{2.78}$$

because the state equation holds true for both the nominal and perturbed values of h. Furthermore, by noting that[1]

$$\frac{\mathrm{d}(\cdot)}{\mathrm{d}\bar{\mathbf{q}}} = \frac{\partial(\cdot)}{\partial\boldsymbol{\sigma}^{\mathrm{D}}}\frac{\mathrm{d}\boldsymbol{\sigma}^{\mathrm{D}}}{\mathrm{d}\bar{\mathbf{q}}} + \frac{\partial(\cdot)}{\partial\bar{\mathbf{q}}} \tag{2.79}$$

with $\mathrm{d}\boldsymbol{\sigma}^{\mathrm{D}}/\mathrm{d}\bar{\mathbf{q}}$ given by Eq. (2.69), we have

$$\frac{\mathrm{d}G^*}{\mathrm{d}h} = \frac{\partial G^*}{\partial h} + \frac{\mathrm{d}G^*}{\mathrm{d}\bar{\mathbf{q}}}\frac{\mathrm{d}\bar{\mathbf{q}}}{\mathrm{d}h} \tag{2.80}$$

which by Eqs. (2.76) and (2.78) becomes

$$\frac{\mathrm{d}G}{\mathrm{d}h} = \frac{\partial G^*}{\partial h} \tag{2.81}$$

and can be directly used for the computation of the sensitivity $\mathrm{d}G/\mathrm{d}h$ required. The vector $\boldsymbol{\lambda}$ is computed in a non-iterative way from Eq. (2.76) written as

$$\frac{\mathrm{d}G^*}{\mathrm{d}\bar{\mathbf{q}}} = \frac{\mathrm{d}G}{\mathrm{d}\bar{\mathbf{q}}} + \boldsymbol{\lambda}^{\mathrm{T}}\left(\frac{\partial\mathbf{K}^{(S)}}{\partial\bar{\mathbf{q}}}\bar{\mathbf{q}} + \mathbf{K}^{(S)}\right) = \frac{\mathrm{d}G}{\mathrm{d}\bar{\mathbf{q}}} + \boldsymbol{\lambda}^{\mathrm{T}}\mathbf{K}^{(T)} = \mathbf{0} \tag{2.82}$$

i.e. as

$$\overset{\mathrm{T}}{\mathbf{K}}{}^{(T)}\boldsymbol{\lambda} = -\left(\frac{\mathrm{d}G}{\mathrm{d}\bar{\mathbf{q}}}\right)^{\mathrm{T}} \tag{2.83}$$

We observe that the system matrix in Eq. (2.83) is the transpose of the tangent stiffness matrix of the equilibrium problem. Usually the ASM makes use of symmetry of this matrix to directly solve the sensitivity problem after finding the solution to the equilibrium problem without further manipulations. However, in this case we see from Eqs. (2.45), (2.46) and (2.33) that the tangent stiffness matrix $\mathbf{K}^{(T)}$ is unsymmetric. Therefore, it is the transpose of the inverted system matrix that must be used to obtain the vector $\boldsymbol{\lambda}$.

[1] This notation becomes slightly awkward when $(\cdot)$ stands for a function of $\boldsymbol{\sigma}^{\mathrm{D}}$, $\bar{\mathbf{q}}$ and any additional variable, say h. In such a case the left-hand side of Eq. (2.79) should, in accordance with standard mathematical notation, read $\partial(\cdot)/\partial\bar{\mathbf{q}}$, which would be confusing in the present context, though.

2.3.1.3 Iterative form of sensitivity expressions

Experience with solving the metal forming problems described by Eq. (2.27) and reported in [1, 6, 67], for instance, shows that the Newton–Raphson scheme, Eq. (2.30), is applicable (i.e. it converges) only for markedly rate-dependent materials, like steel in hot working conditions. This roughly corresponds to the exponent values $n < 2$ in the model (2.3), cf. [67]. Thus, for a material behaviour closer to perfect plasticity direct iterations involving the secant matrix $\mathbf{K}^{(S)}$, cf. Eq. (2.28), i.e. based on

$$\mathbf{K}^{(S)}(\bar{\mathbf{q}}^{(\omega)})\,\bar{\mathbf{q}}^{(\omega+1)} = \bar{\mathbf{Q}} \tag{2.84}$$

must be performed instead. This iterative scheme is always convergent, although only linearly. Procedures for accelerating convergence were analyzed in [6].

In each specific problem the crucial question thus is: Which of the matrices ($\mathbf{K}^{(T)}$ versus $\mathbf{K}^{(S)}$) should be used for calculating the sensitivity? In the latter case an iterative version of the DDM results in the form (cf. Eq. (2.74))

$$\mathbf{K}^{(S)}\left(\frac{\mathrm{d}\bar{\mathbf{q}}}{\mathrm{d}h}\right)^{(\omega+1)} = -\left(\int_\Omega \frac{\partial \mu}{\partial h}\bar{\mathbf{k}}_0\,\mathrm{d}\Omega\right)\bar{\mathbf{q}} - \left[\int_\Omega \left(\bar{\mathbf{k}}_0\bar{\mathbf{q}}\right)\frac{\mathrm{d}\mu}{\mathrm{d}\bar{\mathbf{q}}}\,\mathrm{d}\Omega\right]\left(\frac{\mathrm{d}\bar{\mathbf{q}}}{\mathrm{d}h}\right)^{(\omega)} \tag{2.85}$$

Similarly, for the ASM the iterative form equivalent to Eq. (2.83) results as

$$\overset{\mathrm{T}}{\mathbf{K}}{}^{(S)}\boldsymbol{\lambda}^{(\omega)} = -\left(\frac{\mathrm{d}G}{\mathrm{d}\bar{\mathbf{q}}}\right)^{\mathrm{T}} - \left(\frac{\partial \mathbf{K}^{(S)}}{\partial \bar{\mathbf{q}}}\bar{\mathbf{q}}\right)^{\mathrm{T}}\boldsymbol{\lambda}^{(\omega)} \tag{2.86}$$

To compare both versions of the solution algorithm (tangent versus secant stiffness) for sensitivity analysis we have to keep in mind that frequently, as has been stated above, the equilibrium problem is solved by using the secant stiffness matrix so that its inverse is available at the end of that stage. If the equilibrium problem could be solved by using the tangent stiffness matrix, then the decision that this matrix should also be used for sensitivity is straightforward. Unfortunately, the Newton–Raphson method (which involves the use of the tangent stiffness matrix) is virtually always divergent in situations of most practical importance regarding sensitivity analysis, namely when no non-zero velocities are prescribed. Therefore, it is important from a practical point of view to critically assess both versions of the solution algorithm.

The tangent stiffness option with a well-conditioned matrix yields the sensitivity solution in one step. On the other hand, whenever the equilibrium problem cannot be solved by the use of the tangent stiffness matrix, a solution to the new set of equations is required. In contrast, the secant stiffness option requires iterations but no new solution of the equations system. Moreover, when the material behaviour is close to ideal plasticity, the numerical inverse of the matrix $\mathbf{K}^{(T)}$ does not yield the solution in one step: it may then be necessary to iterate even with the tangent stiffness matrix just to improve the numerically unreliable one-pass solution. And it sometimes happens that this iterative procedure is divergent

so that the solution using the secant stiffness matrix as given by Eqs. (2.85) and (2.86) is anyhow compulsory. The question of superiority of one approach over the other is thus strongly dependent on the material behaviour, the way the loads are applied and the boundary conditions. This is further illustrated in Section 2.3.5. In particular, for a perfectly plastic material the tangent matrix is singular and the solution becomes infinitely sensitive to changes in the physical properties if only the loads are held constant.

2.3.1.4 Equivalence between DDM and ASM

As we already know, both the sensitivity methodologies, i.e. the DDM and the ASM, are theoretically equivalent (although it is by no means so in terms of the computational time required by each of them). In the present context their equivalence may be most easily shown by considering the case of $G = q_{\hat{\alpha}}$ ($\hat{\alpha}$ being a specified component number), i.e. when the sensitivity function coincides with a given nodal velocity. By Eqs. (2.67) and (2.74) we have for the DDM

$$\frac{\mathrm{d}q_{\hat{\alpha}}}{\mathrm{d}h} = \mathbf{i}_{(\hat{\alpha})}\frac{\mathrm{d}\bar{\mathbf{q}}}{\mathrm{d}h} = -\mathbf{i}_{(\hat{\alpha})}\bar{\mathbf{K}}^{-1(T)}\left(\int_{\Omega}\frac{\partial\mu}{\partial h}\bar{\mathbf{k}}_0\,\mathrm{d}\Omega\right)\bar{\mathbf{q}} \tag{2.87}$$

where the βth component of the vector $\mathbf{i}_{(\hat{\alpha})}$ is defined as $i^{\beta}_{(\hat{\alpha})}=\delta^{\beta}_{\hat{\alpha}}$, $\beta=1,2,\ldots,N+S$. For the ASM, Eqs. (2.81) and (2.83) assume the form

$$\frac{\mathrm{d}q_{\hat{\alpha}}}{\mathrm{d}h} = \boldsymbol{\lambda}^{\mathrm{T}}_{(\hat{\alpha})}\frac{\partial\mathbf{R}}{\partial h} = \boldsymbol{\lambda}^{\mathrm{T}}_{(\hat{\alpha})}\left(\int_{\Omega}\frac{\partial\mu}{\partial h}\bar{\mathbf{k}}_0\,\mathrm{d}\Omega\right)\bar{\mathbf{q}} \tag{2.88}$$

and

$$\bar{\mathbf{K}}^{\mathrm{T}(T)}\boldsymbol{\lambda}_{(\hat{\alpha})} = -\mathbf{i}_{(\hat{\alpha})} \tag{2.89}$$

where $\boldsymbol{\lambda}_{(\hat{\alpha})}$ is the adjoint vector corresponding to $G = q_{\hat{\alpha}}$. By substituting $\boldsymbol{\lambda}_{(\hat{\alpha})}$ from Eq. (2.89) into (2.88) we obtain Eq. (2.87). Moreover, taking the set of sensitivity functionals as $\mathbf{G} = \{G_{\hat{\alpha}}\} = \{q_{\hat{\alpha}}\} = \bar{\mathbf{q}}$, Eq. (2.83) takes the form

$$\bar{\mathbf{K}}^{\mathrm{T}(T)}\boldsymbol{\Lambda} = -\mathbf{I} \tag{2.90}$$

where the $\hat{\alpha}$th column of the matrix $\boldsymbol{\Lambda}$ is the adjoint vector $\boldsymbol{\lambda}_{(\hat{\alpha})}$ corresponding to the constraint $G = q_{\hat{\alpha}}$. From Eq. (2.81) we substitute $\boldsymbol{\Lambda}^{\mathrm{T}}$ in the expression for the sensitivities obtained by replacing in Eq. (2.81) G by $\bar{\mathbf{q}}$, $\boldsymbol{\lambda}$ by $\boldsymbol{\Lambda}$ and G^* as given by Eq. (2.75), to get

$$\frac{\mathrm{d}\bar{\mathbf{q}}}{\mathrm{d}h} = \boldsymbol{\Lambda}^{\mathrm{T}}\frac{\partial\mathbf{R}}{\partial h} = -\bar{\mathbf{K}}^{-1(T)}\int_{\Omega}\left(\frac{\partial\mu}{\partial h}\bar{\mathbf{k}}_0\right)\bar{\mathbf{q}}\,\mathrm{d}\Omega \tag{2.91}$$

which is equivalent to Eq. (2.74).

2.3.1.5 Sensitivity expressions for chosen design variables

The forming processes are usually conceived of as controlled (typically holding constant) by either the imposed velocity or the applied force. In the numerical model, as a result of the elimination during the solution procedure of rows and columns corresponding to the fixed degrees of freedom, the former case is equivalent to the application of external forces which are proportional to the viscosity. Through this dependence the applied forces are then also functions of the design parameters. It turns out from the sensitivity analysis of problems with constant imposed velocities that the velocity field exhibits very low sensitivity to material parameters whereas the pressure is sensitive to them. On the other hand, when fixed loads are imposed it is the velocity field that exhibits a strong dependence on the design parameters while the pressure is almost constant. For this reason, the latter case seems to be more interesting and is thus discussed in the applications below.

To calculate the sensitivity of the solution to the material parameters entering the viscoplastic law we have to find, by Eq. (2.74), the partial derivative of the viscosity with respect to a given parameter. Equation (2.3) suggests the static yield stress σ_0, the fluidity γ and the exponent n of the viscoplastic law as possible parameters with respect to which we can analyze the sensitivity of the solution. We have for each of them

$$\begin{aligned}
\frac{\partial \mu}{\partial \sigma_0} &= \frac{1}{3\dot{\bar{\varepsilon}}} \\
\frac{\partial \mu}{\partial \gamma} &= -\frac{1}{3\dot{\bar{\varepsilon}}\gamma n}\left(\frac{\dot{\bar{\varepsilon}}}{\gamma}\right)^{\frac{1}{n}} \\
\frac{\partial \mu}{\partial n} &= -\frac{1}{3\dot{\bar{\varepsilon}}n^2}\left(\frac{\dot{\bar{\varepsilon}}}{\gamma}\right)^{\frac{1}{n}} \ln\left(\frac{\dot{\bar{\varepsilon}}}{\gamma}\right)
\end{aligned} \tag{2.92}$$

By appropriately differentiating Eq. (2.36) we can find sensitivity to the friction coefficient. This derivative will be non-zero only for some of the friction elements (those which are referred to in Eq. $(2.37)_2$). It has the form

$$\frac{\partial \mu}{\partial \nu} = \frac{p}{3\dot{\bar{\varepsilon}}} \tag{2.93}$$

In the case of friction modelled by the contact–friction elements, sensitivity to the friction coefficient is calculated by simply differentiating the friction force, cf. Eq. (2.43), with respect to ν to obtain

$$\frac{\partial \mathbf{f}_i}{\partial \nu} = \begin{cases} \mathbf{0} & \text{for} \quad \hat{f}_i > ||\mathbf{f}_i^s|| \\ \dfrac{\mathbf{v}}{||\mathbf{v}||}\hat{f}_i & \text{for} \quad 0 < \hat{f}_i < ||\mathbf{f}_i^s|| \\ \mathbf{0} & \text{for} \quad \hat{f}_i < 0 \end{cases} \tag{2.94}$$

It is worth pointing out that in the sticking case these derivatives are zero, i.e. the solution is not sensitive to variations of the friction coefficient at all.

The next issue of potentially great practical significance is an attempt to find solution sensitivity with respect to imposed velocities. The velocity-type parameters may be singled out, for instance, in the form of the ram or forging hammer velocity, or the tangential velocity of the roll for extrusion, forging and rolling operations, respectively. In such a case only the loads depend on the design parameter through the viscosity. Thus, if the tool action is modelled by prescribing for all workpiece degrees of freedom whose numbers belong to a subset $A = \{\hat{1}, \hat{2}, \ldots, \hat{\alpha}, \ldots, N_A\} \in \{1, 2, \ldots, N\}$ a velocity value proportional to the tool velocity v_0

$$q_{\hat{\alpha}} = a_{\hat{\alpha}} v_0 , \quad \hat{\alpha} \in A \tag{2.95}$$

then a vector $\boldsymbol{\gamma} = \{\gamma_{\hat{\alpha}}\}, \hat{\alpha} = 1, 2, \ldots, N_A$, is defined such that

$$\gamma_{\hat{\alpha}} = \begin{cases} \dfrac{q_{\hat{\alpha}}}{v_0} & \text{if} \quad \hat{\alpha} \in A \\ 0 & \text{otherwise} \end{cases} \tag{2.96}$$

We have $\gamma_{\hat{\alpha}} = 0$ if either no value is imposed at the $\hat{\alpha}$th degree of freedom or this unknown is set to zero or a velocity is imposed independently of v_0. In such a case, by recalling the sensitivity functional Eq. (2.66) we have

$$\frac{\mathrm{d}G}{\mathrm{d}v_0} = \frac{\mathrm{d}G}{\mathrm{d}q_{\hat{\alpha}}} \gamma_{\hat{\alpha}} = \frac{\mathrm{d}G}{\mathrm{d}\bar{\mathbf{q}}} \boldsymbol{\gamma} \tag{2.97}$$

where $\mathrm{d}G/\mathrm{d}q_{\hat{\alpha}}$ is the sensitivity of G with respect to the velocity $q_{\hat{\alpha}}$ (i.e. $q_{\hat{\alpha}}$ is taken as the design parameter).

2.3.2 Material model at low effective strain rates

A critical look at the use of the tangent stiffness matrix as the system matrix for the sensitivity problem demonstrates a possible lack of accuracy of the standard flow approach implementation. To briefly discuss it let us return for a moment to the material model. It is widely known that the flow approach leads to numerical problems when the velocity field tends to be uniform, making the effective strain rate $\dot{\bar{\varepsilon}}$ approach zero and the viscosity μ approach infinity, cf. Eq. (2.3). The traditional way out of this difficulty (cf. [111]) is to define a cutoff value $\dot{\bar{\varepsilon}}_{\mathrm{lim}}$ for the effective strain rate so that $\mu = \mu_{\mathrm{lim}}$ for every $\dot{\bar{\varepsilon}} < \dot{\bar{\varepsilon}}_{\mathrm{lim}}$. In addition, by the so-called *pressure scaling* [6, 7] a uniform order of magnitude can be obtained for the stiffness matrix entries thus allowing a very small value for the effective strain rate limit. Nevertheless, in some parts of the domain an 'approximate' value of the viscosity will always be obtained. For a mechanical solution this is quite acceptable since the strain rate–viscosity curve is continuous. However, if we consider the tangent stiffness matrix (which is also the system matrix for the sensitivity problem as demonstrated in Eqs. (2.74) and (2.83)), we notice that the elements of the partial derivative $\partial \mathbf{K}^{(S)}/\partial \mathbf{q}$ are proportional to $\dot{\bar{\varepsilon}}^{-3}$ in the viscoplastic range but are null in the 'rigid flow' limit when a constant cutoff

value is adopted, cf. $(2.34)_1$, for $\dot{\bar{\varepsilon}} < \dot{\bar{\varepsilon}}_{\text{lim}}$. This means that if the cutoff value for the effective strain rate is, say, 10^{-6}, then there is a discontinuity of the order 10^{18} in the effective strain rate limit. The jump clearly affects both the convergence of the Newton–Raphson scheme and, as it came out in some of our tests, coincidence of sensitivities calculated by one of the analytical methods and by finite differences. However, the difficulty can be overcome in a simple way by replacing $\mu = \mu_{\text{lim}}$ in the interval $0 \leq \dot{\bar{\varepsilon}} \leq \dot{\bar{\varepsilon}}_{\text{lim}}$ by

$$\mu = \left.\frac{\mathrm{d}\mu}{\mathrm{d}\dot{\bar{\varepsilon}}}\right|_{\dot{\bar{\varepsilon}}=\dot{\bar{\varepsilon}}_{\text{lim}}} (\dot{\bar{\varepsilon}} - \dot{\bar{\varepsilon}}_{\text{lim}}) - \mu_{\text{lim}} \tag{2.98}$$

i.e. by requiring the derivative of the equivalent viscosity in the effective strain rate interval considered be equal to the derivative at the strain rate limit.

2.3.3 Sensitivity analysis for the thermo-mechanical problem

We can now recall the model accounting for the thermo-mechanical coupling as presented in Section 2.2.6 and derive the corresponding sensitivity expressions, following the patterns of the preceding section. Now we have one more independent variable, the temperature, and a few additional material parameters, which may be chosen as our design variables. Besides, the upwind scheme has introduced some numerical parameters, and we may be interested on the effect the assumption of particular values for them has on the results.

If now the response functional is written as

$$\mathcal{G}(h) = G(\boldsymbol{\sigma}^{\mathrm{D}}(h), \tilde{\mathbf{q}}(h); h) \tag{2.99}$$

where $\tilde{\mathbf{q}}$ is the vector of discretized variables, i.e. $\bar{\mathbf{q}}$ enlarged by the nodal temperatures $\mathbf{T}$, and h is any of the design parameters entering the equations: material properties, numerical parameters, etc., then the sensitivity problem consists now in finding the gradient

$$\frac{\mathrm{d}G}{\mathrm{d}h} = \frac{\partial G}{\partial h} + \frac{\partial G}{\partial \boldsymbol{\sigma}^{\mathrm{D}}}\frac{\mathrm{d}\boldsymbol{\sigma}^{\mathrm{D}}}{\mathrm{d}h} + \frac{\partial G}{\partial \tilde{\mathbf{q}}}\frac{\mathrm{d}\tilde{\mathbf{q}}}{\mathrm{d}h} \tag{2.100}$$

By applying similar considerations as in the non-temperature-dependent case, we conclude that, to calculate the above quantity using DDM, it is only necessary to obtain the derivatives of the discretized variables (i.e. sensitivities) $\mathrm{d}\tilde{\mathbf{q}}/\mathrm{d}h$. By differentiating Eq. (2.60) with respect to the design variable h we have

$$\frac{\mathrm{d}}{\mathrm{d}h}(\tilde{\mathbf{K}}^{(s)}\tilde{\mathbf{q}} - \tilde{\mathbf{Q}}) = \frac{\mathrm{d}\tilde{\mathbf{K}}^{(s)}}{\mathrm{d}h}\tilde{\mathbf{q}} + \tilde{\mathbf{K}}^{(s)}\frac{\mathrm{d}\tilde{\mathbf{q}}}{\mathrm{d}h} - \frac{\mathrm{d}\tilde{\mathbf{Q}}}{\mathrm{d}h} = \mathbf{0} \tag{2.101}$$

where

$$\begin{aligned} \frac{\mathrm{d}\tilde{\mathbf{K}}^{(s)}}{\mathrm{d}h} &= \frac{\partial \tilde{\mathbf{K}}^{(s)}}{\partial h} + \frac{\partial \tilde{\mathbf{K}}^{(s)}}{\partial \tilde{\mathbf{q}}}\frac{\mathrm{d}\tilde{\mathbf{q}}}{\mathrm{d}h} \\ \frac{\mathrm{d}\tilde{\mathbf{Q}}}{\mathrm{d}h} &= \frac{\partial \tilde{\mathbf{Q}}}{\partial h} + \frac{\partial \tilde{\mathbf{Q}}}{\partial \tilde{\mathbf{q}}}\frac{\mathrm{d}\tilde{\mathbf{q}}}{\mathrm{d}h} \end{aligned} \tag{2.102}$$

By regrouping terms, we recognize (see Eq. (2.61)) the tangent stiffness matrix as the system matrix for finding the sensitivity vector, while the right-hand-side vector is formed by the terms containing explicit derivatives of $\bar{\mathbf{K}}^{(s)}$ and $\bar{\mathbf{Q}}$ with respect to h

$$\bar{\mathbf{K}}^{(T)}\frac{\mathrm{d}\bar{\mathbf{q}}}{\mathrm{d}h} = -\frac{\partial \bar{\mathbf{K}}^{(s)}}{\partial h}\bar{\mathbf{q}} + \frac{\partial \bar{\mathbf{Q}}}{\partial h} \tag{2.103}$$

We obtain a linear system in the sensitivity variables $\mathrm{d}\bar{\mathbf{q}}/\mathrm{d}h$, where we need only to substitute the appropriate load term to get the solution, since the system matrix has already been factorized or inverted. We can thus investigate the effect of any material or numerical parameter on the solution.

If we consider any of the material parameters entering the constitutive relation (2.2)–(2.3) used to define the equivalent viscosity (i.e. any of the static yield stress σ_0, the fluidity γ, or the viscoplastic index n), the right hand side of Eq. (2.103) reads

a-c) $h = \sigma_0$, or γ or n

$$\text{RHS of Eq. (2.103)} = -\frac{\partial \bar{\mathbf{K}}^{(s)}}{\partial \mu}\bar{\mathbf{q}}\frac{\partial \mu}{\partial h} + \frac{\partial \bar{\mathbf{Q}}}{\partial \mu}\frac{\partial \mu}{\partial h} \tag{2.104}$$

where (cf. Eqs. (2.2), (2.3), (2.22), (2.51) and (2.53))

$$\frac{\partial \bar{\mathbf{K}}^{(s)}}{\partial \mu} = \begin{bmatrix} \mathbf{K}_{(1)} & \mathbf{0} & \mathbf{0} \\ \mathbf{0} & \mathbf{0} & \mathbf{0} \\ \mathbf{0} & \mathbf{0} & \mathbf{0} \end{bmatrix} \qquad \mathbf{K}_{(1)} = \int_\Omega 2\mathbf{B}^{\mathrm{T}}\mathbf{B}\,\mathrm{d}\Omega \qquad \frac{\partial \bar{\mathbf{Q}}}{\partial \mu} = \begin{bmatrix} \mathbf{0} \\ \mathbf{0} \\ \dfrac{\eta \dot{\bar{\varepsilon}}^2}{3} \end{bmatrix} \tag{2.105}$$

and $\partial\mu/\partial h$ is calculated from Eq. (2.3).

We also have as possible design parameters those entering the energy balance equation (2.50) (i.e. k, ρc_{p}) and the boundary conditions (h_{s}, $\bar{h}$ and T_{m}). Then we have (cf. Eqs. (2.56) and (2.58))

d) $h = k$

$$\text{RHS of Eq. (2.103)} = -\frac{\partial \bar{\mathbf{K}}^{(s)}}{\partial k}\bar{\mathbf{q}} = -\begin{bmatrix} \mathbf{0} \\ \mathbf{0} \\ \left(\displaystyle\int_\Omega \nabla\tilde{\boldsymbol{\phi}}(\mathbf{I} + \frac{\partial \mathbf{k}'}{\partial k})\nabla\tilde{\boldsymbol{\phi}}^{\mathrm{T}}\,\mathrm{d}\Omega\right)\mathbf{T} \end{bmatrix} \tag{2.106}$$

e) $h = \rho c_{\mathrm{p}}$

$$\text{RHS of Eq. (2.103)} = -\frac{\partial \bar{\mathbf{K}}^{(s)}}{\partial (\rho c_{\mathrm{p}})}\bar{\mathbf{q}} = -\begin{bmatrix} \mathbf{0} \\ \mathbf{0} \\ \left(\displaystyle\int_\Omega \left(\tilde{\boldsymbol{\phi}}\mathbf{v}\cdot\nabla\tilde{\boldsymbol{\phi}}^{\mathrm{T}} + \nabla\tilde{\boldsymbol{\phi}}\frac{\partial \mathbf{k}'}{\partial \rho c_{\mathrm{p}}}\cdot\nabla\tilde{\boldsymbol{\phi}}^{\mathrm{T}}\right)\mathrm{d}\Omega\right)\mathbf{T} \end{bmatrix} \tag{2}$$

f) $h = \bar{h}$

$$\text{RHS of Eq. (2.103)} = -\begin{bmatrix} 0 \\ 0 \\ \left(\int_{\partial\Omega_q} \tilde{\boldsymbol{\phi}}\tilde{\boldsymbol{\phi}}^{\mathrm{T}}\,\mathrm{d}(\partial\Omega)\right)\mathbf{T} \end{bmatrix} + \begin{bmatrix} 0 \\ 0 \\ \int_{\partial\Omega_q} \tilde{\boldsymbol{\phi}} T_{\mathrm{m}}\,\mathrm{d}(\partial\Omega) \end{bmatrix} \tag{2.108}$$

g) $h = h_s$

$$\text{RHS of Eq. (2.103)} = \begin{bmatrix} 0 \\ 0 \\ \int_{\partial\Omega_q} \tilde{\boldsymbol{\phi}}\,\mathrm{d}(\partial\Omega) \end{bmatrix} \tag{2.109}$$

h) $h = T_m$

$$\text{RHS of Eq. (2.103)} = \begin{bmatrix} 0 \\ 0 \\ \int_{\partial\Omega_q} \tilde{\boldsymbol{\phi}}\bar{h}\,\mathrm{d}(\partial\Omega) \end{bmatrix} \tag{2.110}$$

We have still another important application of the sensitivity analysis to the present problem, which can also be used in any method involving numerical parameters. It should be a desirable property of the upwind scheme to yield results the least sensitive to the actual values of the numerical parameters as possible. We can investigate the behaviour of the numerical scheme by calculating the appropriate load term. In the present context we consider the coefficient '2', by which the local Peclet number is divided to obtain the upwind coefficient (see Eq. (2.56) and the text below). In particular we have

$$\frac{\partial\alpha}{\partial\text{'2'}} = \operatorname{cosech}^2\left(\frac{\gamma}{2}\right)\frac{\gamma}{4} - \frac{1}{\gamma} \tag{2.111}$$

which we replace in the corresponding expression of the explicit derivative with respect to h:

i) $h =$ '2'

$$\text{RHS of Eq. (2.103)} = \begin{bmatrix} 0 \\ 0 \\ \left(\int_{\Omega} \nabla\tilde{\boldsymbol{\phi}}\boldsymbol{\Theta}^{\mathrm{T}}\mathbf{k}'_o\boldsymbol{\Theta}\nabla\tilde{\boldsymbol{\phi}}^{\mathrm{T}}\frac{1}{\alpha}\frac{\partial\alpha}{\partial\text{'2'}}\,\mathrm{d}\Omega\right)\mathbf{T} \end{bmatrix} \tag{2.112}$$

Also the element size d is involved in Eq. (2.56). The generalization to two- and three- dimensions poses the question: how to calculate d? In practice this quantity is measured along the flow direction, but this still does not uniquely define d. The question about the importance of this factor may be studied by considering the sensitivity with respect to d. Explicit differentiation now yields

j) $h = d$

$$\text{RHS of Eq. (2.103)} = \begin{bmatrix} 0 \\ 0 \\ \left(\int_{\Omega} \nabla\tilde{\boldsymbol{\phi}}\boldsymbol{\Theta}^{\mathrm{T}}\mathbf{k}'_o\boldsymbol{\Theta}\nabla\tilde{\boldsymbol{\phi}}^{\mathrm{T}}\left(\frac{1}{d} + \frac{1}{\alpha}\frac{\partial\alpha}{\partial d}\right)\mathrm{d}\Omega\right)\mathbf{T} \end{bmatrix} \tag{2.113}$$

with $\frac{\partial\alpha}{\partial d}$ calculated explicitly from the expressions given below Eq. (2.56).

2.3.4 Analytical illustrations

2.3.4.1 Pure shear strain

Let us consider the configuration shown in Fig. 2.3. The rectangular domain is

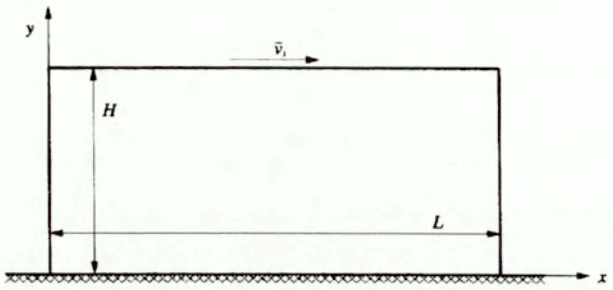

Figure 2.3 Sensitivity analysis of pure shear strain

fixed along the lower edge while a horizontal uniform velocity $\bar{v}_1$ is imposed along its upper boundary. Consequently, the velocity in the body can be represented as

$$v_x = \bar{v}_1 \frac{y}{H}, \qquad v_y = 0 \tag{2.114}$$

The strain rate tensor components result as

$$\dot{\varepsilon}_x = \frac{\partial v_x}{\partial x} = 0, \qquad \dot{\varepsilon}_y = \frac{\partial v_y}{\partial y} = 0, \qquad \dot{\varepsilon}_{xy} = \frac{1}{2}\left(\frac{\partial v_x}{\partial y} + \frac{\partial v_y}{\partial x}\right) = \frac{1}{2}\frac{\bar{v}_1}{H} \tag{2.115}$$

while the effective strain rate becomes

$$\dot{\bar{\varepsilon}} = \sqrt{\frac{4}{3}\dot{\varepsilon}_{xy}^2} = \frac{\bar{v}_1}{\sqrt{3}H} = \text{const} \tag{2.116}$$

from which the viscosity is calculated by using Eq. (2.3) as

$$\mu = \frac{H}{\sqrt{3}\bar{v}_1}\left[\sigma_0 + \left(\frac{\bar{v}_1}{\sqrt{3}H\gamma}\right)^{\frac{1}{n}}\right] \tag{2.117}$$

By using the constitutive equation (2.2) we calculate the shear stress as

$$\sigma_{xy} = 2\mu\dot{\varepsilon}_{xy} = \frac{1}{\sqrt{3}}\left[\sigma_0 + \left(\frac{\bar{v}_1}{\sqrt{3}H\gamma}\right)^{\frac{1}{n}}\right] \tag{2.118}$$

The sensitivity coefficients result in the form

$$\begin{aligned} \frac{\mathrm{d}v_x}{\mathrm{d}h} &= \frac{\mathrm{d}v_y}{\mathrm{d}h} = 0 \\ \frac{\mathrm{d}\dot{\varepsilon}_x}{\mathrm{d}h} &= \frac{\mathrm{d}\dot{\varepsilon}_y}{\mathrm{d}h} = \frac{\mathrm{d}\dot{\varepsilon}_{xy}}{\mathrm{d}h} = 0 \\ \frac{\mathrm{d}\dot{\bar{\varepsilon}}}{\mathrm{d}h} &= 0 \end{aligned} \tag{2.119}$$

while for the viscosity we have

$$\frac{\mathrm{d}\mu}{\mathrm{d}h} = \frac{\partial \mu}{\partial h} + \frac{\partial \mu}{\partial \dot{\bar{\varepsilon}}} \frac{\mathrm{d}\dot{\bar{\varepsilon}}}{\mathrm{d}h} = \frac{\partial \mu}{\partial h} \tag{2.120}$$

The specific expressions for the partial derivatives with respect to the design parameters, σ_0, γ, and n are given in Eqs. (2.92).

If we take as the constraint functional the deformation energy rate

$$G = \int_\Omega \sigma_{ij}\, \dot{\varepsilon}_{ij}\, \mathrm{d}\Omega = \int_\Omega 2\sigma_{xy}\, \dot{\varepsilon}_{xy}\, \mathrm{d}\Omega = 4\Omega\, \mu\, \dot{\varepsilon}_{xy}^2 \qquad \text{(no sum on } x, y\text{)} \tag{2.121}$$

then its sensitivity coefficient with respect to the generic design parameter h is

$$\frac{\mathrm{d}G}{\mathrm{d}h} = 4\Omega \frac{\partial \mu}{\partial h} \dot{\varepsilon}_{xy}^2 \tag{2.122}$$

2.3.4.2 Free forging

Let us now consider the free forging operation defined in Fig. 2.4. A uniformly distributed compression force $t = F/L$ is applied to the upper and lower faces of the workpiece, which is assumed to undergo a plane strain deformation.

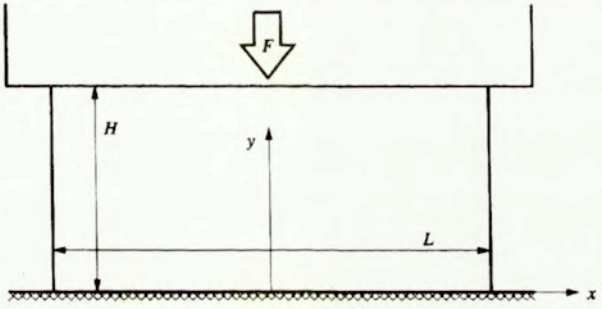

Figure 2.4 Sensitivity analysis of free forging

By elementary equilibrium considerations the stress field is described in this case by

$$\begin{aligned} \sigma_x &= 0 \\ \sigma_y &= t \\ \sigma_{xy} &= 0 \end{aligned} \tag{2.123}$$

from which the pressure and stress deviator components result as

$$\begin{aligned} p &= -\sigma_m = -\frac{\sigma_x + \sigma_y}{2} = -\frac{t}{2} \\ \sigma_x^{\mathrm{D}} &= \sigma_x + p = -\frac{t}{2} \\ \sigma_y^{\mathrm{D}} &= \sigma_y + p = \frac{t}{2} \\ \sigma_{xy}^{\mathrm{D}} &= \sigma_{xy} = 0 \end{aligned} \tag{2.124}$$

The velocity field is unknown a priori. By symmetry considerations we can expect v_y to have a linear variation along the y direction for all points of the domain so that denoting the velocity on the upper edge by $\bar{v}_y$ we arrive at

$$v_y = \frac{2y}{H}\bar{v}_y \tag{2.125}$$

Since there is no friction, the domain preserves its rectangular shape in the process but the aspect ratio changes. Therefore, v_x can be assumed uniform along each of the left and right boundaries, i.e. for $x = L/2$ and $x = -L/2$, respectively. By the incompressibility condition and symmetry considerations we can write

$$\bar{v}_x H + \bar{v}_y L = 0\,, \qquad \dot{\varepsilon}_x + \dot{\varepsilon}_y = 0\,, \qquad \dot{\varepsilon}_{xy} = 0 \tag{2.126}$$

from which we have that

$$v_x = \frac{2x}{L}\bar{v}_x \tag{2.127}$$

The components of the rate of deformation tensor are

$$\begin{aligned} \dot{\varepsilon}_x &= \frac{2}{L}\bar{v}_x = -\frac{2}{H}\bar{v}_y \\ \dot{\varepsilon}_y &= \frac{2}{H}\bar{v}_y \\ \dot{\varepsilon}_{xy} &= 0 \end{aligned} \tag{2.128}$$

while the effective strain rate becomes

$$\dot{\bar{\varepsilon}} = \frac{4}{\sqrt{3}}\frac{\bar{v}_y}{H} = \frac{2\dot{\varepsilon}_y}{\sqrt{3}} \tag{2.129}$$

By recalling that

$$\sigma_y^D = 2\mu\dot{\varepsilon}_y \tag{2.130}$$

we arrive at

$$\dot{\bar{\varepsilon}} = -\gamma\left(\frac{\sqrt{3}t}{2} + \sigma_0\right)^n \tag{2.131}$$

from which

$$\bar{v}_y = -\gamma\left(\frac{\sqrt{3}t}{2} - \sigma_0\right)^n \frac{\sqrt{3}H}{4} \tag{2.132}$$

Finally, we calculate the sensitivity coefficients with respect to the parameters of the constitutive equations for the viscoplastic material model. From Eqs. (2.123) and (2.124) we see that the pressure and stress deviator do not depend on the material parameters, i.e.

$$\frac{\mathrm{d}p}{\mathrm{d}h} = 0\,, \qquad \frac{\mathrm{d}\sigma_{ij}^D}{\mathrm{d}h} = 0 \tag{2.133}$$

From Eq. $(2.133)_2$ and the constitutive equations (2.2) and (2.3), we have

$$\frac{\mathrm{d}\mu}{\mathrm{d}h}\dot{\varepsilon}_{ij} + \mu\frac{\mathrm{d}\dot{\varepsilon}_{ij}}{\mathrm{d}h} = 0 \tag{2.134}$$

while, by differentiating Eq. (2.132) and then inserting the result into Eqs. (2.125) and (2.128), we get

$$\begin{aligned}
\frac{\mathrm{d}\bar{v}_y}{\mathrm{d}\sigma_0} &= -\gamma n\left(\frac{\sqrt{3}t}{2}+\sigma_0\right)^{n-1}\frac{\sqrt{3}H}{4}\\
\frac{\mathrm{d}\bar{v}_y}{\mathrm{d}\gamma} &= -\left(\frac{\sqrt{3}t}{2}+\sigma_0\right)^{n}\frac{\sqrt{3}H}{4}\\
\frac{\mathrm{d}\bar{v}_y}{\mathrm{d}n} &= -\gamma\left(\frac{\sqrt{3}t}{2}+\sigma_0\right)^{n}\frac{\sqrt{3}H}{4}\ln\left(\frac{\sqrt{3}t}{2}+\sigma_0\right)
\end{aligned} \tag{2.135}$$

The sensitivity coefficients of the velocity and strain rate components with respect to any of the design parameters are then arrived at in the form

$$\begin{aligned}
\frac{\mathrm{d}v_y}{\mathrm{d}h} &= \frac{2y}{H}\frac{\mathrm{d}\bar{v}_y}{\mathrm{d}h}\\
\frac{\mathrm{d}\dot{\varepsilon}_x}{\mathrm{d}h} &= \frac{2}{H}\frac{\mathrm{d}\bar{v}_y}{\mathrm{d}h}\\
\frac{\mathrm{d}\dot{\varepsilon}_y}{\mathrm{d}h} &= -\frac{2}{H}\frac{\mathrm{d}\bar{v}_y}{\mathrm{d}h}\\
\frac{\mathrm{d}\dot{\varepsilon}_{xy}}{\mathrm{d}h} &= 0
\end{aligned} \tag{2.136}$$

The viscosity sensitivity coefficients $\mathrm{d}\mu/\mathrm{d}h$ can be obtained in different ways. For example, we can substitute Eqs. $(2.128)_1$ and $(2.136)_1$ (or $(2.128)_2$ and $(2.136)_2$) into Eq. (2.134) to obtain

$$\frac{\mathrm{d}\mu}{\mathrm{d}h} = -\frac{1}{\dot{\varepsilon}_y}\mu\frac{\mathrm{d}\dot{\varepsilon}_y}{\mathrm{d}h} = -\frac{\mu}{h}\frac{\mathrm{d}\bar{v}_y}{\mathrm{d}h} \tag{2.137}$$

Finally, the sensitivity coefficient for the deformation energy functional reduces to

$$\frac{\mathrm{d}G}{\mathrm{d}h} = \int_\Omega \frac{\mathrm{d}\dot{\varepsilon}_y}{\mathrm{d}h}\sigma_y\,\mathrm{d}\Omega = -\frac{2\Omega}{H}\frac{\mathrm{d}\bar{v}_y}{\mathrm{d}h}t \tag{2.138}$$

By comparing both the examples an interesting conclusion of practical importance can be re-iterated: the sensitivity coefficients depend strongly on the way the boundary conditions are imposed. In the first case a constant imposed velocity implies a non-constant load, which should also be design differentiated to derive the sensitivity expressions. As a result of the analysis an insensitive velocity field is obtained in the first example. The conclusion is that in any sensitivity analysis the description of the boundary conditions is an essential part of the sensitivity problem definition, and thus strongly affects the results.

2.3.5 Computational illustrations

2.3.5.1 Direct extrusion

As a first computational illustration of the sensitivity analysis for a forming process, an extrusion matrix is considered as shown in Fig. 2.5, with the given constant load applied at the left boundary simulating the ram. The applied load **F** is such calculated to induce a ram velocity of 1cm/s Sticking friction conditions are assumed. The material model described by Eq. (2.3) is adopted with $\sigma_0 = 200\text{N/cm}^2$, $\gamma = 0.1$ and $n = 1.5$. It corresponds to 18M5 steel (0.18%C, 1.37%Mn) at 1200°C [36, 78]. Free surface conditions prevail when the material gets out of the extrusion die. Sensitivity of the nodal variables **v** and p with respect to the static yield stress σ_0 is calculated. Sensitivity isocurves for the velocity module are plotted in Fig. 2.6. The character of the graph is very similar to that for the isocurves of the velocity module. Both the DDM and the ASM have been employed yielding the same results, which are also in full agreement with the finite difference approach—no noticeable differences appear in the graphs.

We can more easily analyze the sensitivity results by plotting their values at selected points against our design variable. In Figs. 2.7 and 2.8 the pressure and velocity solutions and their respective sensitivities for the points indicated (cf. Fig. 2.5) as a function of the static yield stress are displayed. In each case the results for two different meshes are shown: mesh 2, defined in Fig. 2.5, and mesh 1 such that every element contains four elements of mesh 2.

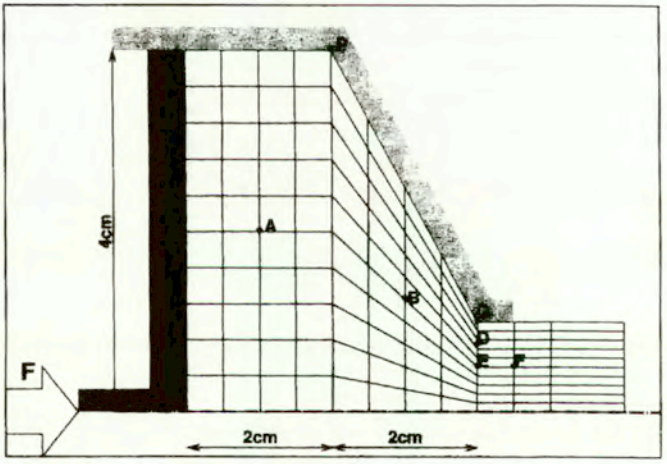

Figure 2.5 Layout of the extrusion process and mesh 2

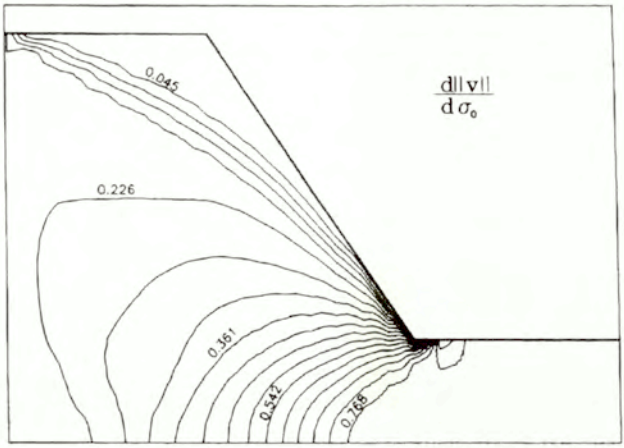

Figure 2.6 Sensitivity of the velocity module to the static yield stress, $\mathrm{d}||\mathbf{v}||/\mathrm{d}\sigma_0$

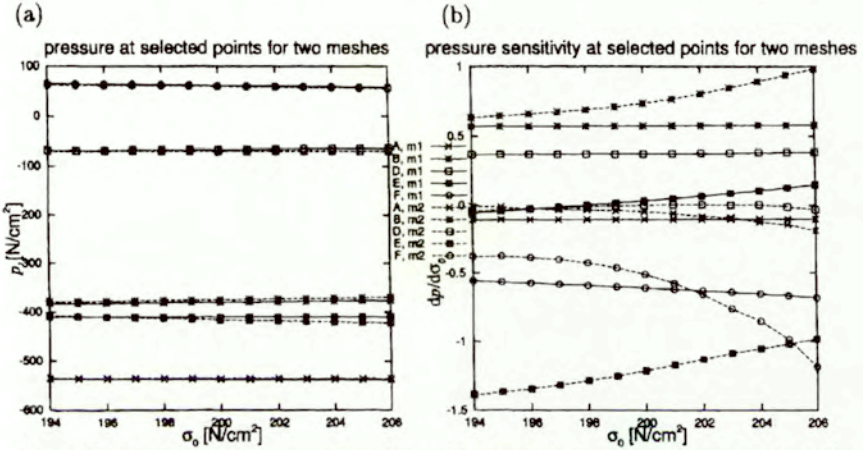

Figure 2.7 Pressure and pressure sensitivity with respect to static yield stress versus static yield stress at different points as obtained with two different meshes (m1 and m2)

In both the cases the results are in very good agreement with the sensitivities calculated by the finite difference approach with the perturbation taken as $\Delta\sigma_0 = 0.005\sigma_0 = 1$. The plots are virtually identical for any of the methods employed and the same mesh. Pressure results appear to be roughly mesh-independent while relatively significant discrepancies are observed for the pressure sensitivity. On the other hand, the equilibrium and sensitivity results exhibit a similar mesh dependency in the case of velocity solutions: for small relative values of a given velocity component a more noticeable mesh dependency is obtained than for

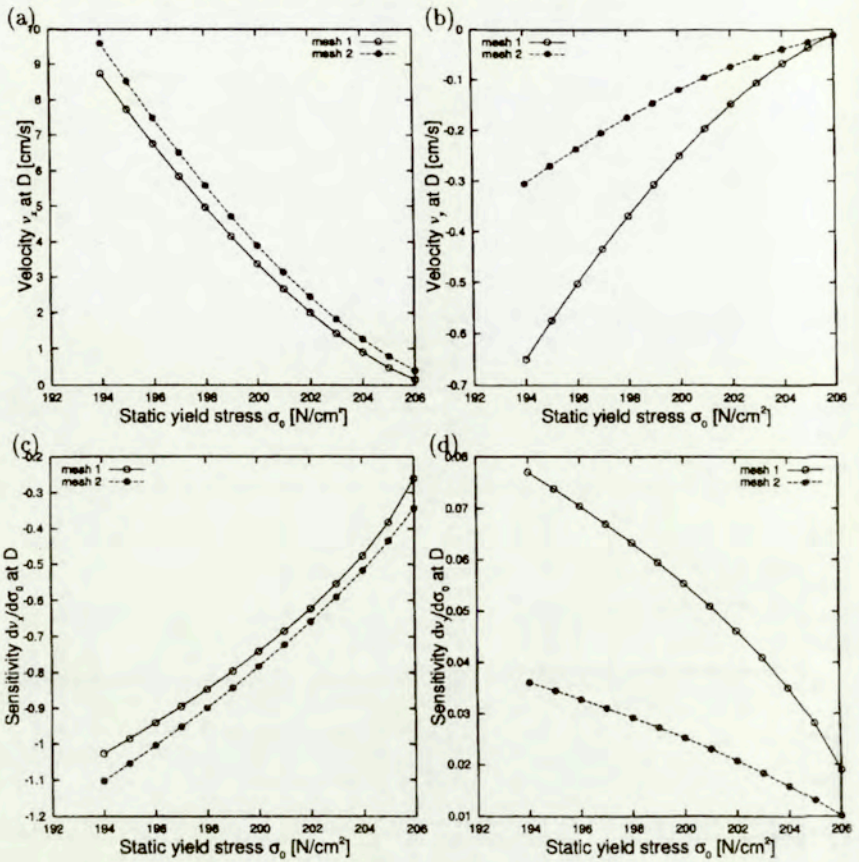

Figure 2.8 Velocity components and velocity sensitivity with respect to static yield stress versus static yield stress at point D

large ones. As expected, velocities are more sensitive to changes in the static yield stress as the cross-section becomes smaller, i.e. near the outlet of the die. Also, for constant loads the sensitivity of the velocity component in the direction at which the tool acts is negative, since an increase in the yield stress results in a slower process. In addition, nodal pressures are almost constant, as they should be in the case of applied loads. If fixed velocities are imposed, then the load happens to be nearly proportional to the viscosity. In such a case the velocities are virtually insensitive to variations in the yield stress whereas pressure sensitivity is positive and tends to be linearly proportional to changes in the yield stress for materials exhibiting behaviour close to perfect plasticity.

A similar analysis is performed with the other parameters entering the con-

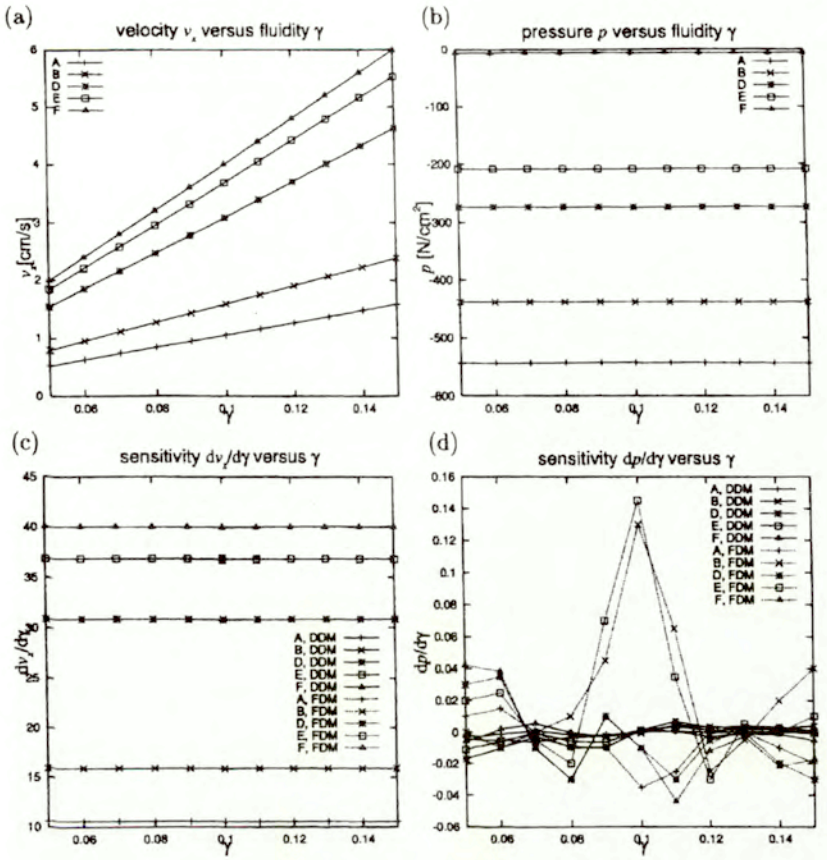

Figure 2.9 Velocity and pressure and their sensitivity with respect to the fluidity coefficient versus the fluidity coefficient at different points

stitutive model (fluidity γ, exponent of the viscoplastic law n, cf. Eq. (2.3)), and the friction coefficient ν, cf. Eq. (2.37), as design parameters. The results for the chosen set of points are shown in Figs. 2.9 – 2.11, where the velocity, pressure and their design derivatives calculated by direct differentiation (full line, denoted DDM) and by finite differences (dotted line, denoted FDM) are plotted.

It turns out from the sensitivity analysis accounting for the different parameters entering the constitutive model that the fluidity γ and the exponent n have a negligible effect on the pressure when loads are held constant. It should be noted that the discrepancies (the DDM versus the FDM) shown in Fig. 2.9(d) for the pressure sensitivities with respect to the fluidity γ are negligible when compared with the values of the pressure. Irregular results are obtained by the FDM, which seems to be due to insufficient precision while solving the

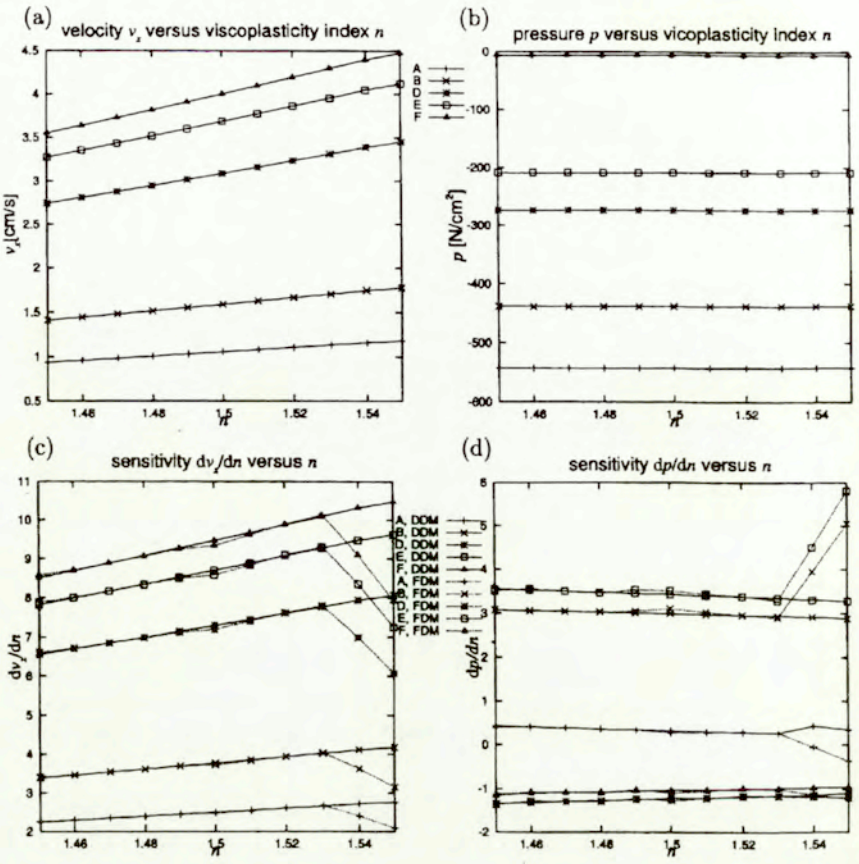

Figure 2.10 Velocity and pressure and their sensitivity with respect to the parameter n versus n at different points

perturbed problem and by the truncation errors inherent when the finite length of the perturbation $\Delta\gamma$ is taken ($\Delta\gamma = 0.01$ in this case). Similarly, irregular sensitivity results for the FDM in the upper range of the considered values of n suggest similar errors in the application of this method. The analysis of sensitivity to the friction coefficient ν leads to a different situation. Unlike the previous cases, the sensitivity coefficients for the problem variables with respect to the friction coefficient calculated by the FDM are very sensitive to the size of the perturbation $\Delta\nu$ used to calculate the numerical derivatives. In fact, no range of $\Delta\nu$ could be found for which a stable value of sensitivities resulted. Considering the friction phenomenon, we can expect a non-smooth transition between the

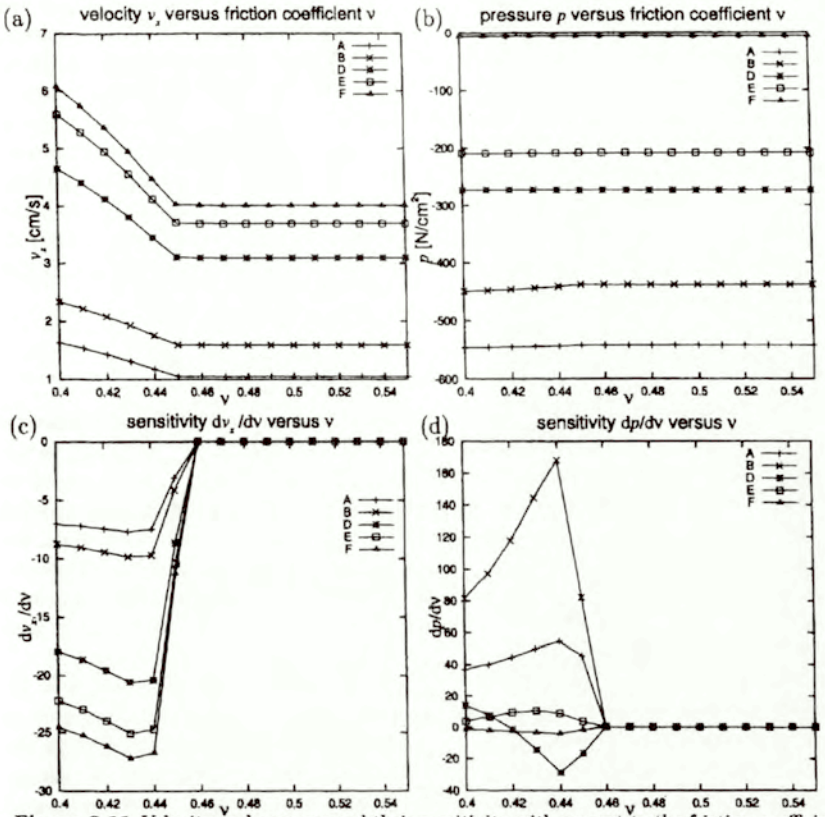

Figure 2.11 Velocity and pressure and their sensitivity with respect to the friction coefficient ν versus ν at different points, as obtained with two different meshes

two different friction types: sticking (with zero tangential velocity) and sliding friction. In terms of the friction elements used for this analysis, we may find points alternating between both types of friction along with the friction coefficient changing according to the local pressure value. The specific friction model we deal with has two aspects, which seem to explain the failure of the sensitivity analysis in this case: the non-smoothness of the friction law leading to a discontinuous derivative, and the treatment of the surface contact phenomenon as a volumetric one, which implies numerical integration over an essentially discontinuous zone. This means that the elements which can provide an adequate friction description in the equilibrium problem may turn out to be unsuitable for sensitivity analysis. In view of the above we have performed the sensitivity analysis using the DDM without confronting the results against those by the FDM. The

DDM results are plotted in Fig. 2.11, in which important response changes are obtained until a certain value of the friction coefficient is reached (for a constant value of the imposed extrusion load), starting at which all the boundary exhibits sticking friction and therefore no sensitivity to the friction coefficient appears.

In this example the equilibrium problem has been solved by direct iterations so that the secant stiffness matrix was available at the end of this step. However, since the material properties were typical of a material with a relatively high rate dependence, the sensitivity problem converged in a few iterations only when the tangent stiffness matrix $\mathbf{K}^{(T)}$ was used. Therefore, the $\mathbf{K}^{(T)}$ option was preferred, even though it required an additional solution of the equations system at the sensitivity stage.

2.3.5.2 Cutting

Another experience resulting from the previous example is that for low material rate sensitivity the direct solution method based on Eq. (2.74) or (2.83) is not possible, because the tangent matrix is nearly singular and cannot be used to obtain an exact solution in one iteration. In spite of this, the matrix, when applied iteratively to find the solution, usually yields convergence much faster than the direct iterative scheme defined by Eqs. (2.85) and (2.86), cf. [10, 72]. However, in some extreme cases the $\mathbf{K}^{(T)}$ scheme is not convergent and the solution is only possible by direct iterations. In addition, convergence is very slow and it may take thousands of iterations.

This problem may be illustrated by the following example in which a 2D cutting problem is simulated by placing a cutting tool at a given depth of an incoming metal flow causing a flow separation—a chip is separated from the main flow. Figure 2.12(a) shows the initial finite element mesh used. Constant loads are imposed on the upper boundary of the body. They are such calculated as to produce a downward directed material flow of 1cm/s. The metal properties are those of a nearly perfectly plastic material ($n = 40$ in Eq. (2.3)). A major part of the domain undergoes rigid body flow, as almost all the plastic deformation is concentrated in the vicinity of the flow separation region. The problem has two free surfaces which are iteratively modified to make the velocity tangent to them. For the lower surface the contact elements impose a penalty-based restriction on the normal velocity when a no-penetration condition requires so, and release it if normal traction is obtained in the fixed part of the curve. Figure 2.12(b) shows the final mesh we arrive at, once the equilibrium problem has been solved with simultaneous fulfillment of the contact and free surface conditions.

In the above example the iterative scheme of Eq. (2.85) had to be employed. In Fig. 2.13 sensitivity results for the velocity module with respect to the visco-plastic law index n obtained by the central FDM and the DDM are compared. Both methods give basically the same solution which consists, similarly to the velocity field, of subdomains with constant velocity sensitivity separated by a narrow band of the shear deformation rate sensitivity coefficients (i.e. a band

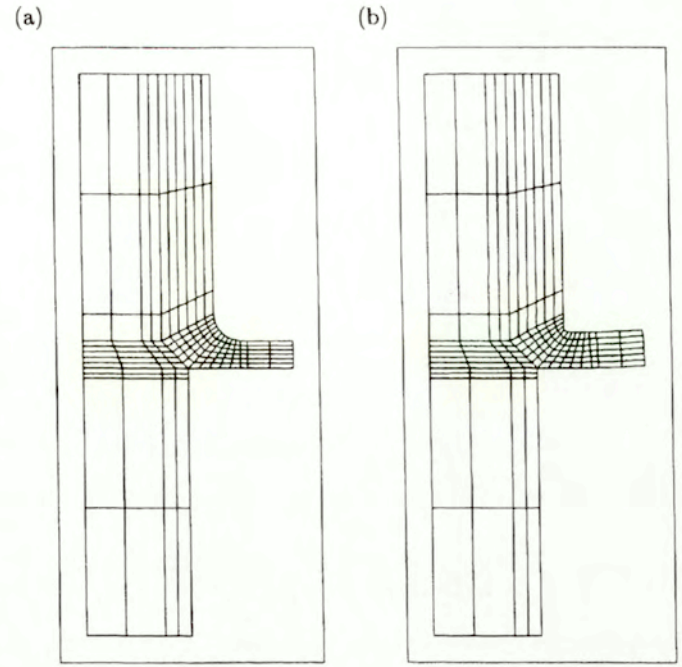

Figure 2.12 Cutting: (a) initial mesh, (b) final mesh

with high values of $d\dot{\varepsilon}_{12}/dn$) corresponding to the plastic deformation zone.

Difficulties in using the tangent matrix have a physical interpretation in the fact that a perfectly plastic material under constant loads is infinitely sensitive to variations in the material properties. The whole process is numerically stable if the boundary conditions consist of non-zero imposed velocities; it is then seen that the velocity sensitivities are virtually zero. As a matter of fact, in this case the variations in the applied loads are proportional to the variations of the material parameters. Hence, no response change is observed.

2.3.5.3 Extrusion with thermo-mechanical model

Direct extrusion

The model for sensitivity analysis of thermally coupled processes has been tested in two metal forming simulations. All sensitivity results obtained by DDM have been checked with their counterpart obtained by the finite difference method

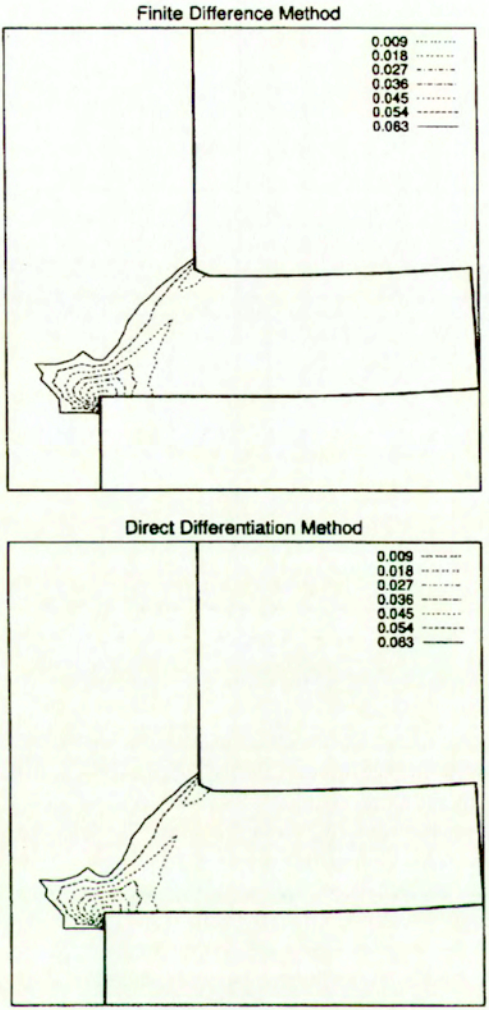

Figure 2.13 Velocity sensitivity with respect to the viscoplastic index n by the FDM and the DDM

(FDM). Since no noticeable discrepancies were obtained, only results from DDM will be shown.

In the first example a plane direct extrusion process is considered. The sensitivity analysis shown in Paragraph 2.3.5.1 is extended to the case of temperature dependent mechanical properties. Attention is focussed to the temperature sensitivity to mechanical and thermal properties, where results seem to be more interesting. The static yield stress and the viscoplastic index have been assumed linearly temperature dependent

$$\begin{aligned} \sigma_0 &= \sigma_{0R}[1 - 0.0025(T - T_R)] \\ n &= n_R[1 - 10^{-4}(T - T_R)] \end{aligned} \tag{2.139}$$

where σ_{0R} and n_R are the values of both properties at the reference temperature $T_R = 1050°C$. The reference values are those of Paragraph 2.3.5.1. Although the coefficients of Eq. (2.139) have been assumed, the proposed functions follow qualitatively some empirical data available ([101], cited in [119], [77, 49]). Figure 2.14 shows the viscosity as a function of the effective strain rate and the temperature. It is seen that opposite behaviour with respect to $\dot{\bar{\varepsilon}}$ takes place at high and low temperature. The layout of the process is the one already presented in Fig. 2.5, while Fig. 2.15 shows (a) the temperature, and the sensitivity-of-temperature contours with respect: (b) to the static yield stress σ_0, and (c) to the heat transfer coefficient of the interface with the tool $\bar{h}$ (cf. Eq. (2.53)). A large heat transfer coefficient $\bar{h} = 200\text{cal/s cm}^2\,°\text{C}$ is assumed for the interface with the extrusion matrix (measured values range from 0.07 to 0.5.), which is kept at a fixed temperature lower than that of the metal. Therefore the highest temperatures appear around the symmetry axis, although the heat generation rate is maximum on the boundary. The similar aspect between the isocurves of Figs. 2.15(a) and (b) suggests that the temperature field is linearly dependent on the yield stress. The

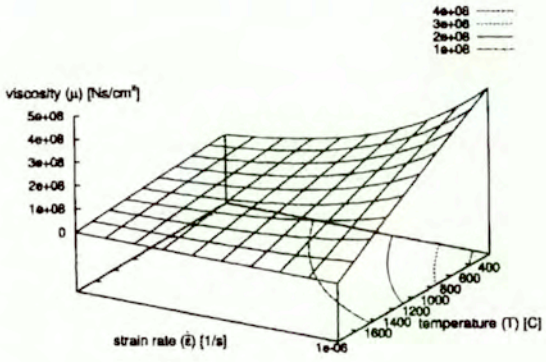

Figure 2.14 Viscosity as a function of the effective strain rate $\dot{\bar{\varepsilon}}$ and temperature T

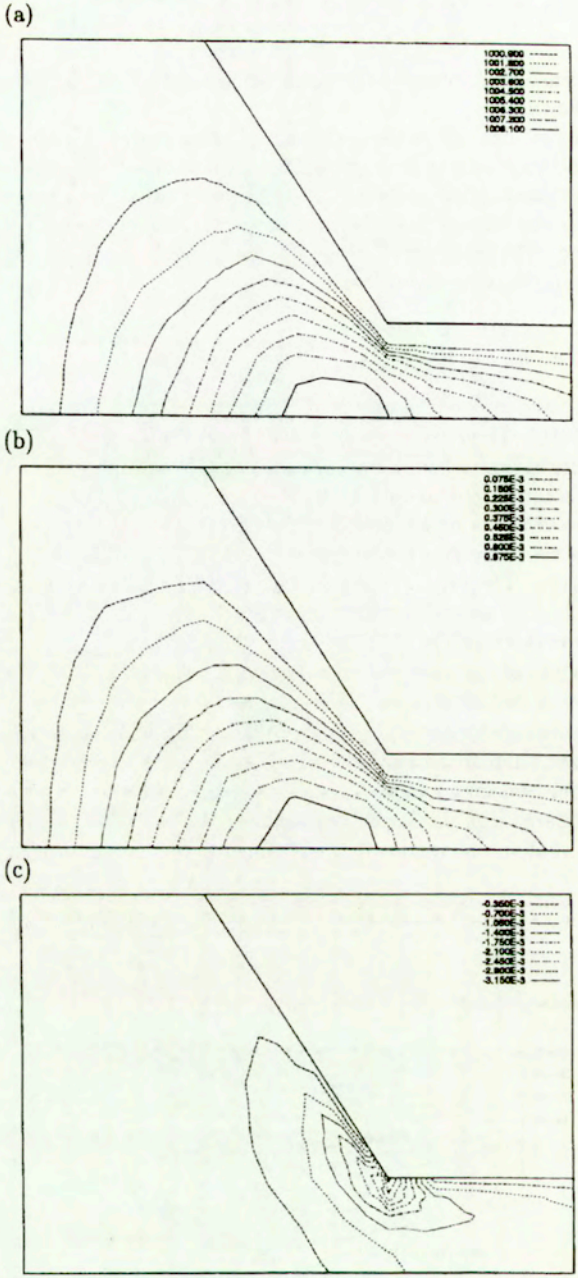

Figure 2.15 Direct extrusion process: (a) temperature contours [°C] and sensitivity (b) to the static yield stress σ_0, [°C cm^2/s] and (c) to the heat transfer coefficient of the interface with the tool

coolant effect is also responsible for a temperature field not too sensitive to the yield stress. On the other hand, changes in the heat transfer coefficient have their most noticeable effect on the temperature field near the wall, especially where the heat generation rate is maximal. This fact is evidenced by the relatively higher temperature sensitivities in this zone. The negative sensitivity values confirm the intuitive fact that increasing the heat transfer coefficient to a cooler region lowers the temperature. All the analytical derivatives have been checked with their finite-difference-based counterparts, and very good agreement was found.

Combined Direct-inverse extrusion

Next we consider a combined direct-inverse extrusion process. This problem develops within a rather unstable equilibrium between the direct and inverse flows. Their relative proportion depends on the extrusion ratio, the friction coefficient, yield stress, viscoplastic material properties and ram velocity. Small changes in them may affect this proportion. Some of these quantities in turn depend on the temperature, as in the previous example. Namely, the following temperature dependent properties of Ti-6Al-4V (cf. [101]) have been used:

$$\sigma_0 = \begin{cases} 1155\text{N/cm}^2 & T < 760°C \\ 794 + 0.011664(T - T_R) - 5.85)(T - T_R) & 760° \leq T \leq 1065° \\ 60.5\text{N/cm}^2 & T > 1065°C \end{cases}$$

$$n = \begin{cases} 8.2497 & T < 982°C \\ 8.2497 - 0.02476728(T - 982) & 982°C < T < 1149°C \\ 4.12182 & T > 1149°C \end{cases}$$

$$\rho = 4.598\text{E-3Kg/cm}^3\,, \quad c = 150.12\text{cal/Kg}\,°\text{C}\,, \quad k = 2.772\text{cal/cm s}\,°\text{C}$$

The layout of the process is shown in Fig. 2.16(a). Imposed ram velocity is assumed. the temperature contours and their sensitivity with respect to the temperature of the extrusion matrix are presented in Figs. 2.16(b) and (c). A relatively cold wall removes the heat generated by plastic deformation and for this reason the temperature contours decrease towards the interface. On the other hand the effect of this imposed temperature on the wall is only important in its neighbourhood. A rather large value has been taken for the interface heat transfer coefficient $\bar{h}$. This explains the maximum sensitivity values close to unity. It should be noticed that in this case the design parameter and the variable whose sensitivity we are investigating have the same units. Further, in Fig. 2.17 the extrusion force and its sensitivity is plotted with respect to the extrusion matrix temperature. A good agreement of sensitivities calculated by both methods can be seen in Fig. 2.17(b). The extrusion force decreases with increasing temperature values, as should be expected. The sensitivity curve puts in evidence a slight oscillation in the derivative of the extrusion force with respect to the die

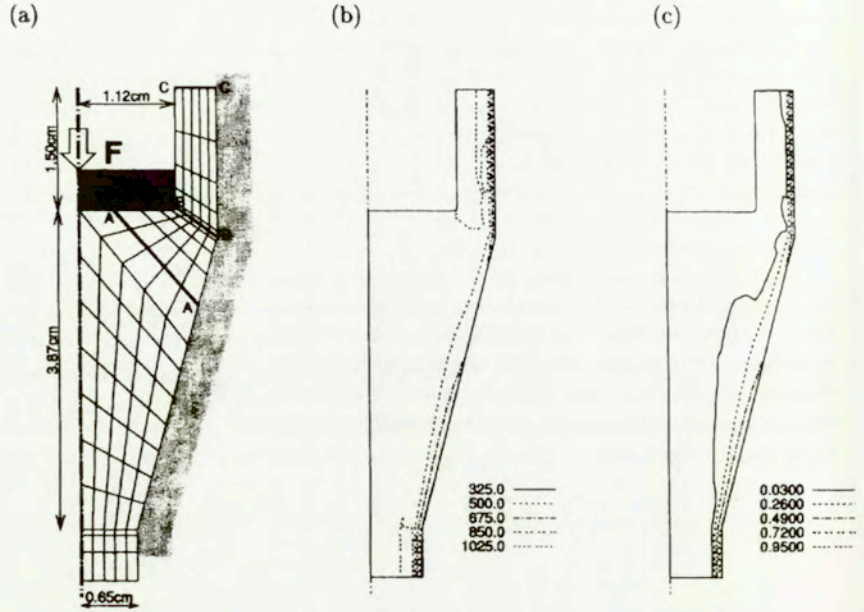

Figure 2.16 Combined direct-inverse extrusion: (a) layout, (b) temperature contours [°C], (c) contours of temperature sensitivity with respect to the matrix temperature $\overline{T}$ [°C/°C]

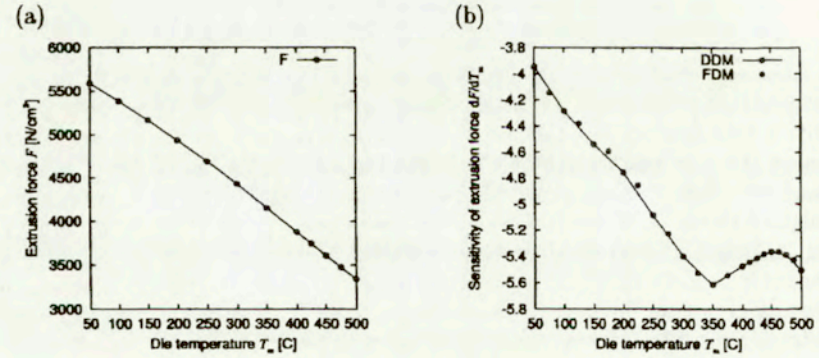

Figure 2.17 Combined direct-inverse extrusion: (a) Extrusion force and (b) its sensitivity with respect to the temperature of the matrix

temperature. This effect is produced by changes in the relative proportion of the two parts of the extrusion flow: forward and backward, whose variation with temperature is a clear consequence of the thermo-mechanical coupling. This in turn suggests the possibility (which should be investigated) of controlling such direct-backward extrusion process by regulating the die temperature through appropriate cooling. As a final point of discussion let us mention that the model assumed with Eq. (2.139) gave an increasing extrusion force with increasing temperatures. This unrealistic behaviour results from the assumed temperature dependent properties. Indeed, Eq. (2.139) foretells growing temperature-viscosity curves at constant rate of deformation for a certain range of the latter. Two opposite effects are contained in Eq. (2.139): a) the static yield stress σ_0 is a decreasing function of temperature and this softens the material at higher temperatures; but b) the material becomes more rate-sensitive (as n lowers) at higher temperatures, thus it hardens. This second effect does not prevail in practical cases, but it did within our firstly assumed fictitious material, with the puzzling results mentioned above. Although this facts may be not relevant from a practical point of view, it shows that the numerical model and its sensitivity module are able to put in evidence inconsistencies in the material data.

We can also make use of the sensitivity analysis to evaluate the stability of the numerical scheme, as it has been pointed out at the end of Section 2.3.3. Figs. 2.18(a) and (b) show the sensitivity isocurves of the temperature and the velocity module with respect to the coefficient '2'. We find that this coefficient has negligible effect on both variables analyzed. For the temperature field, the sensitivities are concentrated around the edge of the ram, in which the velocity gradient and hence the heat generation rate are at their maximum. On the rest of the domain the field is uniform and practically zero. The maximum sensitivity value (lower than unity) should be compared with the temperature range, which exceeds 700 C. In addition, it should be noticed that, according to the meaning of the sensitivity coefficients, such variation lower than 1 C would result upon a unity variation of the design parameter, whose value in this case is 2, therefore small temperature variations result from relatively high design variations (n.b.: in this argumentation we assume the linearization implied by the use of the first derivative: for a more rigorous analysis of this point, among other methods, second order sensitivity would be necessary). Similar observations can be formulated for the velocity module, which is shown in Fig. 2.18(b). Now the small effect on the temperature field is transmitted to the velocity solution by means of the coupling. The contours seem to reflect a quite non-uniform field, but we notice that the values are of six orders of magnitude lower than those of the velocity module (plotted in Fig. 2.18(c)). The contour patterns are somewhat similar to each other, especially in the fact that towards the lower exit both velocities and their sensitivity grow due to the incompressibility condition. However, in the rest of the domain the isocurves are quite different. We therefore conclude that the upwind scheme shows (at least for the present case) acceptable behaviour with respect to the coefficient '2'.

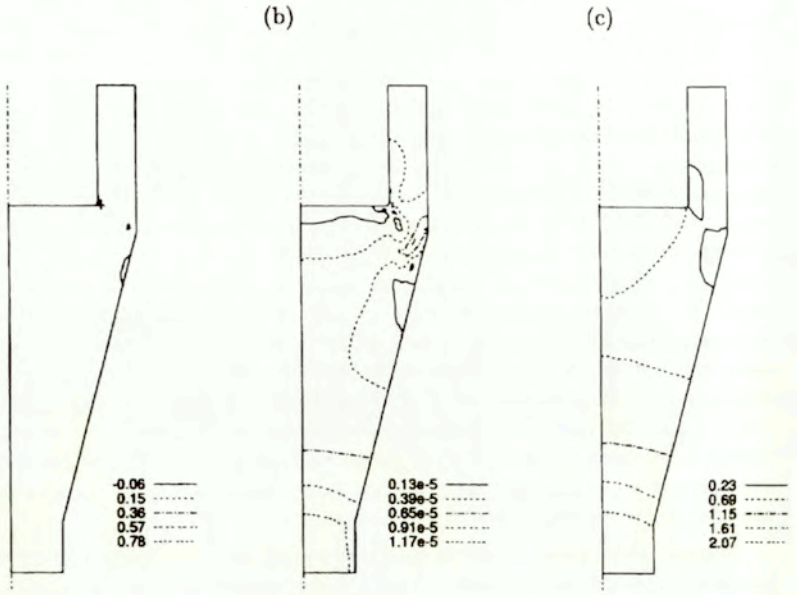

Figure 2.18 Combined direct-inverse extrusion: Sensitivity contours of (a) temperature [°C] and (b) velocity module [cm/s], with respect to numerical parameters of the upwind scheme, (c) velocity module contours [cm/s]

On the other hand, things are different if we consider the effect on the solution of the local mesh measure d (see Eq. (2.56)). We can see in Fig. 2.19(a) the contours of the temperature sensitivity. The values are more than two orders of magnitude bigger than in the previous case, and show more evidences of "wiggles" which do not appear in the temperature solution. Also the sensitivities are high for the velocity module, Fig. 2.19(b). We conclude that the local mesh size has a crucial effect in determining the amount of numerical dissipation that should be added within a given problem. We may notice that the meaning of this sensitivity is not the effect of refining the mesh, but that of varying (almost linearly, cf. Eq. (2.56)) the upwind parameter. If we plot the temperature and its sensitivity along certain mesh lines (cuts AA, BB and CC, Fig. 2.16(a)), we have a more clear picture of this effect. We observe a stable temperature solution with a wiggled temperature sensitivity, Fig. 2.20. It means that wiggles will appear if we do not introduce enough amount of numerical diffusivity, and that much attention should be paid to the way the local mesh size and hence the artificial viscosity are evaluated.

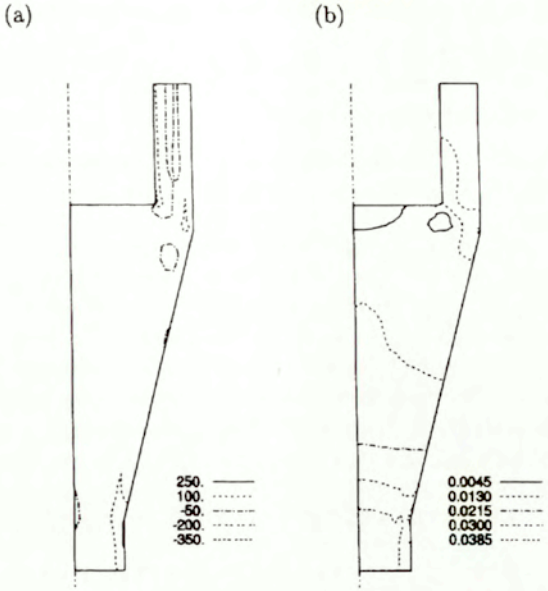

Figure 2.19 Combined direct-inverse extrusion: Sensitivity contours of (a) temperature [°C/cm] and (b) velocity module [1/s], with respect to the local mesh size d calculated for the upwind scheme

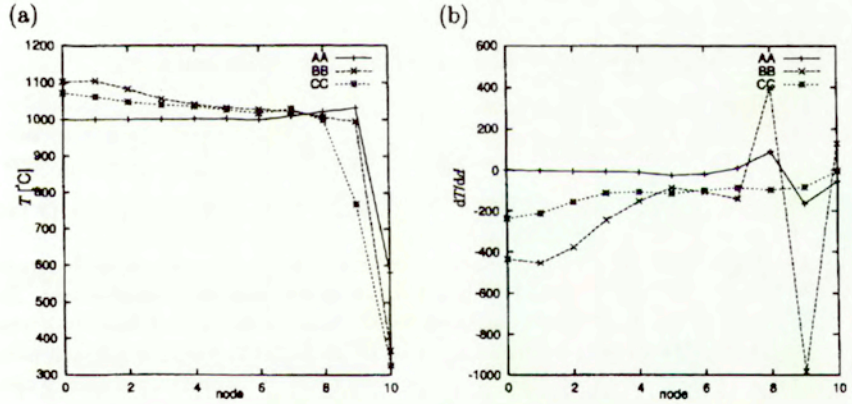

Figure 2.20 Combined direct-inverse extrusion: (a) Temperature and (b) its sensitivity with respect to the local mesh size d

2.4 Shape sensitivity for steady-state problems

2.4.1 General comments

Having successively presented the numerical model of metal forming processes and the way to assess its sensitivity with respect to material parameters, we now proceed in this section by deriving the corresponding equations for shape sensitivity. For the specific case of metal forming processes the results will have a great significance for optimization of the forming tools or, more generally, the process itself. Solving the equilibrium and sensitivity problems allows for the evaluation of cost functionals and their derivatives with respect to shape variables. By combining the procedures with an optimization algorithm the cost functionals may be minimized with respect to the shape parameters subject to given design restrictions. In this way the optimal shape for a given forming tool or for intermediate shapes in a multi-step forming process may be achieved.

As we already know quite well, different sensitivity methodologies can be adopted. Having such a wide range of options one should recall that the equations resulting from different approaches are theoretically equivalent but may have quite different numerical implementations. Taking into account all the particular features previously discussed e.g. in [70] and our personal experience we have opted for the direct differentiation method (DDM) based on the continuum approach (discretization carried out after design differentiation) combined with the domain parameterization approach (DPA). DDM has been presented and compared to its counterpart ASM in Section 2.3 when dealing with parameter sensitivity. The available methods for shape sensitivity will be discussed in a more general context in Appendix A.

2.4.2 The domain parameterization approach

Let us consider a generic response functional

$$\mathcal{G} = \int_{\Omega} g(\boldsymbol{\sigma}, \dot{\boldsymbol{\varepsilon}}, \mathbf{v}; \mathbf{h}) \, \mathrm{d}\Omega + \int_{\partial\Omega_v} g^{(v)}(\hat{\mathbf{v}}, \mathbf{t}; \mathbf{h}) \, \mathrm{d}(\partial\Omega_v) + \int_{\partial\Omega_\sigma} g^{(\sigma)}(\mathbf{v}, \hat{\mathbf{t}}; \mathbf{h}) \, \mathrm{d}(\partial\Omega_\sigma) \tag{2.140}$$

to be the subject of sensitivity analysis, where $\hat{\mathbf{v}}$ and $\hat{\mathbf{t}}$ are the specified velocity and traction vectors, imposed on the boundaries $\partial\Omega_v$ and $\partial\Omega_\sigma$, respectively. The integrand in Eq. (2.140) are assumed to be known functions of their indicated arguments. The general form (2.140) may be specified to describe selected point or (sub)domain design constraints or cost functions to be minimized during optimization. These conditions may be imposed on stress, strain and/or displacement components at selected points or averaged over some domains, or may concern such quantities as the rate of dissipation energy, heat generated, etc. The problem in the shape sensitivity analysis is to find the derivatives of the response

functionals with respect to shape parameters such as one of the coordinates of a given point, the radius of a roller or punch edge, the extrusion ratio, the angle of a die, etc. The design sensitivity expression in this case reads

$$\bar{\delta}G = \bar{\delta}\int_{\Omega} g \, \mathrm{d}\Omega + \bar{\delta}\int_{\partial\Omega_v} g^{(v)} \, \mathrm{d}(\partial\Omega_v) + \bar{\delta}\int_{\partial\Omega_\sigma} g^{(\sigma)} \, \mathrm{d}(\partial\Omega_\sigma) \tag{2.141}$$

in which the integration domain can clearly be design-dependent. Equation (2.141) involves expressions containing the design derivatives of the problem's basic variables (velocities, possibly pressure), dependent quantities (strains, stresses) and geometric characteristics (coordinates, Jacobian, area metrics). The design variations of the problem's variables are derived in Section 2.4.2.2 below. As it will be seen in Appendix A, regardless of which method (the DDM or the ASM) is used to compute the sensitivity expression (2.141), there still exist different possibilities to evaluate the shape design sensitivities. Among them, the DPA is by far the most popular technique in the numerical context, as explained in Appendix A; it will also be adopted below. Hence, the methodology to be employed can be symbolically denoted as DDM/DPA (the adjoint system method could also be used with no difficulty).

2.4.2.1 Transformation to reference configuration

To express the 'old' reference coordinates in terms of the design variables and the 'new' reference coordinates ${}^r\mathbf{x}$ we define the mapping $\mathbf{x} = \mathbf{x}({}^r\mathbf{x}; h_d)$ which enables us to calculate the Jacobian transformation matrix $\mathbf{F} = F_{ij} = \partial x_i/\partial {}^r x_j$ and to relate the volume and surface differential elements between the actual and the reference configurations as

$$\begin{aligned} \mathrm{d}\Omega &= \mathrm{d}\Omega^r J \\ \mathrm{d}(\partial\Omega) &= \mathrm{d}(\partial\Omega^r) J_\partial \end{aligned} \tag{2.142}$$

where $J = \|\mathbf{F}\|$, $J_\partial = \|\mathbf{F}^{-r}\mathbf{n}\|$ and $\mathbf{n}$ is the unit outward normal to the 'old' reference boundary.[1] Likewise, all the spatial derivatives in Eqs. (2.1) and (2.6) can be written in terms of the reference coordinates. In this way we obtain the equilibrium equation

$$\int_{\Omega^r} (\boldsymbol{\sigma}^{\mathrm{T}}\delta\dot{\boldsymbol{\varepsilon}} - \mathbf{f}^{\mathrm{T}}\delta\mathbf{v}) J \, \mathrm{d}\Omega^r - \int_{\partial\Omega_t} \mathbf{t}^{\mathrm{T}}\delta\mathbf{v} J_\partial \, \mathrm{d}(\partial\Omega^r) = 0 \tag{2.143}$$

where

$$\begin{aligned} \dot{\varepsilon}_{ij}(v_k) &= \frac{1}{2}\left(\frac{\partial v_i}{\partial {}^r x_k}\frac{\partial {}^r x_k}{\partial x_j} + \frac{\partial v_j}{\partial {}^r x_k}\frac{\partial {}^r x_k}{\partial x_i}\right) \\ \delta\left(\dot{\varepsilon}_{ij}(v_k)\right) = \dot{\varepsilon}_{ij}(\delta v_k) &= \frac{1}{2}\left(\frac{\partial(\delta v_i)}{\partial {}^r x_k}\frac{\partial {}^r x_k}{\partial x_j} + \frac{\partial(\delta v_j)}{\partial {}^r x_k}\frac{\partial {}^r x_k}{\partial x_i}\right) \end{aligned} \tag{2.144}$$

[1] A simplified notation $J = {}_r^t J$, etc. is used here since no confusion is likely to arise below regarding the definition of either C^r or C^t.

2.4.2.2 Design variation of problem's variables

In Section 2.3 we have dealt with sensitivities directly as derivatives of the different problem quantities with respect to the design variables. In shape sensitivity the same approach is valid, however it seems more intuitive to think of design variations meaning some variational-like perturbations in the parameters defining the actual shape of the problem-related quantities (including the arbitrary variations introduced to solve the equilibrium problem).

Within these design variations we distinguish an explicit part, only depending on the design variables, and an implicit part, which arise as a result of the explicit variations of other related quantities.[1]

Denoting a generic quantity as $f = f(\bar{\mathbf{q}}; \mathbf{h})$ we write the total design variation as the sum of both explicit an implicit parts

$$\bar{\delta} f = \underbrace{\frac{\partial f}{\partial \mathbf{h}} \delta \mathbf{h}}_{\partial f} + \underbrace{\frac{\partial f}{\partial \bar{\mathbf{q}}} \frac{\mathrm{d}\bar{\mathbf{q}}}{\mathrm{d}\mathbf{h}} \delta \mathbf{h}}_{\bar{\delta} f} \tag{2.145}$$

In some cases one of them may vanish. In particular, upon the introduction of design variations in Eqs. (2.1) and (2.6) the problem's variables (including now the geometric ones) undergo variations which can be expressed in terms of implicit and explicit components as

$$\begin{aligned} &\bar{\delta}\mathbf{x} = \partial \mathbf{x}\,, \quad \bar{\delta}\mathbf{F} = \partial \mathbf{F}\,, \quad \bar{\delta}\mathbf{v} = \tilde{\delta}\mathbf{v}\,, \\ &\bar{\delta} p = \tilde{\delta} p\,, \quad \bar{\delta}(\delta \mathbf{v}) = \partial(\delta \mathbf{v})\,, \quad \bar{\delta}(\delta p) = \partial(\delta p) \end{aligned} \tag{2.146}$$

Furthermore, by using Eqs. $(2.144)_1$ and $(2.146)_3$ we have the implicit variation of the strain rate given as

$$\bar{\delta}\dot{\varepsilon}_{ij} = \frac{1}{2}\left[\tilde{\delta}\left(\frac{\partial v_i}{\partial {}^{\tau}x_k}\right)\frac{\partial {}^{\tau}x_k}{\partial x_j} + \tilde{\delta}\left(\frac{\partial v_j}{\partial {}^{\tau}x_k}\right)\frac{\partial {}^{\tau}x_k}{\partial x_i}\right] = \frac{1}{2}\left(\frac{\partial(\tilde{\delta} v_i)}{\partial {}^{\tau}x_k}\frac{\partial {}^{\tau}x_k}{\partial x_j} + \frac{\partial(\tilde{\delta} v_j)}{\partial {}^{\tau}x_k}\frac{\partial {}^{\tau}x_k}{\partial x_i}\right) \tag{2.147}$$

so that

$$\bar{\delta}\dot{\varepsilon}_{ij} = \dot{\varepsilon}_{ij}(\bar{\delta}\mathbf{v}) \tag{2.148}$$

provided the variation is smooth enough to allow the permutation of the differentials. The explicit strain rate variation reads

$$\partial\dot{\varepsilon}_{ij} = \frac{1}{2}\left[\frac{\partial v_i}{\partial {}^{\tau}x_k}\partial\left(\frac{\partial {}^{\tau}x_k}{\partial x_j}\right) + \frac{\partial v_j}{\partial {}^{\tau}x_k}\partial\left(\frac{\partial {}^{\tau}x_k}{\partial x_i}\right)\right] \tag{2.149}$$

since, by Eq. $(2.146)_2$, $\bar{\delta}(\partial {}^{\tau}x_k/\partial x_j) = \partial(\partial {}^{\tau}x_k/\partial x_j)$. In Eq. (2.149) the expression for the design variation of the inverse Jacobian has to be developed on the basis

[1] In Appendix A the explicit part of the design variation will include everything not requiring the solution of a system of equations, such as the previously obtained sensitivities in an incremental process.

of that for the Jacobian itself. From the sometimes called Nanson's formula for the derivative of a matrix in terms of the derivative of its inverse,[2]

$$\frac{\partial F^{-1}_{ji}}{\partial h_d} = -F^{-1}_{jk}\frac{\partial F_{kl}}{\partial h_d}F^{-1}_{li} \tag{2.150}$$

we have

$$\partial\left(\frac{\partial {}^r x_i}{\partial x_j}\right) = -\frac{\partial {}^r x_i}{\partial x_k}\frac{\partial {}^r x_l}{\partial x_j}\partial\left(\frac{\partial x_k}{\partial {}^r x_l}\right) \tag{2.151}$$

In the case of the viscosity parameter, using Eqs. (2.3) and (2.4) results in

$$\begin{aligned}\bar{\delta}\mu &= \frac{\partial \mu}{\partial \dot{\bar{\varepsilon}}}\frac{\partial \dot{\bar{\varepsilon}}}{\partial \dot{\varepsilon}_{ij}}\bar{\delta}\dot{\varepsilon}_{ij}\\ \partial\mu &= \frac{\partial \mu}{\partial \dot{\bar{\varepsilon}}}\frac{\partial \dot{\bar{\varepsilon}}}{\partial \dot{\varepsilon}_{ij}}\partial\dot{\varepsilon}_{ij}\end{aligned} \tag{2.152}$$

and in the case of the stress tensor, by Eq. (2.2), in

$$\begin{aligned}\bar{\delta}\boldsymbol{\sigma} &= 2\,(\bar{\delta}\mu)\,\dot{\boldsymbol{\varepsilon}} + 2\,\mu\,\bar{\delta}\dot{\boldsymbol{\varepsilon}} - \boldsymbol{\Gamma}\,\bar{\delta}p\\ \partial\boldsymbol{\sigma} &= 2\,(\partial\mu)\,\dot{\boldsymbol{\varepsilon}} + 2\,\mu\,\partial\dot{\boldsymbol{\varepsilon}}\end{aligned} \tag{2.153}$$

Analogous to Eqs. (2.147) and (2.149) we can also write

$$\begin{aligned}\bar{\delta}\,(\delta\dot{\varepsilon}_{ij}) &= \frac{1}{2}\left[\bar{\delta}\left(\frac{\partial(\delta v_i)}{\partial {}^r x_k}\right)\frac{\partial {}^r x_k}{\partial x_j} + \bar{\delta}\left(\frac{\partial(\delta v_j)}{\partial {}^r x_k}\right)\frac{\partial {}^r x_k}{\partial x_i}\right]\\ \partial\,(\delta\dot{\varepsilon}_{ij}) &= \frac{1}{2}\left[\frac{\partial(\delta v_i)}{\partial {}^r x_k}\partial\left(\frac{\partial {}^r x_k}{\partial x_j}\right) + \frac{\partial(\delta v_j)}{\partial {}^r x_k}\partial\left(\frac{\partial {}^r x_k}{\partial x_i}\right)\right]\end{aligned} \tag{2.154}$$

2.4.2.3 Sensitivity expressions

We make use of the preceding relations to obtain the design variations of the equilibrium equation (2.143) in the form

$$\int_{\Omega^r}\bar{\delta}(\boldsymbol{\sigma}^{\mathrm{T}}\delta\dot{\boldsymbol{\varepsilon}}\,J)\,\mathrm{d}\Omega^r - \int_{\Omega^r}\bar{\delta}(\mathbf{f}^{\mathrm{T}}\delta\mathbf{v}J)\,\mathrm{d}\Omega^r - \int_{\partial\Omega^r_t}\bar{\delta}(\mathbf{t}^{\mathrm{T}}\delta\mathbf{v}J_\partial)\,\mathrm{d}(\partial\Omega^r) = 0 \tag{2.155}$$

which, by Eqs. (2.146), results in

$$\begin{aligned}&\int_{\Omega^r}[\bar{\delta}\boldsymbol{\sigma}^{\mathrm{T}}\delta\dot{\boldsymbol{\varepsilon}}\,J + \boldsymbol{\sigma}^{\mathrm{T}}\bar{\delta}(\delta\dot{\boldsymbol{\varepsilon}})J + \boldsymbol{\sigma}^{\mathrm{T}}\delta\dot{\boldsymbol{\varepsilon}}\,\partial J]\,\mathrm{d}\Omega^r - \int_{\Omega^r}[\partial(\mathbf{f}^{\mathrm{T}}J)\delta\mathbf{v} + \mathbf{f}^{\mathrm{T}}J\bar{\delta}(\delta\mathbf{v})]\,\mathrm{d}\Omega^r\\ &\quad - \int_{\partial\Omega^r_t}[\partial(\mathbf{t}^{\mathrm{T}}J_\partial)\delta\mathbf{v} + \mathbf{t}^{\mathrm{T}}J_\partial\,\bar{\delta}(\delta\mathbf{v})]\,\mathrm{d}(\partial\Omega^r) = 0\end{aligned} \tag{2.156}$$

or, separating the implicit from the explicit variations, in

$$\begin{aligned}&\left\{\int_{\Omega^r}\boldsymbol{\sigma}^{\mathrm{T}}\bar{\delta}(\delta\dot{\boldsymbol{\varepsilon}})J\,\mathrm{d}\Omega^r - \int_{\Omega^r}\mathbf{f}^{\mathrm{T}}\bar{\delta}(\delta\mathbf{v})J\,\mathrm{d}\Omega^r - \int_{\partial\Omega^r}\mathbf{t}^{\mathrm{T}}\bar{\delta}(\delta\mathbf{v})J_\partial\,\mathrm{d}(\partial\Omega^r)\right\}\\ &\quad + \int_{\Omega^r}[\bar{\delta}\boldsymbol{\sigma}^{\mathrm{T}}\delta\dot{\boldsymbol{\varepsilon}}\,J + \boldsymbol{\sigma}^{\mathrm{T}}\partial(\delta\dot{\boldsymbol{\varepsilon}})J + \boldsymbol{\sigma}^{\mathrm{T}}\delta\dot{\boldsymbol{\varepsilon}}\,\partial J]\,\mathrm{d}\Omega^r\\ &\quad - \int_{\Omega^r}\partial(\mathbf{f}^{\mathrm{T}}J)\delta\mathbf{v}\,\mathrm{d}\Omega^r - \int_{\partial\Omega^r}\partial(\mathbf{t}^{\mathrm{T}}J_\partial)\delta\mathbf{v}\,\mathrm{d}(\partial\Omega^r) = 0\end{aligned} \tag{2.157}$$

[2] which is trivially proved by considering the derivative of $\mathbf{F}\cdot\mathbf{F}^{-1} = \mathbf{I}$

We assume the arbitrary variation $\bar{\delta}(\delta \mathbf{v})$ to be a kinematically admissible velocity field satisfying the smoothness requirements needed to ensure continuous derivatives. Since $\bar{\delta}(\delta \dot{\boldsymbol{\varepsilon}})$ is assumed to be compatible with $\bar{\delta}(\delta \mathbf{v})$ we get from Eq. $(2.154)_1$ that $\bar{\delta}(\delta \dot{\boldsymbol{\varepsilon}}) = \dot{\boldsymbol{\varepsilon}}(\bar{\delta}(\delta \mathbf{v}))$. Therefore, $\bar{\delta}(\delta \dot{\boldsymbol{\varepsilon}})$ is compatible with $\bar{\delta}(\delta \mathbf{v})$ and, since $\bar{\delta}(\delta \mathbf{v})$ is arbitrary, the term in braces in Eq. (2.157) represents the equilibrium equation (2.1) and thus vanishes.

By separating the stress variations and using also Eq. $(2.146)_6$ we obtain

$$\int_{\Omega} \bar{\delta}\boldsymbol{\sigma}^{\mathrm{T}} \delta \dot{\boldsymbol{\varepsilon}}\, J \, \mathrm{d}\Omega^r = \int_{\Omega} \partial(\mathbf{f}^{\mathrm{T}} J) \delta \mathbf{v} \, \mathrm{d}\Omega^r + \int_{\partial\Omega} \partial(\mathbf{t}^{\mathrm{T}} J_s) \delta \mathbf{v} \, \mathrm{d}(\partial\Omega^r) - \int_{\Omega} [\partial \boldsymbol{\sigma}^{\mathrm{T}} \delta \dot{\boldsymbol{\varepsilon}}\, J + \boldsymbol{\sigma}^{\mathrm{T}} \partial(\delta \dot{\boldsymbol{\varepsilon}}) J + \boldsymbol{\sigma}^{\mathrm{T}} \delta \dot{\boldsymbol{\varepsilon}}\, \partial J] \, \mathrm{d}\Omega^r \tag{2.158}$$

Similarly, we perform the design variation on the incompressibility condition (2.6) to get

$$\int_{\Omega^r} \left(\bar{\delta} \dot{\boldsymbol{\varepsilon}}^{\mathrm{T}} \boldsymbol{\Gamma}\, \delta p\, J + \dot{\boldsymbol{\varepsilon}}^{\mathrm{T}} \boldsymbol{\Gamma}\, \bar{\delta}(\delta p)\, J + \dot{\boldsymbol{\varepsilon}}^{\mathrm{T}} \boldsymbol{\Gamma}\, \delta p\, \partial J \right) \mathrm{d}\Omega^r = 0 \tag{2.159}$$

in which the second term vanishes by Eq. (2.6). By applying Eqs. $(2.146)_2$ and (2.148), Eq. (2.159) yields

$$\int_{\Omega^r} \dot{\boldsymbol{\varepsilon}}^{\mathrm{T}} (\bar{\delta}\mathbf{v}) \boldsymbol{\Gamma}\, \delta p\, J \, \mathrm{d}\Omega^r = - \int_{\Omega^r} \partial \dot{\boldsymbol{\varepsilon}}^{\mathrm{T}} \boldsymbol{\Gamma}\, \delta p\, J \, \mathrm{d}\Omega^r - \int_{\Omega^r} \dot{\boldsymbol{\varepsilon}}^{\mathrm{T}} \boldsymbol{\Gamma}\, \delta p\, \partial J \, \mathrm{d}\Omega^r \tag{2.160}$$

2.4.3 Discretization

We now proceed to evaluate different terms resulting from the combined solution of Eqs. (2.158) and (2.160) after the finite element expansion. It can be a matter of discussion whether to attempt analytical differentiation of each term (and thus, the matrices), or to use a central difference approach as suggested in a different context in [17], at least for those terms which may involve differentiation of complicated expressions. In the cited paper, although only linear problems were under discussion, the central difference scheme for the evaluation of the equivalents of $\partial\bar{\mathbf{Q}}$ and $\partial\mathbf{K}^{(s)}\bar{\mathbf{q}}$ (cf. Eq. (2.27), which correspond to the right-hand side of the equation system (2.158) and (2.160)) was preferred. In our case, however, we see no reason to avoid analytical differentiation of the expressions, either in the discretized or in the continuous form. It is a known fact that one of the main drawbacks of the finite difference approach is the requirement to properly choose the size of the adopted perturbation, which should meet two opposite error criteria of being neither too large nor too small, in order to avoid numerical differentiation and truncation errors, respectively. This holds true if applied 'externally', that is by solving twice a perturbed problem and calculating afterwards a finite difference approximation to the derivative, as well as in the case described in the quoted paper, where only some terms are numerically differentiated, the rest being differentiated analytically. It is also necessary to keep track of the mapping to get the perturbed terms from a perturbation in the design parameter. This means no saving concerning the necessary information

that must be available, in comparison with the case where the explicit variations are analytically calculated. Moreover, as shown in what follows, analytical differentiation leads to matrices built in analogy with those of the analysis phase. Thus, the approach is straightforward to implement.

Having discretized the analysis problem we have the variables expressed by Eqs. (2.7). By using Eqs. (2.148) and $(2.152)_1$ together with the constitutive law (2.2) we write Eq. $(2.153)_1$ in the discrete form as

$$\begin{aligned}\bar{\delta}\boldsymbol{\sigma} &= \bar{\delta}(2\mu\mathbf{B}\dot{\mathbf{q}}) + \bar{\delta}p\,\boldsymbol{\Gamma}^{\mathrm{T}} = 2\bar{\delta}\mu\mathbf{B}\,\dot{\mathbf{q}} + 2\mu\mathbf{B}\bar{\delta}\dot{\mathbf{q}} + \bar{\delta}p\,\boldsymbol{\Gamma}^{\mathrm{T}} \\ &= 2\left(\mathbf{B}\,\dot{\mathbf{q}}\frac{\partial\mu}{\partial\dot{\boldsymbol{\epsilon}}} + \mu\,\mathbf{I}\right)\mathbf{B}\bar{\delta}\dot{\mathbf{q}} + \bar{\delta}p\,\boldsymbol{\Gamma}^{\mathrm{T}}\end{aligned} \tag{2.161}$$

Moreover, we have from the discretization assumptions, cf. Eqs. (2.7) and (2.13)

$$\begin{aligned}\delta\mathbf{v} &= \boldsymbol{\phi}\,\delta\dot{\mathbf{q}} \\ \delta\dot{\boldsymbol{\epsilon}} &= \mathbf{B}\,\delta\dot{\mathbf{q}} \\ \delta p &= \hat{\mathbf{B}}\,\delta\bar{\mathbf{p}}\end{aligned} \tag{2.162}$$

which, inserted into Eqs. (2.158) and (2.160), yield

$$\begin{aligned}&\mathbf{K}_{(\mu)}\bar{\delta}\dot{\mathbf{q}} + \int_{\Omega^r}\mathbf{k}_0\dot{\mathbf{q}}\frac{\partial\mu}{\partial\dot{\mathbf{q}}}J\,\mathrm{d}\Omega^r\bar{\delta}\dot{\mathbf{q}} + \mathbf{K}^{\mathrm{T}}_{(p)}\bar{\delta}p \\ &\quad= \int_{\Omega^r}\boldsymbol{\phi}^{\mathrm{T}}\partial(\mathbf{f}J)\,\mathrm{d}\Omega^r + \int_{\partial\Omega^r_t}\boldsymbol{\phi}^{\mathrm{T}}\partial(\mathbf{t}J_s)\,\mathrm{d}(\partial\Omega^r) \\ &\quad\quad- \int_{\Omega^r}2\mathbf{B}^{\mathrm{T}}\left[(\partial\mu)\mathbf{B} + \mu\partial\mathbf{B}\right]\dot{\mathbf{q}}J\,\mathrm{d}\Omega^r \\ &\quad\quad- \int_{\Omega^r}2\mu(\partial\mathbf{B})^{\mathrm{T}}\mathbf{B}\,\dot{\mathbf{q}}\,J\,\mathrm{d}\Omega^r - \int_{\Omega^r}2\mu\,\mathbf{B}^{\mathrm{T}}\mathbf{B}\,\dot{\mathbf{q}}\,\partial J\,\mathrm{d}\Omega^r \\ &\quad\quad- \int_{\Omega^r}\left[(\partial\mathbf{k}_{(p)})^{\mathrm{T}}J + \mathbf{k}^{\mathrm{T}}_{(p)}\,\partial J\right]\,\mathrm{d}\Omega^r\,\dot{\mathbf{q}}\end{aligned} \tag{2.163}$$

and

$$\mathbf{K}_{(p)}\bar{\delta}\dot{\mathbf{q}} = -\int_{\Omega^r}\left[(\partial\mathbf{k}_{(p)})J + \mathbf{k}_{(p)}\,\partial J\right]\,\mathrm{d}\Omega^r\,\dot{\mathbf{q}} \tag{2.164}$$

In the above system we recognize the tangent matrix $\mathbf{K}^{(T)}$ of the equilibrium analysis problem (Eqs. (2.30), (2.33) and (2.35)). Moreover, the right-hand side can be computed by using products of the already calculated matrices with the new matrices $\partial\mathbf{B}$ and $\partial\mathbf{k}_{(p)}$ formed analogously to the sub-matrices entering $\mathbf{K}^{(T)}$, so that

$$\begin{aligned}\partial\dot{\boldsymbol{\epsilon}} &= (\partial\mathbf{B})\dot{\mathbf{q}} \\ \partial\mathbf{k}_{(p)} &= \hat{\mathbf{B}}^{\mathrm{T}}\boldsymbol{\Gamma}^{\mathrm{T}}\partial\mathbf{B}\end{aligned} \tag{2.165}$$

In comparison with the matrices $\mathbf{B}$ and $\mathbf{k}_{(p)}$, cf. Eqs. (2.13) and $(2.22)_2$, respectively, the components of the inverse Jacobian matrix have now been replaced by their explicit variation obtained from Eq. (2.151). The terms containing explicit variations of the external forces or surface traction are to be calculated from the appropriate expressions defining them.

The last step to complete the derivation of the expression for $\bar{\delta}\mathbf{q}$ is to define the mapping $\mathbf{x} = \mathbf{x}(\boldsymbol{\zeta}, \mathbf{h})$, which enables us to calculate $\partial\mathbf{x} = (\partial\mathbf{x}/\partial\mathbf{h})\bar{\delta}\mathbf{h}$, from which the variations of any other geometric quantity can be obtained.[1] There are different ways to solve this problem. Probably the most natural one is to divide the domain into as many so-called master elements as to completely define the discretized domain and the possible design variations. These elements, which may contain from one to several finite elements each, connect the master nodes. The mapping can be defined by the use of shape functions. By means of the inverse transformation we find the native coordinates $\boldsymbol{\zeta}$ of every node in each parent element, and after checking that the point belongs to the element we evaluate the shape functions and recover the nodal coordinates as a linear combination of the master node coordinates. Denoting by $\mathbf{X}_i$ the vector containing the ith coordinate of the master nodes we have

$$x_i = \boldsymbol{\phi}^M(\boldsymbol{\zeta})\mathbf{X}_i = \phi_{ii}^{M(s)}(\boldsymbol{\zeta}(\mathbf{x}))X_i^s \qquad \text{(sum on } s\text{)} \tag{2.166}$$

with $s = 1, 2, \ldots, S_M$, S_M being the number of master nodes and $\boldsymbol{\phi}^M$ the interpolating functions of the parent element.

The explicit variation of the jth nodal coordinate then becomes

$$\partial x_j = \boldsymbol{\phi}^M(\boldsymbol{\zeta})\,\partial\mathbf{X}_i\,\delta_{ij} \tag{2.167}$$

Next, we have to find an expression for the explicit variations $\partial\mathbf{X}_i$ in terms of the design parameter variations. The actual form of this relation will depend on the design parameter, which may affect the coordinates of either one master point only or several of them (such as an angle, etc.). The simplest situation is when the design parameter coincides with just one nodal coordinate, say the $\underline{k}$th, of the $\underline{t}$th master node, $h = X_{\underline{k}}^{\underline{t}}$, so that $\partial X_i^s = \delta_{i\underline{k}}\,\delta_{\underline{t}}^s\bar{\delta}h$. We may also have a more elaborate relation. For example, if the roller radius ρ is assumed to be the design parameter in a plane rolling operation (as it will be in the second example below), and the imposed reduction in thickness is kept constant, then the master nodes are defined as remaining on the roller surface under the design variations, with an additional constraint, e.g. the requirement that they have only horizontal, vertical or radial coordinate variation ($\partial X_2^s = 0$, $\partial X_1^s = 0$, $\partial\theta^s = 0$, respectively, where $\theta^s = \arcsin((X_1^s - x_{1C})/\rho)$ and $s = 1, 2, \ldots, S_M$, see Fig. 2.21). Because of the restriction of the constant reduction in thickness, assuming that x_1 is the rolling direction, the coordinate of the center of the roller will have the variations

$$\begin{aligned} \partial x_{1C} &= 0 \\ \partial x_{2C} &= \bar{\delta}h \end{aligned} \tag{2.168}$$

For the master nodes placed on the roller surface we may calculate the variations ∂X_i^s by using a transformation to polar coordinates. Considering the case of $\partial X_2^s = 0$, we have this condition ensured by the relation

$$\rho\cos\theta^s + \delta\rho = (\rho + \delta\rho)\cos(\theta^s + \delta\theta^s), \quad s = 1, 2, \ldots, S_M \tag{2.169}$$

[1] We denote by $\boldsymbol{\zeta}$ the parent element coordinates in the isoparametric transformation. They are here equivalent to the more general concept of the reference coordinates ${}^r\mathbf{x}$ used so far.

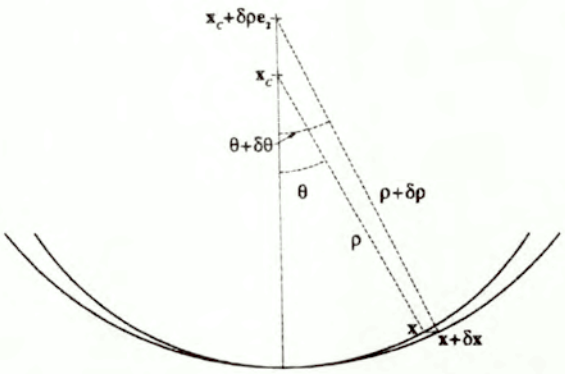

Figure 2.21 Nodal coordinates of the roller surface as a function of the roller radius

from which we obtain $\delta\theta^s$. Then, the horizontal variation of the nodal coordinates reads

$$\partial X_1^s = (\rho + \delta\rho)\sin(\theta^s + \delta\theta^s) - \rho\sin\theta^s \tag{2.170}$$

For $s = \underline{s}$ such that $\theta^{\underline{s}} = 0$, we get, by Eq. (2.169), $\delta\theta^{\underline{s}} = 0$. Then, the condition $\partial X_1^{\underline{s}} = 0$ results from Eq. (2.170).

Up to this point, the interpolating (i.e. shape) functions of the design element have not been discussed. A first, quite obvious and natural option is to use the same functions as those used in the isoparametric finite elements. However, for some implementational reasons, alternative shape functions for the design elements have been introduced. The need for such development arises because it is necessary to determine to which design element a given node belongs, given its nodal coordinates. Once this question is solved the "local coordinates" of the node within the design element are calculated, which finally allows to calculate their derivatives with respect to the design-element nodal coordinates, $\partial x_i/\partial X_j$. But for some non-rectangular domains it may be difficult to determine to which element belong nodes laying in between two design elements. For this reason a set of shape functions have been proposed, which assures straight lines to be transformed (mapped) into straight lines. Such mapping is illustrated in Fig. 2.22, where A, B, C and D are the middle points of the element sides. Every point in the quadrilateral has local coordinates in the interval $(-1, 1)$, while those located on any side have one coordinate constant equal to either 1 or -1. Still another set of shape functions based on bi-spline interpolation will be presented in Section 2.5.3, which allows a more efficient class of design variables, including angles in addition to nodal coordinates.

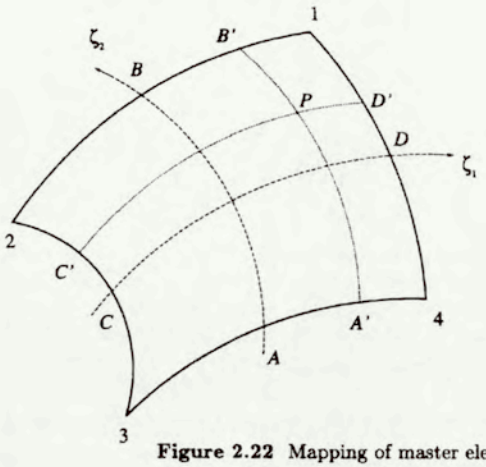

$$\zeta_{1P} = \frac{\overline{AA'}}{\overline{A4}} = \frac{\overline{BB'}}{\overline{B1}}$$

$$\zeta_{2P} = \frac{\overline{CC'}}{\overline{C2}} = \frac{\overline{DD'}}{\overline{D1}}$$

Figure 2.22 Mapping of master elements

2.4.4 Analytical illustrations

Before we continue with computational illustrations, we shall discuss two simple analytical examples of shape sensitivity analysis. First, we recall the results obtained for non-shape parameter sensitivity (see Section 2.3.4 for the pure shear deformation and free forging cases, respectively). In the first example we consider the effect of changing the workpiece height H while keeping the imposed velocity $\bar{v}_1$ constant. Making use of Eqs. (2.114)–(2.118) we compute the derivatives with respect to the design variable H as

$$\frac{\mathrm{d}\dot{\varepsilon}_{xy}}{\mathrm{d}H} = -\frac{\bar{v}_1}{H^2}, \quad \frac{\mathrm{d}\dot{\bar{\varepsilon}}}{\mathrm{d}H} = -\frac{\bar{v}_1}{\sqrt{3}H^2} \tag{2.171}$$

$$\frac{\mathrm{d}\mu}{\mathrm{d}H} = \frac{1}{\sqrt{3}\bar{v}_1}\left[\sigma_0 + \left(1 - \frac{1}{n}\right)\left(\frac{\bar{v}_1}{\gamma\sqrt{3}H}\right)^{\frac{1}{n}}\right] \tag{2.172}$$

whereas

$$\Omega = HL, \qquad \frac{\mathrm{d}\Omega}{\mathrm{d}H} = L \tag{2.173}$$

The above relationships allow us to calculate the sensitivity of the deformation energy rate as

$$\frac{\mathrm{d}G}{\mathrm{d}H} = 4\frac{\mathrm{d}\Omega}{\mathrm{d}H}\mu\dot{\varepsilon}_{xy}^2 + 4\Omega\left(\frac{\mathrm{d}\mu}{\mathrm{d}H}\dot{\varepsilon}_{xy}^2 + \mu\frac{\mathrm{d}\dot{\varepsilon}_{xy}^2}{\mathrm{d}H}\right) \tag{2.174}$$

Free forging solution sensitivity with respect to the billet height H is considered next.

By combining Eqs. (2.128) and (2.132) we observe that

$$\frac{\mathrm{d}\dot{\varepsilon}_{ij}}{\mathrm{d}H} = 0 \tag{2.175}$$

because, as results from Eq. (2.132), for the constant load imposed the punch velocity depends linearly on the billet height H. This means that the strain rate will also be constant. We similarly find that the viscosity μ is not sensitive to changes in the billet height H, which, together with the previous result, confirms the validity of Eq. (2.133) also for this design variable, since by Eq. (2.123) the stresses do not depend on H.

Finally, the expression for the deformation energy reads

$$G = \int_{\Omega_0} \sigma_y \dot{\varepsilon}_y J \, \mathrm{d}\Omega_0 \tag{2.176}$$

where $J = \Omega/\Omega_0 = H/H_0$ is the Jacobian transforming the actual to the reference configuration. In Eq. (2.176), this is the only quantity that depends on H, and hence the deformation energy functional sensitivity is given only by the change in the integration area, i.e.

$$\frac{\mathrm{d}G}{\mathrm{d}H} = \sigma_y \dot{\varepsilon}_y \frac{\mathrm{d}J}{\mathrm{d}H}\Omega_0 = -t\gamma \left(\frac{\sqrt{3}}{2}t + \sigma_0\right)^n \frac{\sqrt{3}}{2}L \tag{2.177}$$

If we consider, instead, the billet width as the design variable, then we have, for a constant load F, a uniformly distributed force, which is inversely proportional to the design variable, $t = F/L$. Combining Eqs. (2.131) and (2.129) we have

$$\dot{\varepsilon}_y = -\gamma \frac{\sqrt{3}}{2}\left(\frac{\sqrt{3}F}{2L} + \sigma_0\right)^n \tag{2.178}$$

Then the sensitivity reads

$$\frac{\mathrm{d}\dot{\varepsilon}_y}{\mathrm{d}H} = \frac{3}{4}n\gamma \left(\frac{\sqrt{3}F}{2L} + \sigma_0\right)^{n-1} \frac{F}{L^2} \tag{2.179}$$

From Eq. (2.134) we find the derivative of the viscosity

$$\frac{\mathrm{d}\mu}{\mathrm{d}H} = -\frac{\mu}{\dot{\varepsilon}_y}\frac{\mathrm{d}\dot{\varepsilon}_y}{\mathrm{d}L} \tag{2.180}$$

Unlike the previous example, we obtain a non-zero derivative for σ_y (cf. Eq. (2.123))

$$\frac{\mathrm{d}\sigma_y}{\mathrm{d}L} = -\frac{F}{L^2} \tag{2.181}$$

while the other components remain identically equal to zero. The Jacobian now reads

$$J = \frac{\Omega}{\Omega_0} = \frac{L}{L_0} \tag{2.182}$$

So the deformation energy functional sensitivity reads

$$\frac{\mathrm{d}G}{\mathrm{d}L} = \frac{\mathrm{d}\sigma_y}{\mathrm{d}L}\,\dot{\varepsilon}_y\,J\Omega_0 + \sigma_y\frac{\mathrm{d}\dot{\varepsilon}_y}{\mathrm{d}L}J\Omega_0 + \sigma_y\,\dot{\varepsilon}_y\frac{\mathrm{d}J}{\mathrm{d}L}\Omega_0 \tag{2.183}$$

which, after replacing the corresponding expressions, simplifies to

$$\frac{\mathrm{d}G}{\mathrm{d}L} = t\,\dot{\varepsilon}_y H n\left(1+\frac{2\sigma_o}{\sqrt{3}t}\right) \tag{2.184}$$

It is interesting to note that the first and third term of Eq. (2.183) (stress and domain variations) cancel out so that only the term corresponding to strain rate variations remains.

2.4.5 Computational illustrations

The procedure for shape sensitivity analysis is first illustrated with an extrusion problem in which the horizontal coordinate of the die corner (point P in Fig. 2.5) is subject to changes, thus causing a variation of the die angle. (The segment $\overline{PC}$ is, by definition, a straight line.) Next, a flat rolling problem is presented, in which the effect of changing the roller diameter while keeping the reduction in thickness unchanged is shown.

2.4.5.1 Extrusion

In the first example we consider an extrusion process in which the material is forced to pass through the extrusion die by the action of the ram, on which a constant force **F** acts. The layout is the same as presented in Fig. 2.5; the horizontal coordinate x_1 of point P is subject to design variations. (An alternative analysis can be performed by considering a constant imposed ram velocity—the applied force has then to be regarded as a function of the design variable.)

The velocities obtained appear to be almost insensitive to the design parameter, whereas the pressures depend on it in an almost linear fashion. Figures 2.23 and 2.24 show the sensitivity coefficients of the velocity module and pressure at selected points indicated in Fig. 2.5. This is followed by the contours of the effective strain rate, Fig. 2.25(a), and its sensitivity with respect to the x-coordinate of point P, Fig. 2.25(b), as well as of the effective stress, Fig. 2.26(a), and its sensitivity, Fig. 2.26(b).

The results are shown for the primary variables, Figs. 2.23 and 2.24, in terms of the design parameter h, where $x_1 = x_1^0 + h$, and x_1^0 is the given value of the coordinate x_1 of point P at the initial configuration from which other configurations corresponding to different values of the design parameter are obtained.

The results obtained by the DDM (full lines) are compared with the solution obtained by the central difference-based FDM (dotted lines). It is seen that the results compare very well. The sensitivity contours obtained by both methods show no noticeable difference. Comparing the respective maxima, we have for the strain rate and its sensitivity (cf. Fig. 2.25) that they do not coincide in the same

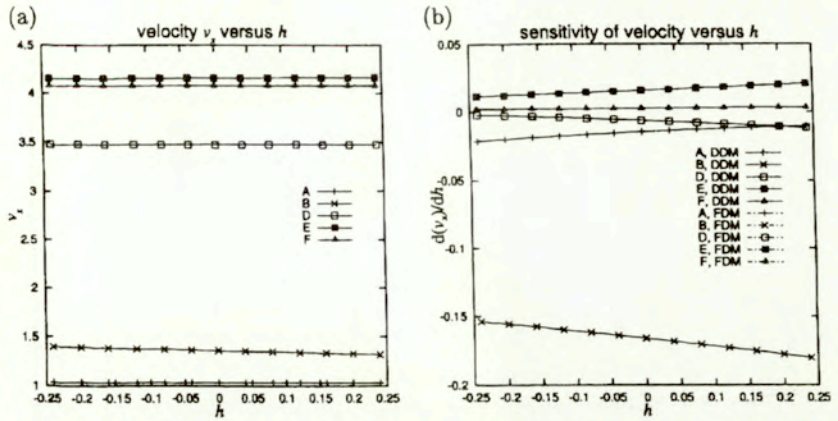

Figure 2.23 Variation of velocity at different points with h: (a) v versus h, (b) $\mathrm{d}v/\mathrm{d}h$ versus h

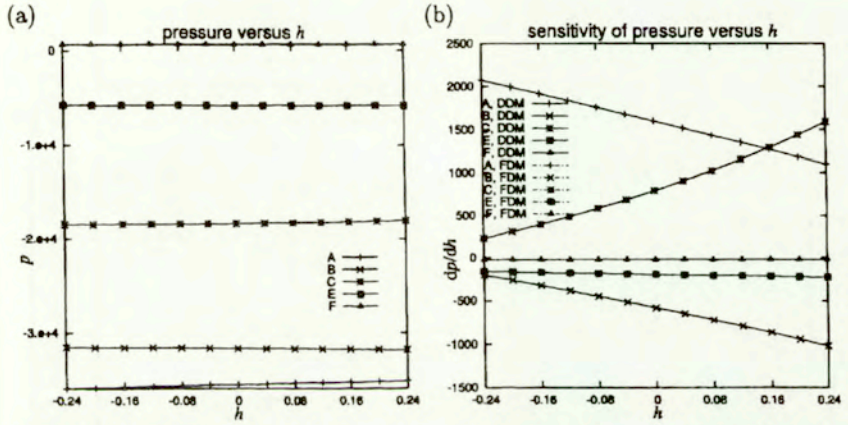

Figure 2.24 Variation of pressure at different points with h: (a) p versus h, (b) $\mathrm{d}p/\mathrm{d}h$ versus h

place, but the one for the strain rate sensitivity is in correspondence with the maximum strain rate gradient, which is concentrated in a small area and farther from the exit with respect to the maximum strain rate. Similar considerations can be stated for the effective stress and its sensitivity (cf. Fig. 2.26). However, it was necessary to reproduce very precisely the mapping of the design elements when the perturbed meshes were considered in the FDM. Small errors in this calculation have in this case a large effect on the results because different rules to generate the mesh following the variations of the design parameters are adopted in different parts of the analysis.

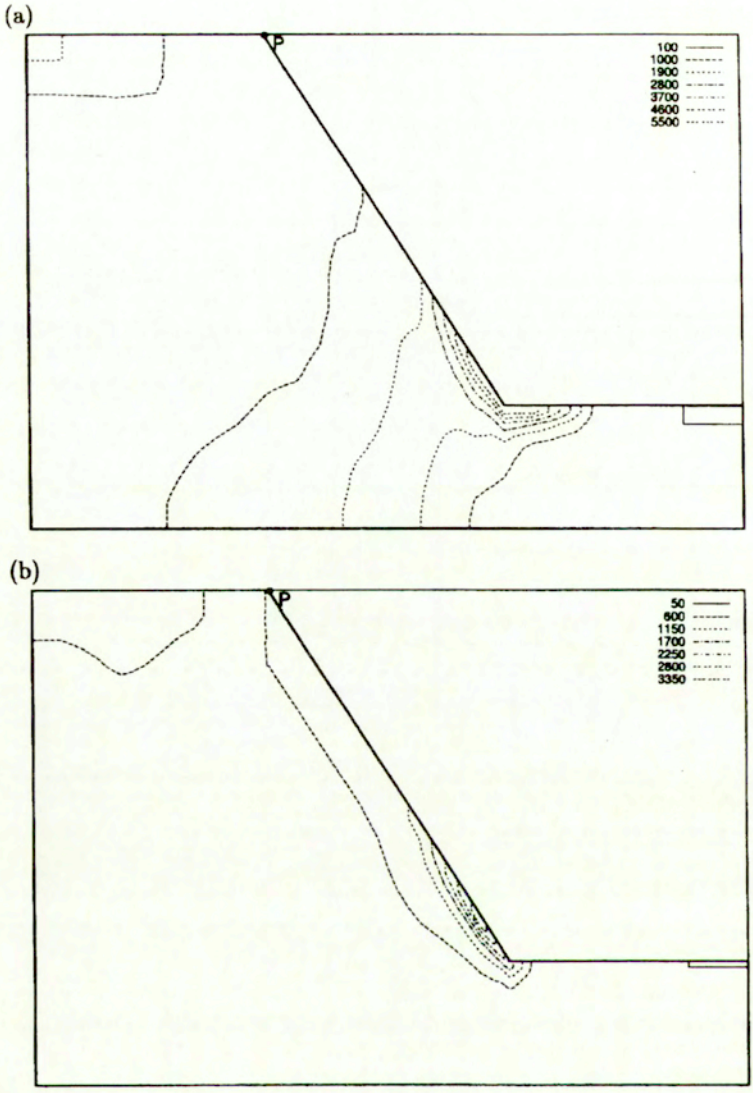

Figure 2.25 (a) Effective strain rate. (b) Effective strain rate sensitivity with respect to the x-coordinate of P

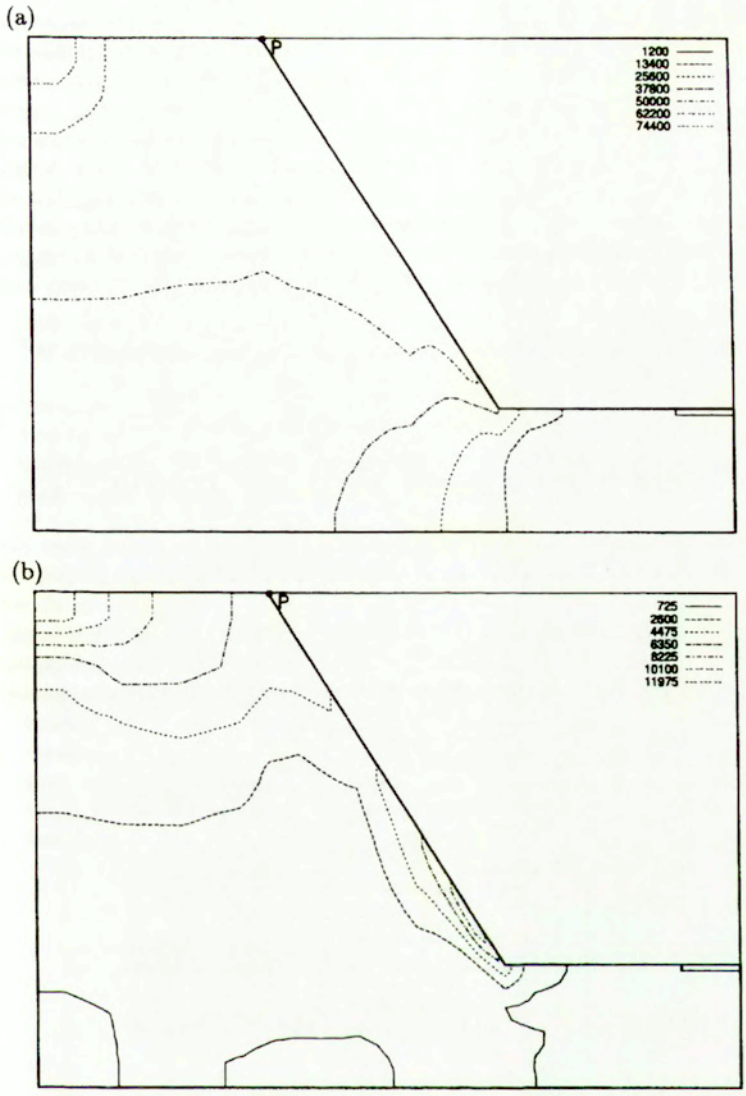

Figure 2.26 (a) Effective stress. (b) Effective stress sensitivity with respect to the x-coordinate of P

2.4.5.2 Rolling

A slab undergoing a reduction in thickness due to the action of two rollers shown in Fig. 2.27 is considered. The rollers impose a prescribed tangential velocity to the material in contact with them. As an illustration of the shape sensitivity formalism presented in Section 2.4.3, the roller radius is taken as the design parameter (although it is not likely to be so in practice). Either a constant angular velocity or a constant tangential velocity may be assumed in the design process. In any case we obtain an explicit variation of the velocity in terms of the design parameter, which will be reflected in the expressions for the explicit variation of the strain rate tensor and, therefore, of the viscosity and stress tensor. Thus, in Eq. (2.147) $\bar{\delta}\mathbf{v}$ should be written instead of $\tilde{\delta}\mathbf{v}$, and Eqs. $(2.146)_3$ and (2.149) read

$$\bar{\delta}\mathbf{v} = \tilde{\delta}\mathbf{v} + \partial\mathbf{v}$$

while

$$\partial\dot{\epsilon}_{ij} = \frac{1}{2}\left[\frac{\partial v_i}{\partial {}^{\tau}x_k}\,\bar{\delta}\left(\frac{\partial {}^{\tau}x_k}{\partial x_j}\right) + \frac{\partial v_j}{\partial {}^{\tau}x_k}\,\bar{\delta}\left(\frac{\partial {}^{\tau}x_k}{\partial x_i}\right)\right] + \frac{1}{2}\left[\frac{\partial(\partial v_i)}{\partial {}^{\tau}x_k}\frac{\partial {}^{\tau}x_k}{\partial x_j} + \frac{\partial(\partial v_j)}{\partial {}^{\tau}x_k}\frac{\partial {}^{\tau}x_k}{\partial x_i}\right]$$

From the algorithmic point of view, the resulting terms can be added when the imposed boundary conditions change in magnitude and/or direction during the design process. Alternatively, the explicit variation of the velocity can be shown to be equivalent to a non-zero 'imposed sensitivity' of the velocity. In other words, a preset value is assigned to it on the surface in contact with the roller, as happens with the velocity in the analysis problem. This imposed sensitivity is calculated

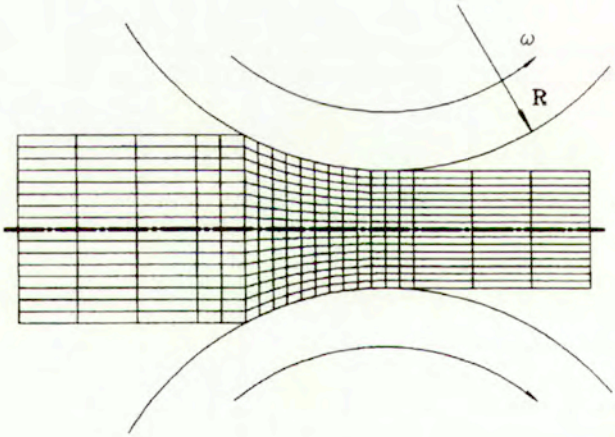

Figure 2.27 Layout of the rolling process

from geometrical considerations taking into account the mapping with which the mesh is modified as a function of the design parameter variations. In the present case, the additional assumptions to uniquely determine the mapping of the mesh to specific designs are: that the roller has a constant tangential velocity (therefore variations in the roller radius imply variations in its angular velocity) and the reduction in thickness (rolling ratio) is also kept constant. Considering the generality required by the FEM analysis programs it is possible to foresee the most common situations encountered in practice and to introduce for them the necessary parameters to define the geometry and the variations. Additionally, it may be preferable to define some general functions by a set of parameters and differentiate them in order to get the explicit variations.

In our reference configuration the roller diameter is 10cm, and the initial and final thickness amount 1.6cm and 1.0cm respectively. The material data from Paragraph 2.3.5.1 has been used.

The equivalent stresses and their sensitivities are plotted in Fig. 2.28. The isocurves show no noticeable difference whether calculated by direct differentiation or by the finite difference approach. Figures 2.29 to 2.31 show some analyzed functionals and their sensitivities versus the roller radius. We have in turn considered the overall distortion, the total deformation energy, the average deviation of the effective strain rate defined as

$$D_{\dot{\bar{\varepsilon}}} = \frac{1}{\Omega}\int_{\Omega}(\dot{\bar{\varepsilon}} - \dot{\bar{\varepsilon}}^{*})^2 \, \mathrm{d}\Omega \quad \text{where} \quad \dot{\bar{\varepsilon}}^{*} = \frac{1}{\Omega}\int_{\Omega}\dot{\bar{\varepsilon}} \, \mathrm{d}\Omega \tag{2.185}$$

and the local maxima of: the distortion rate, the effective strain rate and deformation energy, and finally the material flow rate (i.e. velocity integrated throughout a cross-section). Only some of the plots are shown, since the remaining have a similar pattern to that of the corresponding global or local quantity, or of another measure of the same type (e.g. components of the strain rate). It can be seen that the variation is smooth for the range of the roller radius r considered in the figures, and that better conditions are obtained when a bigger roller is used: less deformation energy, the material is less distorted, etc. The improvement is

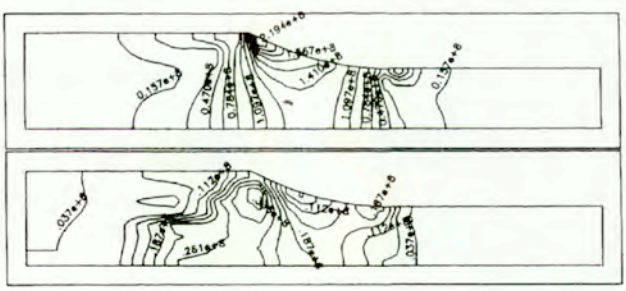

Figure 2.28 Equivalent stress and sensitivity

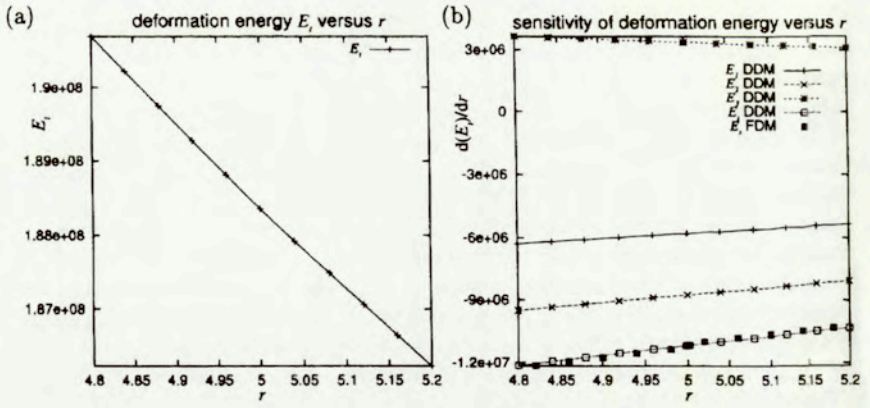

Figure 2.29 Deformation energy rate and sensitivity

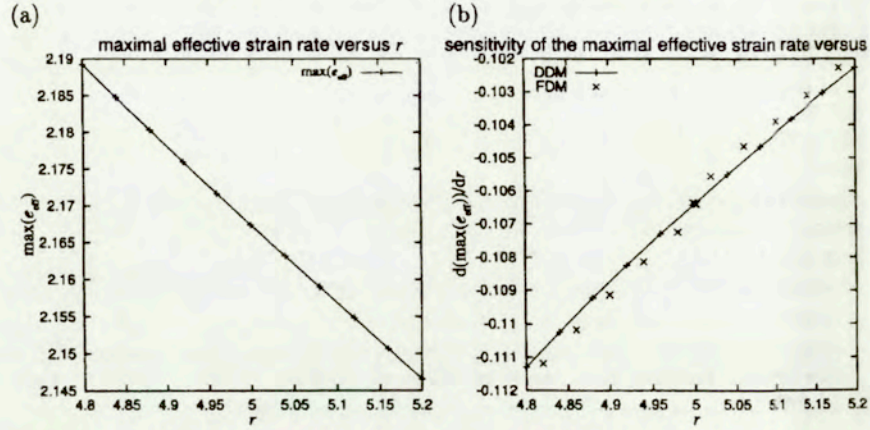

Figure 2.30 Maximal effective strain rate and sensitivity

seen for both global and local quantities. We can explain this fact by noting that the deformation is distributed over an area which grows with the radius. The larger the area, the more homogeneous the process. We can also note that the sensitivity of the deformation energy is calculated as the sum of three terms (see Fig. 2.29), corresponding to the derivative of the product of three functions,

$$\frac{\mathrm{d}E}{\mathrm{d}r} = \frac{\mathrm{d}}{\mathrm{d}r}\left[\int_{\Omega_0} \sigma_{ij}\dot{\varepsilon}_{ij} J \, \mathrm{d}\Omega_0\right] = E_1 + E_2 + E_3$$

with

$$E_1 = \int_{\Omega_0} \frac{\mathrm{d}\sigma_{ij}}{\mathrm{d}r}\dot{\varepsilon}_{ij} J \, \mathrm{d}\Omega_0$$

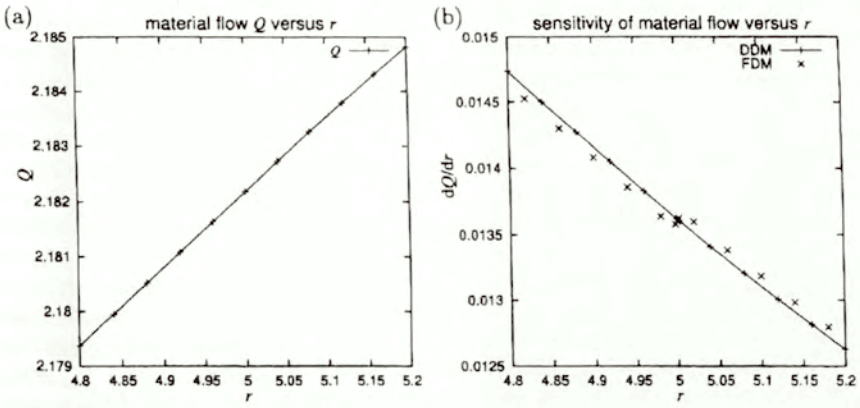

Figure 2.31 Material flow and sensitivity

$$E_2 = \int_{\Omega_0} \sigma_{ij} \frac{\mathrm{d}\dot{\varepsilon}_{ij}}{\mathrm{d}r} J \, \mathrm{d}\Omega_0$$

$$E_3 = \int_{\Omega_0} \sigma_{ij} \dot{\varepsilon}_{ij} \frac{\mathrm{d}J}{\mathrm{d}r} \, \mathrm{d}\Omega_0$$

Two of them, (E_1, E_2) involve implicit derivatives, while E_3 accounting for domain variations, is an explicit function of design. This term is positive since an increment in the roller radius makes the integration area bigger so that the variation of the inverse Jacobian is positive, whereas the product of strain times stress (which are kept constant for this term) is also positive. However, the first two terms and the overall are negative, what results in a decreasing total energy with increasing roller radius, as said. In the sensitivity plots we also see the results of the central finite differences approach (denoted FDM in the figures). They show some minor disagreements with the DDM solution. These differences are reduced when smaller increments are considered for the numerical derivative, which can be seen near the value of $r = 5$, where $\Delta r = 0.004$ (instead of 0.04) was taken for the finite difference verification. In addition, it is seen that the results calculated by finite differences match very well the analytical ones if they are considered as forward, rather than central differences. In fact, the meshes following each increment in the roller radius are generated in terms of the instantaneous mesh velocity of the present configuration multiplied by the roller radius increment. However, as can be seen from Eqs. (2.169) and (2.170), the mesh variations are a nonlinear function of the radius increment. The meshes are explicitly generated and this causes the differences between the finite difference and direct differentiation solutions.

Some final comments can be made about the numerical performance of the shape sensitivity analysis presented in this section. They are valid for both examples. Calculations have been carried out on a Sparc Station-2 (33 MHz). For a problem with 2100 degrees of freedom, as in the first example, each iteration of the analysis problem takes 57 s, of which 8 s correspond to the generation of the element matrices for the direct iteration scheme. However, when the Newton–Raphson method is applied, this time grows to 14 s. The system of equations is solved by the frontal method [65]. For a selected set of material parameters, which allows a fast convergence at the analysis stage ($\sigma_0 = 200, \gamma = 0.1, n = 1.5$, see Eq. (2.3) and cf. [6, 67]), the whole problem is solved in 718 s, of which only 15.5 correspond to the sensitivity stage (namely, the right-hand-side evaluation and its multiplication by the inverse matrix). The relative low cost of the sensitivity analysis is even more spectacular if materials with a lower strain rate hardening effect are considered. In such cases the number of iterations needed in the analysis problem is greatly increased and the Newton–Raphson method frequently does not converge. Therefore, direct iterations are performed, but still the tangent matrix can be used at the sensitivity stage, thus requiring an additional solution of the system of equations. In very extreme cases the iterative scheme is the only possible solution also for the sensitivity analysis. A detailed discussion of this aspect is beyond the scope of the present work. In the context of (non-shape) parameter sensitivity analysis it has been considered in Section 2.3.5, especially in Paragraph 2.3.5.2.

2.5 Shape optimization

2.5.1 Introductory comments

As it has been pointed out earlier, results from sensitivity analysis yield the derivatives of a design functional with respect to the design variables, either directly (ASM) or by building them from those of the problem variables (DDM). (Let us remind that still exists the possibility of calculating them by solving perturbed problems and obtaining the derivatives by finite differences, FDM, which in our understanding is unacceptable for practical applications). This fact suggests that the set formed by the functional and its gradient in the design space can be introduced into an optimization algorithm which, by solving the problem for different sets of the design parameters, can minimize the design functional subject to appropriate design constraints.

Although there are non-gradient-based optimization procedures available, it is obvious that their applicability is largely limited by the cost of each functional evaluation. When such functional evaluation involves the solution by finite elements of a nonlinear problem, such methods may be simply discouraging. Their lack of effectiveness is very clearly seen here in comparison with their gradient-based counterpart. For this reason shape optimization was practically not undertaken until the concept of sensitivity analysis —in particular to

shape parameters—, became more popular. The first works concern other areas, mainly structural analysis [84, 83] and thermal problems [106]. One such attempt, related to metal forming problems can be found in [75, 76]. In these works non-gradient optimization is performed, together with a gradient-based using FDM to calculate the numerical derivatives, In a similar context, that is, making no use of analytical shape sensitivity, optimum design of forging die shapes was presented in [54], which obviously involves a higher degree of complexity due to the transient nature of this process.

The importance of these results is out of discussion. If numerical simulation means a dramatic reduction in the number of necessary prototypes, now the use of optimization algorithms may lead to a sensible reduction in the number of necessary numerical simulations in order to obtain the optimum design. In addition, it provides a rigorous methodology to perform this task. A certain degree of automation and generality is required if the procedure aims to have practical applications. Besides, for such tool to be effective a series of conditions must still be fulfilled. First, the numerical model must reflect the key features of the process. Second, a complete sensitivity analysis must be carried out, which requires a proper description of the discretized domain in terms of (as few as possible) design parameters, and this in turn implies the definition of the functions by which each node depends on those design parameters. Next, the design functional and its gradient in the design space must be evaluated. The optimization algorithm will make use of these quantities to find a new trial for the optimum shape until the functional is minimized subject to some necessary design constraints which limit the trials of design sets. Let us notice that the proper definition of the design criterion and constraints still requires the advice of an expert. But now different functionals may be easily tested and minimized, compared their respective optima and their values and their behaviour at the optima of other functionals.

The lack of some of the above mentioned elements will probably deteriorate the performance of the optimization procedure. For this reason it is crucial to have a complete and consistent treatment of the whole problem. However, the idea of optimization is not new and does not involve special theoretical difficulties. Instead, once the analysis and the sensitivity stages are available, its application to optimization is straightforward, however the main difficulty may have been to achieve those tools. In the last years some works concerning shape optimization of metal forming processes have been presented, assuming the usage of advanced techniques for sensitivity analysis. In [66] the shape optimization of a 3D extrusion die is presented. Even if the tangent matrix is used to evaluate the sensitivity coefficients, the explicit derivatives with respect to the design variables are calculated by FDM, using the so-called 'discrete semi-analytical direct differentiation approach to sensitivity evaluation'. The authors analyze the effect of the perturbation size which, as expected, deserves special attention. In the reported work after analyzing perturbations ranging from 10^{-2} to 10^{-12} an area was found were apparently similar results are obtained for either backward, centered

and forward differences. However the optimum size of the perturbation seems to be different for each design variable. This fact further complicates the problem, and supports the use of analytical evaluation of the explicit derivatives, in the way it has been presented in Section 2.4. In addition, it is clear that the FDM implies more calculation time and results in an awkward code as compared with the analytical version. Concerning again forging, matrix shape optimization was presented in [44, 45, 46], and more recently in [25, 34]. Again the merits of such approaches are apparent, even if they did not get rid of finite difference-based explicit derivatives.

In what follows some results concerning extrusion die shape optimization are presented. They have been obtained connecting the formalism for shape optimization presented in Section 2.4 with two available optimization procedures [43, 95]. The DDM is used in connection with DPA for the shape sensitivity calculations. First, design variables are chosen. They determine a domain partition into so-called design elements (connecting design nodes, some of which contain the design variables as one or more of its coordinates), which are used to identify every point in the domain and to calculate explicit derivatives of geometric quantities with respect to the design variables. Such procedure (i) provides a way to describe any kind of shapes thus is applicable to any forming process and (ii) as seen in Section 2.4, carries out an analytical calculation of all the necessary derivatives, which assures their proper evaluation, as required by the optimization algorithm.

In addition to the bilinear elements used in Section 2.4.3, design elements with bispline interpolation functions are introduced, which allow for the use of angles as design variables, resulting in a more efficient mapping procedure. Different design functionals are considered and, as a result, it is shown that the final shape is highly dependent on the particular optimization criterion adopted.

2.5.2 Optimization algorithm

The optimum design is searched for by iteratively solving the analysis problem and (as its byproduct) the sensitivity problems at each design point. This information is used by the optimization algorithm to find a new set of design parameters aiming at minimizing the response functional, cf. Eq. (2.66).

$$\mathcal{G}=\int_0^t\left[\int_{\Omega(\mathbf{h})}G(\boldsymbol{\sigma}^{\mathrm{D}},\bar{\mathbf{q}};\mathbf{h})\,\mathrm{d}\Omega+\int_{\partial\Omega_v(\mathbf{h})}g(\bar{\mathbf{q}}_F,\mathbf{t};\mathbf{h})\,\mathrm{d}(\partial\Omega_v)+\int_{\partial\Omega_t(\mathbf{h})}h(\bar{\mathbf{q}},\mathbf{t}_F,\mathbf{h})\,\mathrm{d}(\partial\Omega_\sigma)\right]\mathrm{d}\tau \quad (2.186)$$

with respect to the design variables. Two optimization algorithms have been employed: the first one is based on the conjugate gradient method[43] and the second is the Schittkowski's algorithm[95] and both gave the same results.

The optimization problem we are to solve is stated mathematically as follows:

Find the vector of design variables $\mathbf{h} = \{h_1, ..., h_D\} \in \mathrm{R}^D$ that minimizes the objective functional (2.186) subject to

$$\begin{array}{ll} \Upsilon_a(\boldsymbol{\sigma}^{\mathrm{D}}, \bar{\mathbf{q}}; \mathbf{h}) = 0 & a = 1, ..., A \\ \Upsilon_b(\boldsymbol{\sigma}^{\mathrm{D}}, \bar{\mathbf{q}}; \mathbf{h}) \leq 0 & b = 1, ..., B \\ h_d^- \leq h_d \leq h_d^+ & d = 1, ..., D \\ \textit{Equilibrium} & \textit{equations} \end{array} \tag{2.187}$$

where h_d^-, h_d^+ are lower and upper bounds imposed on the design basis h_d, $d = 1, 2, ..., D$. Objective and constraint (referred to as performance) functionals in the above optimization formulation call for design sensitivity analysis.

The optimization algorithm can be summarized as follows:

0. initial estimate for $\mathbf{h}$
1. evaluation of $\mathcal{G}$ and $\dfrac{\mathrm{d}\psi}{\mathrm{d}\mathbf{h}}$
2. if $||\dfrac{\mathrm{d}\psi}{\mathrm{d}\mathbf{h}}|| \leq tol$ exit
3. calculation of $\Delta\mathbf{h}$
4. update $\mathbf{h}$: $\mathbf{h}^{(\mathrm{new})} = \mathbf{h}^{(\mathrm{old})} + \Delta\mathbf{h}$
5. go to 1.

2.5.3 Domain parameterization with bispline design elements

Following the methodology of the DPA, in order to define the mapping from the reference configuration to an actual design, defined as a point in the design space, the domain shape must be parametrized by a number of design variables in terms of which every point in the reference configuration can be associated to a point in the actual design. Specifically, the domain boundary must be interpolated in terms of the design variables.

In Section 2.4.3 the boundary shape was linearly interpolated between the design nodes, some of which contained the design variables as one (or more) of its coordinates. The mapping was then completed to define internal points by the use of bilinear design elements. In this section another boundary description and domain mapping is described. It consists of:

1) *Spline interpolation of the contour subject to design.* The boundary of the discretized domain must be described as a combination of straight lines and some higher order curves. To define each of them, the coordinates and possibly the angle with respect to a selected coordinate axis of a set of nodes is used. For such purpose cubic splines (which may be reduced trivially to a straight line segment) are very commonly used and defined by an appropriate set of nodal coordinates and angles with respect to a reference direction. These nodal coordinates and angles are thus the (natural) design variables. However, it may be sometimes useful to take the spline coefficients instead.

2) *Double-spline-interpolated 4×4-node design elements,* in terms of which it is possible to find the derivative of the coordinates of any point (finite element

discretization node) with respect to the nodal coordinates of the design element. It should be noticed that these nodal coordinates of the design element may not be independent. In fact, in order to get a smooth field of local coordinates the nodes which do not define a border may be calculated as linearly interpolated from the corner nodes.

1) Spline interpolation of the boundary subject to design.

The basic shape optimization problem may be formulated as that of obtaining the shape that minimizes a given cost functional. For different reasons, not all the boundary may be subject to optimization: most frequently some design constrains have to be met. On the other hand we have the problem of choosing the geometric variables that can describe the boundary upon design. Most probably, it will not be a good choice to use as design variables the coordinates of each of the boundary nodes arising from the finite element discretization. It is well known that optimization algorithms may become very slow and even have convergence problems for a large number of design variables. Moreover, such a large number may be not necessary if, additionally, the nodes on the border subject to optimal design are interpolated with sufficiently smooth functions which, in turn, are defined in terms of a few master nodes.

Any cubic spline segment involves the evaluation of four coefficients resulting from the fulfillment by the function of four conditions on its value or its derivatives at given points. Neighbouring segments must satisfy the continuity condition of the curve and of its first derivative. So, a simple way of assuring the conditions between segments and automatizing the addition of more segments in the description of the boundary under design is to take as design variables one of the spatial coordinates and its derivative with respect to the internal variable of the spline. In this way, when the boundary under design is described with only one spline segment, four design variables appear (some of which may be fixed by a design constraint). However, for every new added segment, although four more parameters enter, only two more design variables are added, because of the continuity conditions between spline segments. In addition, this set of variables allows us to find out the spline coefficients separately for each segment. The other coordinate may be chosen as linearly dependent on the spline variable.

For a generic segment we have thus a vector of design variables

$$\mathbf{h}^k = \{x_k, x'_k, x_{k+1}, x'_{k+1}\}$$

and we find the coefficients of the spline

$$\chi(\xi) = e_0 + e_1\xi + e_2\xi^2 + e_3\xi^3\,; \qquad -1 \le \xi \le 1$$

by stating that

$$x_k = \chi(-1)\,; \quad x'_k = \chi'(-1)\,; \quad x_{k+1} = \chi(1)\,; \quad x_{k+1} = \chi(1)$$

2) Interpolation inside the design element

In terms of the internal coordinates ξ, η we define the double spline functions

$$\Psi_x = a_1 + a_2\xi + a_3\eta + a_4\xi^2 + a_5\xi\eta + a_6\eta^2 + a_7\xi^3 + a_8\xi^2\eta + a_9\xi\eta^2 + a_{10}\eta^3 + a_{11}\xi^3\eta + a_{12}\xi^2\eta^2 + a_{13}\xi\eta^3 + a_{14}\xi^3\eta^2 + a_{15}\xi^2\eta^3 + a_{16}\xi^3\eta^3 \quad (2.188)$$

$$\Psi_y = b_1 + b_2\xi + b_3\eta + b_4\xi^2 + b_5\xi\eta + b_6\eta^2 + b_7\xi^3 + b_8\xi^2\eta + b_9\xi\eta^2 + b_{10}\eta^3 + b_{11}\xi^3\eta + b_{12}\xi^2\eta^2 + b_{13}\xi\eta^3 + b_{14}\xi^3\eta^2 + b_{15}\xi^2\eta^3 + b_{16}\xi^3\eta^3 \quad (2.189)$$

where $-1 \leq \xi, \eta \leq 1$, and the sixteen coefficients of each function are determined by the nodal coordinates at $\xi, \eta = \{-1, -\frac{1}{3}, \frac{1}{3}, 1\}$ For practical purposes the nodal coordinates may be mutually independent or, better, those which are unnecessary to describe the geometry may be calculated in terms of the other nodes. In this case the local coordinate field will be smoother and the finite element mesh will conserve its regular aspect.

The whole shape that is being optimized may be piecewise described by spline lines, as seen above. Each of these spline segments may correspond to one side of the design elements in which the whole domain can be subdivided. Then, the number of design elements is roughly determined by the number of segments needed to define the geometry with a given accuracy (plus a few more elements for those areas not subject to design). Most frequently, only one side (or none) of the design element will be a spline segment. The remaining three sides can be straight lines. In such an element we have to define the above Ψ_x and Ψ_y functions in order to relate the coordinates of each point contained in the element with the design variables via the nodal coordinates of the design element and the spline coefficients of the design-boundary segment corresponding to the design element. Having defined this mapping, the way the nodes change their position with design variations is uniquely determined, and we can calculate the derivatives $\mathrm{d}x_i/\mathrm{d}d_j$, which are needed to obtain the global sensitivity coefficients and, with them, the objective function gradients.

To specifically obtain these derivatives we proceed design-element wise as follows:

1) define a spline for the design element side subject to design in terms of the design variables which the design element connects, as shown above. The other coordinate (y in this case) is linearly interpolated within the internal variable ξ and does not enter the design variables. The other three sides of the design element are straight lines.

2) Define a double-spline in the design element. We need a set of sixteen points (x and y coordinates) from which we obtain two sets of sixteen constants. We take as reference points those located at $(\xi, \eta) = \{-1, -\frac{1}{3}, \frac{1}{3}, 1\}$ (Fig. 2.32). Points 1, 4, 13 and 16 are known. We obtain points 2, 3, 5, 8, 9 and 12 as linearly interpolated from the corner nodes. Points 14 and 15 are obtained by evaluating χ at $\xi = -\frac{1}{3}$ and $\xi = \frac{1}{3}$ respectively, and finally, points 6 and 10, and 7 and 11, by linear interpolation on the η direction between points 2 and 14, and 3 and 15 respectively.

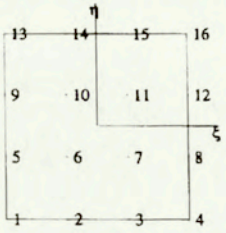

Figure 2.32 Design element

If we arrange the local coordinates and the interpolating functions in the vectors (see Fig. 2.32)

$$\boldsymbol{\xi} = \{-1, -\tfrac{1}{3}, \tfrac{1}{3}, 1, -1, -\tfrac{1}{3}, \tfrac{1}{3}, 1, -1, -\tfrac{1}{3}, \tfrac{1}{3}, 1, -1, -\tfrac{1}{3}, \tfrac{1}{3}, 1\} \tag{2.190}$$

$$\boldsymbol{\eta} = \{-1, -1, -1, -1, -\tfrac{1}{3}, -\tfrac{1}{3}, -\tfrac{1}{3}, -\tfrac{1}{3}, \tfrac{1}{3}, \tfrac{1}{3}, \tfrac{1}{3}, \tfrac{1}{3}, 1, 1, 1, 1\} \tag{2.191}$$

$$\boldsymbol{\psi} = \{1, \xi, \eta, \xi^2, \xi\eta, \eta^2, \xi^3, \xi^2\eta, \xi\eta^2, \eta^3, \xi^3\eta, \xi^2\eta^2, \xi\eta^3, \xi^3\eta^2, \xi^2\eta^3, \xi^3\eta^3\} \tag{2.192}$$

we can rewrite the double splines as

$$\Psi_x = a_i\psi_i\,, \qquad \Psi_y = b_i\psi_i\,, \qquad i = 1, 16 \tag{2.193}$$

Arranging accordingly the global coordinates in vectors $\mathbf{X}, \mathbf{Y}$, by evaluating the functions ψ_i at the points (ξ_j, η_j) we have[1]

$$\mathbf{X} = \mathbf{CA}\,, \qquad \mathbf{Y} = \mathbf{CB} \tag{2.194}$$

with $c_{ji} = \psi_i(\xi_j, \eta_j)$, from which

$$\mathbf{A} = \mathbf{C}^{-1}\mathbf{X}\,, \qquad \mathbf{B} = \mathbf{C}^{-1}\mathbf{Y} \tag{2.195}$$

Now we can calculate the derivative

$$\frac{\partial x}{\partial h_i} = \frac{\partial x}{\partial a_j}\frac{\partial a_j}{\partial X_k}\frac{\partial X_k}{\partial \chi_l}\frac{\partial \chi_l}{\partial e_m}\frac{\partial e_m}{\partial h_i} \tag{2.196}$$

where $\dfrac{\partial a_j}{\partial X_k} = (c^{-1})_{jk}$. We also notice that in this case $\dfrac{\partial y}{\partial h_i} = 0$.

It is worth to notice that for elements having all four sides straight, the above mapping reduces to the bilinear one described in Section 2.4.3.

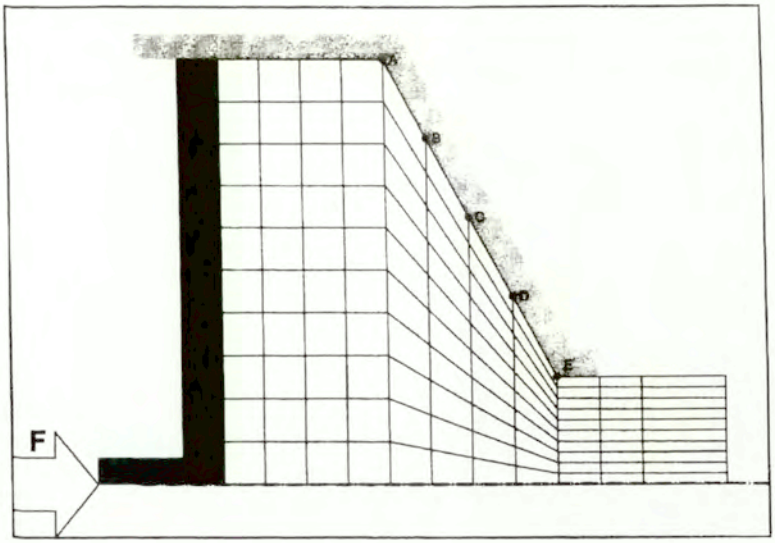

Figure 2.33 Layout of the extrusion process.

2.5.4 Computational illustrations

The shape optimization procedure is illustrated by finding the optimum design of an extrusion matrix, where the extrusion ratio is fixed. Optimization criteria of minimizing the deformation energy, the maximum strain rate and uniform rate of deformation are investigated. A layout of the problem is shown in Fig. 2.33, together with its discretization into finite elements. A constant velocity is imposed on the left boundary. The design variables are the x coordinates of some nodal points defining the matrix shape (marked A-D in the figure) and the slope on the die boundary at them. The shape sensitivity analysis of such problem within bilinear design elements has been presented in [12] (see Section 2.4.3). In that paper the die profile was supposed to be a straight line, so that only one design parameter (the horizontal coordinate of the upper die corner) was sufficient to define any geometry variation.

Using the flow approach we obtain the velocity, strain and stress solution. Further, for any given configuration the shape sensitivities may be obtained by application of the procedure presented in Section 2.4.3 for appropriately defined shape parameters.

On this basis, optimum shapes resulting from different design functionals and obtained using the bilinear design elements are first shown. Then, taking

[1] where the notation $\mathbf{A} = [a_i], \mathbf{C} = [c_{ij}], \mathbf{X} = [X_i]$, etc., has been adopted

one design functional, the effect of friction boundary conditions on the optimum shape is shown. Finally, optimum shapes are obtained with different number of design variables using both bilinear and bispline design elements.

1) Design functionals

The following functionals have been employed:

energy rate

$$\Psi_E = \int_\Omega \sigma_{ij}\dot{\varepsilon}_{ij}\, d\Omega \tag{2.197}$$

maximum local energy rate

$$\Psi_e = \max_\Omega(\tfrac{1}{2}\sigma_{ij}\dot{\varepsilon}_{ij}) \tag{2.198}$$

averaged effective strain rate deviation

$$\Psi_{D\dot{\varepsilon}} = \frac{1}{\Omega}\int_\Omega (\dot{\bar{\varepsilon}} - \dot{\bar{\varepsilon}}^*)^2\, d\Omega,\ \dot{\bar{\varepsilon}}^* = \frac{1}{\Omega}\int_\Omega \dot{\bar{\varepsilon}}\, d\Omega \tag{2.199}$$

maximum effective strain rate

$$\Psi_{\dot{\varepsilon}_l} = \max_\Omega(\dot{\bar{\varepsilon}}) \tag{2.200}$$

overall distortion rate

$$\Psi_D = \tfrac{1}{2}\int_\Omega \dot{\varepsilon}_{12}\, d\Omega \tag{2.201}$$

maximum distortion rate

$$\Psi_{\dot{\varepsilon}_{12}} = \max_\Omega(\dot{\varepsilon}_{12}) \tag{2.202}$$

The corresponding optimized die profiles are shown in Figs. 2.34 to 2.36.

Since the optimized profile is defined by a polygonal line joining the design points, we impose restrictions on the coordinates of every two neighbouring design points in order to avoid unrealistic situations which may appear during the optimization iterations and disturb the convergence process. Numbering the design nodes from left to right and taking only the horizontal components x_i as design variables, we should have $x_{i+1} \geq x_i$.

Table 2.1 shows the reduction in the value of all the considered functionals achieved after optimization with respect to the x coordinate of the four nodes defining the die profile. We can see in Figs. 2.34 to 2.36 two different families of optimal shapes corresponding to either local or global functional character. For the specific case of the overall deformation energy (Fig. 2.34) the global functional presents a nearly straight optimal die profile while the corresponding local criterion (i.e. minimization of the maximum local plastic deformation energy

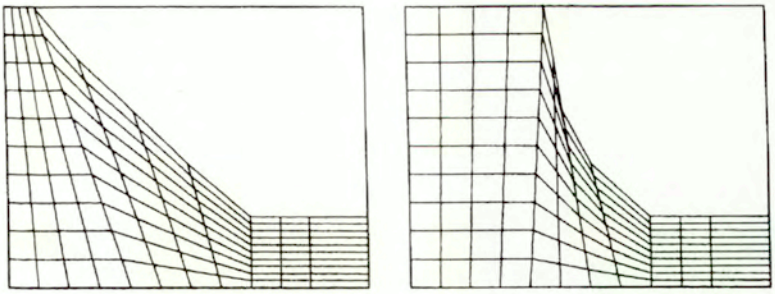

Figure 2.34 Optimal shape – Minimization criteria: energy rate (left) and maximum local energy rate (right).

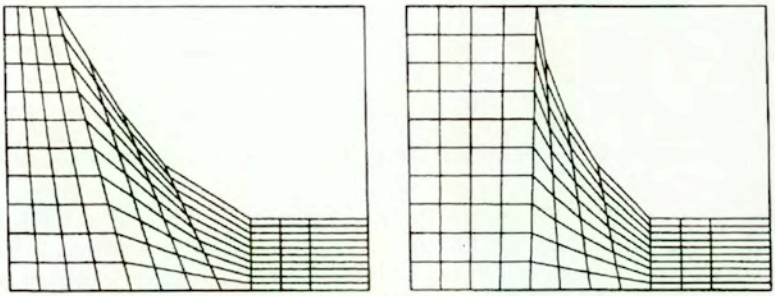

Figure 2.35 Optimal shape – Minimization criteria: averaged effective strain rate deviation (left) and maximum local effective strain rate (right).

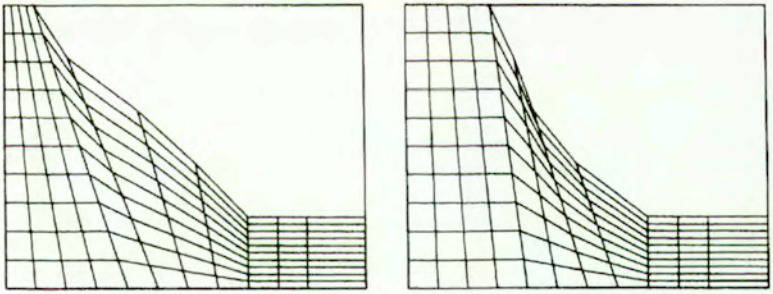

Figure 2.36 Optimal shape – Minimization criteria: overall distortion rate (left) and maximum local distortion rate (right).

Functional	Ψ_E	Ψ_e	$\Psi_{D\dot{\varepsilon}}$	$\Psi_{\dot{\varepsilon}_1}$	Ψ_D	$\Psi_{\dot{\varepsilon}_{12}}$
Initial value	0.8658E+5	0.3684E+6	4.802	6.8844	7.119	5.068
Optimal value	0.7922E+5	0.2686E+6	2.913	5.3424	6.358	3.997

Table 2.1 Initial and optimal values of the design functionals.

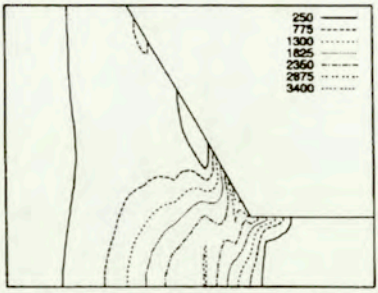

Figure 2.37 Energy rate isocurves for the initial die.

rate) exhibits a strongly concave profile. It is interesting to notice, however, that both give approximately the same angle between the die and the material outlet, which is the most critical zone with concentrated strain rates and stresses.

Comparative plots of the energy rate are shown for the initial (Fig. 2.37), and modified (Fig. 2.38, (a) and (b)) configurations, optimized with respect to both globally and locally defined cost functionals. It can be seen that the last plot shows visible differences with respect to the original and the globally-optimized ones, which suggests that the minimum for both the criteria (local and global) are very different. On the other hand, the isocurves for the energy rate have a similar pattern in both the initial and the global-optimized configurations: in the latter, smoother energy gradients and the deformation zone more spread throughout the

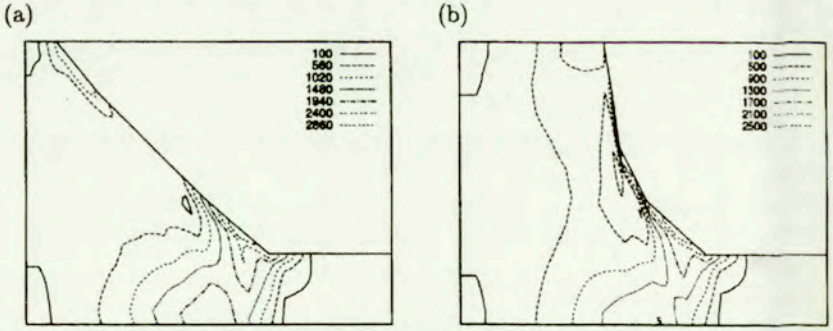

Figure 2.38 Energy rate isocurves for the (a) global- and (b) local- energy rate optimized die.

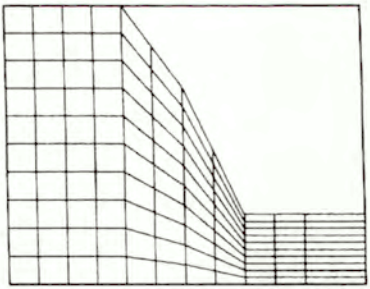

Figure 2.39 Optimal shape with sticking condition; energy rate minimization.

domain can, be seen.

2) Effect of boundary conditions

The optimal solution also strongly depends on the boundary conditions. In contrast with the solutions already shown, where no friction conditions have been assumed, Fig. 2.39 shows the optimal solution with respect to the deformation energy rate criterion (2.197) for a problem modeled with sticking (i.e. no slip) condition. Now the design variable is the y-coordinate of the central node of the die profile. A different optimal shape is obtained, as compared to the case with frictionless boundaries. As before, the die shape is mainly characterized by the die angle at the outlet, which now is much larger. Besides, a much less significant reduction of the cost fuctional has been achieved: from $\Psi_{E0} = 0.1552E + 6$ down to $\Psi_{Ef} = 0.1530E + 6$. This behaviour results from the effect of the boundary conditions: a zone is developed where the material remains attached to the boundary, thus roughly speaking, design variations only change the size of this zone, which however has a small contribution to the energy integral.

Next, the same problem of minimizing the global energy rate when the sticking condition is assumed is solved using the bispline design elements presented in Section 2.5.3. Figure 2.40 shows the optimal shapes of the extrusion die for such boundary condition assumed along the whole boundary. In the first case the x coordinate of the upper edge of the die profile and the slope at both profile ends (x_A, θ_A, θ_E, see Fig. 2.33) have been taken as design variables. In the second case, also the x-coordinate and the slope at the middle point of the profile are used.

We can see that the solution with more design variables approximates better a "square" profile at the die corner, with a transition at the die exit. The angle at the die exit is very similar in both cases, as results from Table 2.2. The solution is in agreement with the empirically optimized dies for such boundary conditions, where the dead zone forms a kind of internal optimal die. However, we can see also from Table 2.2 that the cost functional is roughly the same for both solutions, which means that it may not be worth to reach an exact optimum if this involves some technological difficulties. Moreover, the same example using

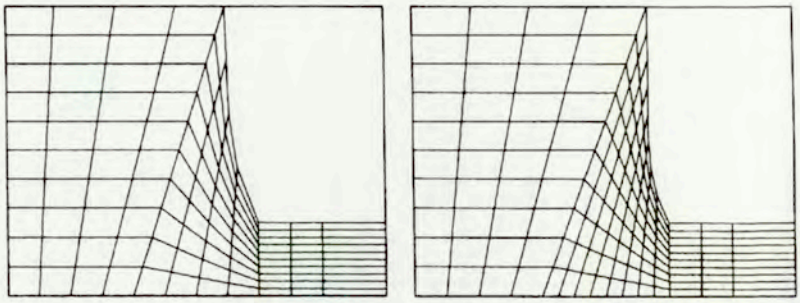

Figure 2.40 Optimal shape – three (left) and five (right) design variables.

	$\mathcal{G}_{Ei}$	$\mathcal{G}_{Ef}$	x_A	θ_A	θ_E
D=3	0.1563E+6	0.1511E+6	3.50	93.76°	121.38°
D=5	0.1563E+6	0.1507E+6	3.65	94.89°	122.05°

Table 2.2 Initial and optimal values of the design functionals and of the design variables.

only one degree of freedom (the x-coordinate of the middle point, x_C) already shown, see Fig. 2.39, solved using bilinear design elements, yields a functional value of $\mathcal{G}_{Ef}$=0.153E+6 with, again, a similar die angle at the exit [13], which shows to be the most critical variable for optimization. In the present discussion, however, it should be noticed that the constitutive model used here fails to model the real material behaviour at the shear band that develops within the dead-zone formation. The extrusion force drops when the dead zone arises, as it comes out from experiments, but this fact is not reflected within this model.

3) Design elements

Finally, to further investigate the performance of the design elements with different design variables, the problem of finding the optimal shape, which minimizes the overall deformation energy rate has been solved using both bilinear and bispline design elements and different sets of design parameters. Again, the initial shape is that given in Fig. 2.33. The initial value of the design functional is given as reference to be compared with the optimized results. The optimal shapes arrived at are shown in Figs. 2.41 and 2.42 for the frictionless and sticking condition cases, respectively. All the results are summarized in Table 2.3. It can be seen that the relative reduction in the cost functional is much noticeable in the frictionless case than with sticking condition boundaries. Moreover, for the former the bispline elements show to be very effective. With the same number of degrees of freedom (i.e. design parameters), a more important reduction in the design functional is obtained. The case with sticking friction shows, as before, a non-significant gain. As already argued, in such case a dead zone develops with

	Frictionless boundaries		Sticking friction	
Init. Value:	$\mathcal{G}_o = 86343$	$\mathcal{G}/\mathcal{G}_o$	$\mathcal{G}_o = 156282$	$\mathcal{G}/\mathcal{G}_o$
bilinear elements:				
$3X + 0\theta$	$\mathcal{G} = 67667$	0.784	$\mathcal{G} = 152120$	0.973
$4X + 0\theta$	$\mathcal{G} = 67388$	0.780	$\mathcal{G} = 152461$	0.976
$5X + 0\theta$	$\mathcal{G} = 64618$	0.748	$\mathcal{G} = 152522$	0.976
bispline elements:				
$1X + 2\theta$	$\mathcal{G} = 63408$	0.734	$\mathcal{G} = 152609$	0.976
$2X + 3\theta$	$\mathcal{G} = 60903$	0.705	$\mathcal{G} = 152575$	0.976

Table 2.3 Initial and optimal values of the design functionals.

which the same material finds its own optimal internal die, since our numerical solution minimizes the same energy functional. Besides, it is even noticed that increasing the number of design parameters the optimized functional is higher than with less design parameters. This fact suggests the presence of local minima which are probably connected with the material model in the $\dot{\bar{\varepsilon}} \to 0$ limit, in which, as said in Section 2.2, a cutoff value is applied for the viscosity μ.

The computations presented in this section were carried out using Schittkowski's algorithm [95]. The case shown in Fig. 2.39 (like many others not presented here) was also solved using the Conjugate Gradient Method. The same results were obtained in both cases; the number of iterations was also similar. However, the implementation of [95] available to the authors had better possibilities for imposing constraints and for this reason was preferred.

2.6 Summary of the chapter

In this chapter sensitivity evaluation techniques were employed to study different metal forming processes in the framework of the flow approach.

First, the constitutive parameters were taken as the design variables. The methodology developed turned out generally reliable and effective. Problems involving the friction model described in Section 2.2.2 proved to be very sensitive to changes in the friction coefficient; serious difficulties in finding the size of the parameter perturbations for calculating the sensitivity gradients by the finite difference approach were encountered. On the contrary, the techniques yielding the sensitivity information as a by-product of the equilibrium analysis were demonstrated to work well even for this challenging class of problems.

An iterative form of the sensitivity formulation based on the secant stiffness matrix was also presented. An example was shown, in which the tangent matrix could not be employed at all, implying the importance of the iterative scheme. Similar situations will typically arise in solving problems for which at the same

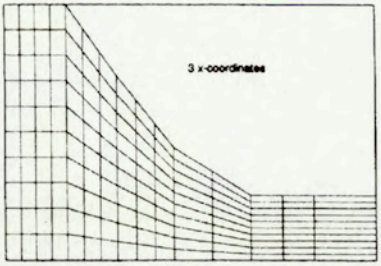

$\mathcal{G}/\mathcal{G}_o = 0.784$

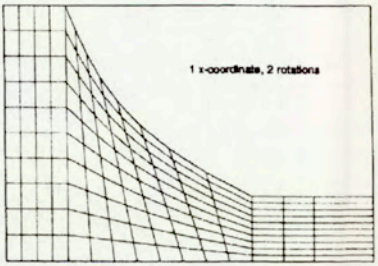

$\mathcal{G}/\mathcal{G}_o = 0.734$

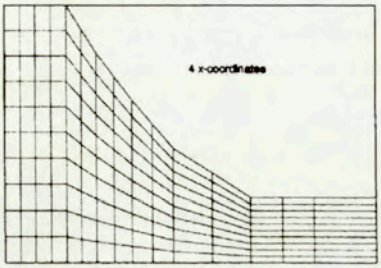

$\mathcal{G}/\mathcal{G}_o = 0.780$

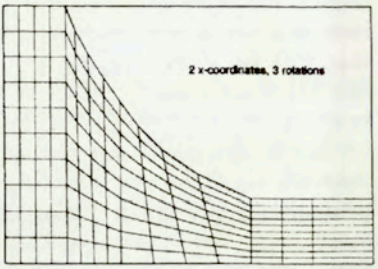

$\mathcal{G}/\mathcal{G}_o = 0.7054$

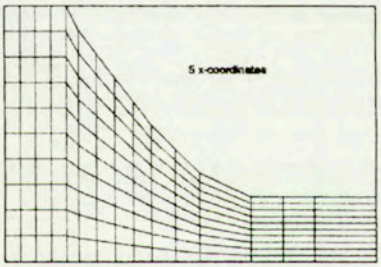

$\mathcal{G}/\mathcal{G}_o = 0.748$

Figure 2.41 Shape optimization for frictionless boundary. Bilinear and bispline elements

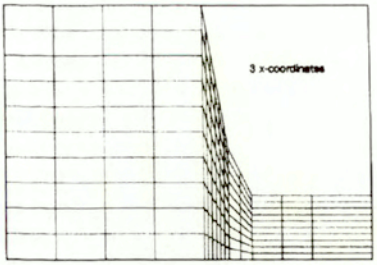

$\mathcal{G}/\mathcal{G}_o = 0.973$

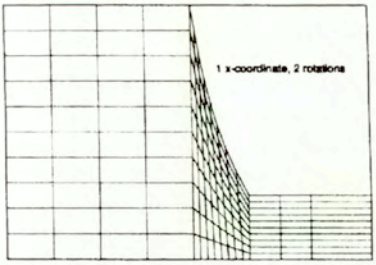

$\mathcal{G}/\mathcal{G}_o = 0.976$

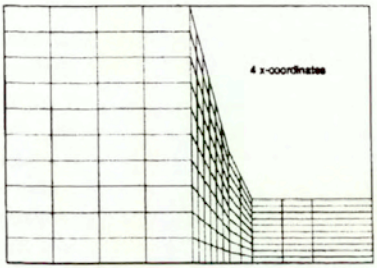

$\mathcal{G}/\mathcal{G}_o = 0.976$

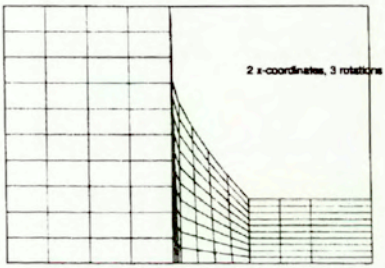

$\mathcal{G}/\mathcal{G}_o = 0.976$

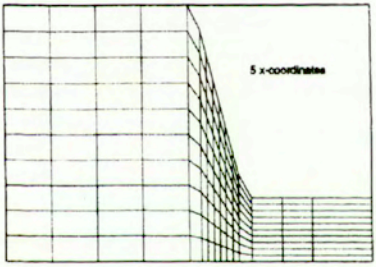

$\mathcal{G}/\mathcal{G}_o = 0.976$

Figure 2.42 Shape optimization for sticking condition. Bilinear and bispline elements

time (i) the material model exhibits no or very little hardening and (ii) no non-zero boundary velocities are prescribed.

Techniques developed for shape sensitivity analysis of metal forming processes offer an effective way to generate valuable information about the influence of the tool shape modification on different forming process characteristics. Tool shape optimization is thus an immediate and natural application of the results. As before, serious drawbacks of using the finite difference method for sensitivity assessment were demonstrated. On the other hand, the direct differentiation method combined with the domain parameterization approach made it possible to solve the problem at hand in an elegant and straightforward way.

Finally, the formalism for shape sensitivity is used to find the optimal shape of an extrusion die according to different design functionals, boundary conditions, so-called design elements and design variables. The two mappings used in the context of the DPA for shape sensitivity analysis are conceived as to be applicable to any kind of geometry and thus can be used in other optimization problems.

Chapter 3

Transient processes by an incremental approach

3.1 Introductory comments

In the last two decades computer modelling of metal forming processes has been experimenting a continuous development. We have already mentioned that, concerning the physics of the problem, attention has been paid to constitutive equations, geometry description, boundary conditions, piece-tool interaction, metallurgical aspects, etc. Additionally, a set of issues has been covered on the numerical side, such as mesh generation and adaptivity, stabilization techniques, efficient solution of the system of equations. One of the latest steps in this direction has been the adaptation of the codes to parallel processing. This has resulted from real needs arising from the solution of industrial problems. In this sense, it can be said that the growth of the computational requirements has even over-passed the computer developments. Besides, searching for more efficient computational solutions, explicit methods, which were already commonly used in other fields as compressible fluid dynamics, have attracted the attention of researchers. Explicit methods become competitive with respect to implicit ones whenever the critical time step for the former is comparable to the time step required for accuracy of the solution. Although it is difficult to make a general statement in this matter, it can be said that this situation arises in the simulation of many metal forming operations. The following features of the explicit methods are highlighted when compared with their implicit counterpart: (i) conditional stability, (ii) no solution of equation system required, (iii) simplicity of implementation and usage. In addition, explicit methods are very well suited for parallelization and an almost ideal (linear) speed-up may be obtained. On the other hand, a drawback arises as a consequence of the incompressibility condition: as we will see later on, in the procedures for circumventing the Brezzi-Babuska condition at least a small amount of artificial compressibility is required in explicit methods, otherwise the critical time step becomes zero.

Discrete methods for time integration of a set of differential equations have sometimes taken advantage of time step splitting, which gives place to the split algorithms, also called fractional step methods. Indeed, most commonly used in fluid mechanics, they produce some positive effects by a proper choice of the split, as the long series of works initiated by Chorin [32, 33] shows. Schneider *et al.* [96] and afterwards Kawahara and Ohmiya [68] noticed that the split allows for the use of equal velocity and pressure interpolation functions for incompressible flows. Some new directions and applications have been covered recently by Zienkiewicz and co-workers [112, 118] based on the characteristic method, with also an application to elastic-plastic metal forming [120]. In that work and, using a different approach, in the paper of Bonet and Burton [22] linear triangles and tetrahedra are used. With such elements automatic mesh generators and adaptive refinement may be more easily used.

In this chapter the fractional step method is applied to metal forming problems described with the rigid-viscoplastic material model used so far [4]. The final form arrived at after discretization tells us that interpolating function of the same order can be used for both velocity and pressure. Hence linear triangles and tetrahedra are implemented. The method is illustrated with numerical simulation of extrusion and upsetting. At the same time the role of some material and numerical parameters on the stabilizing effect and on the convergence rate is discussed. Comparison of the stabilization scheme with the so-called Galerkin least squares formulation proposed by Hughes *et al.* [63] and extended by the author for metal forming [10] is also given.

Further, sensitivity analysis of metal-forming problems as described by this method [5] is presented. The Direct Differentiation Method (DDM) is used to obtain the parameter sensitivity expressions corresponding to the model for metal forming simulation in terms of the flow approach with explicit time integration and time step splitting. The sensitivity coefficients are obtained also in two substeps but independently of the solution that is being calculated at each sub-step, hence there are no additional time steps for the sensitivity stage. As numerical illustrations of the method, a steady state extrusion process is obtained as the result of a pseudo-transient evolution. Afterwards, upsetting is presented to show the full transient solution. In each case sensitivity results with respect to chosen design parameters are given.

To avoid possible confusions, it is worth to mention that the concept of *stability* is used here in the two senses it usually has in the literature: one refers to the evolution of the solution during the time integration. This is the most classical meaning. The second one refers to the absence of spurious modes in the solution, either at steady state or at a given time step. This particularly refers to the pressure solution as a consequence of the incompressibility condition and requires the application of so-called stabilizing methods. It should become clear from the context which concept is referred to at any time.

3.2 Split-based explicit flow approach

3.2.1 Extension of the flow approach to transient processes

We have discussed in Section 2.2 the formalism of the flow approach with the assumption that the process has reached a steady state. Now, the explicit approach we are interested in calls for a transient formulation of the problem, which will be presented below.

But before going further let us recall a key issue, which lays at the core of the very idea of time step splitting, as we will see later on. As it is well known, the formulation we are dealing with, in which the velocities are differentiated by one order higher than the pressure (from which zero diagonal terms result), requires upon discretization the fulfillment of the Babuska-Brezzi condition. Usually this implies the use of different interpolation orders for both variables. Different procedures have been proposed to overcome this restriction. One such has been the Galerkin least squares formulation proposed by Hughes *et al* [63] and applied by the author in metal forming processes within the flow approach [10] and has been presented in Section 2.2.4. As we have seen, the method —and others equivalent to it— aims at having a Laplacian matrix instead of zero in Eq. (2.26). In particular, this so-called stabilizing sub-matrix within the system matrix is achieved in the quoted papers by adding the first equation weighted by the gradient of the shape functions to the second equation. Since the first equation is fulfilled, this addition does not affect the incompressibility condition, but well poses the system matrix. In this way the zero diagonal is avoided, the system matrix is positive definite and thus stable pressure solutions can be obtained. We will come back to this point later on, in the next section.

The flow approach as presented in Section 2.2, although is formulated as a steady state problem, has sometimes been used for transient analysis [111]. Indeed, dynamic terms have most frequently no practical relevance, as can be observed from the fact that the equivalent Reynolds number of a typical metal forming operation is of the order of 10^{-6} to 10^{-9}. In addition, if we work within a material —Lagrangian— approach, that is, the coordinate system deforms with the body, then convective terms do not appear in the equation. Therefore we can follow up the whole process as a sequence of equilibrium states, and update the coordinates from step to step as ${}^{t+\Delta t}\mathbf{x} = {}^{t}\mathbf{x} + {}^{t}\mathbf{v}\Delta t$. Nevertheless, we are here interested in the full transient solution, which, as we shall see, will be more efficient than the quoted one. Since we will still neglect dynamic effects for the already discussed reasons, we shall be dealing in fact with a pseudo-time integration (i.e. only acceleration terms are included, but not convective). As it will be shown, such formulation may give rise, under appropriate conditions to additional terms which allow us to use equal-order interpolation of all the problem variables. The final form we are aiming at is that of an incremental approach, which yields solution by a sequence of linear steps. In particular, we will apply

an explicit scheme for time integration, which does not require inversion of the system matrix.

So, we write the equilibrium equations in a non-steady form. The non-linear counterpart of the pseudo-compressible formulation [32] of the Stokes problem reads

$$\frac{\partial(\rho v_i)}{\partial t} = \frac{\partial \sigma^{\mathrm{D}}_{ij}}{\partial x_j} - \frac{\partial p}{\partial x_i} - g_i \tag{3.1}$$

$$\frac{\partial \rho}{\partial t} = -\frac{\partial(\rho v_i)}{\partial x_i} \tag{3.2}$$

where, assuming small changes in density, we can write

$$\rho_o \frac{\partial v_i}{\partial t} = \frac{\partial \sigma^{\mathrm{D}}_{ij}}{\partial x_j} - \frac{\partial p}{\partial x_i} - g_i \tag{3.3}$$

$$\frac{1}{c^2}\frac{\partial p}{\partial t} = -\rho_o \frac{\partial v_i}{\partial x_i} \tag{3.4}$$

In Eq. (3.4), c is the speed of sound, $c^2 = K/\rho_o$, where K is the bulk modulus. Thus extended equations yield, by discretization

$$\begin{bmatrix} \mathbf{M}_{(v)} & \mathbf{0} \\ \mathbf{0} & \mathbf{M}_{(p)} \end{bmatrix} \frac{\mathrm{d}}{\mathrm{d}t} \begin{bmatrix} \dot{\mathbf{q}} \\ \dot{\bar{\mathbf{p}}} \end{bmatrix} = - \begin{bmatrix} \mathbf{K}_{(\mu)} & \mathbf{K}^{\mathrm{T}}_{(p)} \\ -\mathbf{K}_{(p)} & \mathbf{0} \end{bmatrix} \begin{bmatrix} \dot{\mathbf{q}} \\ \dot{\bar{\mathbf{p}}} \end{bmatrix} + \begin{bmatrix} \mathbf{Q} \\ \mathbf{0} \end{bmatrix} \tag{3.5}$$

where the mass matrices read

$$M_{(v)\alpha\beta} = \int_\Omega \rho_o \phi_i^{(\alpha)} \phi_i^{(\beta)} \, \mathrm{d}\Omega \qquad M_{(p)\alpha\beta} = \int_\Omega \frac{1}{\rho_o c^2} \hat{\phi}_i^{(\alpha)} \hat{\phi}_i^{(\beta)} \, \mathrm{d}\Omega \tag{3.6}$$

and $\boldsymbol{\phi}$ and $\hat{\boldsymbol{\phi}}$ are the shape functions for velocity and pressure, as defined in Eqs. (2.8), (2.9) and (2.12).

The mass balance equation tells us that some (fictitious) compressibility is allowed. Its magnitude is inversely proportional to $\rho_o c^2$. In fact, c represents the propagation velocity of a pressure perturbation, but since, as said, dynamic effects are not relevant in the model, c can be thought of as a scaling factor for the incompressibility constraint, which can be accordingly adjusted. On the other hand, explicit time integration methods are limited by the distance that such pressure perturbation travels in a time step, in relation with the element size. More accurately satisfied incompressibility means then, a higher c and thus a smaller critical time step, which, in the limit of perfect incompressibility, becomes zero.

3.2.2 The split algorithm

The split algorithm, initially proposed by Chorin [32, 33] has been successfully used in fluid mechanics. A detailed survey and its generalization based in the characteristic method has been presented by Zienkiewicz *et al.* [112, 118]. Later,

Zienkiewicz *et al.* [120] applied the idea to dynamic forming processes within a displacement-based approach and for an elasto-plastic material. In the sequel we use the split algorithm aiming at a formulation suitable for nonlinear Stokes problems, by means of which the flow approach describes metal forming problems.

In the papers already quoted in this section the splitting technique has been applied to solve various discretized differential equations. They show the convenience of performing each time step in two sub-steps. A proper choice of the split can produce a desired effect such as to uncouple a set of equations or to introduce stabilizing terms. The choice of the split is arbitrary as long as the original equation is exactly recovered by summing the respective equations of both sub-steps.

We consider a generic time step from time t to $t+\Delta t$. All the problem variables at time t are known. The unknowns to be solved for at each time step are the velocity and pressure increments, $\Delta \mathbf{v}, \Delta p$. According to previous works [14, 68, 96, 112, 118, 120], in the first sub-step we obtain an intermediate velocity increment $\Delta \tilde{\mathbf{v}}$ by not including the pressure gradient term in the momentum balance, Eq. (3.3)

$$\rho_o \frac{\Delta \tilde{v}_i}{\Delta t} = \frac{\rho_o}{\Delta t}(\tilde{v}_i - {}^{t}v_i) = \frac{\partial {}^{t}\sigma^{D}_{ij}}{\partial x_j} - g_i \tag{3.7}$$

No index is used for the intermediate velocity to emphasize that it does not correspond to any time instant. The velocity correction will be done after the new pressure ${}^{t+\Delta t}p$ is calculated. Then we will have

$${}^{t+\Delta t}v_i = \tilde{v}_i - \frac{\Delta t}{\rho_o} \; {}^{t+\theta_2 \Delta t}\left(\frac{\partial p}{\partial x_i}\right) \tag{3.8}$$

where

$${}^{t+\theta_2 \Delta t}\left(\frac{\partial p}{\partial x_i}\right) = \theta_2 \; {}^{t+\Delta t}\left(\frac{\partial p}{\partial x_i}\right) + (1-\theta_2) \; {}^{t}\left(\frac{\partial p}{\partial x_i}\right) \qquad 0 \le \theta_2 \le 1 \tag{3.9}$$

Meanwhile, the mass conservation equation (3.4), when discretized in time, reads

$$\frac{1}{c^2}\left(\frac{{}^{t+\Delta t}p - {}^{t}p}{\Delta t}\right) = -\rho_o \frac{\partial}{\partial x_i}\left(\theta_1 \, {}^{t+\Delta t}v_i + (1-\theta_1) {}^{t}v_i\right) \qquad 0 \le \theta_1 \le 1 \tag{3.10}$$

and using Eq. (3.8) we get

$$\frac{1}{c^2}\left(\frac{{}^{t+\Delta t}p - {}^{t}p}{\Delta t}\right) = -\rho_o \frac{\partial}{\partial x_i}\left\{\theta_1 \left[\tilde{v}_i - \frac{\Delta t}{\rho_o} \; {}^{t+\theta_2 \Delta t}\left(\frac{\partial p}{\partial x_i}\right)\right] + (1-\theta_1) {}^{t}v_i\right\} \tag{3.11}$$

We still have to define the boundary conditions related to Eq. (3.7), that is, for the intermediate velocity $\tilde{\mathbf{v}}$. Upon discretization of Eq. (3.7), a force term results from the body forces plus the integral of the deviatoric part of the boundary traction over the whole boundary. In the second sub-step (Eq. (3.8)) a second force term results from the integral of the volumetric part of the boundary

traction. The combined effect of both forces gives us the total boundary traction, which either vanish on $\partial\Omega - (\partial\Omega_\sigma + \partial\Omega_v)$, are known on $\partial\Omega_\sigma$ or result as a reaction of imposed velocities on $\partial\Omega_v$. As argued by Zienkiewicz *et al.* [120], since the choice of how to split the time step is arbitrary, we can include both force terms in the first sub-step. We could have arrived to the same conclusion by splitting the step after discretization. On the other hand, essential boundary conditions must be satisfied by the velocity ${}^{t+\Delta t}\mathbf{v}$. But to impose them also to the intermediate velocity $\tilde{\mathbf{v}}$ would mean to apply a set of forces which would have to be also included —with opposite sign— on the second sub-step. Using a similar argumentation as before, the $\tilde{\mathbf{v}}$ field is calculated with no essential boundary conditions applied.

With the above considerations in mind, space discretization of equations (3.7), (3.8) and (3.11) yields

$$\begin{aligned}
\tilde{\mathbf{q}} &= {}^{t}\dot{\mathbf{q}} - \Delta t \mathbf{M}_{(v)}^{-1}(\mathbf{K}_{(\mu)}{}^{t}\dot{\mathbf{q}} - {}^{t}\mathbf{Q}) \\
{}^{t+\Delta t}\dot{\mathbf{q}} &= \tilde{\mathbf{q}} - \Delta t \mathbf{M}_{(v)}^{-1}\left[\theta_2 \mathbf{K}_{(p)}^{T}{}^{t+\Delta t}\bar{\mathbf{p}} + (1-\theta_2)\mathbf{K}_{(p)}^{T}{}^{t}\bar{\mathbf{p}}\right] \\
{}^{t+\Delta t}\bar{\mathbf{p}} &= {}^{t}\bar{\mathbf{p}} - \Delta t \mathbf{M}_{(p)}^{-1}\left(\theta_1\left\{\mathbf{K}_{(p)}\tilde{\mathbf{q}} + \frac{\Delta t}{\rho_o}\mathbf{H}\left[\theta_2{}^{t+\Delta t}\bar{\mathbf{p}} + (1-\theta_2){}^{t}\bar{\mathbf{p}}\right] - {}^{t}\mathbf{Q}_{(p)}\right\}\right. \\
&\qquad \left. +(1-\theta_1)\mathbf{K}_{(p)}{}^{t}\dot{\mathbf{q}}\right)
\end{aligned} \tag{3.12}$$

where the discretized Laplacian operator

$$H_{\alpha\beta} = \int_\Omega \frac{\partial\hat{\phi}^{(\alpha)}}{\partial x_i}\frac{\partial\hat{\phi}^{(\beta)}}{\partial x_i}\,\mathrm{d}\Omega \tag{3.13}$$

has been obtained, and the load vector ${}^{t}\mathbf{Q}_{(p)}$, resulting from integration by parts of the pressure gradient term, reads

$${}^{t}Q_{(p)\alpha} = \frac{\Delta t}{\rho}\int_{\partial\Omega}\hat{\phi}^{(\alpha)}\frac{\partial\hat{\phi}^{(\beta)}}{\partial x_i}n_i\,\mathrm{d}(\partial\Omega)(\theta_2{}^{t+\Delta t}p_\beta + (1-\theta_2){}^{t}p_\beta) \tag{3.14}$$

As we have said in advance in the previous section, this results allow us to expect stabilized pressure solution under appropriate values of Δt and c^2, for any choice of interpolating functions for velocity and pressure.

Summarizing, the sequence of calculations consists in finding first the estimated velocity, then the pressure increment and finally the velocity correction. We notice that the two weighting coefficients θ_1 and θ_2 have the following effect:

- θ_1 tells at which time instant the mass conservation is imposed. It is convenient to do it at the end of the time step, therefore we take $\theta_1 = 1$;
- if θ_2 is different from zero we get an implicit scheme and iterations are necessary to obtain ${}^{t+\Delta t}\bar{\mathbf{p}}$. Since we are interested in the fully explicit version we use $\theta_2 = 0$.

Replacing in Eq. (3.12) these values for θ_1 and θ_2 we get

$$\begin{aligned}
\tilde{\mathbf{q}} &= {}^{t}\dot{\mathbf{q}} - \Delta t \mathbf{M}_{(v)}^{-1}(\mathbf{K}_{(\mu)}{}^{t}\dot{\mathbf{q}} - {}^{t}\mathbf{Q}) \\
{}^{t+\Delta t}\dot{\mathbf{q}} &= \tilde{\mathbf{q}} - \Delta t \mathbf{M}_{(v)}^{-1}\mathbf{K}_{(p)}^{T}{}^{t}\bar{\mathbf{p}} \\
{}^{t+\Delta t}\bar{\mathbf{p}} &= {}^{t}\bar{\mathbf{p}} - \Delta t \mathbf{M}_{(\rho)}^{-1}(-\mathbf{K}_{(p)}\tilde{\mathbf{q}} + \frac{\Delta t}{\rho_o}\mathbf{H}{}^{t}\bar{\mathbf{p}} - {}^{t}\mathbf{Q}_{(p)})
\end{aligned} \tag{3.15}$$

In matrix form, the split algorithm reads

sub-step 1

$$\frac{1}{\Delta t}\begin{bmatrix} \mathbf{M}_{(v)} & \mathbf{0} \\ \mathbf{0} & \mathbf{M}_{(\rho)} \end{bmatrix}\begin{bmatrix} \tilde{\mathbf{q}} - {}^{t}\dot{\mathbf{q}} \\ \tilde{\bar{\mathbf{p}}} - {}^{t}\bar{\mathbf{p}} \end{bmatrix} + \begin{bmatrix} \mathbf{K}_{(\mu)} & \mathbf{0} \\ \mathbf{0} & \mathbf{0} \end{bmatrix}\begin{bmatrix} {}^{t}\dot{\mathbf{q}} \\ {}^{t}\bar{\mathbf{p}} \end{bmatrix} - \begin{bmatrix} {}^{t}\mathbf{Q} \\ \mathbf{0} \end{bmatrix} = \mathbf{0} \tag{3.16}$$

sub-step 2

$$\frac{1}{\Delta t}\begin{bmatrix} \mathbf{M}_{(v)} & \mathbf{0} \\ \mathbf{0} & \mathbf{M}_{(\rho)} \end{bmatrix}\begin{bmatrix} {}^{t+\Delta t}\dot{\mathbf{q}} - \tilde{\mathbf{q}} \\ {}^{t+\Delta t}\bar{\mathbf{p}} - \tilde{\bar{\mathbf{p}}} \end{bmatrix} + \begin{bmatrix} \mathbf{0} & \mathbf{K}_{(p)}^{T} \\ -\mathbf{K}_{(p)} & \frac{\Delta t}{\rho_o}\mathbf{H} \end{bmatrix}\begin{bmatrix} \tilde{\mathbf{q}} \\ \tilde{\bar{\mathbf{p}}} \end{bmatrix} - \begin{bmatrix} \mathbf{0} \\ {}^{t}\mathbf{Q}_{(p)} \end{bmatrix} = \mathbf{0} \tag{3.17}$$

As it is the usual practice in explicit time integration schemes, the mass matrix is diagonalized by lumping. Therefore, the global matrix needs not to be assembled nor inverted. The solution for the next time step is obtained by multiplying element by element two vectors (inverse of mass, and residual forces).

3.2.2.1 Steady state limit

If we apply constant loads or imposed velocities, the present method should lead us, as a limit case, to the steady state solution. In such case, the time integration is just the transient process between the initial conditions and the steady state. Two approaches are then possible: to update the nodal coordinates according to a suitable rule (the simplest being ${}^{t+\Delta t}x_\alpha = {}^{t}x_\alpha + {}^{n}\dot{q}_\alpha \Delta t$) — i.e. Lagrangian approach — or to consider a fixed mesh in space — Eulerian approach. The latter is more natural for the analysis of the steady case and will be followed in this section. It should require the inclusion of the convective term in the momentum balance. However, it is a common practice to neglect this term for practical metal forming cases, as pointed out in Section 3.2.1. We look for the form the system (3.15) takes when steady state is reached. Since we will have, obviously,

$$\begin{aligned}
{}^{t+\Delta t}\dot{\mathbf{q}} &= {}^{t}\dot{\mathbf{q}} = \dot{\mathbf{q}} \neq \tilde{\mathbf{q}} \\
{}^{t+\Delta t}\bar{\mathbf{p}} &= {}^{t}\bar{\mathbf{p}} = \bar{\mathbf{p}} = \tilde{\bar{\mathbf{p}}}
\end{aligned} \tag{3.18}$$

we notice that the dynamic terms will vanish (no acceleration). We arrive at the steady state form by eliminating $\tilde{\mathbf{q}}$ from Eq. (3.15). Summing Eq. $(3.15)_1$ and Eq. $(3.15)_2$ we obtain again the momentum equation as in Eq. (2.26). Besides, we can replace $\tilde{\mathbf{q}}$ in Eq. $(3.15)_3$ either as taken from Eq. $(3.15)_1$ or from Eq. $(3.15)_2$. The complete system will be, respectively

$$\begin{bmatrix} \mathbf{K}_{(\mu)} & \mathbf{K}_{(p)}^{T} \\ \mathbf{K}_{(p)} - \Delta t \mathbf{K}_{(p)}\mathbf{M}_{(v)}^{-1}\mathbf{K}_{(\mu)} & -\frac{\Delta t}{\rho_o}\mathbf{H} \end{bmatrix}\begin{bmatrix} \dot{\mathbf{q}} \\ \bar{\mathbf{p}} \end{bmatrix} = \begin{bmatrix} \mathbf{Q} \\ -\Delta t \mathbf{K}_{(p)}\mathbf{M}_{(v)}^{-1}\mathbf{Q} + \mathbf{Q}_{(p)} \end{bmatrix} \tag{3.19}$$

or

$$\begin{bmatrix} \mathbf{K}_{(\mu)} & \mathbf{K}^{\mathrm{T}}_{(\mathrm{p})} \\ \mathbf{K}_{(\mathrm{p})} & \Delta t \mathbf{K}_{(\mathrm{p})} \mathbf{M}^{-1}_{(\nu)} \mathbf{K}^{\mathrm{T}}_{(\mathrm{p})} - \frac{\Delta t}{\rho_o} \mathbf{H} \end{bmatrix} \begin{bmatrix} \dot{\mathbf{q}} \\ \bar{\mathbf{p}} \end{bmatrix} = \begin{bmatrix} \mathbf{Q} \\ \mathbf{Q}_{(\mathrm{p})} \end{bmatrix} \tag{3.20}$$

where Eq. (3.19) is similar to the form obtained by Hughes *et al.* [63] and Eq. (3.20) looks more attractive because it yields a symmetric system matrix, as we have in Eq. (2.26) (note that the second-row equation has been multiplied by -1). In any case, we can recognize the negative Laplacian in the pressure-pressure sub-matrix which adds the stabilizing effect, thus allowing the use of equal order interpolation for the velocity and pressure, $\phi_i^{(s)} = \hat{\phi}_i \ \forall i, s$, cf. Eqs. (2.8), (2.9) and (2.12), also for the transient analysis. In particular, linear triangles and tetrahedra for 2D and 3D, respectively, have been used in this chapter.

$\phi_i^{(s)} = \hat{\phi}_i$ The following remarks can be made:

1) As said before, Eq. (3.19) is comparable to the Galerkin least-squares formulation proposed by Hughes *et al.* [63], who added to the incompressibility equation the result of weighting the momentum equation with the gradient of the shape functions scaled by the mesh size and the viscosity. If we examine the pressure-pressure sub-matrix, we see that in the present scheme it is multiplied by $\Delta t/\rho_o$, whereas according to Hughes *et al.*, by the factor $\alpha h_e^2/2\mu$, where α is a numerical parameter (typically $\alpha = 0.5$), h_e is the element size and μ is the viscosity. (We notice that $\alpha h_e^2 \rho/2\mu$ has time units and it has been sometimes called the intrinsic time scale.) The whole factor should be a constant if we want to keep the incompressibility equation unchanged by the addition of another equation which is itself fulfilled. However both the element size and the viscosity are non constant quantities throughout the elements. So, in order to have comparable methods and for the sake of the correctness of Hughes' *et al.* method [63], mean or other equivalent values of h_e and μ should be adopted. Obviously, these requirements are automatically satisfied if the mesh is uniform and the fluid of a Newtonian kind, as is the case in the quoted paper.

2) If we try to obtain the equation for the steady state prior to discretization i.e. substitute $\bar{v}$ in Eq. (3.11) either taken from Eq. (3.7) or (3.8), we obtain, respectively

$${}^{t+\Delta t}p = {}^{t}p - \rho_o c^2 \Delta t \frac{\partial}{\partial x_i} \left[{}^{t}v + \left\{ \frac{\Delta t}{\rho_o} \frac{\partial {}^{t}\sigma'^{\mathrm{p}}_{ij}}{\partial x_i} - \frac{\Delta t}{\rho_o} \frac{\partial {}^{t}p}{\partial x_i} - \frac{\Delta t}{\rho_o} f_i \right\} \right] \tag{3.21}$$

$${}^{t+\Delta t}p = {}^{t}p - \rho_o c^2 \Delta t \frac{\partial}{\partial x_i} \left[{}^{t+\Delta t}v + \left\{ \frac{\Delta t}{\rho_o} \frac{\partial {}^{t}p}{\partial x_i} - \frac{\Delta t}{\rho_o} \frac{\partial {}^{t}p}{\partial x_i} \right\} \right] \tag{3.22}$$

where the terms in curled braces vanish trivially in Eq. (3.22) and because they form the equilibrium equation in Eq. (3.21), respectively.

It results from the derivation of Eq. (3.22) that the stabilizing method given by equation Eq. (3.20) results only from discretization features. In fact, the addition of the other term should counteract the effect of the stabilizing matrix

alone, and from our experience, it does. Fortunately, as observed by Hughes *et al.* [63], stabilization according to Eq. (3.19) is achieved with no noticeable lack of compressibility with the only addition of the stabilizing matrix. This fact also allows us in the steady state model to avoid the complete calculation of the matrix product, which involves, for a given element, the element matrices of all the surrounding elements.

3) With respect to the version quoted here, the Galerkin least squares formulation has been extended and corrected by similar addition of the mass conservation equation with appropriate weighting factor [47], from which a so-called bulk viscosity arises. Its role for the linear Stokes problem has been investigated by Fourier analysis by Idelsohn *et al.* [64] for the one-dimensional case and for the general case by De Mulder [85]. It results, from their analysis, that the effect of the bulk viscosity in the stabilization scheme is relevant for high Reynolds numbers. Since we are working clearly in the range of low Reynolds numbers, we can conclude that the stabilized system Eq. (3.19) is acceptable.

4) As pointed out in [120], the merits of the split algorithm become clear if we consider that with other strategy the stabilization matrix $\mathbf{H}$ will not appear. For example, if we calculate the approximate velocity $\tilde{\mathbf{v}}$ using the pressure gradient at time t (instead of not writing it at all) and later on change accordingly the velocity correction, we obtain again a zero diagonal for the pressure. Strictly speaking, the velocity $\tilde{\mathbf{v}}$ is neither intermediate (in the sense that is does not correspond to a time between t and $t + \Delta t$) neither approximate (otherwise a better one would improve results), but just a velocity field obtained as uncoupled from the pressure.

5) Finally, let us notice that the factor $\Delta t/\rho_o$, from the point of view of stabilization, should be large enough to stabilize the pressure solution, but it should not "over-stabilize" it. Therefore we have, also for the transient case, upper and lower limits for the time step size. It has been noticed, in our numerical tests, that the upper bound is not reached because the critical time step for the explicit method is more restrictive, although it is possible to find a problem where it happens otherwise. Besides, the same restrictions would be present if we were using an implicit method. Probably more serious is the one about the lower bound for the time step, which may collide with the aim of improving accurateness by reducing the time step length.

3.2.2.2 About joining the two sub-steps

Coming back to the transient solution, we see that the analysis of the steady state limit also suggests that a single-step expression may be derived from the two-step algorithm. Proceeding similarly with Eq. (3.15) as we did in the steady state analysis, but now without using Eq. (3.18), we obtain

$$^{t+\Delta t}\tilde{\mathbf{q}} = {}^{t}\tilde{\mathbf{q}} - \Delta t \mathbf{M}^{-1}(\mathbf{K}^{(s)*}\,{}^{t}\tilde{\mathbf{q}} - {}^{n}\bar{\mathbf{Q}}^{*}) \tag{3.23}$$

in one step, where $\mathbf{K}^{(s)*}$ and $\bar{\mathbf{Q}}^{*}$ are the system matrix and right-hand-side vector of Eq. (3.19). Unfortunately, the convenience of this one step solution is not clear

because the evaluation of the $\mathbf{K}^{(s)*}$ matrix requires also, for every element, the element matrices of the patch of neighbouring elements, thus the diagonality of the system is lost.

3.2.3 Boundary conditions

The solution to the system (3.5) is obtained by imposing velocities in selected nodes corresponding to the movement of the forming tool or, alternatively, by applying nodal forces in them. When the pseudo-transient problem is solved to obtain the steady state solution, these loads or velocities may be imposed at once or incrementally. It can be easily checked by considering the accuracy with which the equilibrium equations are fulfilled at each time step that the latter is better.

Other boundary velocities may be forced to have zero normal component as the point comes in contact with a solid boundary. In the present model this has been achieved by describing the solid boundaries with a function that is problem dependent. When a node is in contact with the solid boundary, its velocity is rotated to a local system, the normal component is zeroed and the tangential component rotated back to the global system. Points coming in contact with the solid boundary have their path modified so that, keeping the total step length, the final part —since contact begins— is done along the boundary.

Boundary friction may be treated by using contact friction elements as was presented in [11] (Section 2.2.3), where a force opposite to the velocity of the metal at the boundary is imposed. A Coulomb friction law is used, and the magnitude of the friction force is calculated as proportional to the pressure at the boundary.

For 2D problems, the boundary in which friction is to be modelled is defined by a set of two-node elements connecting the appropriate nodes. A geometrical condition tells for each node on each friction element whether it is in contact with the solid boundary. If so, the normal-to-boundary velocity component is zeroed (cf. Fig. 3.1).

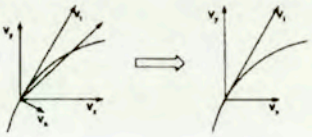

Figure 3.1 Boundary condition for velocity.

Then, a pressure condition decides whether the friction force should be applied. In the present model a negative nodal pressure means compression. Only

in that case a friction force calculated as

$$f_f = -p\nu\frac{l_e}{2} \tag{3.24}$$

and opposite direction to the (tangential) velocity is added to both nodes of the friction element, where p is the mean element pressure, ν the Coulomb friction coefficient and l_e the element length.

Among different possibilities of implementation, our choice has been to perform the velocity operations on each node, but to apply element-wise the friction force on both nodes, at elements with a mean pressure satisfying the compression condition.

The above model may lead to some instabilities for problems where a dead zone (i.e. with sticking friction) develops. In such cases, the velocity may oscillate around zero and thus the friction force will change in sign while its module remains roughly the same. To avoid such oscillations a restriction in the velocity module is imposed:

$$|v_t| > \delta \tag{3.25}$$

while its direction remains positive with respect to the expected direction of the flow, which, in most cases, can be *a priori* stated.

3.2.4 Computational illustrations

In this section some forming processes are simulated with the method presented in this chapter. Apart from the aim of showing the possibilities of the method concerning the simulation itself, we also pay attention to some features regarding the numerical parameters present. On the basis of their comparison with other methods we can learn more about the way these factors act on the solution process and about their meaning. Special emphasis on the numerical side of the solution is placed in the first example, where a steady state 2D extrusion is simulated. The following simulations concern 2D and 3D upsetting and transient extrusion.

3.2.4.1 Steady state extrusion

The interest of this example lays in that it is very well known and that it can be readily solved by other methods, with which we can evaluate our results by comparison. In addition, the form of the equations arrived at when steady state is reached allows us to compare them easily with other stabilization methods, as pointed out in Section 3.2.2. Figure 3.2 shows the process layout and the finite element mesh. A set of velocities imposed on the left side of the domain simulates the effect of the ram. As a result of the pseudo-time integration with fixed mesh the steady state solution is obtained. The initial velocity and pressure fields are assumed to be zero on the rest of the domain, and they develop from left to right along the iterations, until convergence to a stable solution is obtained.

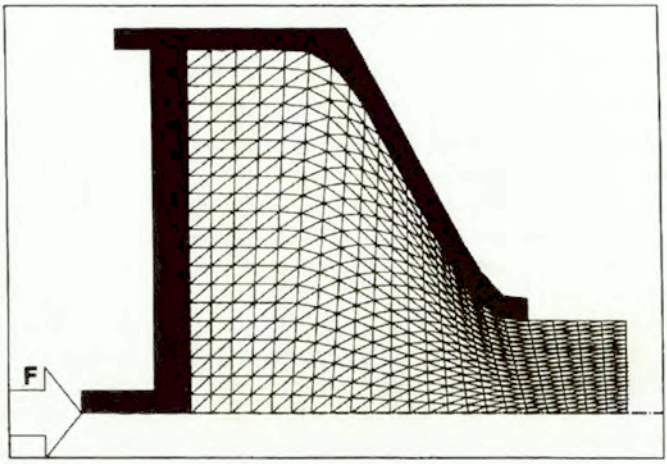

Figure 3.2 Layout of the extrusion process.

From Eq. (3.15) we see that the three parameters, Δt, ρ and c are grouped into two factors: $\Delta t/\rho$ and $\Delta t \rho c^2$, which can be taken as two independent variables that affect: the convergence rate to the steady state, the accuracy with which the incompressibility condition is fulfilled (in transient cases), and the pressure stabilization. In addition, their values should be such as to prevent hourglass modes in the velocity solution and, with explicit time integration, be within the stability region. For steady state we notice from Eq. (3.19) or Eq. (3.20) that the artificial compressibility vanishes (leading to "exact" incompressibility). Thus, only $\Delta t/\rho$ remains as a coefficient for the stabilization terms. Moreover, the density ρ is not responsible for dynamic effects, hence it may be arbitrarily given as long as the quotient $\Delta t/\rho$ remains in its due value. For the (pseudo-) transient evolution to steady state, the factor $\Delta t \rho c^2$ must fulfill the stability condition upon explicit time integration. It also affects the convergence rate and the solution history: the solution may evolve monotonically to, or oscillate around the equilibrium values. When comparing the same process for materials of different rate dependency we notice that highly-viscoplastic materials converge within a small number of oscillations, whereas others with (almost) ideal-plastic behaviour require a very big number of cycles, and it may even occur that the stable solution is not found in practice. This fact, also present with imposed boundary velocities (instead of forces) suggests the existence of non-uniqueness associated with viscoplastic materials with a low rate dependency, as it has been discussed in Section 4.2 [2].

With the above considerations in mind, and before using the explicit split

algorithm, we have solved the present example by a direct method that uses the scheme of Eq. (3.19) and with different values of the coefficient for the stabilization terms, $\Delta t/\rho$. These results are plotted in Fig. 3.3, where the velocity module and the pressure (left and right columns, respectively) are shown for values of $\Delta t/\rho$ ranging from 10^{-8} to 10^{-4}. Frictionless boundaries have been assumed.

To have a better view of the whole field, the viewpoint has been placed at the upper right corner of Fig. 3.2. We see the velocity solutions practically insensitive to this parameter, growing smoothly from a value of 1 (in contact with the ram) to 4, at the exit (the extrusion ratio is 4). However, the pressure field exhibits spurious modes for low values of $\Delta t/\rho$, which means that the stabilizing effect is not sufficient. On the other hand, for high values the pressure field looks over-smoothed.

Now, recalling the discussion of remark 1, in Section 3.2.2, about the comparison of Eq. (3.19) with the Galerkin least squares formulation [63], we see that the (non-constant) factor $\alpha h_e^2/2\mu$ of that method, which should be compared to $\Delta t/\rho$ of our method, ranges between 10^{-6} and 10^{-5}. We have found that the solution by that method lies between the split method solutions obtained with those values of $\Delta t/\rho$, hence the same effect is obtained by adding a similar term calculated with two different methods.

Up to now we have analyzed the effect of the stabilizing term. Now, by solving the problem with the explicit split algorithm we superpose to the previous analysis of the direct solution method the effect of the time step and of the compressibility. The results, again for different choices of $\Delta t/\rho$ are shown in Fig. 3.4. We have verified that, for given mesh, ram velocity and material properties, the critical time-step is inversely proportional to c. We recall here the discussion of the end of Section 3.2.2 about the effect of c on the incompressibility condition to conclude that within the explicit split method at least a small amount of artificial compressibility must be always added to the model. As noticed, in the steady state limit the artificial compressibility vanishes, so it may be used to improve the numerical performance of the algorithm.

For fixed $\Delta t/\rho$, an increase in $\Delta t\rho c^2$ causes a faster convergence to the steady state solution, as long as the stability limit is not exceeded, obviously. For low values of $\Delta t/\rho$ an extended pressure stability (i.e. no spurious modes) with respect to the direct solution is obtained for a same value of the stabilizing coefficient. As expected, the steady state solution normally does not depend on the choice of $\Delta t\rho c^2$. However, for high values of $\Delta t/\rho$, instead of the over-smoothing observed in the direct solution, also velocity hour-glass has been obtained, which in turn deteriorates the pressure solution and makes it dependent on $\Delta t\rho c^2$ due to numerical effects. The numerical behaviour of the explicit split algorithm is schematized in Fig. 3.5, as a function of the two coefficients. The stability limit in the log-log graph is represented by a straight line of slope -1.

Finally, we show in Fig. 3.6 the isocurves for the velocity module and pressure with $\Delta t/\rho = 10^{-7}$. We recognize the standard patterns: velocity module growing from the inlet to the outlet, the frictionless wall and the rounded corner of the die

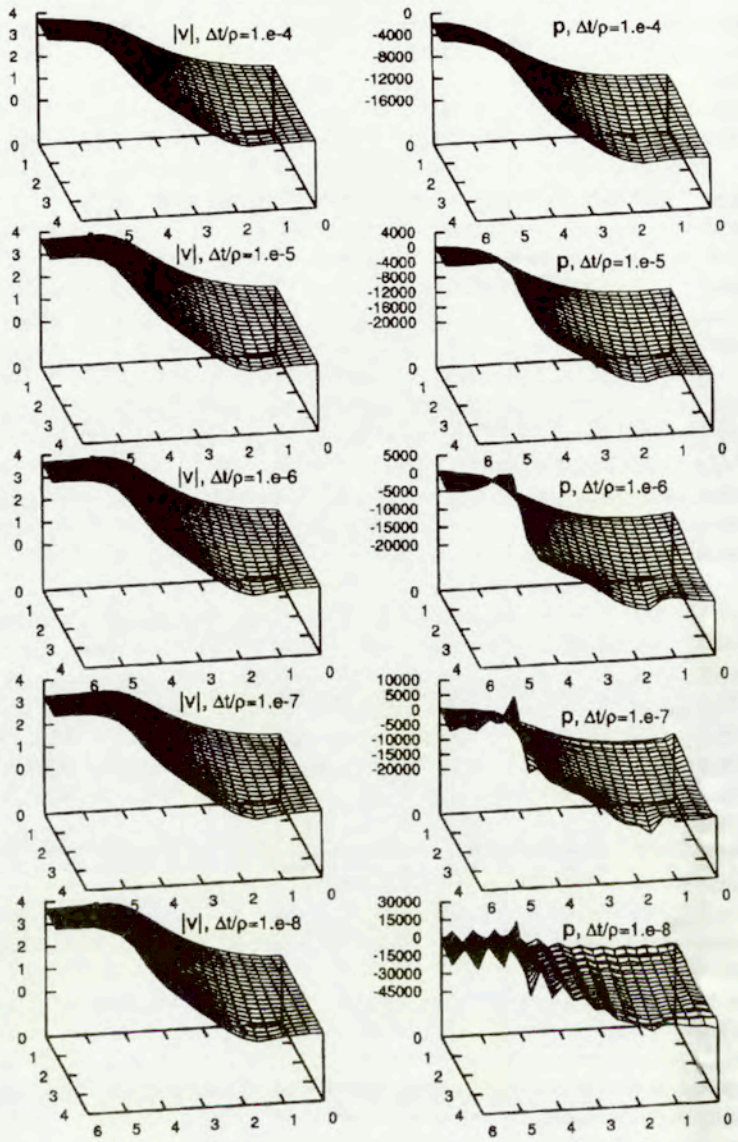

Figure 3.3 Velocity module and pressure for different values of $\Delta t/\rho$ using a direct solution method.

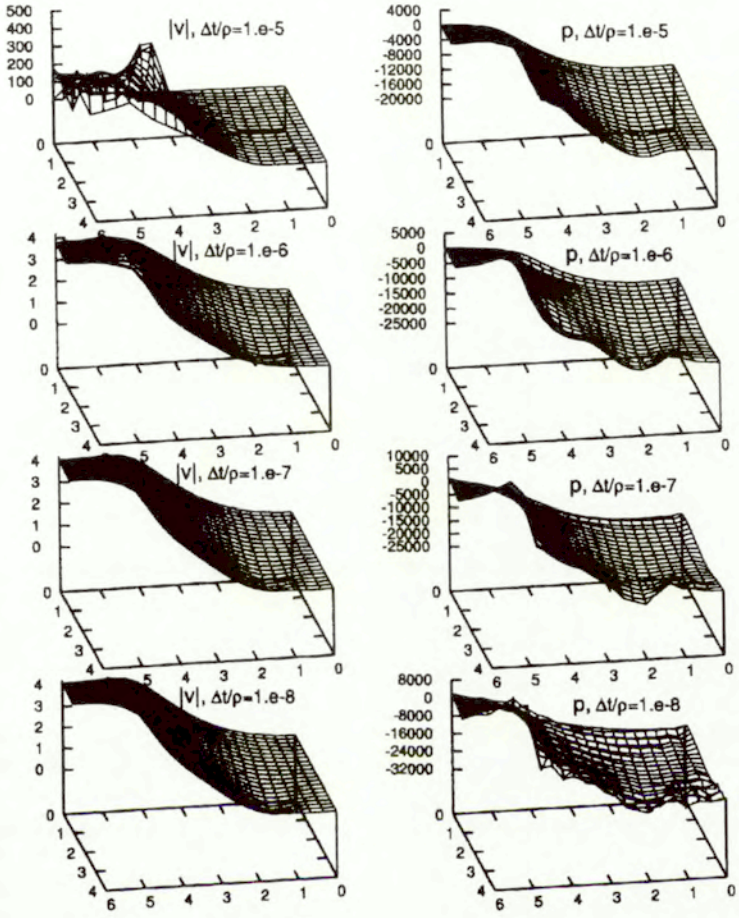

Figure 3.4 Velocity module and pressure for different values of $\Delta t/\rho$ using the explicit method.

prevent the appearance of a dead zone; maximum compression in contact with the die, near the outlet; material unloading right outside the die.

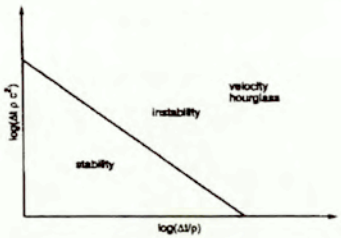

Figure 3.5 Stability range.

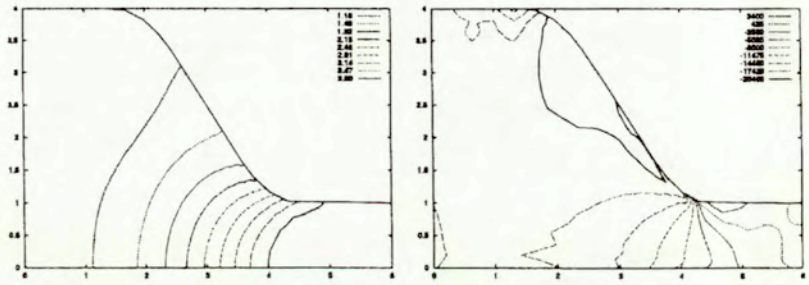

Figure 3.6 Velocity and pressure contours for the steady state.

3.2.4.2 Upsetting

In the next example a workpiece with uniform velocity meets a solid wall. The vertical velocities on the boundary nodes of the first elements (on the left part of the mesh) are constrained to assure the above condition. As the process advances the right end spreads normal to the die velocity. Figure 3.7 shows the meshes obtained for different time stations. All the non-constrained part of the workpiece experiments thickening, Small changes in the deformation patterns have been observed when comparing a highly viscoplastic material with an almost perfectly plastic one. These two cases have been calculated by assuming values of 1.5 and 40 for the viscoplastic index n, respectively.

By inspection of the deformed mesh, we can notice some instabilities in the free boundary which are due to a local time step over the critical value. However, the instabilities have not propagated to the rest of the solution. In fact, some small instabilities are also present in the pressure field, cf. Fig. 3.7h, but also the general patterns of the isocurves are correct.

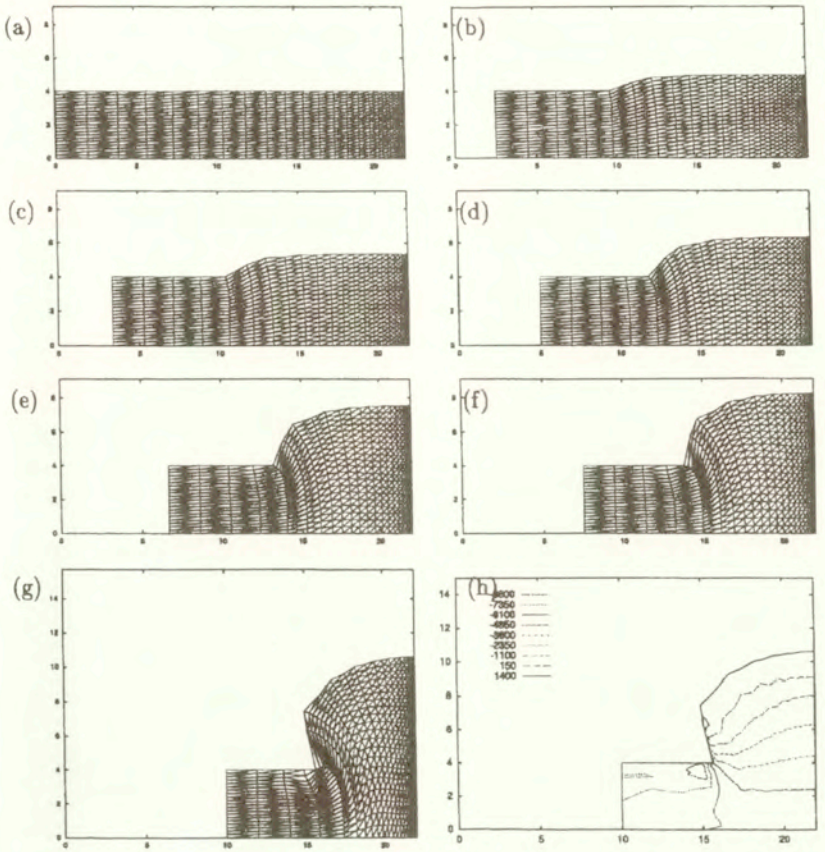

Figure 3.7 Upsetting. Meshes at a) t=0, b) 0.25, c) 0.33, d) 0.50, e) 0.66, f) 0.75 and g) 1.0, and h) pressure isocurves at t=1.

3.2.4.3 Transient extrusion

We now model the filling of an extrusion matrix by plastic deformation of an initially rectangular piece. The layout of the process is similar to that given in Fig. 3.2. The die corners have been rounded to avoid singularities in the velocity field and to reduce the dead zone. The problem is governed by the movement of the ram. A constant friction coefficient of $\nu = 0.2$ (cf. Eq. (3.24)) has been assumed. The sequence of meshes as the material gets into the extrusion die is shown in Fig. 3.8.

It can be seen that as an effect of friction the mesh is moderately distorted, and only over the end of the process remeshing becomes necessary. The velocity and

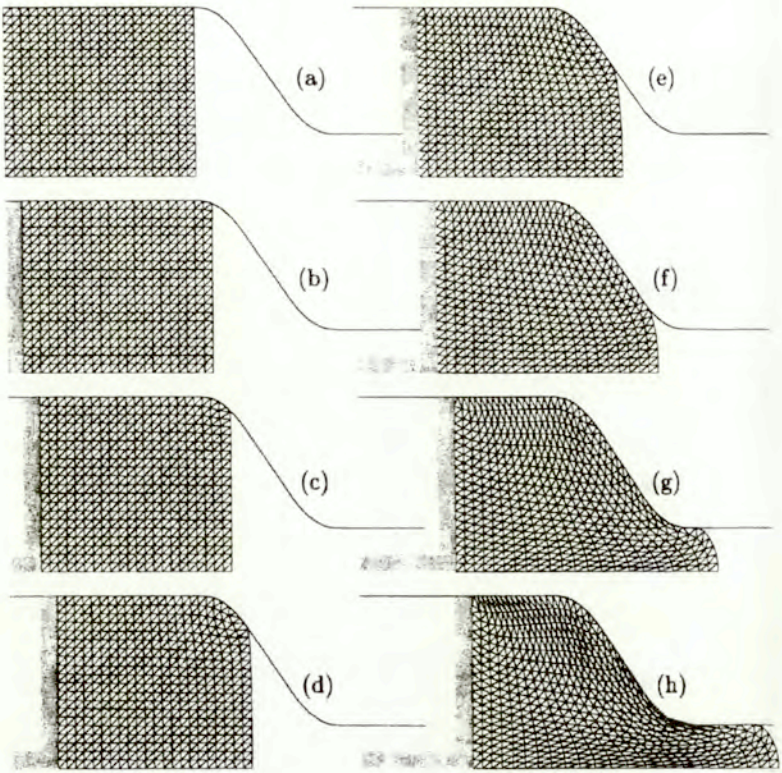

Figure 3.8 Transient extrusion, meshes at a) t=0, b) t=0.4, c) t=0.7, d) t=1.0, e) t=1.4, f) t=1.8, g) t=2.2, h) t=2.5.

pressure contours for the final mesh are shown in Fig. 3.9, in which the standard patterns can be recognized. Now a dead zone appears because of friction, and maximum pressure occurs at the upper left corner for the same reason.

The positive (from the point of view of simulation) effect of friction on the mesh distortion is further illustrated by comparison with the solution of the frictionless case. The upper right corner undergoes plastic deformation first. For the assumed process conditions (extrusion ratio, die angle, ram velocity, no boundary friction) the maximal velocity and velocity gradient occur in this zone. Therefore it is the most critical part of the domain and where the largest mesh distortion takes place. In Fig. 3.10a the mesh at $t = 1.6$ is shown, after an intermediate remeshing at $t = 1.0$. The unrealistic shape of the front edge results from the frictionless boundary condition. Because of the elongation of the

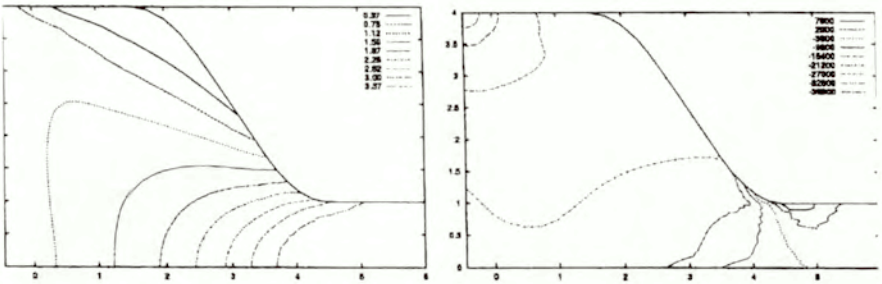

Figure 3.9 Transient extrusion: velocity module and pressure contours at t=2.5.

elements, the error in describing the boundary shape is noticeable. Nevertheless, the pressure contours, shown in Fig. 3.10b follow the standard patterns, the same as other quantities.

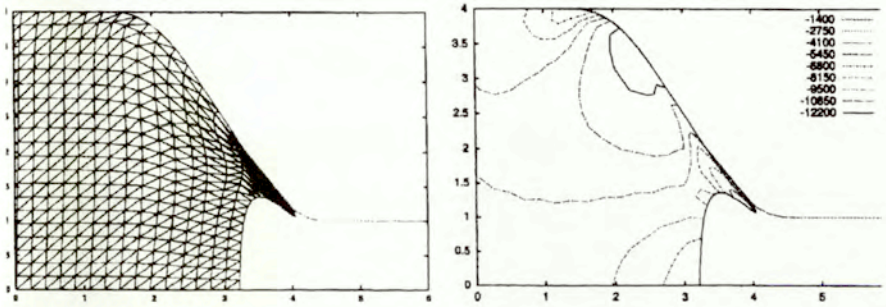

Figure 3.10 Frictionless transient extrusion: final mesh, and pressure contours at t=1.60.

3.2.4.4 3D upsetting

Finally, the upsetting of the prismatic bar schematically shown together with the finite element mesh in Fig. 3.11, is modeled. The right end constitutes a symmetry plane and thus the corresponding boundary conditions have been assigned: constrained longitudinal (z) and free in-plane (x, y) velocity components. Conversely, on the left end, simulating the effect of a tool with sticking (no slip) condition contact, longitudinal velocities are imposed and in-plane velocities are fixed to zero. The mesh represents one eighth of the bar, and xz and yz are also symmetry planes.

The velocity and pressure contours are shown in Fig. 3.12 for a length reduction of $r = 30\%$. The respective velocity components grow smoothly from

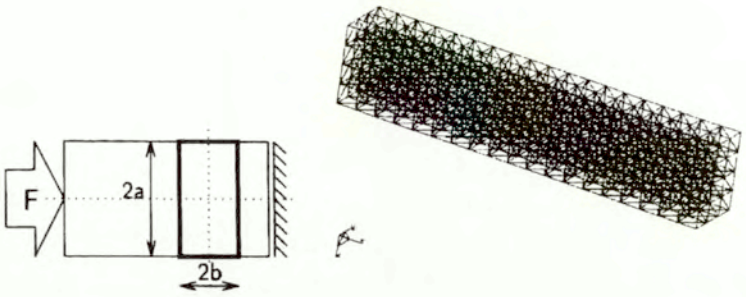

Figure 3.11 3D upsetting. Finite element mesh.

zero at the symmetry planes towards the opposite external face. The pressure field reflects the effect of the boundary conditions: in contact with the punch the pressure is maximal at the middle sides, while on the symmetry plane the pressure are maximal at the center and at the corners.

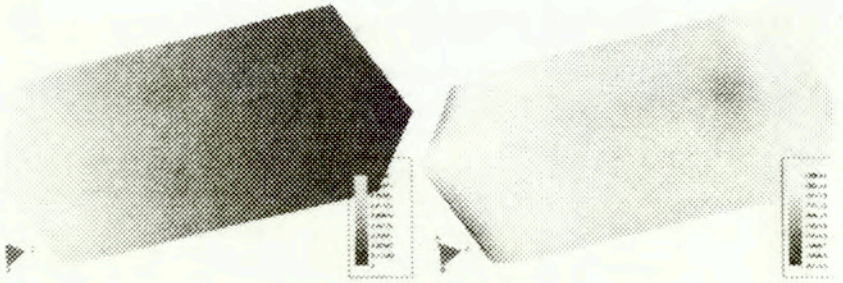

Figure 3.12 3D upsetting. Velocity module and pressure contours for a 30% reduction.

The above mentioned features can be seen with more detail in Fig. 3.13 for $r = 0\%$ and Fig. 3.14 for $r = 30\%$, where the in-plane velocities and the pressure have been plotted for the center ($x = 0$, $y = 0$), the middle side points ($x = a$, $y = 0$ and $x = 0$, $y = b$), and the corner ($x = a$, $y = b$), where the section is $2a \times 2b$, with $a > b$. At the beginning the border effects are concentrated on both mesh edges, while a relatively long constant zone for the solution is obtained. This zone is smaller as the upsetting process develops. The two v_x and the two v_y velocities plotted are similar. A different constant value for each of the

pairs is due to section shape ($a \neq b$). The pressures at both middle side points are similar and decrease toward the symmetry axis. Instead, the pair center-of-section–corner points show an opposite behaviour: when one increases the other decreases. This fact, as stated, results from the boundary conditions.

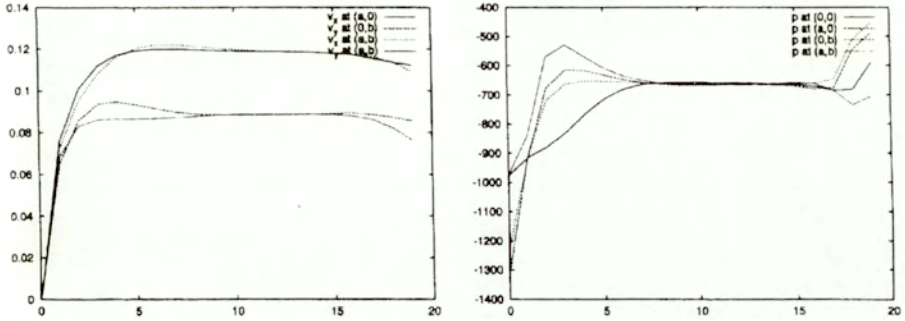

Figure 3.13 3D upsetting. x and y velocity components and pressure in selected points at t=0.

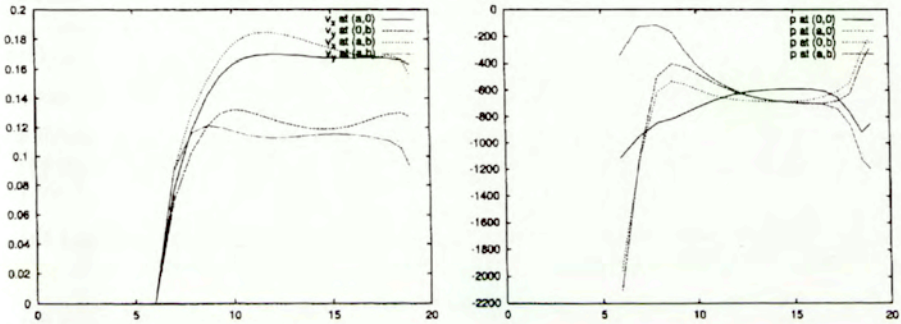

Figure 3.14 3D upsetting. x and y velocity components and pressure in selected points at t=0.6.

3.3 Sensitivity analysis

Having solved the analysis problem by use of the split algorithm, we may proceed as in Chapter 2 and derive the sensitivity expressions for this problem and its numerical model [5]. Again, we expect additional information about the process and the numerical parameters involved in the model.

The most straightforward way for sensitivity analysis of the present problem together with its numerical model is to apply the Direct Differentiation Method to the discrete set of equations. We differentiate the already discretized equilibrium equations, Eqs. (3.16) and (3.17) with respect to a design parameter h. Equivalently, we can differentiate the continuum equations and then discretize the problem, which would also include time-step splitting for the time integration of the sensitivity coefficients, although we can also assume another strategy and even another discretization for the sensitivity stage. If that is not the case, we obtain, with either method, the design-differentiated system

$$\begin{aligned}
&\frac{\partial}{\partial h}\left(\frac{1}{\Delta t}\mathbf{M}\right)(\bar{\tilde{\mathbf{q}}}-{}^{t}\bar{\mathbf{q}})+\frac{1}{\Delta t}\mathbf{M}\left(\frac{\mathrm{d}\bar{\tilde{\mathbf{q}}}}{\mathrm{d}h}-\frac{\mathrm{d}{}^{t}\bar{\mathbf{q}}}{\mathrm{d}h}\right)\\
&\qquad+\frac{\partial \mathbf{K}_1}{\partial h}{}^{t}\bar{\mathbf{q}}+\mathbf{K}_1^{(T)}\frac{\mathrm{d}{}^{t}\bar{\mathbf{q}}}{\mathrm{d}h}-\frac{\partial {}^{t}\bar{\mathbf{Q}}}{\partial h}=0\\
&\frac{\partial}{\partial h}\left(\frac{1}{\Delta t}\mathbf{M}\right)({}^{t+\Delta t}\bar{\mathbf{q}}-\bar{\tilde{\mathbf{q}}})+\frac{1}{\Delta t}\mathbf{M}\left(\frac{\mathrm{d}^{t+\Delta t}\bar{\mathbf{q}}}{\mathrm{d}h}-\frac{\mathrm{d}\bar{\tilde{\mathbf{q}}}}{\mathrm{d}h}\right)\\
&\qquad+\frac{\partial \mathbf{K}_2}{\partial h}\bar{\tilde{\mathbf{q}}}+\mathbf{K}_2\frac{\mathrm{d}\bar{\tilde{\mathbf{q}}}}{\mathrm{d}h}-\frac{\mathrm{d}{}^{t}\bar{\mathbf{Q}}_{(\mathrm{p})}}{\mathrm{d}h}=0
\end{aligned}\tag{3.26}$$

where the tangent matrix of $\mathbf{K}_1$ reads

$$\mathbf{K}_1^{(T)}=\begin{bmatrix}\mathbf{K}_{(\mu)}^{(T)} & \mathbf{0}\\ \mathbf{0} & \mathbf{0}\end{bmatrix}=\mathbf{K}_1+\begin{bmatrix}\dfrac{\partial K_{(\mu)\alpha\gamma}}{\partial q_\beta}q_\gamma & \mathbf{0}\\ \mathbf{0} & \mathbf{0}\end{bmatrix}\tag{3.27}$$

while $\mathbf{K}_2$ is identical to its tangent $\mathbf{K}_2^{(T)}$, since Eq. (3.17) is linear in $\tilde{\mathbf{q}}$ and the pressure entries of the derivative of $\bar{\mathbf{Q}}_{(\mathrm{p})}$ read

$$\frac{\mathrm{d}{}^{t}Q_{(\mathrm{p})\alpha}}{\mathrm{d}h}=\frac{\partial {}^{t}Q_{(\mathrm{p})\alpha}}{\partial h}+\frac{\Delta t}{\rho}\int_{\partial\Omega}\hat{\phi}^{(\alpha)}\frac{\partial\hat{\phi}^{(\beta)}}{\partial x_i}n_i\,\mathrm{d}(\partial\Omega)\frac{\mathrm{d}{}^{t}p_\beta}{\mathrm{d}h}\tag{3.28}$$

If we obtain from Eqs. (3.16) and (3.17) and replace into Eq. (3.26) respectively $(\bar{\tilde{\mathbf{q}}}-{}^{t}\bar{\mathbf{q}})$ and $({}^{t+\Delta t}\bar{\mathbf{q}}-\bar{\tilde{\mathbf{q}}})$, we arrive at expressions for $\mathrm{d}\bar{\tilde{\mathbf{q}}}/\mathrm{d}h$ and $\mathrm{d}^{t+\Delta t}\bar{\mathbf{q}}/\mathrm{d}h$ —our only unknowns— which do not depend, respectively, on $\bar{\tilde{\mathbf{q}}}$ and ${}^{t+\Delta t}\bar{\mathbf{q}}$,

$$\begin{aligned}
&\frac{\partial}{\partial h}\left(\frac{1}{\Delta t}\mathbf{M}\right)\Delta t\mathbf{M}^{-1}(\mathbf{K}_1{}^{t}\bar{\mathbf{q}}-{}^{t}\bar{\mathbf{Q}})+\frac{1}{\Delta t}\mathbf{M}\left(\frac{\mathrm{d}\bar{\tilde{\mathbf{q}}}}{\mathrm{d}h}-\frac{\mathrm{d}{}^{t}\bar{\mathbf{q}}}{\mathrm{d}h}\right)\\
&\qquad+\frac{\partial \mathbf{K}_1}{\partial h}{}^{t}\bar{\mathbf{q}}+\mathbf{K}_1^{(T)}\frac{\mathrm{d}{}^{t}\bar{\mathbf{q}}}{\mathrm{d}h}-\frac{\partial {}^{t}\bar{\mathbf{Q}}}{\partial h}=0\\
&\frac{\partial}{\partial h}\left(\frac{1}{\Delta t}\mathbf{M}\right)\Delta t\mathbf{M}^{-1}(\mathbf{K}_2\bar{\tilde{\mathbf{q}}}-{}^{t}\bar{\mathbf{Q}}_{(\mathrm{p})})+\frac{1}{\Delta t}\mathbf{M}\left(\frac{\mathrm{d}^{t+\Delta t}\bar{\mathbf{q}}}{\mathrm{d}h}-\frac{\mathrm{d}\bar{\tilde{\mathbf{q}}}}{\mathrm{d}h}\right)\\
&\qquad+\frac{\partial \mathbf{K}_2}{\partial h}\bar{\tilde{\mathbf{q}}}+\mathbf{K}_2\frac{\mathrm{d}\bar{\tilde{\mathbf{q}}}}{\mathrm{d}h}-\frac{\mathrm{d}{}^{t}\bar{\mathbf{Q}}_{(\mathrm{p})}}{\mathrm{d}h}=0
\end{aligned}\tag{3.29}$$

therefore the sensitivity coefficients can be obtained simultaneously to them, which means that the sensitivity stage does not introduce additional steps or sub-steps, and can be obtained together with the solution of the analysis problem.

The boundary conditions for the sensitivity stage are similar to those of the analysis stage[120, 4] (see Section 3.2.3): only natural for the intermediate quantities ($\mathrm{d}\bar{\mathbf{q}}/\mathrm{d}h$), and essential and natural for the end-of-step quantities ($\mathrm{d}^{t+\Delta t}\bar{\mathbf{q}}/\mathrm{d}h$), according to the imposed geometrical restrictions. It should be noticed that to boundaries with non-zero imposed values zero sensitivity corresponds.

The design parameter h can be any material, shape and numerical parameter (as the time step), which means that sensitivity analysis may be used to asses the effect of assuming certain values of them.

The general expression Eq. (3.29) further simplifies by considering particular choices of the design parameter. By inspection of Eq. (3.29) it comes out that only the following derivatives are needed

$$\frac{\partial \mathbf{K}_1}{\partial h}\ ;\ \frac{\partial {}^t\bar{\mathbf{Q}}}{\partial h}\ ;\ \frac{\partial \mathbf{K}_2}{\partial h}\ ;\ \frac{\mathrm{d}\,{}^t\bar{\mathbf{Q}}_{(\mathrm{p})}}{\mathrm{d}h}\ ;\ \frac{\partial}{\partial h}\left(\frac{1}{\Delta t}\mathbf{M}\right)\Delta t\mathbf{M}^{-1} \tag{3.30}$$

The first three quantities can be calculated from what we know from Section 2.3. The next one results in a term involving already calculated pressure sensitivities, and another term involving the pressure multiplied by factors which can be design parameters, in which case the corresponding term is non-zero. Only $\mathbf{K}_1$ depends on parameters entering Eq. (2.3) i.e. through the viscosity μ which multiplies the whole matrix. $\mathbf{K}_2$ is constant and does not depend on material nor numerical parameters. Finally, to calculate the product $\frac{\partial}{\partial h}\left(\frac{1}{\Delta t}\mathbf{M}\right)\Delta t\mathbf{M}^{-1}$ let us notice (cf. Eq. (3.6)) that $\mathbf{M}$ is diagonal, thus so it will be the whole product. Writing separately the matrices $\mathbf{M}_{(v)}$ and $\mathbf{M}_{(\rho)}$, results

a) for $h = \Delta t$

$$\begin{aligned}\frac{\partial}{\partial \Delta t}\left(\frac{1}{\Delta t}\mathbf{M}_{(v)}\right)\Delta t\mathbf{M}_{(v)}^{-1} &= -\frac{1}{\Delta t}\mathbf{I}\\ \frac{\partial}{\partial \Delta t}\left(\frac{1}{\Delta t}\mathbf{M}_{(\rho)}\right)\Delta t\mathbf{M}_{(\rho)}^{-1} &= -\frac{1}{\Delta t}\mathbf{I}\end{aligned} \tag{3.31}$$

b) for $h = \rho$

$$\begin{aligned}\frac{\partial}{\partial \rho}\left(\frac{1}{\Delta t}\mathbf{M}_{(v)}\right)\Delta t\mathbf{M}_{(v)}^{-1} &= \frac{1}{\rho}\mathbf{I}\\ \frac{\partial}{\partial \rho}\left(\frac{1}{\Delta t}\mathbf{M}_{(\rho)}\right)\Delta t\mathbf{M}_{(\rho)}^{-1} &= -\frac{1}{\rho}\mathbf{I}\end{aligned} \tag{3.32}$$

c) for $h = c$

$$\begin{aligned}\frac{\partial}{\partial c}\left(\frac{1}{\Delta t}\mathbf{M}_{(v)}\right)\Delta t\mathbf{M}_{(v)}^{-1} &= \mathbf{0}\\ \frac{\partial}{\partial \rho}\left(\frac{1}{\Delta t}\mathbf{M}_{(\rho)}\right)\Delta t\mathbf{M}_{(\rho)}^{-1} &= -\frac{2}{\rho}\mathbf{I}\end{aligned} \tag{3.33}$$

while it will vanish for any other already considered design parameter.

3.3.1 Computational illustrations

3.3.1.1 Steady state extrusion

First, sensitivity analysis is carried out for a steady state extrusion process as shown in the first example of Section 3.2.4. The layout and finite element mesh are shown in Fig. 3.2. Let us remind that velocities are imposed on the left side thus simulating the effect of the ram. Boundary friction is simulated using contact elements that impose a Coulomb friction force proportional to the pressure, with a velocity restriction to avoid oscillations around sticking friction. Time integration is carried out within a fixed mesh until steady state is achieved.

Figure 3.15 shows the velocity module and pressure surfaces as seen from the upper right corner of the extrusion matrix. The velocity grows smoothly from 1 to 4, according to the extrusion ratio. The pressure reflects compression inside the die with unloading towards the exit. A slight oscillation takes place due to the effect of boundary conditions near the outlet. Figures 3.16 to 3.18 show the sensitivity of both quantities (i.e. velocity module and pressure) with respect to the parameters of the constitutive equation: yield stress σ_0, fluidity γ and index of the viscoplastic law n, respectively. The assumed values for these quantities are: $\sigma_0 = 200$, $\gamma = 10^{-6}$ and $n = 1.5$, corresponding to a rather rate sensitive material as steel in hot working conditions. In every case the DDM and FDM solutions are in good agreement, either when the sensitivity coefficients are small with respect to the values of the variable (Fig. 3.16a) or very large (Fig. 3.17b)

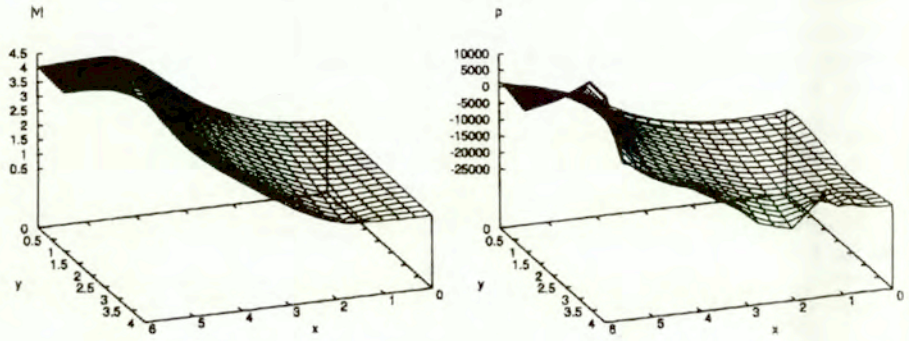

Figure 3.15 Velocity module $|\mathbf{u}|$ and pressure p

The characteristics of these results are the same as for the solution by a direct method, as has been presented in [10]: for this case of imposed velocities (instead of imposed boundary force) the pressure sensitivity with respect to the yield stress is quite proportional to the pressure itself, and the velocity module is almost insensitive. Results are very sensitive to the fluidity, which is in agreement

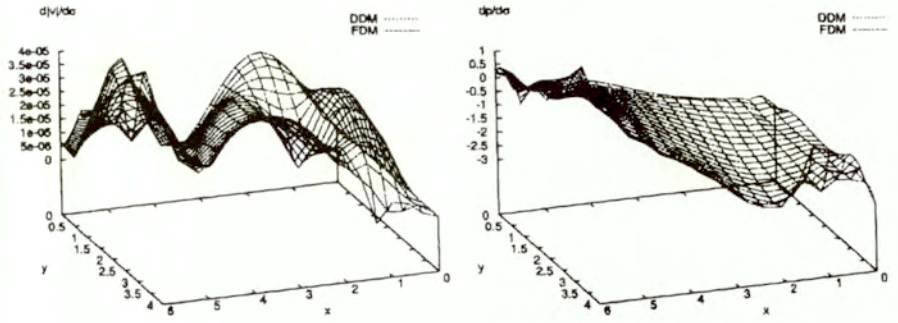

Figure 3.16 Sensitivity of |u| and p with respect to the static yield stress σ

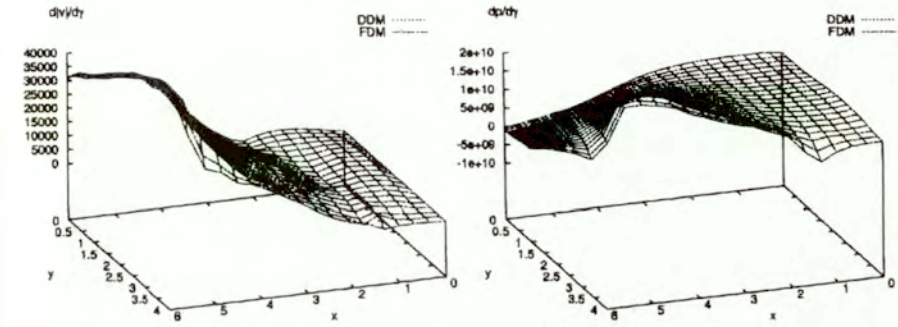

Figure 3.17 Sensitivity of |u| and p with respect to the fluidity parameter γ

with its small nominal value. Velocity sensitivities grow from zero in contact with the ram (where velocity is imposed) to its maximal value at the exit. Conversely, pressure sensitivities are at their maximum near the ram and drop to zero at the exit.

Sensitivity analysis can also be applied to obtain information about the numerical method used to simulate a given process[3]. In particular, in the present example the time step Δt, the material density ρ_o and the sound velocity c have been taken as design parameters for nominal values of 10^{-6}, 10, and 10^{-11}, respectively. The sensitivities of the velocity module and pressure with respect to them are shown in Figs. 3.19 to 3.21. Again, agreement is found between FDM and DDM. We can see that sensitivities with respect to material density are proportional to those with respect to the time step, with a negative proportionality constant for the pressure. From Figs. 3.19 and 3.20 we can get 10^{-7} as the value of the constant, which is equal to $\Delta t/\rho_o$. (This result also comes out easily by

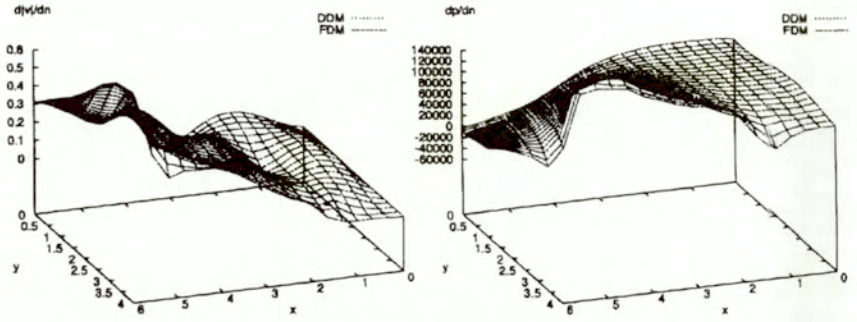

Figure 3.18 Sensitivity of $|\mathbf{u}|$ and p with respect to the viscoplastic index n

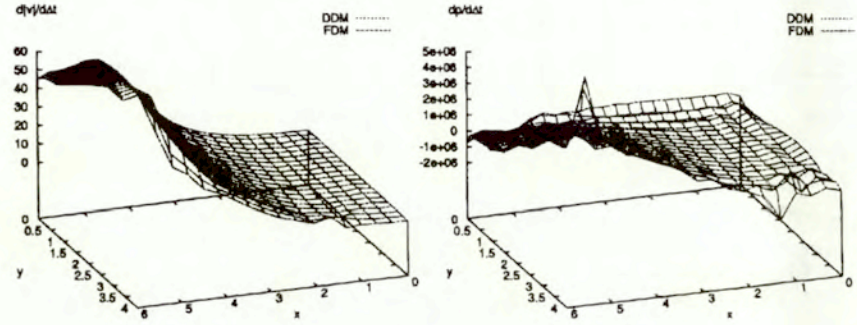

Figure 3.19 Sensitivity of $|\mathbf{u}|$ and p with respect to the time step size Δt

comparing Eq. (3.31) with Eq. (3.32).) Besides, the relatively large values for the sensitivity coefficients $\mathrm{d}|v|/\mathrm{d}h$ and $\mathrm{d}p/\mathrm{d}h$ (Fig. 3.19) result from the small nominal values of the time step. For steady state exact incompressibility is achieved, and c is only relevant for speed of convergence to the steady state. We can verify this fact in Fig. 3.21, where the sensitivities are zero except for a small local perturbation at the exit which may be due to a local loss of stability.

3.3.1.2 Upsetting

In the next example a transient process is simulated. An initially rectangular specimen moves in the x-direction by the action of a punch placed on the left end and meets a solid wall oriented perpendicularly to the movement on the right. The punch further imposes its velocity and induces a sidewise deformation on the piece. Sticking friction is assumed between the punch and the specimen.

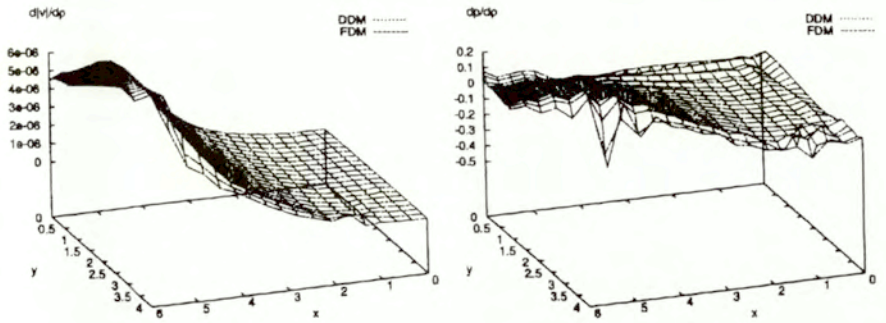

Figure 3.20 Sensitivity of $|\mathbf{u}|$ and p with respect to the density ρ_o

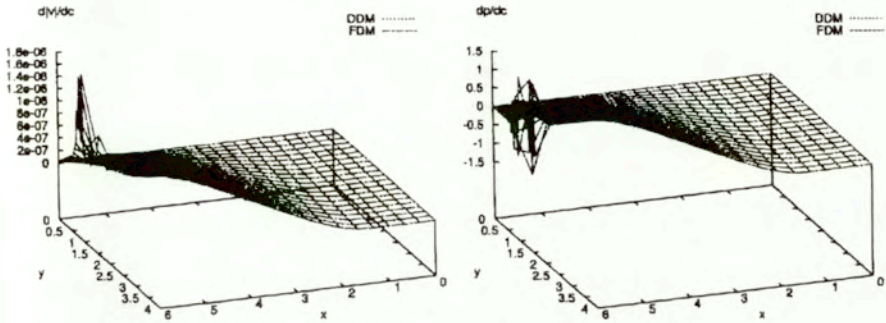

Figure 3.21 Sensitivity of $|\mathbf{u}|$ and p with respect to the velocity c

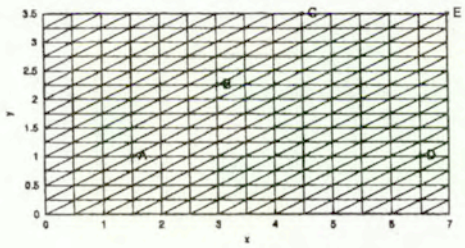

Figure 3.22 Upsetting: initial mesh and selected points

The finite element mesh is shown in Fig. 3.22, together with the position of some selected points which shall be used to illustrate the results. The velocity

components (denoted here u and v) and pressure are shown together with their sensitivity with respect to the static yield stress σ_0 at a 30% reduction of the initial length, Figs. 3.23 to 3.25. Again we notice similar features for this design variable: velocity sensitivities are several orders of magnitude lower than the nominal value of velocity, pressure sensitivity is approximately proportional to the nominal pressure. In the sensitivity plots we notice some differences when comparing both methods, FDM and DDM.

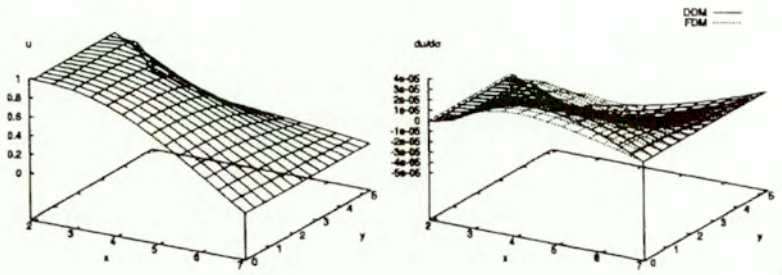

Figure 3.23 x-velocity component and sensitivity wrt σ_0 at r=30%

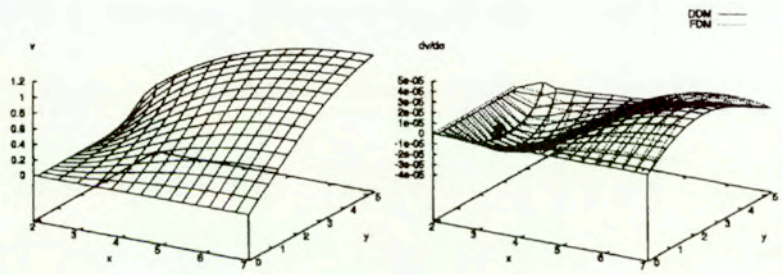

Figure 3.24 y-velocity component and sensitivity wrt σ_0 at r=30%

This fact is further illustrated in Figs. 3.26 to 3.30, where velocity components and pressure at selected points (shown in Fig. 3.22) in terms of their x-coordinate along the process, except for point E, which only moves vertically hence the y-coordinate is used. The differences grow as the process develops. However, it has been noticed that the differences between the curves yielded by DDM and

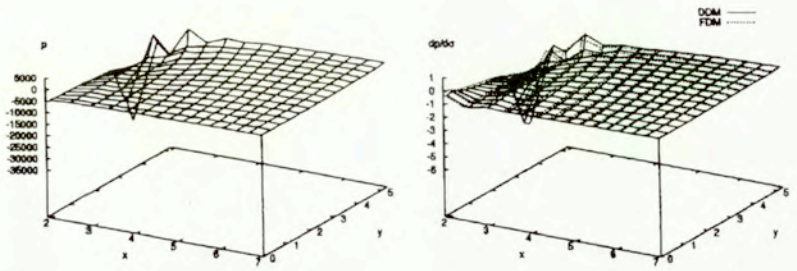

Figure 3.25 pressure and sensitivity wrt σ_0 at r=30%

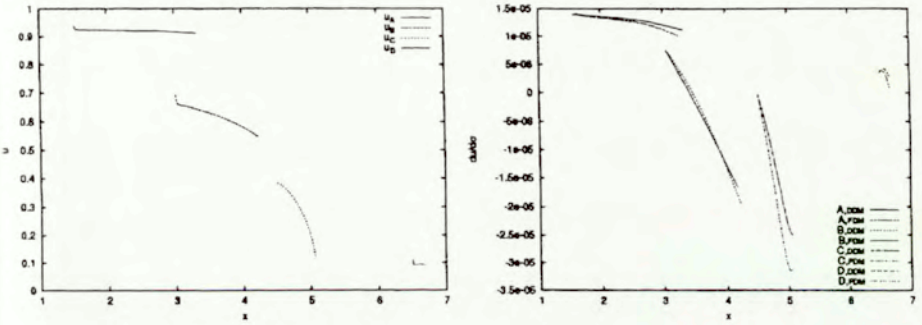

Figure 3.26 x-velocity component and sensitivity wrt σ_0 *vs* x-coordinate

FDM decrease both when a smaller perturbation is taken and when the time step size Δt is reduced. These facts highlight the cumulative nature of the error, characteristic of explicit methods, and suggest that FDM results will converge to those of DDM when both sources of error —i.e. of finite size of the perturbation in FDM and that of time integration, are further reduced.

3.4 Concluding remarks

Linear elements for analysis of metal forming processes have been presented in the context of explicit time integration. The method shows a capability of efficient simulation of different metal forming operations. Good agreement has been found with other methods. The effect of the time step and of some material properties which act as numerical parameters has been analyzed. It comes out that a proper

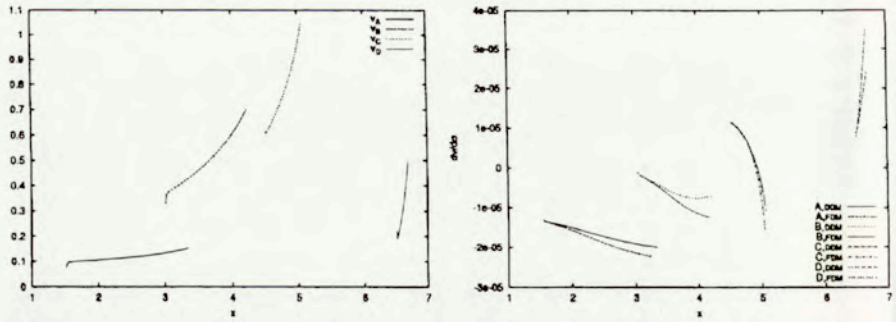

Figure 3.27 y-velocity component and sensitivity wrt σ_0 *vs* x-coordinate

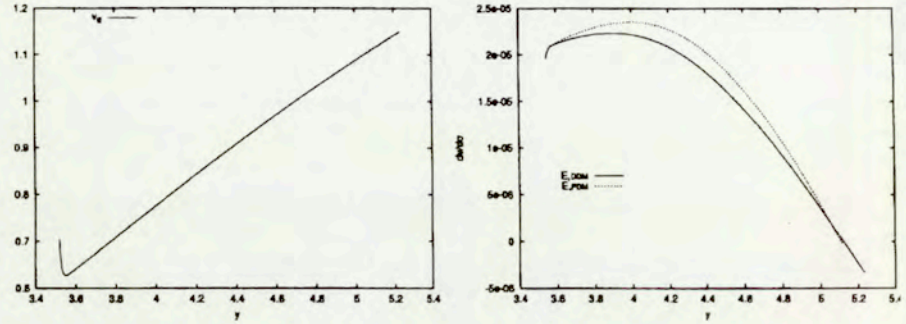

Figure 3.28 y-velocity component and sensitivity wrt σ_0 *vs* y-coordinate

choice of the set is crucial to obtain good results. The key point is the appropriate choice of the split, which allows for the use of equal order interpolation for both discretized variables, while holding (at least approximately, in the explicit case) the incompressibility condition. This is an interesting result because it allows for the use of linear (i.e. triangles and tetrahedra) elements, for which simpler and more robust automatic mesh generators than for quadrilaterals and hexahedra are available. In turn, mesh generators are required for remeshing during operations where large deformations develop, such as metal forming.

The reformulation for the implicit method of most of the results and analyses performed for the full explicit case is straightforward. The explicit version, although it is restricted by the time step size, may be easily parallelized, with an almost ideal, linear speed-up.

The method has been extended with sensitivity analysis by direct differentia-

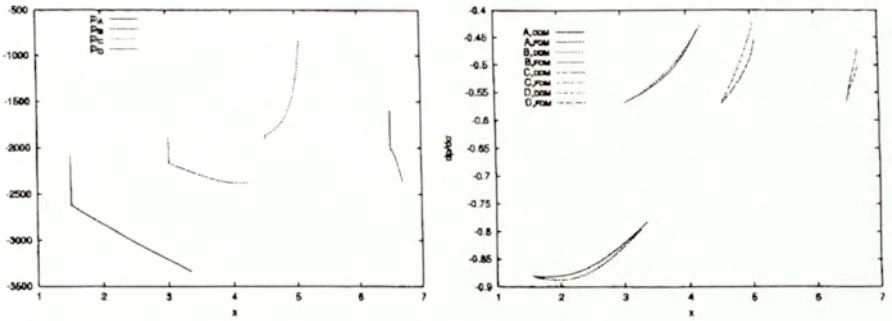

Figure 3.29 pressure and sensitivity wrt σ_0 *vs* x-coordinate

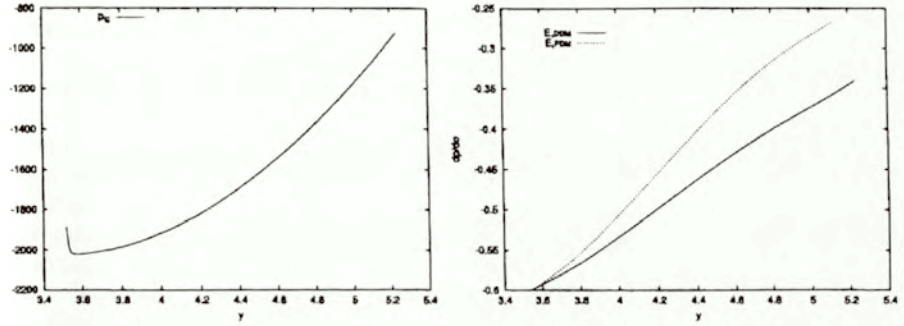

Figure 3.30 pressure and sensitivity wrt σ_0 *vs* y-coordinate

tion of the governing equations. The goal of this technique lays on the calculation of the sensitivity coefficients simultaneously to the analysis problem solution. Although the cost of the sensitivity stage in terms of computational time is comparatively larger than in direct solution methods, the solution is clearly more convenient than that obtained by using finite differences, and besides it does not depend on the size of the perturbation which, as shown, introduces a cumulative error in the sensitivity coefficients. The method is especially suited for large problems, where explicit time integration becomes more convenient than implicit.

The effect of numerical parameters introduced by solution methods has been shown to be also an interesting subject of sensitivity analysis. In particular, for explicit time integration the sensitivity with respect to the time step 'amplifies' the information already available with the solution of the equilibrium problem. Some local lack of stability can be noticed, which hardly would be visible otherwise, e.g. because it would require special post-processing of the numerical solution, such as Fourier analysis.

Chapter 4

Special topics on metal forming

4.1 Introductory comments

This chapter is devoted to two subjects which, although make use of the model we have been dealing with in this work, could not be discussed (for didactic reasons) in the sequence

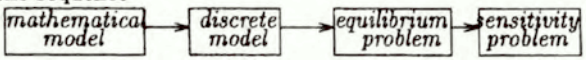

which has been assumed throughout the preceding chapters. Both are fully based on the flow approach and apply to metal-forming processes. Moreover, it is believed that they highlight some aspects of the model behaviour under particular conditions, which surely helps to a better and deeper knowledge of metal-forming issues.

On the basis of the numerical simulation of cutting problems, where the (a priori unknown) free surface plays a key role, a nearly ideally plastic material is used to investigate on the existence of non-uniqueness.

Secondly, transient problems are considered in the context of the so-called pseudo-concentration method [7, 103, 104] and on this basis a semi-analytical model is developed to deal with cylindrical geometry with non-axisymmetric loads, boundary conditions and free surfaces.

4.2 Non–unique numerical solutions in visco–plasticity

4.2.1 Introductory comments

The behavior of a perfectly plastic material under continuous deformation has attracted the attention of researchers for several decades. Although in most of the contributions severe assumptions have been stated —namely, no strain hardening, no stress rate dependence, two dimensional flow, isothermal conditions, etc.—,

astonishingly accurate results can be obtained as compared with experimental data.

The mathematical model for rigid–perfectly plastic material yields a hyperbolic system of differential equations. Among traditional methods for solving this system of equations, the slip line field theory [102] is for sure the most popular, and the one that has been used in most different problems. Special attention was devoted to the presence of non–unique solutions, all of which are complete in the sense that they satisfy all the static and kinematic requirements. This non–uniqueness is partly due to the idealized nature of the material model, but in addition, it has been proved [90, 91, 92] that free surfaces introduce the possibility of non–unique solutions, since the final configuration is not known. Different positions of the free surface can be shown to satisfy the governing equations, by application of the slip line theory.

On the other hand, computer numerical methods as those we have been dealing here have constituted an alternative and complementary approach to these problems. It has been possible to reproduce slip line theory results and, in addition, to find out solutions where that method is not applicable. We have discussed the flow approach in Chapters 1 and 2. As we have seen, the theory is developed for rigid–viscoplastic materials, and the perfectly plastic material is seen and obtained as its non-strain-rate-dependent limit. However, this limit involves a singular problem, from the mathematical and, therefore, numerical point of view. In [6] an effective method has been proposed which, based on matrix scaling, makes the problem better posed (by lowering the condition number of the system matrix) and, as a byproduct, substantially extends the range of strain rates for which the model can be applied without being distorted, e.g. by means of any of the methods described in Section 2.3.2.

In this section we solve the problem of cutting out a thin strip from a semi–infinite domain of a perfectly plastic material by the movement of a rigid sharp wedge parallel to the metal surface [2]. As we know, the model considers the material as a non–Newtonian fluid, and therefore the crack formation and propagation is not taken into account. The boundary conditions in most of the boundary are that of free surfaces. Its position is found as part of the solution by the procedure described in Section 2.2.5, an essential feature of which is the ability of modelling free surfaces where large variations in shape and orientation from the initial configuration may develop. As said, this behavior is taken into account by an integration along a streamline using an intrinsic coordinate system with an additional condition for determining the updated configuration. In order to avoid excessive mesh distortion, an algorithm for mesh rearrangement has also been introduced.

It has been found that the final configuration depends on the initial guess. These results appear to be sensitive to the specific configuration, *i.e.* to the wedge angle.

4.2.2 Physical and computational model

The model used in this section follows the formalism already dealt with in Section 2.2, to which the reader is referred for details. Let us only remind, for completeness, that a non-linear Stokes flow is solved via the virtual work equation in rate form together with the incompressibility condition. The equivalent viscosity for the fluid-type constitutive equation, cf. Eq. (2.2)

$$\sigma_{ij} = \sigma^{D}_{ij} - p\,\delta_{ij} = 2\mu\,\dot{\epsilon}_{ij} - p\,\delta_{ij} \tag{4.1}$$

is written as cf. Eq. (2.3)

$$\mu = \frac{1}{3\dot{\bar{\epsilon}}}\left[\sigma_0 + \left(\frac{\dot{\bar{\epsilon}}}{\gamma}\right)^{\frac{1}{n}}\right] \tag{4.2}$$

The perfectly plastic limit is obtained by letting $n \to \infty$, in Eq. (4.2).

4.2.3 Free surfaces

Upon focusing our attention to cutting simulation, we can say that the task of finding the free surfaces plays a crucial role in the solution of the overall problem. The procedure presented in Section 2.2.5, based on curvilinear integration along the free surface, which calculates its 'correction' in order to fulfill the streamline condition (i.e. zero flow of material across it, cf. Eq. (2.48)) at each iteration. This technique gives us the necessary tool to localize free surfaces of the type we find in these processes. They must be allowed to have any orientation and to reproduce possible sharp changes in direction in correspondence to zones of strain localization. This feature means an essential difference with other problems (typically of fluid mechanics) where free surfaces also take place. In such problems the parameters defining the free surface enter in the equation system as part of the unknowns. Conversely, here we calculate them externally to the set of equations, as an additional condition. Such procedure is usually referred to as *staggered* solution of a coupled problem, as we may considered the one at hand. As a result the convergence of the nonlinear set of equations is somewhat slower than it would be using a full coupled solution method, but a serious complication in the computer model is avoided. Moreover, recalling that we are interested in virtually perfectly plastic materials, we know in advance that Newton-Raphson solution of the nonlinear equation system is inapplicable [6], thus we can foretell that the calculation time would be similar with either methods for handling free surfaces.

In addition to the free surface correction at each iteration, an auxiliary Laplace problem is solved to relocate all the nodes on the domain in order to keep the mesh aspect i.e. to avoid mesh distortion (and even singularity). This procedure was also described in Section 2.2.5.

4.2.4 Plastic material with a residual viscous effect

For the numerical applications we have taken $n = 40$ in Eq. (4.2) to obtain the viscoplastic limit. If, in addition, $\sigma_0 = 200$, $\gamma = 1$, and $\sigma_{vp} = \sigma_0 + (\dot{\bar{\varepsilon}}/\gamma)^{\frac{1}{n}}$, we have

$\dot{\bar{\varepsilon}}$	σ_{vp}
10^{-6}	200.7
1	201.0
10^{6}	201.5

This means a very little, but non–null, viscous effect. A perfectly plastic material would yield to a singular stiffness matrix, making impossible the numerical solution by this method. Besides, we are interested in solving this problem with this residual viscous effect, since it has been an open question whether such behavior would eliminate any non–uniqueness. It should be kept in mind that Hill's uniqueness theorem [59] does not apply to problems involving unspecified boundaries.

4.2.5 Numerical results

For the numerical calculations we use a steady state module of a finite element code written by the author [1]. The program implements the model presented in Section 2.2, following standard finite element techniques as presented therein: mixed, velocity/pressure formulation with isoparametric nine and four node elements for velocities and pressure, respectively. The non–linear system of equations is iteratively solved by the frontal method. A simple back–substitution scheme is adopted, because the Newton–Raphson method is not applicable —it does not converge—, when the material behaviour is close to perfectly plastic.

We model a cutting problem as a semi-infinite domain, a narrow strip of which, h, is removed by the movement of a rigid sharp wedge parallel to the metal surface. For convenience of simulation, since we are describing the process within an Eulerian approach, the cutting tool is supposed to be fixed and the metal flow, to meet it. Thus a uniform, directed downwards velocity is imposed on the upper boundary. The horizontal component is enforced to be zero on the left boundary, as well as the component normal to the solid boundary. The metal chip and the undeformed matrix constitute two regions with a uniform velocity field, separated by a narrow transition zone where all the plastic deformation is concentrated. In correspondence to these two regions, the free surface has two straight segments which form a sharp angle. The line from this corner to the tool edge separates the two zones of uniform flow, i.e. with rigid body motion.

Figures 4.1 to 4.3 show three initial and final meshes for a wedge angle of 110° with respect to the imposed velocity. Initial configurations are automatically generated by giving a set of parameters defining the geometry, where the assumed chip thickness, e_0 (i.e. the width of the "arm" at the right part of the model),

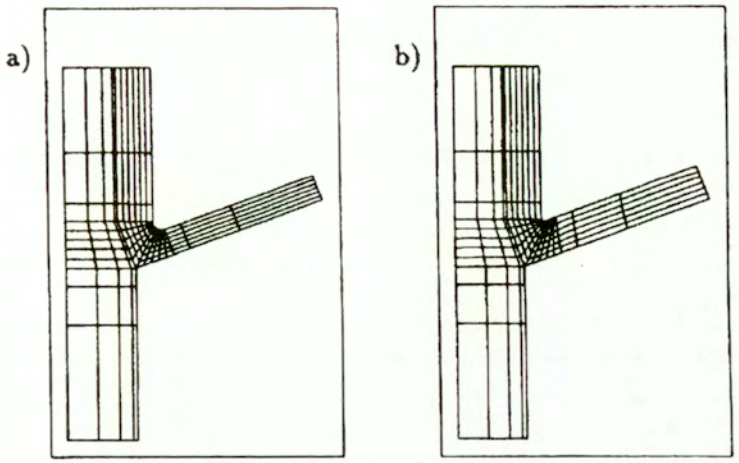

Figure 4.1 Wedge angle = 110°, mesh 1. **a**: Initial mesh. **b**: Final mesh.

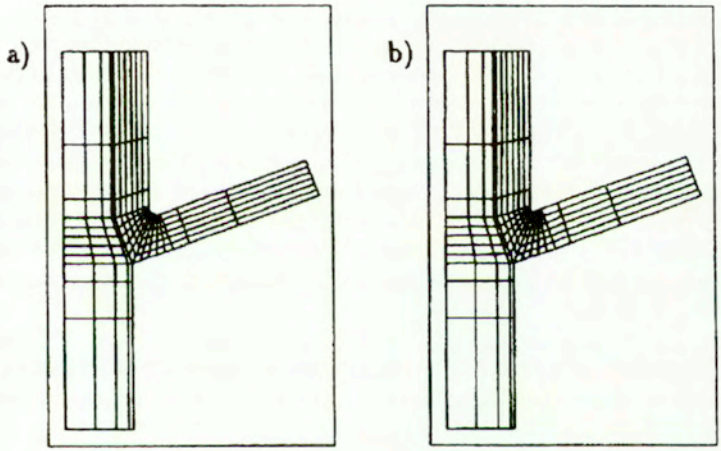

Figure 4.2 Wedge angle = 110°, mesh 2. **a**: Initial mesh. **b**: Final mesh.

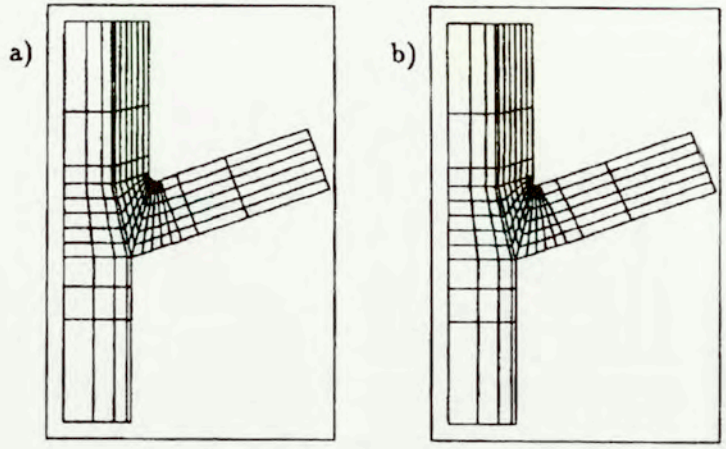

Figure 4.3 Wedge angle = 110°, mesh 3. **a**: Initial mesh. **b**: Final mesh.

is the main variable. It is pointed out that the different final chip thicknesses correspond to the steady–state solutions and result from assuming different initial configurations, as shown in the figures. We state that the solution is not mesh dependent, since we have refined the mesh both in the direction parallel and normal to the free surface, and obtained essentially the same results. Minor variations are produced by changing the initial radius connecting both parts of the domain, which can also be seen as producing different initial configurations.

The range of obtained solutions is shown in Fig. 4.4, where, in terms of the initial chip thickness/cutting depth ratio (e_0/h), both the final chip thickness/cutting depth ratio (e/h) and a thickness/cutting depth ratio normalized in terms of the applied force and the stress at pure shear (ek/Th) are visualized. The latter can be compared with Petryk's non-unique solution [91], whose extreme values are shown by the dashed lines in the same figure. In Fig. 4.5 the strain rate contours are plotted, showing how the velocity gradients are concentrated in a narrow band.

Similar calculations are carried out for tool angles of 90° and 70° (Figs. 4.6 to 4.9) showing final meshes and thickness/cutting depth ratios. It can be pointed out that decreasing the wedge angle, the sensitivity to initial guesses decreases.

4.2.6 Concluding remarks

We have shown the numerical solution of some cutting problems where non-uniqueness is found by considering different initial guesses. Because the rigid–perfectly plastic material is reached as a limit of the rigid–visco–plastic one, a

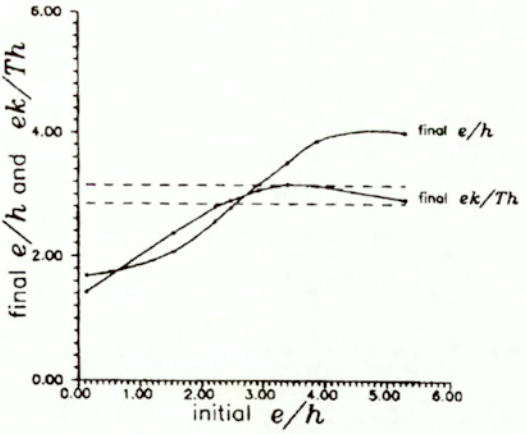

Figure 4.4 Wedge angle = 110°, chip thickness/cutting depth ratio.

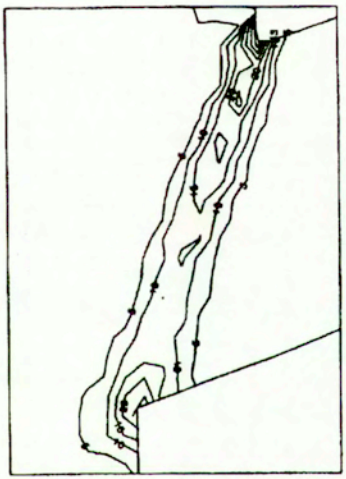

Figure 4.5 Strain rate contours.

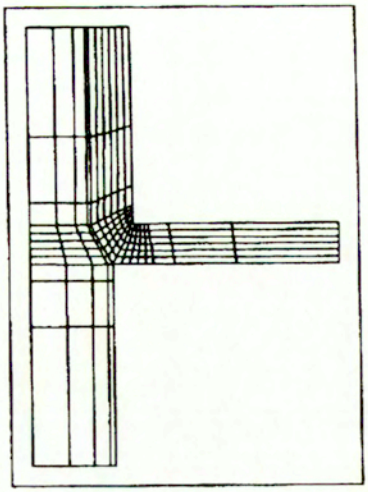

Figure 4.6 Wedge angle = 90°, final mesh.

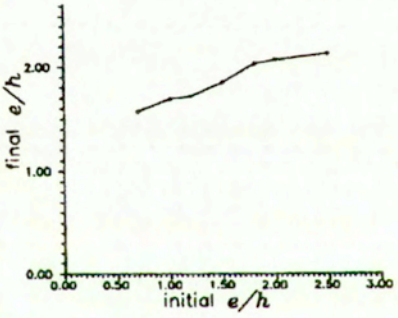

Figure 4.7 Wedge angle = 90°, chip thickness/cutting depth ratio.

residual rate sensitivity is present, and still the non–uniqueness is present. This means that a small amount of rate dependence does not eliminate the non–uniqueness in the cutting problem.

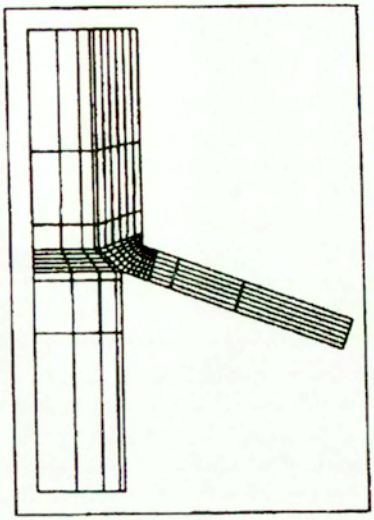

Figure 4.8 Wedge angle = 70°, final mesh.

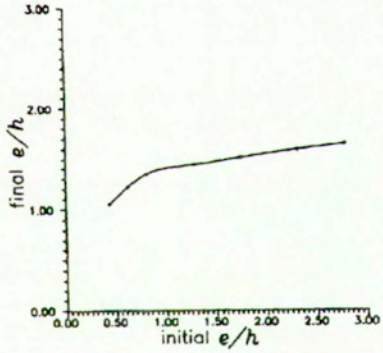

Figure 4.9 Wedge angle = 70°, chip thickness/cutting depth ratio.

4.3 Transient analysis of tube rolling processes by a semi-analytical formulation

4.3.1 Introductory comments

A thorough consideration of computer models that have been developed for metal forming simulation clearly shows their striking variety. We have outlined some of the existing models in different parts of this work. Complex situations present in such processes, together with the interest they awake in industrial applications have encouraged developments of various models, with different degrees of generality. Experience has shown, however, that best results are obtained if special purpose codes are developed, resulting in smaller programs, which handle accurately and efficiently the characteristic features of the given processes.

In this sense, in different areas of numerical analysis, special models have been formulated which take advantage of a given geometric situation, which is useful to state the problem in a simpler way or to solve it with less computational effort. Semi-analytical methods can be placed in this group, and they have been successfully used in many linear problems. The constancy of geometry along a given direction allows to state the variables in terms of a Fourier series expansion in that direction, and in such linear cases an uncoupled, block-diagonal system is obtained, which results in a number of $(n-1)$-dimensional problems, instead of an n-dimensional one. Some particular applications have been presented for non-linear problems, where the modes of the series expansion appear to be coupled [108, 71]. Usually this coupling has been handled by placing the residual due to it as an equivalent load, and iterations are performed until convergence is achieved. In [9] we have presented such semi-analytical model for metal forming processes in which non axisymmetric loads and boundary conditions are applied to an axisymmetric configuration. Such situation is found, for example, in seamless tube rolling. The aim of the work reported here is to extend this formulation to transient processes [8].

Starting from the solution for a given time t, also obtained by Fourier series expansion, we have as initial data the velocity field expanded in its harmonic components, and the position of the free surface of the metal, defined by a number of cuts of it with radial planes at some chosen angles. The resulting curves are used to define a scalar field, which is then expressed in terms of its components harmonic. A reference value of the scalar field is assigned to the free surface, which thus becomes an isosurface of the scalar field. An advective transport is performed for the global set of variables (harmonic components of the "pseudo-concentration" for each node). The system is block diagonal, although there appears a coupling between modes due to the non axi-symmetric terms of the velocity. This coupling can be accurately accounted for by considering the orthogonal properties of the basis functions, in terms of which all the variables of the problem are stated. Such formulation in addition is in good agreement with the semi-analytical approach and provides an elegant solution to the problem of

coupling.

As a result of the advective transport the new position of the interfaces is found by recombining the harmonic transported components in each integrating station. After this step, the new solution for the updated configuration can proceed.

The procedure is illustrated with transient tube rolling simulations.

4.3.2 Outline of the pseudo-concentration method

The flow approach is again recalled (cf. Section 2.2). In this context, the problem of describing transient processes is considered. We already know that dynamic terms in metal-forming problems are negligible. Thus a transient process may be solved as a sequence of stationary problems, for which the velocity field is obtained. Then, according to a given time integration rule, the new configuration is found. This can be done most intuitively by a Lagrangian-type scheme

$$^{t+\Delta t}x_i = {}^{t}x_i + \Delta t\, {}^{t}v_i \tag{4.3}$$

which, as known, is likely to produce unacceptable mesh distortion within a few steps, thus requiring remeshing. For this reason some alternative methods have been conceived. The so-called ALE (Arbitrary Lagrangian-Eulerian) methods [42, 62] use a mixed solution consisting in assigning an 'arbitrary' velocity to the mesh. The normal component of this velocity coincides with that of the deformed body on its boundary. Additionally, this velocity is such calculated as to minimize the mesh distortion (and here lies the difficulty of applying this method). Among some other ideas about how to carry out the simulation of a transient process while keeping the mesh distortion the least as possible, the pseudo-concentration method [7, 103, 104] makes good use of the fixed-time solutions given by the flow approach and provides a way to calculate the configuration for the next time step. This method considers evolving free surfaces along the process as interfaces between two media: the metal and a fictitious material whose properties are 'slight' enough so as not to disturb the flow of the metal. A scalar field is generated with the condition of containing these interfaces as isocurves at a given value of this field. One way of achieving this is to generate this field by assigning to each point the value of the distance from it to the interface, with a sign convention to identify the subdomains occupied respectively by the metal and the fictitious material. In particular problems, some alternative definitions instead of this distance-based one may found to be more convenient. It is noted that the metal will move during the given time step in the same way as the scalar field attached to both materials, when transported in a non-diffusive way. Based on this fact, the advective transport of the scalar field is performed,

$$\frac{Dc}{Dt} = \frac{\partial c}{\partial t} + (\mathbf{v} - \mathbf{v}_M) \cdot \nabla c = 0 \tag{4.4}$$

from which, by proper spatial and time discretization, the values for the incremented time $t + \Delta t$, ${}^{t+\Delta t}c$ can be obtained from the trapezoidal rule

$$ {}^{t+\Delta t}c - {}^{t}c = \Delta t(\mathbf{v} - \mathbf{v}_M) \cdot \nabla((1-\alpha){}^{t}c + \alpha {}^{t+\Delta t}c) \tag{4.5} $$

with $0 \leq \alpha \leq 1$. $\mathbf{v}_M$ stands for a mesh velocity, which in general can be imposed to follow the movement of solid boundaries representing active surfaces, like rams, dies, etc. Usually the definition of this velocity is straightforward, since the tools most frequently have simple paths.

Once ${}^{t+\Delta t}c$ is found, the updated position of the interfaces is obtained by searching for the isocurves of the value that was given to them when the field was generated.

4.3.3 Semi-analytical formulation for transient problems

A number of technical problems are axisymmetric in geometry but not in their loading. An elegant solution to such problems in linear cases is given by semi-analytical methods, in which the loads are decomposed in their harmonic modes and separately applied making use of the principle of superposition. In non-linear problems some methods exist [108, 71, 9] which apply this methodology accordingly treating the coupling between the modes. In tube rolling there is an (approximately) axial geometry; velocity is imposed by the rolls also with lack of axial symmetry. One effect of such imposed velocity is a non-planar and non-axisymmetric front edge of the rolled tube.

The pseudo-concentration method has been used to simulate axisymmetric tube rolling in [7]. Also stationary problems have been analyzed [9] by expanding the imposed velocity with Fourier series making use of the concept of pseudo-concentrations to describe a non-axisymmetric body in an axisymmetric domain by modal decomposition of the accordingly defined scalar field. Thus, the semi-analytical formulation is possible, and a (rather special) class of 3D problems is solved as a set of 2D problems.

In what follows, we present the transient solution provided the velocity field is known from a constant time solution, as described in [9]. In view of the slow speed at which these processes are usually performed, and the characteristics of the pseudo-concentration method, which gives a velocity field for the fictitious material that serves as an estimation of the one the metal will have when reaching a given part of the domain, solution can be obtained by a staggered sequence, i.e. by solving separately the mechanical problem, at constant time, and the transient one, with transport of free surfaces according to a given velocity field. Thus, we are only concerned with finding the updated configuration for time $t + \Delta t$, provided the velocities and the configuration for time t are given.

We define the scalar field as expanded in Fourier series

$$ {}^{t}c = {}^{t}c_0 + \sum_{l=1}^{L} \left({}^{t}c_l \cos l\theta - {}^{t}c_{-l} \sin l\theta \right) \tag{4.6} $$

such that the interfaces at the different angles are isocurves of it. If we are to solve the advective transport equation (4.4), the unknowns will be the harmonic components of the scalar field in each node, which we place in a vector containing sequentially the (planar) vectors of each harmonic component. In correspondence to Eq. (4.5) we will have,

$$(\mathbf{M}_1 - \alpha\mathbf{M}_2)\left\{{}^{t+\Delta t}c\right\} = (\mathbf{M}_1 + (1-\alpha)\mathbf{M}_2)\left\{{}^{t}c\right\} \tag{4.7}$$

where $\{\mathbf{c}\}_{(2L+1)S\times 1}$ is the array of $2L+1$ vectors $\{\mathbf{c}_l\}_{S\times 1}$ (one for each harmonic component), where S is the number of nodes. Similarly, $\mathbf{M}_1$ and $\mathbf{M}_2$ are arrays of $(2L+1)\times(2L+1)$ matrices of that read, for $-L \leq i,j \leq L$

$$\begin{aligned}\mathbf{M}_{1ij} &= \int_\Omega \begin{pmatrix} \boldsymbol{\phi}_c^T\boldsymbol{\phi}_c \cos i\theta \cos j\theta & -\boldsymbol{\phi}_c^T\boldsymbol{\phi}_c \cos i\theta \sin j\theta \\ -\boldsymbol{\phi}_c^T\boldsymbol{\phi}_c \sin i\theta \cos j\theta & \boldsymbol{\phi}_c^T\boldsymbol{\phi}_c \sin i\theta \sin j\theta \end{pmatrix} d\Omega \\ &= \delta_{ij}\pi \int_\Omega \begin{pmatrix} \boldsymbol{\phi}_c^T\boldsymbol{\phi}_c & \mathbf{0} \\ \mathbf{0} & \boldsymbol{\phi}_c^T\boldsymbol{\phi}_c \end{pmatrix} d\Omega \end{aligned} \tag{4.8}$$

and $\boldsymbol{\phi}_c$ are suitable shape functions which interpolate c. However, for $\mathbf{M}_2$ it will be

$$\begin{aligned}\mathbf{M}_{2ij} = \Delta t \int_\Omega \Big[& \cos i\theta \boldsymbol{\phi}_c^T(\mathbf{v}-\mathbf{v}_M)\cdot\nabla\boldsymbol{\phi}_c \cos j\theta \\ & -\sin i\theta \boldsymbol{\phi}_c^T(\mathbf{v}-\mathbf{v}_M)\cdot\nabla\boldsymbol{\phi}_c \cos j\theta \\ & -\cos i\theta \boldsymbol{\phi}_c^T(\mathbf{v}-\mathbf{v}_M)\cdot\nabla\boldsymbol{\phi}_c \sin j\theta \\ & \sin i\theta \boldsymbol{\phi}_c^T(\mathbf{v}-\mathbf{v}_M)\cdot\nabla\boldsymbol{\phi}_c \sin j\theta \Big] d\Omega \end{aligned} \tag{4.9}$$

where it is clear that, being the velocity a function of the circumferential coordinate, the system of equations will couple. We then have two alternatives. The first one is to find the solution with an implicit iterative algorithm, by placing the terms due to the coupling as an equivalent load. In this case we will have

$$\mathbf{M}_2 = \overline{\mathbf{M}}_2 + \overline{\overline{\mathbf{M}}}_2 \tag{4.10}$$

where $\overline{\mathbf{M}}_2$ is a block diagonal matrix given by the axisymmetric term of $(\mathbf{v}-\mathbf{v}_M)$, and $\overline{\overline{\mathbf{M}}}_2$ is a full matrix, given by the other terms.

Then we can write Eq. (4.7) as

$$\left(\mathbf{M}_1 - \alpha\overline{\mathbf{M}}_2\right)\left\{{}^{t+\Delta t}c^{(\omega+1)}\right\} = (\mathbf{M}_1 + (1-\alpha)\mathbf{M}_2)\left\{{}^{t}c\right\} + \alpha\overline{\overline{\mathbf{M}}}_2\left\{{}^{t+\Delta t}c^{(\omega)}\right\} \tag{4.11}$$

and iterate by direct back-substitutions until a given convergence tolerance is reached. Convergence condition for such algorithm is given in [1, 9]. The right hand side can be integrated along the circumferential coordinate by Gaussian quadrature, by evaluating the equivalent load vector in the integrating points.

Alternatively, although the orthogonal properties of the base functions are not directly applicable, if we have the velocity also expanded in Fourier series, we can make use of the following properties of the product of three base functions [1],

developed for $i, j, k > 0$, equivalent cases being obtained by permutations in these formulae

$$\begin{aligned}
\int_0^{2\pi} \cos i\theta \cos j\theta \cos k\theta d\theta &= \begin{cases} \frac{\pi}{2} & \text{if } i = j + k \\ 0 & \text{other cases} \end{cases} \\
\int_0^{2\pi} \cos i\theta \sin j\theta \sin k\theta d\theta &= \begin{cases} \frac{\pi}{2} & \text{if } i = j - k \\ -\frac{\pi}{2} & \text{if } i = j + k \\ 0 & \text{other cases} \end{cases} \\
\int_0^{2\pi} \sin i\theta \cos j\theta \cos k\theta d\theta &= 0 \quad \forall\, i, j, k \\
\int_0^{2\pi} \sin i\theta \sin j\theta \sin k\theta d\theta &= 0 \quad \forall\, i, j, k
\end{aligned} \tag{4.12}$$

In this way, the necessary calculations for computing the modal component coupling can be reduced. Further, if $\alpha = 0$ is taken in Eq. (4.5) (explicit Euler scheme) we have

$$\mathbf{M}_1 \left\{ {}^{t+\Delta t}\mathbf{c} \right\} = (\mathbf{M}_1 + \mathbf{M}_2) \left\{ {}^{t}\mathbf{c} \right\} \tag{4.13}$$

Now the coefficient matrix will be block diagonal, and the solution $\left\{ {}^{t+\Delta t}\mathbf{c} \right\}$ is obtained in one step. The right hand side can be computed by numerical integration, as above, but it can also be integrated analytically in the θ direction. In fact, it is seen by Eqs. (4.12) that the contribution of harmonic component c_i to the residual of component c_j when considering the velocity harmonic component $\mathbf{v}_k$ will be non-zero in a small number of sets (i, j, k). This result provides an elegant way of solving the coupled system of equations, avoiding any numerical integration along θ coordinate. Of course, if $\alpha > 0$ is considered, the same non-zero terms will appear, but now multiplying the harmonic components of ${}^{t+\Delta t}\mathbf{c}$, and an iterative algorithm will be necessary to solve the implicit scheme, but still without numerical integration in θ.

Leaving aside whether the right hand side of Eq. (4.11) or (4.13) is either calculated by numerical integration (usually only if the Fourier series expansion of the velocity $\mathbf{v}$ is not available), or by use of Eqs. (4.12), the direct substitution scheme given in Eq. (4.11) converges if [1, 9]

$$\left\| \left(\mathbf{M}_1 - \alpha \overline{\mathbf{M}}_2 \right)^{-1} \right\| \cdot \left\| \alpha \overline{\overline{\mathbf{M}}}_2 \right\| < 1 \tag{4.14}$$

The convergence rate is linear, and it can be shown that the closer the norms product in Eq. (4.14) is, the faster the algorithm will converge. However this norm product is fixed for a given velocity field, and when non-axisymmetric term are important as related to the axisymmetric one, many iterations will be necessary.

In addition, for fixed mesh, $\mathbf{v}_M = 0$, the mesh geometry will be constant throughout the time interval t to $t + \Delta t$, as already is the velocity. In such case, it is not necessary to recalculate the matrices $\mathbf{M}_1$, $\overline{\mathbf{M}}_2$ and $\overline{\overline{\mathbf{M}}}_2$; in the iterations following the first one only the residual is evaluated.

4.3.4 Transient tube rolling simulation

The model has been tested by simulating the entrance of a seamless tube into a rolling stand. Figure 4.10 shows a scheme of the process to be modelled. It consists of three rolls placed at 120° each other, through which the tube passes, coming from a previous stage. As a result the tube experiences a reduction in wall thickness. We first consider one of the stages corresponding to the beginning of the process, where a mandrel is placed inside the tube, and a big reduction in wall thickness can be achieved. In the present example, a reduction of 30% is imposed.

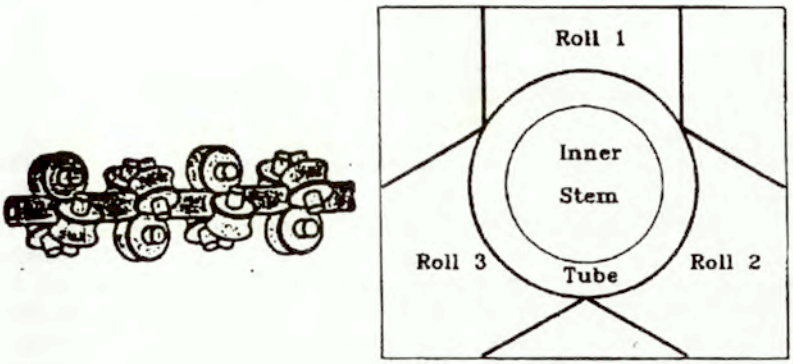

Figure 4.10 Tube rolling station

The process is modeled by sequentially finding the velocity field in its harmonic components, and performing the time integration which yields the new, updated position of the interfaces, according to the given velocity field. The rolls impose a velocity proportional to its radius, so the tube will have imposed velocities as a function of θ. The first constant-time solution corresponds to the moment the tube reaches the rolls. In this moment the interface is plane and normal to the tube axis. From the beginning the discretized domain consists of the zone presently occupied by the metal and that where the material will flow —or may flow— during the process. The zone where the metal has not arrived yet is filled with a fictitious material whose viscosity is four orders of magnitude lower than that of the actual metal. This assures the metal a free flow, and also provides a velocity field to perform the advective transport in the whole domain.

The process is performed in 14 time steps. Figure 4.11 shows the position of the interface during the simulation. They have the same aspect for every value of θ, although small differences are computed. Indeed, it can be said that, from the point of view of the transport problem for c, the metal produces a strong diffusion along the θ coordinate because the material resistance to shear causes the velocity field to be smoothed in the circumferential direction.

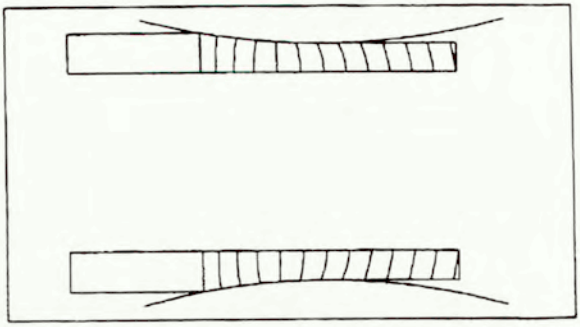

Figure 4.11 Interface evolution along the process

It is worth pointing out how the profile of the leading edge of the tube reflects the relative tube velocity with respect to the rolls. At first the rolls go faster, and it is seen how they pull the tube from the surface. After the so called non-slipping point, where the metal and the rolls have the same velocity, the converse occurs, and in that final part the corresponding free surfaces exhibit the friction force, opposed to the flow, the tube receives. Figures 4.12 and 4.13 show the velocity module at a given time step for two different cuts in θ: 0° and 57° (it should be noticed that, because of the symmetry the domain in θ coordinate is from 0° to 60°). The variation of the velocity distribution in different angles can be seen, as well as the relative velocity with respect to the roll. In fact, this is a procedure for finding the non-slipping point, whose position will vary along θ. In the same figures the interface for that moment, corresponding to the fifth time step is also

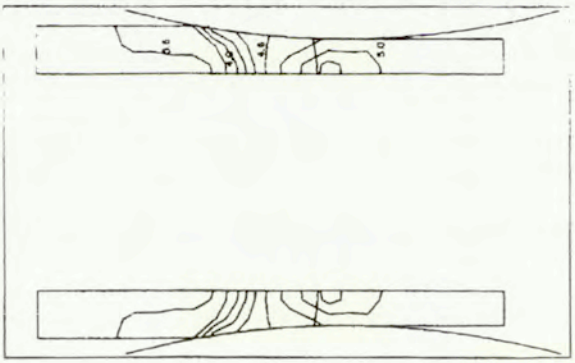

Figure 4.12 Velocity module at t=5.0, $\theta = 0°$

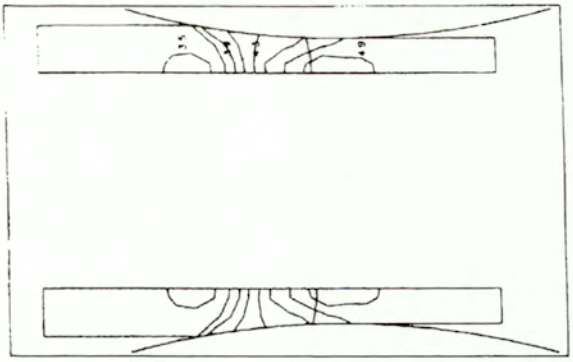

Figure 4.13 Velocity module at t=5.0, $\theta = 57°$

plotted. These concepts about the metal flow and the action it receives from the rolls can also be appreciated if we look at the shear stresses τ_{rz}, which are plotted, for the same time step and integrating stations, in Figs. 4.14 and 4.15.

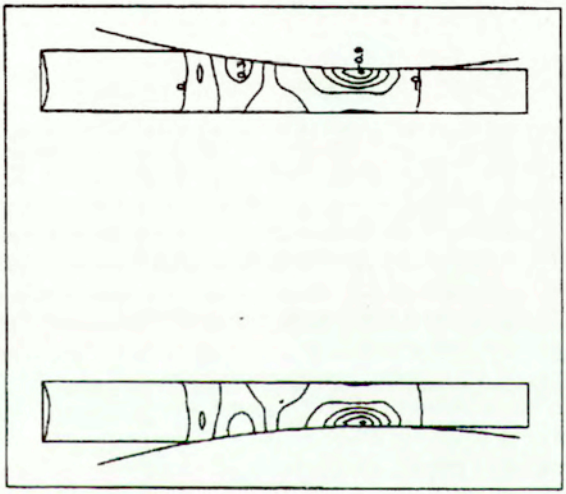

Figure 4.14 Shear stresses τ_{rz} at t=5.0, $\theta = 0°$

It is clearly seen that the maximum and minimum shear stresses take place near the rolls, and that in either sides from the non-slipping point they have different signs, according to the sign of the friction force the rolls impose on the

metal. Near the inner surface these stresses are small. As it can be shown by plotting the maximum shear stresses [6] the material suffers a mild distortion in this zone.

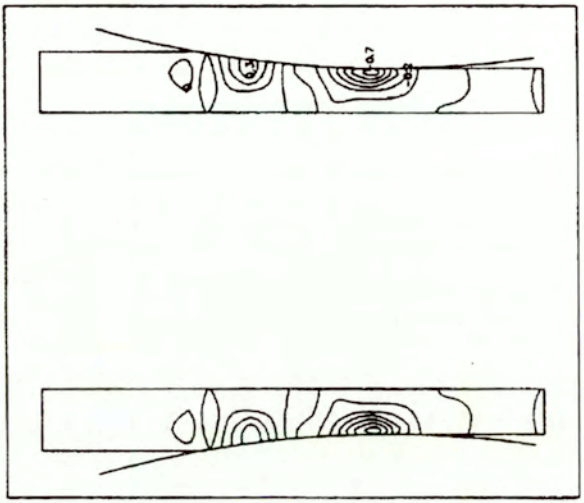

Figure 4.15 Shear stresses τ_{rz} at t=5.0, $\theta = 57°$

With respect to the other stresses, we find that they reach their maxima between the rolls, and that the material is severely compressed. This can be seen in Figs.4.16 to 4.18, where the axial σ_z, radial σ_r and circumferential σ_ϑ stresses are plotted for the same time step and $\theta = 57°$. Similar patterns are obtained for cuts at other values of the angle θ. It is noticed that while σ_r has very high gradients and a non uniform distribution along the tube thickness, σ_z is quite uniform, and decreases very fast outside the rolls. It is worth to notice also that because of this axial compression, which is not obvious, the tube, when rolled without the inner stem tends to increase its thickness [6] as predicted by *e.g.* the slip line theory for a perfectly plastic material. For this reason, in actual rolling processes a traction in the right end is applied by controlling the relative velocity of the following set of rolls.

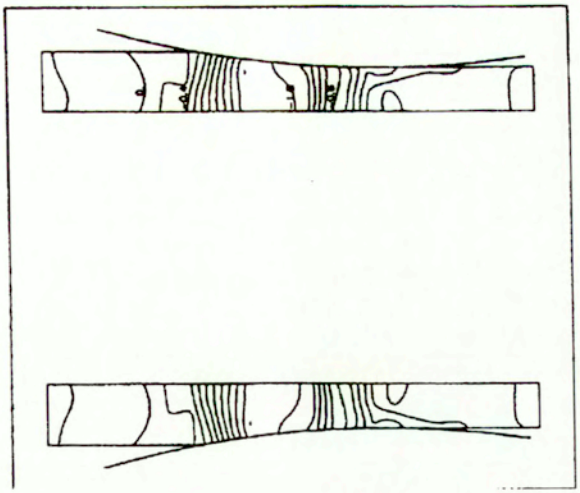

Figure 4.16 Axial stresses σ_z at t=5.0, $\theta = 57°$

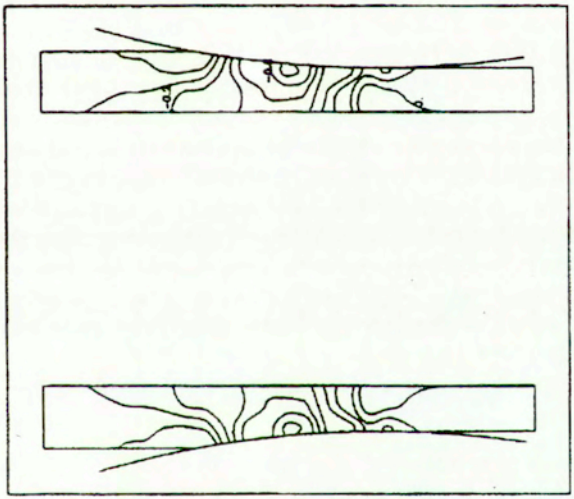

Figure 4.17 Radial stresses σ_r at t=5.0, $\theta = 57°$

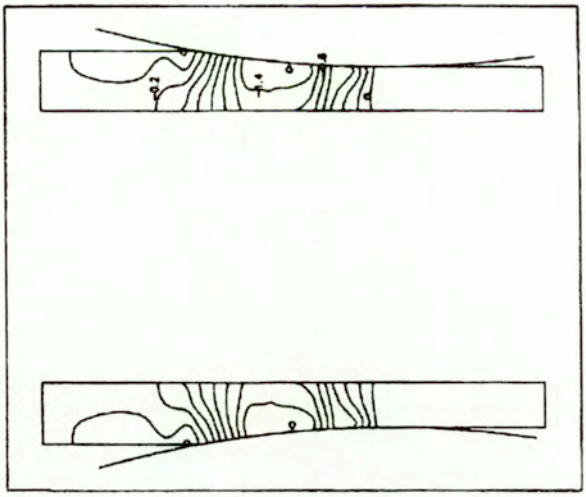

Figure 4.18 Circumferential stresses σ_θ at t=5.0, $\theta = 57°$

As a second example we show the modelling of one of the final stages in tube rolling. For this case the tube passes between two rolls. In order to make more apparent the lack of axial symmetry, the rolls diameter is similar to that of the tube. Also, this example exhibits a small thickness/diameter ratio (1/20), which makes more noticeable the effect of non axi-symmetric imposed velocity. The whole process is performed in ten time steps, starting from a planar front end. Different intermediate shapes of this leading edge are plotted in Figs.4.19 to 4.21, in sequential order. It can be appreciated that at the beginning the circumferential velocity component is relatively important, and this causes an irregular contour, which smoothes both towards the inner surface (Fig. 4.19), and as the process goes further (Figs. 4.20 and 4.21). Away from the rolls the non-axisymmetric velocity components decrease to zero, and finally a stable profile is obtained. This frontal edge shape is familiar to seamless tube producers, who call it "fish mouth" and which constitutes part of the waste which must be cut out from every tube.

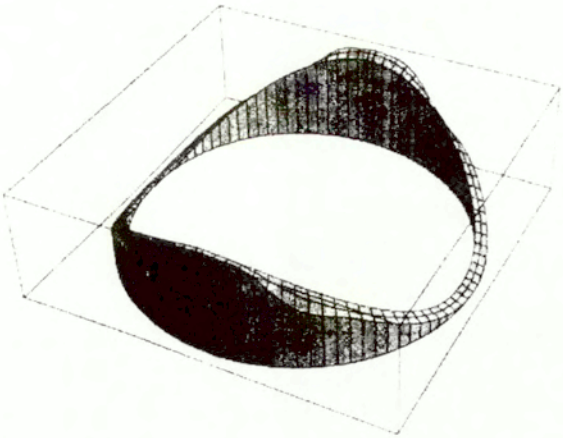

Figure 4.19 Tube rolling: front shape at t=4.0

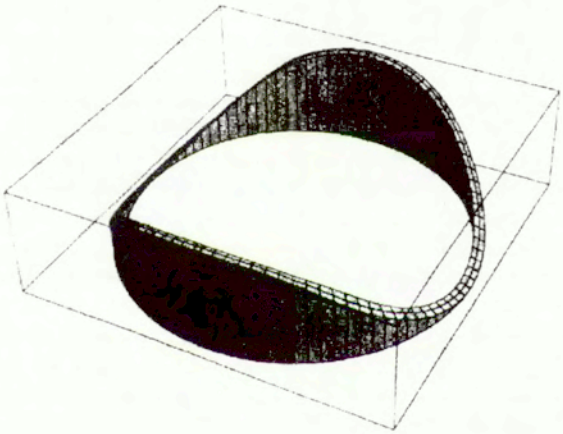

Figure 4.20 Tube rolling: front shape at t=5.0

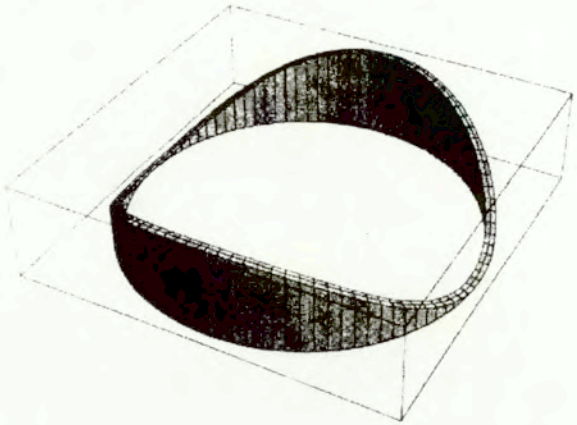

Figure 4.21 Tube rolling: front shape at t=8.0

4.3.5 Concluding remarks

The semi-analytical formulation has been extended to transient metal forming processes, providing a practical way of performing 3-D analysis for some particular configurations. It gives useful information for analysis and design of a given tube rolling process, and by studying the history of stresses and strains on the material, the properties of the final product, at least qualitatively, can be predicted.

As in other applications of the semi-analytical method, the range of problems that can be analyzed by means of it is restricted to cases not too far away from the axial symmetry, or to loads which require small number of terms of harmonic components to be expressed. When this is not the case, a large number of terms must be computed in the Fourier series expansion, which in addition to making the method not worthy to be used, may bring also some difficulties in the convergence of the implicit algorithm [9] which gives the velocity field for the constant time solution.

Further research about the preceding concept is necessary in order to study other applications of this method. In particular, it seems worthy to extend this analysis to plane strip rolling, and to injection problems with axisymmetric configurations, although a proper modelling of the boundary conditions will be necessary.

Appendix A

Shape sensitivity at large deformations

A.1 The domain parameterization approach—basic concepts and notation

In Section 2.4 we have considered the problem of shape sensitivity restricted to metal forming processes described in the framework of the Flow Approach. An Eulerian approach was then used to describe stationary processes. In this Chapter shape sensitivity analysis will be again considered but in a more general context. Problems involving large deformations and nonlinear constitutive equations are to be described. The problem to be discussed now belongs to the most challenging and practically useful design sensitivity formulations. Unfortunately, it also requires the use of some additional complex notation and this is why this section is almost entirely devoted to giving definitions of all the relevant symbols and presenting just the very basic ideas of the shape sensitivity analysis at large deformations. A detailed discussion follows in the subsequent sections. The two available methods for general sensitivity analysis (i.e. DDM and ASM), when combined with the two most popular methodologies for shape sensitivity (i.e. DPA and MDA, see Section 2.4), give rise to four possible couples. In [70] the Domain Parameterization Approach was the framework to develop the two couples DPA/DDM and DPA/ASM. Here the Direct Differentiation Method is used to obtain the sensitivity coefficients, since it shows to be more effective than ASM for history dependent processes (i.e. those were the instantaneous mechanical properties depend on the deformation path and/or on its rate) as, we want to deal with. In this context, the two couples DPA/DDM (Section A.2) and MDA/DDM (Section A.3) are presented, although attention is mainly focussed on the first one. Both are finally compared and shown to be equivalent. A parallel development of the formulation for implicitly and explicitly integrated constitutive equations is given, the latter (notationally simpler and bearing some resemblance to linear mechanics problems) as a particular case of the former.

Calculating the structural response sensitivity to shape variation has generated a lot of interest among researchers in the last several years. Early work on the subject was reviewed in a survey paper [53]; a thorough exposition of this topic can be found in [55]. Other developments of seminal value were reported in [16, 17, 20, 21, 23, 29, 30, 31, 38, 40, 39, 61, 80, 93, 94, 109, 123], for instance. The work done to date has been concerned with both the adjoint approach, which is appropriate for finding the sensitivities of a few response quantities with respect to many design variables, and the direct approach, which is useful for finding the sensitivities of many response quantities with respect to a few design variables. Also, both of the basic methodologies: the domain parameterization approach (DPA) and the material derivative approach (MDA), have been widely employed.

The objective of studying the sensitivity of nonlinear systems in the general framework of incremental methodology, is to find design variations (or derivatives) of displacement and/or stress-type constraints at the load level ${}^{t+\Delta t}Q_\alpha$, given some required sensitivity information at t and the incremental equilibrium solution Δu_i, $\Delta \bar{\sigma}_{ij}$, ..., obtained at the time step $[t, t+\Delta t]$. Adopting the updated Lagrangian strategy (for which the acronym UL is widely accepted), the constraint may be presented in a general form as

$$\begin{aligned} \mathcal{G}(h_d) &= G(\sigma_{ij}, u_i; h_d) \\ &= \int_{\Omega^t} {}^{t+\Delta t}g(\sigma_{ij}, u_i; h_d)\ \mathrm{d}\Omega^t + \int_{\partial\Omega_\sigma^t} {}^{t+\Delta t}g^{(\sigma)}(u_i; h_d)\ \mathrm{d}(\partial\Omega^t) \\ &\quad + \int_{\partial\Omega_u^t} {}^{t+\Delta t}g^{(u)}(t_i; h_d)\ \mathrm{d}(\partial\Omega^t) \end{aligned} \tag{A.1}$$

in which g, $g^{(\sigma)}$ and $g^{(u)}$ are given functions of their indicated arguments, t_i is the reaction vector on the boundary part $\partial\Omega_u$ on which displacements are prescribed, and $\mathbf{h} = \{h_d\}$, $d = 1, 2, \ldots, D$, is a vector of shape (and possibly non-shape) design variables. The notation indicating time instants at which particular functions are taken is employed so that

$${}^{t+\Delta t}g(\sigma_{ij}, u_i; h_d) = g({}^{t+\Delta t}\sigma_{ij}, {}^{t+\Delta t}u_i; h_d), \quad \text{etc.} \tag{A.2}$$

the symbol ${}^{t+\Delta t}(\cdot)$ implying the value of the function at time instant $t+\Delta t$. Finally, the upper-right index for the domain and its boundary indicates the reference configuration.

We note that since this chapter aims at reaching a high level of generality of sensitivity formulations, the constraint functional is taken in a slightly more general form than that employed so far. The integrals in the expression (A.1) defined over the boundaries $\partial\Omega_u^t$ and $\partial\Omega_\sigma^t$ make it possible to evaluate the reactions and free boundary displacements sensitivity with respect to the design parameters h_d.

Before we introduce the necessary concepts to derive the formalism for sensitivity analysis within an UL approach, we have to summarize the UL methodology in order to introduce some concepts and notation we will make use of later on in the rest of the chapter. Section A.1.1 is devoted to this aim. Next, concepts of shape sensitivity are presented in Section A.1.2.

A.1.1 Outline of UL methodology

In this section the equations describing nonlinear solid mechanics involving large deformations and material nonlinearities are presented following the methodology and notation of [70]. In the framework of the UL approach, starting from a rate form of the governing equations (as necessary for such problems) yields, by appropriate time integration, to an incremental formulation. Such time integration may be along the real time t or, for non-rate-dependent materials, use time just as a loading parameter. The specific time integration rule (of the constitutive equation) will produce an implicit or explicit scheme, as we will see later on. For simplicity, we will consider constant length of the time steps Δt, which does not mean loss of generality since with no formal change a sequence of unevenly distributed time instants may be considered as well.

According to the UL conventions, the process starts at time $\tau = 0$ at a configuration Ω^0; we assume we know the solution up to time $\tau = t$, in which we adopt the reference configuration Ω^t, and seek the solution for the next required 'dynamic equilibrium' position at time $\tau = t + \Delta t$. This strategy allows us to follow up the whole process bearing in mind that the reference configuration is *updated* and all the problem quantities duly 'accumulated' after every increment and the calculated solution gives the 'initial' conditions of displacements, strains, stresses and possibly other fields for the next incremental problem. The procedure is schematized in Figure A.1.

On the basis of this general solution strategy we completely specify the problem to be solved by defining the kinematic (i.e. strain-displacements) relations, the constitutive (stress-strain) equations and the equations of motion, from which we derive the variational or weak formulation.

The *incremental Green strain tensor* $\Delta\varepsilon_{ij}$ in the updated Lagrangian description is a nonlinear function of the incremental displacement vector Δu_i and can be presented in the form[1]

$$\Delta\varepsilon_{ij} = \overline{\Delta\varepsilon}_{ij} + \overline{\overline{\Delta\varepsilon}}_{ij}\,, \qquad x_i \in \Omega^t \tag{A.3}$$

in which

$$\begin{aligned} \overline{\Delta\varepsilon}_{ij} &= \tfrac{1}{2}\left(\Delta u_{i,j} + \Delta u_{j,i}\right) = \overline{A}_{ijk}\,\Delta u_k \\ \overline{\overline{\Delta\varepsilon}}_{ij} &= \tfrac{1}{2}\,\Delta u_{k,i}\,\Delta u_{k,j} = \overline{\overline{A}}_{ij}(\Delta u_k, \Delta u_k) \end{aligned} \tag{A.4}$$

are the linear and nonlinear (quadratic) incremental strain contributions while the differential operators $\overline{A}_{ijk}$ and $\overline{\overline{A}}_{ij}$ are defined as

$$\begin{aligned} \overline{A}_{ijk} &= \frac{1}{2}\left(\frac{\partial}{\partial x_i}\delta_{jk} + \frac{\partial}{\partial x_j}\delta_{ik}\right) \\ \overline{\overline{A}}_{ij}(a_k, b_l) &= \frac{1}{4}\left(\frac{\partial}{\partial x_i}a_k\,\frac{\partial}{\partial x_j}b_l + \frac{\partial}{\partial x_j}a_k\,\frac{\partial}{\partial x_i}b_l\right) \end{aligned} \tag{A.5}$$

[1] Dependence of all the functions on the time (or a time-like) variable is assumed but not explicitly indicated for compactness.

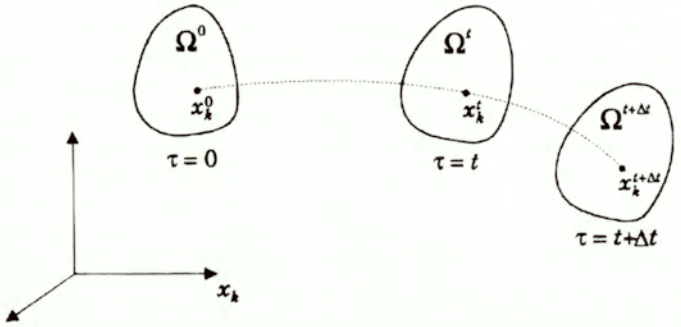

$\Delta u_i({}^t x_j)$ incremental displacement } from incremental solution with configuration at t taken as reference state

${}^{t+\Delta t}u_i({}^t x_j) = {}^t u_i({}^t x_j) + \Delta u_i({}^t x_j)$ 'new' total displacement

${}^{t+\Delta t}x_i({}^t x_j) = {}^t x_i + \Delta u_i({}^t x_j)$ 'new' position of point x_i } update at the end of the step $[t, t+\Delta t]$

Figure A.1 Updated Lagrangian description—basic concept.

for any sufficiently smooth fields $a_i(x_j)$ and $b_i(x_j)$.

It should be noted that the quadratic dependence of $\Delta\varepsilon_{ij}$ on Δu_i is exact and not a second-order approximation only. In the limiting case of $\Delta t \to 0$ the rate expression results from the above equations in the form

$$\dot{\varepsilon}_{ij} = \tfrac{1}{2}\,(\dot{u}_{i,j} + \dot{u}_{j,i}) \tag{A.6}$$

Constitutive equations of many inelastic materials at infinitesimal deformations can be symbolically presented as

$$\dot{\sigma}_{ij}(\sigma_{kl}, p_\zeta; \dot{\varepsilon}_{kl}) = C_{ijkl}(\sigma_{mn}, p_\zeta)\,\dot{\varepsilon}_{kl} + H_{ij}(\sigma_{kl}, p_\zeta)\,, \qquad x_i \in \Omega^t \tag{A.7}$$

in which the buildup of tensors C_{ijkl} and H_{ij} takes specific forms according to the material model used. σ_{ij} is the classical *Cauchy stress tensor* while $\mathbf{p} = \{p_\zeta\}$, $\zeta = 1, 2, \ldots, V$, stands for an array of variables called *internal variables* needed for the description of the history effects and typically includes scalar and second order tensors.

The presence of additional variables in the constitutive relations requires additional equations. These additional equations reflect the hypothesis that if the

local (in time) state that determines the rate form of the constitutive equation (A.7) is defined by σ_{ij} and p_ζ, then the rate of evolution of the internal variables should also be determined using σ_{ij} and p_ζ, i.e.

$$\begin{aligned} \dot{p}_\zeta = \dot{p}_\zeta(\sigma_{ij}, p_\eta; \dot{\varepsilon}_{ij}) &= A_{\zeta ij}(\sigma_{kl}, p_\eta)\,\dot{\varepsilon}_{ij} + N_\zeta(\sigma_{ij}, p_\eta) \\ &\qquad \zeta, \eta = 1, 2, \ldots, V \end{aligned} \tag{A.8}$$

It should be noticed that for materials with a distinct yield surface local loading/unloading conditions must be additionally considered with Eqs. (A.7) and (A.8) describing then only the inelastic (loading) branch of the response.

In the incremental formulation it is the finite time increment $\Delta\sigma_{ij}$ of the stress tensor, and not the stress rate $\dot{\sigma}_{ij}$, that has to be determined. Thus, we look for

$$\Delta\sigma_{ij} = \int_t^{t+\Delta t} \left[C_{ijkl}(\sigma_{mn}, p_\zeta)\,\dot{\varepsilon}_{kl} + H_{ij}(\sigma_{kl}, p_\zeta) \right] \mathrm{d}\tau \tag{A.9}$$

in which the arguments σ_{ij} and p_ζ of the tensors C_{ijkl} and H_{ij} are to be generally considered as functions of time. Putting it another way, instead of using as the constitutive law the mapping

$$({}^t\sigma_{ij}, {}^tp_\zeta; {}^t\dot{\varepsilon}_{ij}) \;\rightarrow\; \dot{\sigma}_{ij} = \dot{\sigma}_{ij}({}^t\sigma_{kl}, {}^tp_\zeta; {}^t\dot{\varepsilon}_{kl}) \tag{A.10}$$

which is in our case linear in $\dot{\varepsilon}_{ij}$, the finitely-incremental nature of the displacement solution Δu_i and, consequently, of the computed incremental strain $\Delta\varepsilon_{ij}$ makes it necessary to use another mapping

$$({}^t\sigma_{ij}, {}^tp_\zeta; \Delta\varepsilon_{ij}) \;\rightarrow\; \Delta\sigma_{ij} = \Delta\sigma_{ij}({}^t\sigma_{kl}, {}^tp_\zeta; \Delta\varepsilon_{kl}) \tag{A.11}$$

which in general (for so-called *implicit algorithms*) will no longer be linear in $\Delta\varepsilon_{ij}$ and require iteration to compute $\Delta\sigma_{ij}$. To see this we may consider Eq. (A.11) in a slightly redefined (but fully equivalent) form as

$$\begin{aligned} \Delta\sigma_{ij} &= \Delta\check{\sigma}_{ij}({}^{t+\Delta t}\sigma_{kl}, {}^{t+\Delta t}p_\zeta; \Delta\varepsilon_{kl}) \\ &= \Delta\check{\sigma}_{ij}({}^t\sigma_{kl} + \Delta\check{\sigma}_{kl}({}^{t+\Delta t}\sigma_{mn}, {}^{t+\Delta t}p_\zeta; \Delta\varepsilon_{mn}), \\ &\qquad {}^tp_\zeta + \Delta\check{p}_\zeta({}^{t+\Delta t}\sigma_{kl}, {}^{t+\Delta t}p_\eta; \Delta\varepsilon_{kl}); \Delta\varepsilon_{kl}) \end{aligned} \tag{A.12}$$

in which $\Delta\sigma_{kl}$ and $\Delta\check{\sigma}_{kl}$ clearly stand for different functions of their indicated arguments—given a value of $\Delta\varepsilon_{ij}$ Eq. (A.12) needs iteration to solve it for $\Delta\sigma_{ij}$.

Time integration of the evolution equations for internal variables presents a similar problem—because of simple forms typically used for these equations closed-form expressions are often arrived at, though.

The constitutive equations in the form (A.7) can be used directly for small deformation problems only. In the UL approach Eq. (A.7) is replaced by

$$\begin{aligned} \mathring{\sigma}_{ij} &= \left[C_{ijkl}(\sigma_{mn}, p_\zeta) - \tfrac{1}{2}\left(\sigma_{ik}\,\delta_{jl} + \sigma_{jk}\,\delta_{il} + \sigma_{il}\,\delta_{jk} + \sigma_{jl}\,\delta_{ik}\right) + \sigma_{ij}\,\delta_{kl} \right] \dot{\varepsilon}_{kl} \\ &\quad + H_{ij}(\sigma_{kl}, p_\zeta) \\ &= \tilde{C}_{ijkl}(\sigma_{mn}, p_\zeta)\,\dot{\varepsilon}_{kl} + H_{ij}(\sigma_{kl}, p_\zeta) \end{aligned} \tag{A.13}$$

where $\dot{\tilde{\sigma}}_{ij}$ is the rate of the *second Piola–Kirchhoff stress tensor* based on the current configuration and coincides with the so-called *Jaumann rate* of the Kirchhoff stress tensor defined on the current configuration with respect to the convective coordinates coinciding at time t with the Cartesian frame of reference.

The incremental equations of motion after neglecting inertial terms can be arrived at in the form

$$\Delta\tilde{\sigma}^1_{ij,j} + {}^t\varrho\,\Delta\hat{f}_i = 0\,, \qquad x_i \in \Omega^t \tag{A.14}$$

in which

$$\Delta\tilde{\sigma}^1_{ij} = {}^{t+\Delta t}\tilde{\sigma}^1_{ij} - {}^t\tilde{\sigma}^1_{ij}\,, \qquad \Delta\hat{f}_i = {}^{t+\Delta t}\hat{f}_i - {}^t\hat{f}_i \tag{A.15}$$

where ${}^t\tilde{\sigma}^1_{ij}$ stands for the *first Piola-Kirchhoff stress tensor* based on the current configuration at time t and ${}^t\hat{f}_i$ is the distributed body force vector per unit mass. Within the present description, the total first and second Piola-Kirchhoff stresses ${}^t\tilde{\sigma}^1_{ij}$ and ${}^t\tilde{\sigma}_{ij}$, are equal to each other at time t and also equal to the classical Cauchy stress tensor ${}^t\sigma_{ij}$ also at time t. The incremental stresses are related as

$$\Delta\tilde{\sigma}^1_{ij} = \Delta\tilde{\sigma}_{ij} + \Delta u_{i,k}\,{}^t\dot{\sigma}_{kj} + \Delta u_{i,k}\,\Delta\tilde{\sigma}_{kj} \tag{A.16}$$

which allows us to express the equation of motion in terms of the symmetric second Piola–Kirchhoff stress components.

The set of equations (A.6), (A.9) and (A.14) is completed by specifying stress-type and/or displacement-type boundary conditions which are written respectively as

$$\Delta\sigma^1_{ij}\,n_j = \Delta\hat{t}_i\,, \qquad x_i \in \partial\Omega^t_\sigma \tag{A.17}$$

and

$$\Delta u_i = \Delta\hat{u}_i\,, \qquad x_i \in \partial\Omega^t_u \tag{A.18}$$

where $\hat{t}_i$ and $\hat{u}_i$ are, respectively, components of the surface traction vector and of the prescribed displacement vector (both assumed known), n_i is the vector normal to the boundary surface $\partial\Omega^t$ at time t while $\partial\Omega^t_\sigma$ and $\partial\Omega^t_u$ are parts of $\partial\Omega^t$ where the respective boundary conditions are applied.

Finally, initial conditions for the first step are specified as

$$\begin{aligned} u_i &= \hat{u}^0_i\,, \\ \dot{u}_i &= \dot{\hat{u}}^0_i\,, \end{aligned} \qquad x_i \in \Omega^0\,; \quad \tau = 0 \tag{A.19}$$

while on subsequent steps the values of $\{{}^tu_i,\ {}^t\dot{u}_i\}$ at the end of the previous step will be used.

The obtained incremental solution Δu_i (from which, we also have $\Delta\varepsilon_{ij}$, $\Delta\tilde{\sigma}_{ij}$ and Δp_ζ) is used to update from time t to time $t+\Delta t$ all the problem quantities as

$${}^{t+\Delta t}(\cdot) = {}^t(\cdot) + \Delta(\cdot) \tag{A.20}$$

i.e., for instance

$$\begin{aligned} {}^{t+\Delta t}u_i &= {}^{t}u_i + \Delta u_i \qquad \text{(displacement updating)} \\ {}^{t+\Delta t}\bar{\sigma}_{ij} &= {}^{t}\sigma_{ij} + \Delta\bar{\sigma}_{ij} \qquad \text{(stress updating)} \qquad \text{etc.} \end{aligned} \tag{A.21}$$

The geometry updating procedure $\Omega^t \to \Omega^{t+\Delta t}$ has the form

$${}^{t+\Delta t}x_i = {}^{t}x_i + \Delta u_i({}^{t}x_j), \qquad {}^{t}x_i \in \Omega^t \tag{A.22}$$

which is followed by the appropriate change of arguments ${}^{t}x_i \to {}^{t+\Delta t}x_i$ in expressions (A.21), so that they become

$${}^{t+\Delta t}u_i({}^{t}x_j) = {}^{t+\Delta t}u_i({}^{t+\Delta t}x_j - \Delta u_j) \stackrel{\text{df}}{=} {}^{t+\Delta t}\mathring{u}_i({}^{t+\Delta t}x_j) \tag{A.23}$$

The notational distinction u , $\mathring{u}$ will not be maintained in the rest of this presentation. The meaning of the function at each time should become clear from the context.

For the second Piola-Kirchhoff stress tensor, the transformation to the new configuration at $t+\Delta t$ (where it will be equal to the Cauchy stress at $t+\Delta t$) reads

$${}^{t+\Delta t}\bar{\sigma}_{ij} \cong (1 - \Delta u_{k,k})(\delta_{il} + \Delta u_{i,l})(\delta_{jm} + \Delta u_{j,m})\, {}^{t+\Delta t}\bar{\sigma}_{lm} \tag{A.24}$$

with ${}^{t+\Delta t}\bar{\sigma}_{ij}$ becoming the stress to be used at the next step. In Eq. (A.24) we have used the approximate expression

$$\frac{{}^{t+\Delta t}\varrho}{{}^{t}\varrho} \cong 1 - \Delta u_{i,i} \tag{A.25}$$

where ${}^{t}\varrho$ is the mass density of the material at time t. All the components are consequently referred to the same fixed Cartesian coordinate system $\{x_i\}$.

The preceding equations conform the so-called local or strong formulation, i.e. they impose point-wise conditions. However in practice weak formulations are used. This fact is supported by theoretical (related with continuum mechanics foundations) as well as practical reasons (concerning e.g. solution methods to the governing equations and the possibility of including in a single functional all the intrinsic features of the problem at hand, also the boundary conditions). To construct the *virtual work equation* in the incremental setting we observe that the equilibrium of the system on hand at time instant t requires in the updated Lagrangian formulation that

$$\int_{\Omega^t} {}^{t}\sigma_{ij}\, \delta\overline{\Delta\varepsilon}_{ij}\ \mathrm{d}\Omega^t = \int_{\Omega^t} {}^{t}\hat{f}_i\, \delta\Delta u_i\ \mathrm{d}\Omega^t + \int_{\partial\Omega^t_\sigma} {}^{t}\hat{t}_i\, \delta\Delta u_i\ \mathrm{d}(\partial\Omega^t) \tag{A.26}$$

for any kinematically admissible[1] (i.e. sufficiently smooth and satisfying the kinematic boundary conditions (A.18)) variation of Δu_i. The strain variation $\delta\overline{\Delta\varepsilon}_{ij}$ is treated here as the function of δu_i according to, cf. Eq. $(A.4)_1$

$$\delta\overline{\Delta\varepsilon}_{ij} = \tfrac{1}{2}\big(\delta\Delta u_{i,j} + \delta\Delta u_{j,i}\big) = \overline{A}_{ijk}\, \delta\Delta u_k \tag{A.27}$$

[1]From now on the acronym k.a. will replace the term 'kinematically admissible'.

The similar condition of equilibrium of the system at $t+\Delta t$ reads

$$\int_{\Omega^t}{}^{t+\Delta t}\tilde{\sigma}_{ij}\,\delta\big(\overline{\Delta\varepsilon}_{ij}+\overline{\overline{\Delta\varepsilon}}_{ij}\big)\,\mathrm{d}\Omega^t=\int_{\Omega^t}{}^{t+\Delta t}\hat{f}_i\,\delta\Delta u_i\,\mathrm{d}\Omega^t+\int_{\partial\Omega^t_\sigma}{}^{t+\Delta t}\hat{t}_i\,\delta\Delta u_i\,\mathrm{d}(\partial\Omega^t) \quad (A.28)$$

in which, cf. Eq. $(A.4)_2$

$$\delta\overline{\overline{\Delta\varepsilon}}_{ij}=\tfrac{1}{2}\big(\delta\Delta u_{k,i}\,\Delta u_{k,j}+\Delta u_{k,i}\,\delta\Delta u_{k,j}\big)=2\overline{\overline{A}}_{ij}(\Delta u_k,\delta\Delta u_k) \quad (A.29)$$

We note that contrary to Eq. (A.26), in Eq. (A.28) no incremental strain linearization has been carried out which is due to the assumed finiteness of the time step. Subtracting sidewise Eq. (A.26) from Eq. (A.28) results in

$$\int_{\Omega^t}\big(\Delta\tilde{\sigma}_{ij}\,\delta\overline{\Delta\varepsilon}_{ij}+{}^{t+\Delta t}\tilde{\sigma}_{ij}\,\delta\overline{\overline{\Delta\varepsilon}}_{ij}\big)\,\mathrm{d}\Omega^t=\int_{\Omega^t}\Delta\hat{f}_i\,\delta\Delta u_i\,\mathrm{d}\Omega^t+\int_{\partial\Omega^t_\sigma}\Delta\hat{t}_i\,\delta\Delta u_i\,\mathrm{d}(\partial\Omega^t) \quad (A.30)$$

or

$$\int_{\Omega^t}\big(\Delta\tilde{\sigma}_{ij}\,\delta\Delta\varepsilon_{ij}+{}^t\sigma_{ij}\,\delta\overline{\overline{\Delta\varepsilon}}_{ij}\big)\,\mathrm{d}\Omega^t=\int_{\Omega^t}\Delta\hat{f}_i\,\delta\Delta u_i\,\mathrm{d}\Omega^t+\int_{\partial\Omega^t_\sigma}\Delta\hat{t}_i\,\delta\Delta u_i\,\mathrm{d}(\partial\Omega^t) \quad (A.31)$$

which is the *incremental virtual work equation* sought. As a matter of fact, Eq. (A.30) is based on the assumption that the equilibrium at t, i.e. Eq. (A.26) is strictly satisfied. Since due to errors of numerical pseudo-time integration Eq. (A.26) will generally be satisfied only approximately, Eq. (A.31) is often replaced by Eq. (A.28) written in the form

$$\int_{\Omega^t}\big(\Delta\tilde{\sigma}_{ij}\,\delta\Delta\varepsilon_{ij}+{}^t\sigma_{ij}\,\delta\overline{\overline{\Delta\varepsilon}}_{ij}\big)\,\mathrm{d}\Omega^t=\int_{\Omega^t}{}^{t+\Delta t}\hat{f}_i\,\delta\Delta u_i\,\mathrm{d}\Omega^t$$
$$+\int_{\partial\Omega^t_\sigma}{}^{t+\Delta t}\hat{t}_i\,\delta\Delta u_i\,\mathrm{d}(\partial\Omega^t)-\int_{\Omega^t}{}^t\sigma_{ij}\,\delta\overline{\Delta\varepsilon}_{ij}\,\mathrm{d}\Omega^t \quad \text{for any k.a. } \delta\Delta u_i \quad (A.32)$$

whose right-hand side clearly is, cf. Eq. (A.31)

$$\int_{\Omega^t}\Delta\hat{f}_i\,\delta\Delta u_i\,\mathrm{d}\Omega^t+\int_{\partial\Omega^t_\sigma}\Delta\hat{t}_i\,\delta\Delta u_i\,\mathrm{d}(\partial\Omega^t)$$
$$+\underbrace{\int_{\Omega^t}{}^t\hat{f}_i\,\delta\Delta u_i\,\mathrm{d}\Omega^t+\int_{\partial\Omega^t_\sigma}{}^t\hat{t}_i\,\delta\Delta u_i\,\mathrm{d}(\partial\Omega^t)-\int_{\Omega^t}{}^t\sigma_{ij}\,\delta\overline{\Delta\varepsilon}_{ij}\,\mathrm{d}\Omega^t}_{=0\ \text{up to time integration accuracy}}$$

Eq. (A.30) is the weak form of the equilibrium equation. A few problems (linear and some other special cases) yield the variational formulation from the stationarity condition of a certain functional. However, in most cases, such functional, due to the nonlinearity of the constitutive equations, does not exist. It does, however, provided we linearize the problem by both using the *explicit integration* of the constitutive law i.e. when, cf. Eq. (A.9)

$$\Delta\sigma_{ij}={}^tC_{ijkl}\,\overline{\Delta\varepsilon}_{kl}+\Delta t\,{}^tH_{ij} \quad (A.33)$$

and neglect the 'higher-order' term $\Delta\bar{\sigma}_{ij}\,\delta\overline{\overline{\Delta\varepsilon}}_{ij}$. Then Eq. (A.30) will read

$$\int_{\Omega^t}\left[{}^tC_{ijkl}\,\overline{\Delta\varepsilon}_{ij}(\Delta u_m)\,\delta\overline{\Delta\varepsilon}_{kl}(\delta\Delta u_n)+{}^t\sigma_{ij}\,\delta\overline{\overline{\Delta\varepsilon}}_{ij}(\Delta u_k,\delta\Delta u_k)\right]\,\mathrm{d}\Omega^t$$
$$=\int_{\Omega^t}\Delta\hat{f}_i\,\delta\Delta u_i\,\,\mathrm{d}\Omega^t+\int_{\partial\Omega^t_\sigma}\Delta\hat{t}_i\,\delta\Delta u_i\,\,\mathrm{d}(\partial\Omega^t)$$
$$-\int_{\Omega^t}\Delta t\,{}^tH_{ij}\,\delta\overline{\Delta\varepsilon}_{ij}(\delta\Delta u_k)\,\,\mathrm{d}\Omega^t \tag{A.34}$$

which also results from the stationarity condition of the functional

$$\mathcal{J}[\Delta u_i]=\int_{\Omega^t}\left[\tfrac{1}{2}\,{}^tC_{ijkl}\,\overline{\Delta\varepsilon}_{ij}(\Delta u_m)\,\overline{\Delta\varepsilon}_{kl}(\Delta u_n)+{}^t\sigma_{ij}\,\overline{\overline{\Delta\varepsilon}}_{ij}(\Delta u_k)\right]\,\mathrm{d}\Omega^t$$
$$+\int_{\Omega^t}\Delta t\,{}^tH_{ij}\,\overline{\Delta\varepsilon}_{ij}(\Delta u_k)\,\,\mathrm{d}\Omega^t$$
$$-\int_{\Omega^t}\Delta\hat{f}_i\,\Delta u_i\,\,\mathrm{d}\Omega^t-\int_{\partial\Omega^t_\sigma}\Delta\hat{t}_i\,\Delta u_i\,\,\mathrm{d}(\partial\Omega^t) \tag{A.35}$$

The resulting problem is linear in Δu_i since Eq. (A.34) has to be satisfied for any $\delta\Delta u_i$ belonging to the class of admissible displacement variations.

By replacing Eqs. (A.27) and (A.29) into Eqs. (A.32) and (A.34) (the latter being extended similarly with the equilibrium equation at t) we obtain, respectively

$$\int_{\Omega^t}\left[\Delta\bar{\sigma}_{ij}\,\overline{A}_{ijk}\,\delta\Delta u_k+2\,{}^t\sigma_{ij}\,\overline{\overline{A}}_{ij}(\Delta u_k,\delta\Delta u_k)\right]\,\mathrm{d}\Omega^t$$
$$=\int_{\Omega^t}{}^{t+\Delta t}\hat{f}_i\,\delta\Delta u_i\,\,\mathrm{d}\Omega^t+\int_{\partial\Omega^t_\sigma}{}^{t+\Delta t}\hat{t}_i\,\delta\Delta u_i\,\,\mathrm{d}(\partial\Omega^t)$$
$$-\int_{\Omega^t}{}^t\sigma_{ij}\,\overline{A}_{ijk}\,\delta\Delta u_k\,\,\mathrm{d}\Omega^t,\qquad\text{for any k.a. }\delta\Delta u_k \tag{A.36}$$

for the general case and, for explicit integration of the constitutive law

$$\int_{\Omega^t}\left[{}^tC_{ijkl}\,\overline{A}_{ijm}\,\overline{A}_{kln}\,\Delta u_m\,\delta\Delta u_n+2\,{}^t\sigma_{ij}\,\overline{\overline{A}}_{ij}(\Delta u_k,\delta\Delta u_k)\right]\,\mathrm{d}\Omega^t$$
$$=\int_{\Omega^t}{}^{t+\Delta t}\hat{f}_i\,\delta\Delta u_i\,\,\mathrm{d}\Omega^t+\int_{\partial\Omega^t_\sigma}{}^{t+\Delta t}\hat{t}_i\,\delta\Delta u_i\,\,\mathrm{d}(\partial\Omega^t)$$
$$-\int_{\Omega^t}({}^t\sigma_{ij}+{}^t\tilde{H}_{ij})\,\overline{A}_{ijk}\,\delta\Delta u_k\,\,\mathrm{d}\Omega^t,\qquad\text{for any k.a. }\delta\Delta u_k \tag{A.37}$$

with the known term containing ${}^t\tilde{H}_{ij}=\Delta t\,{}^tH_{ij}$.

For the case of *implicit integration* of the constitutive law the virtual work equation (A.31) will clearly have to be solved iteratively. For clearness and compactness of notation we define the following operators

$$\Delta Q\circ\delta\Delta u=\int_{\Omega^t}\Delta\hat{f}_i\,\delta\Delta u_i\,\,\mathrm{d}\Omega^t+\int_{\partial\Omega^t_\sigma}\Delta\hat{t}_i\,\delta\Delta u_i\,\,\mathrm{d}(\partial\Omega^t)$$
$$\Delta F(\Delta u_i)\circ\delta\Delta u=\int_{\Omega^t}\left[\Delta\bar{\sigma}_{ij}(\Delta u_k)\,\overline{A}_{ijk}\,\delta\Delta u_k+2\,{}^t\sigma_{ij}\,\overline{\overline{A}}_{ij}(\Delta u_k,\delta\Delta u_k)\right]\mathrm{d}\Omega^t \tag{A.38}$$

standing for the virtual work of the incremental external load and internal forces, respectively. Similarly, the operators for the corresponding total quantities, at time t and $t + \Delta t$ read, respectively

$$\begin{aligned}
{}^{t}Q \circ \delta\Delta u &= \int_{\Omega^t} {}^{t}\hat{f}_i \, \delta\Delta u_i \; \mathrm{d}\Omega^t + \int_{\partial\Omega^t_\sigma} {}^{t}\hat{t}_i \, \delta\Delta u_i \; \mathrm{d}(\partial\Omega^t) \\
{}^{t}F \circ \delta\Delta u &= \int_{\Omega^t} {}^{t}\sigma_{ij} \, \delta\overline{\Delta\varepsilon}_{ij} \; \mathrm{d}\Omega^t = \int_{\Omega^t} {}^{t}\sigma_{ij} \, \overline{A}_{ijk} \, \delta\Delta u_k \; \mathrm{d}\Omega^t \\
{}^{t+\Delta t}Q \circ \delta\Delta u &= \int_{\Omega^t} {}^{t+\Delta t}\hat{f}_i \, \delta\Delta u_i \; \mathrm{d}\Omega^t + \int_{\partial\Omega^t_\sigma} {}^{t+\Delta t}\hat{t}_i \, \delta\Delta u_i \; \mathrm{d}(\partial\Omega^t) \\
{}^{t+\Delta t}F \circ \delta\Delta u &= \int_{\Omega^t} {}^{t+\Delta t}\tilde{\sigma}_{ij} \, \delta\Delta\varepsilon_{ij} \; \mathrm{d}\Omega^t \\
&= \int_{\Omega^t} {}^{t+\Delta t}\tilde{\sigma}_{ij} \Big[\overline{A}_{ijk} \, \delta\Delta u_k + 2 \, \overline{\overline{A}}_{ij}(u_k, \delta\Delta u_k) \Big] \; \mathrm{d}\Omega^t
\end{aligned} \tag{A.39}$$

Then, by defining the incremental and total residuals as

$$\Delta R = \Delta Q - \Delta F \tag{A.40}$$

$${}^{t}R = {}^{t}Q - {}^{t}F \tag{A.41}$$

we may rewrite Eq. (A.31) and Eq. (A.32) as

$$\Delta R(\Delta u_i) \circ \delta\Delta u = \Delta Q \circ \delta\Delta u - \Delta F(\Delta u_i) \circ \delta\Delta u = 0 \tag{A.42}$$

and

$${}^{t+\Delta t}R(\Delta u_i) \circ \delta\Delta u = {}^{t+\Delta t}Q \circ \delta\Delta u - {}^{t+\Delta t}F(\Delta u_i) \circ \delta\Delta u = 0 \tag{A.43}$$

respectively.

Eq. (A.42) is nonlinear in Δu. As long as we do not have the 'exact' solution, $\Delta R(\Delta u_i^{(\omega)})$ will not be equal zero. Using a Newton-Raphson procedure the $(\omega + 1)$-th (variation-type) correction $\gamma\Delta u_i^{(\omega+1)}$ to $\Delta u_i^{(\omega)}$

$$\Delta u_i^{(\omega+1)} = \Delta u_i^{(\omega)} + \gamma\Delta u_i^{(\omega+1)} \tag{A.44}$$

is calculated by linearizing the residual increment $\Delta R(\Delta u_i^{(\omega)})$ (via Taylor series expansion up to the linear term)

$$\Delta R(\Delta u_i^{(\omega)}) \circ \delta\Delta u + \frac{\partial}{\partial\Delta u}\Big[\Delta R(\Delta u_i^{(\omega)}) \circ \delta\Delta u\Big] \circ \gamma\Delta u^{(\omega+1)} = 0 \tag{A.45}$$

i.e., by noting that ΔQ is independent of Δu_i

$$\frac{\partial}{\partial\Delta u}\Big[\Delta F(\Delta u_i^{(\omega)}) \circ \delta\Delta u\Big] \circ \gamma\Delta u^{(\omega+1)} = -\Delta R(\Delta u_i^{(\omega)}) \circ \delta\Delta u \tag{A.46}$$

which yields to the system on $\gamma\Delta u_i^{(\omega+1)}$

$$\begin{aligned}
&\int_{\Omega^t} \Big[\hat{C}^{(\omega)}_{ijkl} \overline{A}_{ijm} \, \overline{A}_{kln} \, \gamma\Delta u_m \, \delta\Delta u_n^{(\omega+1)} + 2 \, {}^{t}\sigma_{ij} \, \overline{\overline{A}}_{ij}(\gamma\Delta u_k^{(\omega+1)}, \delta\Delta u_k) \Big] \; \mathrm{d}\Omega^t \\
&\quad = \Delta R(\Delta u_i^{(\omega)}) \circ \delta\Delta u
\end{aligned} \tag{A.47}$$

where

$$\hat{C}^{(\omega)}_{ijkl} = \frac{\partial \Delta \bar{\sigma}^{(\omega)}_{ij}}{\partial \Delta \varepsilon_{kl}} \tag{A.48}$$

is the so-called *consistent* (with the constitutive law integration scheme) or *algorithmic tangent constitutive tensor* at the solution level corresponding to the displacement ${}^t u_i + \Delta u_i^{(\omega)}$. It is easily observed that for explicit integration scheme, cf. Eq. (A.33)

$$\hat{C}_{ijkl} = {}^t C_{ijkl} \tag{A.49}$$

Since we are involved in an iterative process, it seems reasonable to account at this step for a possible non-equilibrated residual force from the previous step. Instead of the incremental virtual work residual $\Delta R \circ \delta \Delta u$ we then consider the total residual generated so far $({}^t R + \Delta R) \circ \delta \Delta u$ (i.e. Eq. (A.43)) and replace Eq. (A.46) by

$$\frac{\partial}{\partial \Delta u}\Big(\Delta F^{(\omega)} \circ \delta \Delta u\Big) \circ \gamma \Delta u^{(\omega+1)} = -\underbrace{\Big[{}^t R + \Delta R(\Delta u_i^{(\omega)})\Big]}_{t+\Delta t R^{(\omega)}} \circ \delta \Delta u \tag{A.50}$$

for any kinematically admissible $\delta \Delta u$.

A.1.2 Concepts for DPA

In accordance with the updated Lagrangian path-following strategy, we have so far been taking as the reference state the configuration of the body at the beginning of each incremental step. However, our interest in finding changes in the response because of changes in the initial shape of the body requires keeping track of the initial shape parameters during the whole analysis. One of the methods that can be used effectively for this purpose is the domain parameterization (or reference state) approach, for which the acronym DPA was coined in [70]. Its idea is based on adopting a fixed reference (or 'parent') state assumed independent of both the deformation under loading and design variation. To handle the subject in a formal manner, let us define a fixed reference state C^r that is affected neither by any possible design changes (shape variations) nor by any deformation processes. The body in the reference state C^r is assumed to take up the volume Ω^r with the boundary $\partial\Omega^r$, cf. Fig. A.2.

For each specific design, say h_d, a unique one-to-one mapping

$${}^0 x_k = {}^0 x_k({}^r x_l, h_d), \qquad {}^r \mathbf{x} \in \Omega^r \tag{A.51}$$

may be established to map each material point with coordinates ${}^r x_k$ in C^r into its position with coordinates ${}^0 x_k$ in C^0; the mapping is assumed to depend only on design and be independent of the loading history. Moreover, the dependence on h_d in Eq. (A.51) is explicit and can be regarded as known for each specific design parameter set. The variables ${}^r x_k$ in C^r will consequently be used below as the

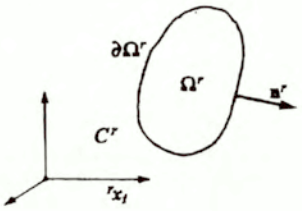

Figure A.2 Reference configuration

independent variables regardless of the step-wise updated reference configurations typical of the UL approach.

Within the isoparametric finite element methodology, the so-called parent element may be used conveniently as the reference domain for the shape sensitivity analysis. Thus, examples of transformation (A.51) can be found in every book on the FEM. More specifically, for an isoparametric element, the coordinate vector ${}^0\mathbf{x}$ of the material point in the initial state C^0 is written as

$$ {}^0\mathbf{x}({}^r\mathbf{x}, \mathbf{h}) = \boldsymbol{\phi}({}^r\mathbf{x})\,\mathbf{X}(\mathbf{h}) \tag{A.52} $$

where $\boldsymbol{\phi}$ is the shape function matrix

$$ \boldsymbol{\phi}_{3\times N} = \begin{bmatrix} \phi_1^{(1)} & & \phi_1^{(2)} & & \cdots & \phi_1^{(S)} & \\ & \phi_2^{(1)} & & \phi_2^{(2)} & \cdots & & \phi_2^{(S)} \\ & & \phi_3^{(1)} & & \phi_3^{(2)} & \cdots & \phi_3^{(S)} \end{bmatrix} $$

so that $\phi_k^{(s)}$, $k = 1, 2, 3$, $s = 1, 2, \ldots, S$, is the shape function for the kth coordinate at the sth node in the element, S is the number of element nodes (i.e. $N = 3S$), $\mathbf{X}$ is the column vector of all element nodal coordinates

$$ \mathbf{X}_{N\times 1} = \left\{ \begin{array}{cccc} \mathbf{X}_{3\times 1}^{(1)} & \mathbf{X}_{3\times 1}^{(2)} & \cdots & \mathbf{X}_{3\times 1}^{(S)} \end{array} \right\} $$

and

$$ \mathbf{X}_{3\times 1}^{(s)} = \left\{ \begin{array}{ccc} X_1^{(s)} & X_2^{(s)} & X_3^{(s)} \end{array} \right\}, \qquad s = 1, 2, \ldots, S $$

is the sth node coordinate vector.[1]

Since the function ${}^0\mathbf{x}$ in Eq. (A.51) has been assumed explicitly given in terms of design, the vector of nodal coordinates $\mathbf{X}$ results by Eq. (A.52) as an explicitly given function of $\mathbf{h}$ as well.

Variations in geometry are represented by variations of the nodal coordinates $\mathbf{X}$, which, in turn, may be related to variation of design by means of the relation

$$ \delta\mathbf{X} = \partial\mathbf{X} = \frac{\partial\mathbf{X}}{\partial\mathbf{h}}\,\delta\mathbf{h} \tag{A.53} $$

[1]The above formalism has been also employed (and explained) in Section 2.2.1.

This assertion becomes trivial if it is the nodal coordinates $\mathbf{X}$ (not necessarily all of them) that are selected as the shape design variables. Nevertheless, as seen in Section 2.4, in such case an interdependence between the nodal coordinates will be preferred. Then the derivative in Eq. (A.53) will be split into $\frac{\partial \mathbf{X}}{\partial \mathbf{X}^{\mathrm{M}}} \frac{\partial \mathbf{X}^{\mathrm{M}}}{\partial \mathbf{h}}$, where $\mathbf{X}^{\mathrm{M}}$ is the array containing the master nodes (i.e. those selected to uniquely define the coordinates of any node in the domain).

Let us now go back to the fundamentals of the DPA. The first step in it consists of transforming all the quantities to the reference domain Ω^r. The compact notation

$$ {}^{t_2}_{t_1}F_{kl} = \frac{\partial\, {}^{t_2}x_k}{\partial\, {}^{t_1}x_l} \tag{A.54} $$

has been found useful to stand for the deformation gradient at any time instant t_2, the state at another time instant t_1 being taken as the reference state. All the transformations to be considered are depicted in Fig. A.3.

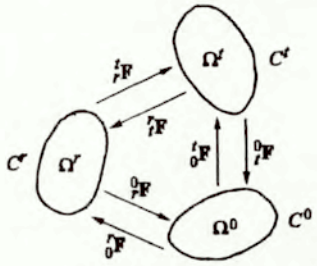

Figure A.3 Transformations from and to the reference, initial and present configurations

To better emphasize the nature of the mathematical task we face, let us first transform the incremental strains Eq. (A.4) from the configuration C^t to the newly defined reference configuration C^r. To this purpose we use the mapping[1]

$$ {}^{t}x_k = {}^{t}x_k({}^{r}x_m; h_d) = {}^{t}x_k({}^{0}x_l({}^{r}x_m; h_d)) \tag{A.55} $$

in which ${}^{0}x_k = {}^{0}x_k({}^{r}x_m; h_d)$ is the mapping introduced in Eq. (A.51), ${}^{t}x_k = {}^{t}x_k({}^{0}x_m; h_d)$ is the deformation function and the (pseudo-) time variable has been suppressed in the deformation function to simplify notation. For the incremental displacement expressed as

$$ \Delta u_i({}^{t}x_k) = \Delta u_i({}^{t}x_k({}^{0}x_m({}^{r}x_n; h_d))) = \Delta u_i({}^{r}x_n; h_d) \tag{A.56} $$

[1] We do not differentiate between symbols standing for functions of original and transformed independent variables. At the small cost of having to pay special attention whenever these functions are differentiated, we gain a lot in simplicity of the notation.

we obtain

$$\Delta u_{i;j} = \frac{\partial \Delta u_i}{\partial {}^r x_j} = \frac{\partial \Delta u_i}{\partial {}^t x_k}\,\frac{\partial {}^t x_k}{\partial {}^0 x_m}\,\frac{\partial {}^0 x_m}{\partial {}^r x_j} = \Delta u_{i,k}\,{}^t_0F_{km}\,{}^0_rF_{mj} = \Delta u_{i,k}\,{}^t_rF_{kj} \tag{A.57}$$

and similarly

$$\Delta u_{i;j} = \Delta u_{i;k}\,{}^r_tF_{kj} = \Delta u_{i;k}\,{}^t_rF^{-1}_{kj} \tag{A.58}$$

By using a similar convention for the incremental strains

$$\begin{aligned} \overline{\Delta\varepsilon}_{ij}({}^t x_k) &= \overline{\Delta\varepsilon}_{ij}({}^r x_k; h_d) \\ \overline{\overline{\Delta\varepsilon}}_{ij}({}^t x_k) &= \overline{\overline{\Delta\varepsilon}}_{ij}({}^r x_k; h_d) \end{aligned} \tag{A.59}$$

we arrive at the linear and quadratic part of the incremental strain in the form

$$\begin{aligned} \overline{\Delta\varepsilon}_{ij} &= \frac{1}{2}\Big(\frac{\partial \Delta u_i}{\partial {}^r x_m}\,{}^r_0F_{mn}\,{}^0_tF_{nj} + \frac{\partial \Delta u_j}{\partial {}^r x_m}\,{}^r_0F_{mn}\,{}^0_tF_{ni}\Big) \\ &= \underbrace{\frac{1}{2}\Big(\delta_{ik}\,{}^0_tF_{nj} + \delta_{jk}\,{}^0_tF_{ni}\Big)}_{\overline{A}^{(t)}_{ijkn}}\,\underbrace{{}^r_0F_{mn}\,\frac{\partial}{\partial {}^r x_m}}_{\overline{A}^{(r)}_{n}}\,\Delta u_k \\ &= \overline{A}^{(t)}_{ijkn}\,\overline{A}^{(r)}_{n}\,\Delta u_k \;=\; \overline{A}_{ijk}\,\Delta u_k \end{aligned} \tag{A.60}$$

$$\begin{aligned} \overline{\overline{\Delta\varepsilon}}_{ij} &= \underbrace{\frac{1}{4}\Big({}^0_tF_{ni}\,{}^0_tF_{pj} + {}^0_tF_{nj}\,{}^0_tF_{pi}\Big)}_{\overline{\overline{A}}^{(t)}_{ijnp}}\,\underbrace{{}^r_0F_{mn}\,{}^r_0F_{sp}\,\frac{\partial \Delta u_k}{\partial {}^r x_m}\,\frac{\partial \Delta u_k}{\partial {}^r x_s}}_{\overline{\overline{A}}^{(r)}_{np}(\Delta u_k, \Delta u_k)} \\ &= \overline{\overline{A}}^{(t)}_{ijnp}\,\overline{\overline{A}}^{(r)}_{np}(\Delta u_k, \Delta u_k) \;=\; \overline{\overline{A}}_{ij}(\Delta u_k, \Delta u_k) \end{aligned} \tag{A.61}$$

In Eqs. (A.60) and (A.61) the matrix operators labelled (t) depend on the 'real' deformation gradient ${}^t_0\mathbf{F}$, while those labelled (r) depend on the 'fictitious' deformation gradient ${}^0_r\mathbf{F}$. We may check by simple inspection that the operator $\overline{\overline{A}}_{ij}$ is symmetric with respect to its arguments, $\overline{\overline{A}}_{ij}(\mathbf{a}, \mathbf{b}) = \overline{\overline{A}}_{ij}(\mathbf{b}, \mathbf{a})$. Later derivations will make use of this property while taking design variations or performing differentiations.

To make subsequent derivations more compact and transparent, the following absolute tensor notation will also be employed:

$$\begin{aligned} \overline{\Delta\boldsymbol{\varepsilon}} &= \overline{\mathbf{A}}^{(t)}\,\overline{\mathbf{A}}^{(r)}\,\Delta\mathbf{u} = \overline{\mathbf{A}}\,\Delta\mathbf{u} \\ \overline{\overline{\Delta\boldsymbol{\varepsilon}}} &= \overline{\overline{\mathbf{A}}}^{(t)}\,\overline{\overline{\mathbf{A}}}^{(r)}(\Delta\mathbf{u}, \Delta\mathbf{u}) = \overline{\overline{\mathbf{A}}}(\Delta\mathbf{u}, \Delta\mathbf{u}) \end{aligned} \tag{A.62}$$

The absolute notation has been here slightly extended by additionally adopting the following rules for any tensors $\mathbf{a}$, $\mathbf{b}$ and $\mathbf{c}$:

$$\begin{aligned} \mathbf{a}\,\mathbf{b}\,\mathbf{c} &= \big(\mathbf{a}\,\mathbf{b}\big)\mathbf{c} = \big\{a_{\ldots k}\,b_{k\ldots}\big\}\mathbf{c} = \big\{(\mathbf{a}\,\mathbf{b})_{\ldots m}\,c_{m\ldots}\big\} \\ \mathbf{a}\cdot\mathbf{b}\cdot\mathbf{c} &= \big(\mathbf{a}\cdot\mathbf{b}\big)\cdot\mathbf{c} = \big\{a_{\ldots kl}\,b_{kl\ldots}\big\}\cdot\mathbf{c} = \big\{(\mathbf{a}\cdot\mathbf{b})_{\ldots mn}\,c_{mn\ldots}\big\} \end{aligned} \tag{A.63}$$

implying that operations involving more than two tensors proceed from left to right (unless parentheses or brackets indicate otherwise) so that, for instance

$$\overline{A}^{(t)}_{ijkn}\,\overline{A}^{(r)}_{n}\,\Delta u_k = \left(\overline{\mathbf{A}}^{(t)}\,\overline{\mathbf{A}}^{(r)}\right)_{ijk}\,\Delta u_k = \left(\overline{\mathbf{A}}^{(t)}\,\overline{\mathbf{A}}^{(r)}\,\Delta\mathbf{u}\right)_{ij}$$

In the framework of this absolute notation, the virtual incremental work equations (A.36) and (A.37) read, respectively

$$\int_{\Omega^t}\left[\Delta\tilde{\boldsymbol{\sigma}}\cdot(\overline{\mathbf{A}}\delta\Delta\mathbf{u}) + 2\,{}^t\boldsymbol{\sigma}\cdot\overline{\overline{\mathbf{A}}}(\Delta\mathbf{u},\delta\Delta\mathbf{u})\right]\,\mathrm{d}\Omega^t$$
$$= \int_{\Omega^t}{}^{t+\Delta t}\hat{\mathbf{f}}\delta\Delta\mathbf{u}\,\mathrm{d}\Omega^t + \int_{\partial\Omega^t_\sigma}{}^{t+\Delta t}\hat{\mathbf{t}}\delta\Delta\mathbf{u}\,\mathrm{d}(\partial\Omega^t) - \int_{\Omega^t}{}^t\boldsymbol{\sigma}\cdot(\overline{\mathbf{A}}\delta\Delta\mathbf{u})\,\mathrm{d}\Omega^t \quad (A.64)$$

and

$$\int_{\Omega^t}\left[{}^t\mathbf{C}\cdot(\overline{\mathbf{A}}\Delta\mathbf{u})\cdot(\overline{\mathbf{A}}\delta\Delta\mathbf{u}) + 2\,{}^t\boldsymbol{\sigma}\cdot\overline{\overline{\mathbf{A}}}(\Delta\mathbf{u},\delta\Delta\mathbf{u})\right]\,\mathrm{d}\Omega^t$$
$$= \int_{\Omega^t}{}^{t+\Delta t}\hat{\mathbf{f}}\,\delta\Delta\mathbf{u}\,\mathrm{d}\Omega^t + \int_{\partial\Omega^t_\sigma}{}^{t+\Delta t}\hat{\mathbf{t}}\,\delta\Delta\mathbf{u}\,\mathrm{d}(\partial\Omega^t)$$
$$- \int_{\Omega^t}({}^t\boldsymbol{\sigma} + {}^t\tilde{\mathbf{H}})\cdot(\overline{\mathbf{A}}\delta\Delta\mathbf{u})\,\mathrm{d}\Omega^t, \qquad \text{for any k.a. } \delta\Delta\mathbf{u} \quad (A.65)$$

We have adopted here again the convention that the symbols $\overline{\mathbf{A}}$ and $\overline{\overline{\mathbf{A}}}$ (instead of $\overline{\Delta\boldsymbol{\varepsilon}}$ and $\overline{\overline{\Delta\boldsymbol{\varepsilon}}}$) are used whenever there is a need to display clearly the arguments of the linear and quadratic incremental strains, respectively. We also emphasize that the bilinear form symbol $\overline{\overline{\mathbf{A}}}(\cdot,\cdot)$ applies, by definition, to contracted vector arguments only so that the compact notation

$$\overline{\overline{\mathbf{A}}}(\Delta\mathbf{u},\Delta\mathbf{u}) = \overline{\overline{A}}(\Delta u_k,\Delta u_k)$$

is not ambiguous.

The transformation between the reference domain Ω^r and the current domain Ω^t is locally characterized by the corresponding gradient (Jacobian) of the transformation ${}^t_r\mathbf{F}$ and its inverse ${}^r_t\mathbf{F}$ defined as, cf. Eq. (A.54)

$${}^t_rF_{kl} = \frac{\partial\,{}^tx_k}{\partial\,{}^rx_l}, \qquad {}^r_tF_{kl} = \frac{\partial\,{}^rx_k}{\partial\,{}^tx_l} = {}^t_rF^{-1}_{kl} \quad (A.66)$$

It will turn out to be useful to explicitly account in the above expressions for the initial body configuration by rewriting Eq. (A.66) in the expanded form

$${}^t_rF_{kl} = \frac{\partial\,{}^tx_k}{\partial\,{}^0x_m}\frac{\partial\,{}^0x_m}{\partial\,{}^rx_l} = {}^t_0F_{km}\,{}^0_rF_{ml}, \qquad {}^r_tF_{kl} = \frac{\partial\,{}^rx_k}{\partial\,{}^0x_m}\frac{\partial\,{}^0x_m}{\partial\,{}^tx_l} = {}^r_0F_{km}\,{}^0_tF_{ml} \quad (A.67)$$

The differential volume and its boundary in the current configuration can be expressed in terms of their reference configuration counterparts as

$$\mathrm{d}\Omega^t = {}^t_rJ\,\mathrm{d}\Omega^r, \qquad \mathrm{d}(\partial\Omega^t) = {}^t_rJ_\theta\,\mathrm{d}(\partial\Omega^r) \quad (A.68)$$

where

$$ {}^t_r J = \det[{}^t_r \mathbf{F}] = \det[{}^t_0 \mathbf{F}\, {}^0_r \mathbf{F}] = \det[{}^t_0 \mathbf{F}]\, \det[{}^0_r \mathbf{F}] = {}^t_0 J\, {}^0_r J $$

is the determinant of the Jacobian, while ${}^t_r J_\partial$ is defined by Nanson's formula as,

$$ {}^t_r J_\partial = {}^t_r J \left\| {}^r_t \mathbf{F}\, \mathbf{n}^r \right\| = {}^t_r J \left\| \left({}^r_0 \mathbf{F}\, {}^0_t \mathbf{F} \right) \mathbf{n}^r \right\| = {}^t_r J \left({}^r_0 F_{ki}\, {}^0_t F_{km}\, n^r_i\, n^r_m \right)^{\frac{1}{2}} $$

The transformation of the virtual work equation in both forms (A.36) and (A.37) gives

$$ \begin{aligned} &\int_{\Omega^r} \left[\Delta\tilde{\boldsymbol{\sigma}} \cdot (\overline{\mathbf{A}} \delta\Delta\mathbf{u}) + 2\, {}^t\boldsymbol{\sigma} \cdot \overline{\overline{\mathbf{A}}}(\Delta\mathbf{u}, \delta\Delta\mathbf{u}) \right] {}^t_r J \, \mathrm{d}\Omega^r \\ &\quad = \int_{\Omega^r} {}^{t+\Delta t}\hat{\mathbf{f}} \delta\Delta\mathbf{u}\, {}^t_r J \, \mathrm{d}\Omega^r + \int_{\partial\Omega^r_\sigma} {}^{t+\Delta t}\hat{\mathbf{t}} \delta\Delta\mathbf{u}\, {}^t_r J_\partial \, \mathrm{d}(\partial\Omega^r) \\ &\quad\quad - \int_{\Omega^r} {}^t\boldsymbol{\sigma} \cdot (\overline{\mathbf{A}} \delta\Delta\mathbf{u})\, {}^t_r J \, \mathrm{d}\Omega^r \end{aligned} \tag{A.69} $$

$$ \begin{aligned} &\int_{\Omega^r} \left[{}^t\mathbf{C} \cdot (\overline{\mathbf{A}}\Delta\mathbf{u}) \cdot (\overline{\mathbf{A}} \delta\Delta\mathbf{u}) + 2\, {}^t\boldsymbol{\sigma} \cdot \overline{\overline{\mathbf{A}}}(\Delta\mathbf{u}, \delta\Delta\mathbf{u}) \right] {}^t_r J \, \mathrm{d}\Omega^r \\ &\quad = \int_{\Omega^r} {}^{t+\Delta t}\hat{\mathbf{f}}\, \delta\Delta\mathbf{u}\, {}^t_r J \, \mathrm{d}\Omega^r + \int_{\partial\Omega^r_\sigma} {}^{t+\Delta t}\hat{\mathbf{t}}\, \delta\Delta\mathbf{u}\, {}^t_r J_\partial \, \mathrm{d}(\partial\Omega^r) \\ &\quad\quad - \int_{\Omega^r} ({}^t\boldsymbol{\sigma} + {}^t\tilde{\mathbf{H}}) \cdot (\overline{\mathbf{A}} \delta\Delta\mathbf{u})\, {}^t_r J \, \mathrm{d}\Omega^r, \qquad \text{for any k.a. } \delta\Delta\mathbf{u} \end{aligned} \tag{A.70} $$

all the functions now being treated as dependent on spatial variables ${}^r x_k$ and design parameters h_d.

The constraint functional (A.1) may be transformed similarly to yield

$$ \begin{aligned} {}^{t+\Delta t}\mathcal{G}(\mathbf{h}) &= {}^{t+\Delta t}G[\boldsymbol{\sigma}, \mathbf{u}; \mathbf{h}] \\ &= \int_{\Omega^r} {}^{t+\Delta t}g(\boldsymbol{\sigma}, \mathbf{u}; \mathbf{h})\, {}^t_r J \, \mathrm{d}\Omega^r + \int_{\partial\Omega^r_\sigma} {}^{t+\Delta t}g^{(\sigma)}(\mathbf{u}; \mathbf{h})\, {}^t_r J_\partial \, \mathrm{d}(\partial\Omega^r) \\ &\quad + \int_{\partial\Omega^r_\mathbf{t}} {}^{t+\Delta t}g^{(u)}(\mathbf{t}; \mathbf{h})\, {}^t_r J_\partial \, \mathrm{d}(\partial\Omega^r) \end{aligned} \tag{A.71} $$

By taking the design variation of the functional $\mathcal{G}$ we arrive at

$$ \begin{aligned} &\bar{\delta}\mathcal{G}(\mathbf{h}) \\ &= \Big\{ \int_{\Omega^r} \Big[\Big(\frac{\partial^{t+\Delta t} g}{\partial\boldsymbol{\sigma}} \frac{\mathrm{d}^{t+\Delta t}\boldsymbol{\sigma}}{\mathrm{d}\mathbf{h}} + \frac{\partial^{t+\Delta t} g}{\partial\mathbf{u}} \frac{\mathrm{d}^{t+\Delta t}\mathbf{u}}{\mathrm{d}\mathbf{h}} + \frac{\partial^{t+\Delta t} g}{\partial\mathbf{h}} \Big) {}^t_r J + {}^{t+\Delta t}g \frac{\mathrm{d}\, {}^t_r J}{\mathrm{d}\mathbf{h}} \Big] \, \mathrm{d}\Omega^r \\ &\quad + \int_{\partial\Omega^r_\sigma} \Big[\Big(\frac{\partial^{t+\Delta t} g^{(\sigma)}}{\partial\mathbf{u}} \frac{\mathrm{d}^{t+\Delta t}\mathbf{u}}{\mathrm{d}\mathbf{h}} + \frac{\partial^{t+\Delta t} g^{(\sigma)}}{\partial\mathbf{h}} \Big) {}^t_r J_\partial + {}^{t+\Delta t}g^{(\sigma)} \frac{\mathrm{d}\, {}^t_r J_\partial}{\mathrm{d}\mathbf{h}} \Big] \, \mathrm{d}(\partial\Omega^r) \\ &\quad + \int_{\partial\Omega^r_\mathbf{t}} \Big[\Big(\frac{\partial^{t+\Delta t} g^{(u)}}{\partial\mathbf{t}} \frac{\mathrm{d}^{t+\Delta t}\mathbf{t}}{\mathrm{d}\mathbf{h}} + \frac{\partial^{t+\Delta t} g^{(u)}}{\partial\mathbf{h}} \Big) {}^t_r J_\partial + {}^{t+\Delta t}g^{(u)} \frac{\mathrm{d}\, {}^t_r J_\partial}{\mathrm{d}\mathbf{h}} \Big] \, \mathrm{d}(\partial\Omega^r) \Big\} \delta\mathbf{h} \end{aligned} \tag{A.72} $$

In Eq. (A.72), values at $t + \Delta t$ of all the derivatives of g, $g^{(\sigma)}$ and $g^{(u)}$ with respect to their arguments can be routinely obtained from the respective explicit expressions provided the equilibrium problem has been solved at the step $[t, t + \Delta t]$,

which is here assumed in accordance with the basic methodology of the step-wise sensitivity assessment. However, the values at $t + \Delta t$ of the design derivatives (sensitivity coefficients) of stresses $\boldsymbol{\sigma}$, surface traction $\mathbf{t}$ and displacements $\mathbf{u}$, i.e. $\mathrm{d}^{t+\Delta t}\boldsymbol{\sigma}/\mathrm{d}\mathbf{h}$, $\mathrm{d}^{t+\Delta t}\mathbf{t}/\mathrm{d}\mathbf{h}$ and $\mathrm{d}^{t+\Delta t}\mathbf{u}/\mathrm{d}\mathbf{h}$, respectively, can only be determined after:

(i) displacement increment sensitivities $\mathrm{d}\Delta\mathbf{u}/\mathrm{d}\mathbf{h}$ have been computed from the current step sensitivity problem,

(ii) beginning-of-step sensitivity values $\mathrm{d}^t\boldsymbol{\sigma}/\mathrm{d}\mathbf{h}$, $\mathrm{d}^t\mathbf{p}/\mathrm{d}\mathbf{h}$, $\mathrm{d}^t\mathbf{t}/\mathrm{d}\mathbf{h}$, $\mathrm{d}^t\mathbf{u}/\mathrm{d}\mathbf{h}$ and $\mathrm{d}\,{}_r^tJ/\mathrm{d}\mathbf{h}$, $\mathrm{d}\,{}_r^tJ_\beta/\mathrm{d}\mathbf{h}$ have been recovered from computer memory, and

(iii) incremental sensitivities $\mathrm{d}\Delta\bar{\boldsymbol{\sigma}}/\mathrm{d}\mathbf{h}$, $\mathrm{d}\Delta\mathbf{p}/\mathrm{d}\mathbf{h}$ and $\mathrm{d}\Delta\mathbf{t}/\mathrm{d}\mathbf{h}$ have been computed using the above-mentioned data and appropriate, design-differentiated equations relating $\Delta\bar{\boldsymbol{\sigma}}$, $\Delta\mathbf{p}$ and $\Delta\mathbf{t}$ with $\Delta\mathbf{u}$.

It is observed that in the UL approach the mapping from the reference domain C^r to the configuration C^t does not depend on the incremental displacement $\Delta\mathbf{u}$, which implies that the Jacobian sensitivities in Eq. (A.68) are independent of $\mathrm{d}\Delta\mathbf{u}/\mathrm{d}\mathbf{h}$. This feature, typical of Lagrangian methodology, is compensated for in the framework of the sensitivity update procedure as described in [70]. Indeed, the second Piola-Kirchhoff stress tensor at time $t + \Delta t$ is transformed from configuration C^t to $C^{t+\Delta t}$ by

$$ {}^{t+\Delta t}\bar{\sigma}_{ij} = \frac{1}{J} F_{ik} F_{jl}\, {}^{t+\Delta t}\bar{\sigma}_{kl} \tag{A.73} $$

where F_{ij} is the deformation gradient relating both the configurations, cf. Eq. (A.22), and J denotes its determinant. (In Eq. (A.24) this transformation was given using an approximate expression of J.) Accordingly, the updated value of the stress sensitivity is transformed with

$$ \begin{aligned} \bar{\delta}\, {}^{t+\Delta t}\bar{\sigma}_{ij} = \frac{1}{J} \Big[\Big(&- F^{-1}_{mn} \bar{\delta} F_{mn} F_{ik} F_{jl} + \bar{\delta} F_{ik} F_{jl} + F_{ik} \bar{\delta} F_{jl} \Big)\, {}^{t+\Delta t}\bar{\sigma}_{kl} \\ &+ F_{ik} F_{jl} \bar{\delta}\, {}^{t+\Delta t}\bar{\sigma}_{kl} \Big] \end{aligned} \tag{A.74} $$

obtained by design-differentiation of Eq. (A.73); the expression for $\bar{\delta} F_{ij}$ will be derived in Eq. (A.96) below. Updating of the stress-type internal parameters (like the back stress tensor) proceeds along similar lines. The above transformation should be applied to complete the theory developed here, which concerns a nonlinear problem at the typical interval $[t, t + \Delta t]$, but where no incremental update procedure for stress sensitivity is further discussed.

Before setting out to deal with further features of the shape sensitivity of the nonlinear response, we shall recall our specific sensitivity-oriented notation for design variations of functions of the form ${}^t f = f({}^t\mathbf{u}(\mathbf{h}); \mathbf{h})$,

$$ \bar{\delta} f = \underbrace{\frac{\partial\, {}^t f}{\partial \mathbf{u}} \frac{\mathrm{d}\, {}^t\mathbf{u}}{\mathrm{d}\mathbf{h}} \delta\mathbf{h}}_{\bar{\delta}\, {}^t f} + \underbrace{\frac{\partial\, {}^t f}{\partial \mathbf{h}} \delta\mathbf{h}}_{\partial\, {}^t f} \tag{A.75} $$

The function f is assumed given in terms of its arguments, while $\mathbf{u}(\mathbf{h})$ is a solution (whose dependence on $\mathbf{h}$ is generally unknown) generated in a step-by-step manner. The symbols $\bar{\delta}$, $\tilde{\delta}$ and ∂ refer to total, implicit and explicit parameter variations, respectively.

An extension of the above formalism, useful when dealing within the incremental methodology with any function f of the form ${}^{t+\Delta t}f = f(\Delta\mathbf{u}(\mathbf{h}), {}^{t}\mathbf{u}(\mathbf{h}); \mathbf{h})$ is recalled to read

$$\bar{\delta}^{t+\Delta t}f = \underbrace{\frac{\partial^{t+\Delta t}f}{\partial \Delta\mathbf{u}}\frac{\mathrm{d}\Delta\mathbf{u}}{\mathrm{d}\mathbf{h}}\delta\mathbf{h}}_{\tilde{\delta}^{t+\Delta t}f} + \underbrace{\frac{\partial^{t+\Delta t}f}{\partial \mathbf{u}}\frac{\mathrm{d}^{t}\mathbf{u}}{\mathrm{d}\mathbf{h}}\delta\mathbf{h} + \underbrace{\frac{\partial^{t+\Delta t}f}{\partial \mathbf{h}}\delta\mathbf{h}}_{\partial^{t+\Delta t}f}}_{\hat{\partial}^{t+\Delta t}f} \tag{A.76}$$

with $\hat{\partial}f$ called the effectively explicit design variation. The difference in the way the term $(\partial f/\partial \mathbf{u})(\mathrm{d}\mathbf{u}/\mathrm{d}\mathbf{h})\delta\mathbf{h}$ is treated in Eq. (A.75) (implicit design variation) and Eq. (A.76) (a part of the effectively explicit design variation) deserves a special comment. Even though the solution $\mathbf{u}$ is generally an unknown function of design —a fact fully accounted for in Eq. (A.69)— from the viewpoint of the current incremental step analysis, the value of $\mathrm{d}^{t}\mathbf{u}/\mathrm{d}\mathbf{h}$ is assumed to have been computed 'earlier' and thus treated just as a collection of known numbers. In other words, the implicit design variation of the function ${}^{t}f = f({}^{t}\mathbf{u}(\mathbf{h}); \mathbf{h})$ denoted at time t as $\bar{\delta}\,{}^{t}f = (\partial\,{}^{t}f/\partial\mathbf{u})(\mathrm{d}^{t}\mathbf{u}/\mathrm{d}\mathbf{h})\delta\mathbf{h}$ becomes a part of the explicit design variation term as soon as we proceed to consider the incremental step $[t, t+\Delta t]$, at which all function values at t are assumed known by the nature of the UL description. Putting it another way still, a design variation of a function f represented as a product of (any number of) terms

$$f(\mathbf{h})\,\delta\mathbf{h} = f_1(\mathbf{h}) f_2(\mathbf{h})\,\delta\mathbf{h}$$

is called the implicit variation of f if at least one of the contributing terms cannot be computed by a straightforward function evaluation. Otherwise, i.e. if all the terms are 'known' in the above sense, the variation is (effectively) explicit. The term 'straightforward function evaluation' means that no solution to another boundary-value problem is needed at the given moment to carry out the calculations.

A.2 The DPA/DDM formalism

Expressing the constraint functional and the virtual work equation in terms of the new reference state C^{r} independent of the deformation and design, accompanied by the appropriate transformation of the domain of all the functions involved, lies at the core of the domain parameterization approach (DPA) to solving shape sensitivity problems. This method, combined with the direct differentiation technique, is taken as the basis for our derivations in this section. As pointed out

in Section A.1, such a combined approach will be referred to in the text by using the acronym DPA/DDM. The so-called material derivative approach (MDA), combined with the DDM, will be developed in the context of the present UL formulation and compared with the DPA later in Section A.3. In fact, both the DPA and the MDA can also be used in conjunction with the adjoint system method (ASM), resulting in what may be called the DPA/ASM and the MDA/ASM techniques, respectively. However, as it is well known (cf. e.g. [70], Chapter 4), the DDM is superior over the ASM in dealing with the history-dependent problems addressed in this chapter, so we shall basically confine ourselves to the DDM-based techniques only.

We shall now derive all the expressions needed to compute the sensitivity of the constraint functional, Eq. (A.72). In the framework of the DDM we shall need for this purpose the design variation of the incremental virtual work equation (A.65). To compute this, we must, in turn, know the design variation of each of the terms involved.

Let us start by observing that the displacement increment depends on design only implicitly, i.e.

$$\bar{\delta}\Delta\mathbf{u} = \bar{\delta}\Delta\mathbf{u} \tag{A.77}$$

The virtual variation of $\Delta\mathbf{u}$ is assumed to depend on design explicitly

$$\bar{\delta}(\delta\Delta\mathbf{u}) = \partial(\delta\Delta\mathbf{u}) \tag{A.78}$$

As we shall soon see, assumption (A.78) has no practical consequences and could be replaced by the more stringent condition

$$\bar{\delta}(\delta\Delta\mathbf{u}) = 0 \tag{A.79}$$

as it is sometimes assumed.

When it comes to evaluating design variations of the matrix operators $\overline{\mathbf{A}}^{(t)}$, $\overline{\mathbf{A}}^{(r)}$, $\overline{\overline{\mathbf{A}}}^{(t)}$ and $\overline{\overline{\mathbf{A}}}^{(r)}$, the following remark seems in place to re-emphasize the discussion on notation given in the previous section, cf. Eqs. (A.60)–(A.63):

The notation

$$\begin{aligned} \bar{\delta}\overline{\mathbf{A}} &= \left(\bar{\delta}\overline{\mathbf{A}}^{(t)}\right)\overline{\mathbf{A}}^{(r)} + \overline{\mathbf{A}}^{(t)}\left(\partial\overline{\mathbf{A}}^{(r)}\right) \\ \bar{\delta}\overline{\overline{\mathbf{A}}} &= \left(\bar{\delta}\overline{\overline{\mathbf{A}}}^{(t)}\right)\overline{\overline{\mathbf{A}}}^{(r)} + \overline{\overline{\mathbf{A}}}^{(t)}\left(\partial\overline{\overline{\mathbf{A}}}^{(r)}\right) \end{aligned} \tag{A.80}$$

may at first sight appear warranted by: (i) the explicit design dependence of the gradient ${}^{\circ}_{r}\mathbf{F}$, cf. Eq. (A.91) below, contributing to the definitions of $\overline{\mathbf{A}}^{(r)}$ and $\overline{\overline{\mathbf{A}}}^{(r)}$, and (ii) the 'real' deformation gradient ${}^{t}_{\circ}\mathbf{F}$ involved in the definitions of $\overline{\mathbf{A}}^{(t)}$ and $\overline{\overline{\mathbf{A}}}^{(t)}$. However, in accordance with the notation introduced in the previous section, at the current incremental step $[t, t+\Delta t]$, the gradient $\mathrm{d}\,{}^{t}_{\circ}\mathbf{F}/\mathrm{d}\mathbf{h}$ is merely a collection of known numbers and not a quantity dependent on incremental solution sensitivity coefficients. Recalling the discussion about Eq. (A.76), we

can make use of the concept of effective explicit design variation we then used. Thus, in view of the algorithmic properties, the notation

$$\begin{aligned} \bar{\delta}\overline{\mathbf{A}} &= \hat{\partial}\overline{\mathbf{A}} = \left(\hat{\partial}\overline{\mathbf{A}}^{(t)}\right)\overline{\mathbf{A}}^{(r)} + \overline{\mathbf{A}}^{(t)}\left(\partial\overline{\mathbf{A}}^{(r)}\right) \\ \bar{\delta}\overline{\overline{\mathbf{A}}} &= \hat{\partial}\overline{\overline{\mathbf{A}}} = \left(\hat{\partial}\overline{\overline{\mathbf{A}}}^{(t)}\right)\overline{\overline{\mathbf{A}}}^{(r)} + \overline{\overline{\mathbf{A}}}^{(t)}\left(\partial\overline{\overline{\mathbf{A}}}^{(r)}\right) \end{aligned} \tag{A.81}$$

turns out to be more appropriate at the time step considered. Consequently, the design variations of incremental strains become

$$\begin{aligned} \bar{\delta}\overline{\Delta\boldsymbol{\varepsilon}} &= \left(\hat{\partial}\overline{\mathbf{A}}\right)\Delta\mathbf{u} + \overline{\mathbf{A}}\bar{\delta}\Delta\mathbf{u} \\ \bar{\delta}\overline{\overline{\Delta\boldsymbol{\varepsilon}}} &= \left(\hat{\partial}\overline{\overline{\mathbf{A}}}\right)(\Delta\mathbf{u},\Delta\mathbf{u}) + 2\overline{\overline{\mathbf{A}}}(\bar{\delta}\Delta\mathbf{u},\Delta\mathbf{u}) \end{aligned} \tag{A.82}$$

and

$$\begin{aligned} \bar{\delta}\delta\overline{\Delta\boldsymbol{\varepsilon}} &= \left(\hat{\partial}\overline{\mathbf{A}}\right)\delta\Delta\mathbf{u} + \overline{\mathbf{A}}\partial\delta\Delta\mathbf{u} \\ \bar{\delta}\delta\overline{\overline{\Delta\boldsymbol{\varepsilon}}} &= 2\left[\left(\hat{\partial}\overline{\overline{\mathbf{A}}}\right)(\delta\Delta\mathbf{u},\Delta\mathbf{u}) + \overline{\overline{\mathbf{A}}}(\bar{\delta}\Delta\mathbf{u},\delta\Delta\mathbf{u})\right] \end{aligned} \tag{A.83}$$

in which $\partial\overline{\mathbf{A}}$ and $\partial\overline{\overline{\mathbf{A}}}$ are given by Eqs. (A.81).

For purely didactic reasons, let us consider first the sensitivity formulation for the problem in which the constitutive law is assumed to have been integrated explicitly. We may then write

$$\begin{aligned} \bar{\delta}\,{}^{t}\tilde{\mathbf{C}}(\boldsymbol{\sigma}(\mathbf{h}),\mathbf{p}(\mathbf{h});\mathbf{h}) &= \bar{\delta}\tilde{\mathbf{C}}({}^{t}\boldsymbol{\sigma}(\mathbf{h}),{}^{t}\mathbf{p}(\mathbf{h});\mathbf{h}) \\ &= \left(\frac{\partial\,{}^{t}\tilde{\mathbf{C}}}{\partial\boldsymbol{\sigma}}\frac{\mathrm{d}\,{}^{t}\boldsymbol{\sigma}}{\mathrm{d}\mathbf{h}} + \frac{\partial\,{}^{t}\tilde{\mathbf{C}}}{\partial\mathbf{p}}\frac{\mathrm{d}\,{}^{t}\mathbf{p}}{\mathrm{d}\mathbf{h}} + \frac{\partial\,{}^{t}\tilde{\mathbf{C}}}{\partial\mathbf{h}}\right)\delta\mathbf{h} = \hat{\partial}\,{}^{t}\tilde{\mathbf{C}} \end{aligned} \tag{A.84}$$

Using the above relationships, the design variation of particular terms in Eq. (A.70) gives successively:

$$\begin{aligned} \bar{\delta}({}^{t}\tilde{\mathbf{C}}\cdot\overline{\Delta\boldsymbol{\varepsilon}}\cdot\delta\overline{\Delta\boldsymbol{\varepsilon}}) = {}&\hat{\partial}\,{}^{t}\tilde{\mathbf{C}}\cdot(\overline{\mathbf{A}}\Delta\mathbf{u})\cdot(\overline{\mathbf{A}}\delta\Delta\mathbf{u}) \\ &+ {}^{t}\tilde{\mathbf{C}}\cdot\left[(\hat{\partial}\overline{\mathbf{A}})\Delta\mathbf{u} + \overline{\mathbf{A}}\bar{\delta}\Delta\mathbf{u}\right]\cdot(\overline{\mathbf{A}}\delta\Delta\mathbf{u}) \\ &+ {}^{t}\tilde{\mathbf{C}}\cdot(\overline{\mathbf{A}}\Delta\mathbf{u})\cdot(\hat{\partial}\overline{\mathbf{A}}\delta\Delta\mathbf{u} + \overline{\mathbf{A}}\partial\delta\Delta\mathbf{u}) \end{aligned} \tag{A.85}$$

$$\begin{aligned} \bar{\delta}({}^{t}\boldsymbol{\sigma}\cdot\delta\overline{\overline{\Delta\boldsymbol{\varepsilon}}}) = {}&2\left[\hat{\partial}\,{}^{t}\boldsymbol{\sigma}\cdot\overline{\overline{\mathbf{A}}}(\delta\Delta\mathbf{u},\Delta\mathbf{u}) + {}^{t}\boldsymbol{\sigma}\cdot(\hat{\partial}\overline{\overline{\mathbf{A}}})(\delta\Delta\mathbf{u},\Delta\mathbf{u})\right. \\ &\left.+ {}^{t}\boldsymbol{\sigma}\cdot\overline{\overline{\mathbf{A}}}(\delta\Delta\mathbf{u},\bar{\delta}\Delta\mathbf{u}) + {}^{t}\boldsymbol{\sigma}\cdot\overline{\overline{\mathbf{A}}}(\partial\delta\Delta\mathbf{u},\Delta\mathbf{u})\right] \end{aligned} \tag{A.86}$$

$$\begin{aligned} \bar{\delta}({}^{t+\Delta t}\hat{\mathbf{f}}\delta\Delta\mathbf{u}) &= (\partial^{t+\Delta t}\hat{\mathbf{f}})\delta\Delta\mathbf{u} + {}^{t+\Delta t}\hat{\mathbf{f}}\partial\delta\Delta\mathbf{u} \\ \bar{\delta}({}^{t+\Delta t}\hat{\mathbf{t}}\delta\Delta\mathbf{u}) &= (\partial^{t+\Delta t}\hat{\mathbf{t}})\delta\Delta\mathbf{u} + {}^{t+\Delta t}\hat{\mathbf{t}}\partial\delta\Delta\mathbf{u} \end{aligned} \tag{A.87}$$

$$\begin{aligned} \hat{\partial}({}^{t}\boldsymbol{\sigma}\cdot\delta\overline{\Delta\boldsymbol{\varepsilon}}) &= \hat{\partial}\,{}^{t}\boldsymbol{\sigma}\cdot\overline{\mathbf{A}}\delta\Delta\mathbf{u} + {}^{t}\boldsymbol{\sigma}(\hat{\partial}\overline{\mathbf{A}}\delta\Delta\mathbf{u} + \overline{\mathbf{A}}\partial\delta\Delta\mathbf{u}) \\ \hat{\partial}({}^{t}\tilde{\mathbf{H}}\cdot\delta\overline{\Delta\boldsymbol{\varepsilon}}) &= \hat{\partial}\,{}^{t}\tilde{\mathbf{H}}\cdot\overline{\mathbf{A}}\delta\Delta\mathbf{u} + {}^{t}\tilde{\mathbf{H}}(\hat{\partial}\overline{\mathbf{A}}\delta\Delta\mathbf{u} + \overline{\mathbf{A}}\partial\delta\Delta\mathbf{u}) \end{aligned} \tag{A.88}$$

$$
\begin{aligned}
\hat{\partial}\,{}^{t}_{r}J &= \partial \det\left[{}^{t}_{r}\mathbf{F}\right] = \frac{\partial \det[{}^{t}_{r}\mathbf{F}]}{\partial\,{}^{t}_{r}F_{kl}}\hat{\partial}\,{}^{t}_{r}F_{kl} \\
&= \det\left[{}^{t}_{r}\mathbf{F}\right]\,{}^{r}_{t}F_{lk}\hat{\partial}\,{}^{t}_{r}F_{kl} = {}^{t}_{r}J\,{}^{r}_{t}F_{lk}\,\hat{\partial}\,{}^{t}_{r}F_{kl} \\
\hat{\partial}\,{}^{t}_{r}J_{\partial} &= \hat{\partial}\left({}^{t}_{r}J\,\|\,{}^{r}_{t}F_{kl}n^{r}_{k}\|\right) = (\hat{\partial}\,{}^{t}_{r}J)\|\,{}^{r}_{t}F_{kl}n^{r}_{k}\| + {}^{t}_{r}J\frac{\|\,{}^{r}_{t}F_{mj}n^{r}_{m}\|}{\partial\,{}^{r}_{t}F_{kl}}\hat{\partial}\,{}^{r}_{t}F_{kl} \qquad \text{(A.89)} \\
&= (\hat{\partial}\,{}^{t}_{r}J)\|\,{}^{r}_{t}F_{kl}n^{r}_{k}\| + {}^{t}_{r}J\frac{n^{k}_{r}\,{}^{r}_{t}F_{ml}n^{r}_{m}}{\|\,{}^{r}_{t}F_{sq}n^{r}_{s}\|}\hat{\partial}\,{}^{r}_{t}F_{kl} \\
&\qquad\qquad \text{(no sum on } r \text{ and } t\text{)}
\end{aligned}
$$

The only 'unknown' terms in all the above relationships are those involving the incremental displacement sensitivity $\bar{\delta}\Delta\mathbf{u}$. With regard to Eq. (A.84) (and, similarly, Eq. (A.88)) we note again that the total design variation of the constitutive moduli tensor $\bar{\mathbf{C}}$ (and $\bar{\mathbf{H}}$), taken at time instant t, is fully explicit at the step $[t, t+\Delta t]$, since the sensitivity coefficients $\mathrm{d}\,{}^{t}\boldsymbol{\sigma}/\mathrm{d}\mathbf{h}$ and $\mathrm{d}\,{}^{t}p/\mathrm{d}\mathbf{h}$ are treated as known arrays of numbers and not as the sensitivity gradients yet to be computed. A different situation will result if an implicit constitutive law time integration is used, the constitutive moduli tensor being then effectively defined at time instant $t+\Delta t$, see the discussion later in this section.

With all the above relationships to hand we may now design-differentiate the virtual work equation (A.70). By doing so and moving over to the right-hand side all the known terms we obtain

$$
\begin{aligned}
&\int_{\Omega^r}\left({}^{t}\bar{\mathbf{C}}\cdot(\bar{\mathbf{A}}\bar{\delta}\Delta\mathbf{u})\cdot(\bar{\mathbf{A}}\delta\Delta\mathbf{u}) + 2\,{}^{t}\boldsymbol{\sigma}\cdot\bar{\bar{\mathbf{A}}}(\delta\Delta\mathbf{u},\bar{\delta}\Delta\mathbf{u})\right){}^{t}_{r}J\,\mathrm{d}\Omega^r \\
&\quad= \int_{\Omega^r}\left[(\partial^{t+\Delta t}\hat{\mathbf{f}}\delta\Delta\mathbf{u} + {}^{t+\Delta t}\hat{\mathbf{f}}(\partial\delta\Delta\mathbf{u}))\,{}^{t}_{r}J + {}^{t+\Delta t}\hat{\mathbf{f}}\delta\Delta\mathbf{u}\,\hat{\partial}\,{}^{t}_{r}J\right]\mathrm{d}\Omega^r \\
&\qquad+ \int_{\partial\Omega^r_{\sigma}}\left[(\partial^{t+\Delta t}\hat{\mathbf{t}}\delta\Delta\mathbf{u} + {}^{t+\Delta t}\hat{\mathbf{t}}(\partial\delta\Delta\mathbf{u}))\,{}^{t}_{r}J_{\partial} + {}^{t+\Delta t}\hat{\mathbf{t}}\delta\Delta\mathbf{u}\,\hat{\partial}\,{}^{t}_{r}J\right]\mathrm{d}(\partial\Omega^r) \\
&\qquad- \int_{\Omega^r}\Big\{\Big[\hat{\partial}({}^{t}\boldsymbol{\sigma} + {}^{t}\bar{\mathbf{H}})\cdot(\bar{\mathbf{A}}\delta\Delta\mathbf{u}) + ({}^{t}\boldsymbol{\sigma} + {}^{t}\bar{\mathbf{H}})\cdot(\hat{\partial}\bar{\mathbf{A}}\delta\Delta\mathbf{u}) \\
&\qquad\qquad + ({}^{t}\boldsymbol{\sigma} + {}^{t}\bar{\mathbf{H}})\cdot\bar{\mathbf{A}}\,\partial\delta\Delta\mathbf{u}\Big]\,{}^{t}_{r}J + ({}^{t}\boldsymbol{\sigma} + {}^{t}\bar{\mathbf{H}})\cdot(\bar{\mathbf{A}}\delta\Delta\mathbf{u})\hat{\partial}\,{}^{t}_{r}J\Big\}\,\mathrm{d}\Omega^r \\
&\qquad- \int_{\Omega^r}\Big\{\Big[\hat{\partial}\,{}^{t}\bar{\mathbf{C}}\cdot(\bar{\mathbf{A}}\Delta\mathbf{u})\cdot(\bar{\mathbf{A}}\delta\Delta\mathbf{u}) + {}^{t}\bar{\mathbf{C}}\cdot(\hat{\partial}\bar{\mathbf{A}}\Delta\mathbf{u})\cdot(\bar{\mathbf{A}}\delta\Delta\mathbf{u}) \\
&\qquad\qquad + {}^{t}\bar{\mathbf{C}}\cdot(\bar{\mathbf{A}}\Delta\mathbf{u})\cdot(\hat{\partial}\bar{\mathbf{A}}\delta\Delta\mathbf{u}) + {}^{t}\bar{\mathbf{C}}\cdot(\bar{\mathbf{A}}\Delta\mathbf{u})\cdot(\bar{\mathbf{A}}\partial(\delta\Delta\mathbf{u}))\Big]\,{}^{t}_{r}J \\
&\qquad\qquad + {}^{t}\bar{\mathbf{C}}\cdot(\bar{\mathbf{A}}\Delta\mathbf{u})\cdot(\bar{\mathbf{A}}\delta\Delta\mathbf{u})\hat{\partial}\,{}^{t}_{r}J\Big\}\,\mathrm{d}\Omega^r \\
&\qquad- 2\int_{\partial\Omega^r_{\sigma}}\Big\{\Big[\hat{\partial}\,{}^{t}\boldsymbol{\sigma}\cdot\bar{\bar{\mathbf{A}}}(\delta\Delta\mathbf{u},\Delta\mathbf{u}) + {}^{t}\boldsymbol{\sigma}\cdot\hat{\partial}\bar{\bar{\mathbf{A}}}(\delta\Delta\mathbf{u},\Delta\mathbf{u}) + {}^{t}\boldsymbol{\sigma}\,\bar{\bar{\mathbf{A}}}(\partial(\delta\Delta\mathbf{u}),\Delta\mathbf{u})\Big]\,{}^{t}_{r}J \\
&\qquad\qquad + {}^{t}\boldsymbol{\sigma}\cdot\bar{\bar{\mathbf{A}}}(\delta\Delta\mathbf{u},\Delta\mathbf{u})\hat{\partial}\,{}^{t}_{r}J\Big\}\,\mathrm{d}(\partial\Omega^r), \qquad \text{for any k.a. } \delta\Delta\mathbf{u} \qquad \text{(A.90)}
\end{aligned}
$$

In the above variational formulation, the value of $\bar{\delta}\Delta\mathbf{u}$ is the only unknown, while the terms involving $\partial(\delta\Delta\mathbf{u})$ represent the equilibrium condition and can therefore be suppressed.[1] The remaining quantities can be expressed in terms of

[1] Which justifies our earlier comments that the assumption of $\delta\Delta\mathbf{u}$ as independent of h is not restrictive at all.

explicit design variations and function values known from the previous step of the analysis. In other words, apart from an arbitrary variation $\delta\Delta\mathbf{u}$, the right-hand side of Eq. (A.90) may be treated as known, while the left-hand side coincides with that appearing in the virtual work equation (A.65) except for $\Delta\mathbf{u}$ now replaced by $\bar{\delta}\Delta\mathbf{u}$. For arbitrary kinematically admissible variations $\delta\Delta\mathbf{u}$, Eq. (A.90) can thus be solved for $\bar{\delta}\Delta\mathbf{u}$ or, effectively, for the sensitivity coefficients $\partial\Delta u_i/\partial h_d$ sought.

To complete the derivations of this section, we need only to find an effective way of computing design variations of all the mappings between the reference, initial and current configurations, respectively. They are clearly needed to determine the (explicit) design variations of the matrix operators $\overline{\mathbf{A}}^{(t)}$, $\overline{\mathbf{A}}^{(r)}$, $\overline{\overline{\mathbf{A}}}^{(t)}$ and $\overline{\overline{\mathbf{A}}}^{(r)}$ required in Eq. (A.81).

The easiest part is to compute the sensitivity of the gradient ${}^{0}_{r}\mathbf{F} = \partial {}^{0}\mathbf{x}/\partial {}^{r}\mathbf{x}$. For we simply have

$$\bar{\delta}\,{}^{0}_{r}\mathbf{F} = \partial\,{}^{0}_{r}\mathbf{F} = \frac{\partial {}^{0}\mathbf{x}({}^{r}\mathbf{x}, \mathbf{h})}{\partial \mathbf{h}}\delta\mathbf{h}, \qquad \bar{\delta}\,{}^{0}_{r}\mathbf{F} = 0 \tag{A.91}$$

since the mapping ${}^{0}\mathbf{x}({}^{r}\mathbf{x}, \mathbf{h})$ is explicitly given in terms of its arguments, cf. Eq. (A.51). Equation (A.91) allows us to determine the matrix operators $\overline{\mathbf{A}}^{(r)}$ and $\overline{\overline{\mathbf{A}}}^{(r)}$ by using their definitions given in Eqs. (A.60) and (A.61).

Let us now find the design variations of the 'real' deformation gradient ${}^{t}_{0}\mathbf{F}$ (or, for convenience of notation, the 'next' value of it, ${}^{t+\Delta t}_{0}\mathbf{F}$, which algorithmically amounts to the same, bearing in mind the repetitive nature of the approach). The value of this variation is needed to determine by Eqs. (A.60) and (A.61) the terms in Eq. (A.90) containing the matrices $\partial\overline{\mathbf{A}}^{(t)}$ and $\partial\overline{\overline{\mathbf{A}}}^{(t)}$. In accordance with the basic methodology of the incremental analysis, we assume that the 'incremental' gradient, cf. Eq. (A.22),

$${}^{t+\Delta t}_{t}F_{ij} = \frac{\partial\,{}^{t+\Delta t}x_i}{\partial\,{}^{t}x_j} = \delta_{ij} + \Delta u_{i,j} \tag{A.92}$$

and the first corresponding sensitivity coefficients

$$\bar{\delta}\,{}^{t+\Delta t}_{t}F_{ij} = \bar{\delta}\Delta u_{i,j} \tag{A.93}$$

have been determined as a result of the current step equilibrium and sensitivity calculations, while the values of ${}^{t}_{0}\mathbf{F}$ and $\hat{\partial}\,{}^{t}_{0}\mathbf{F}$ can be recovered from computer memory; the value of $\bar{\delta}\,{}^{t+\Delta t}_{0}\mathbf{F}$ needed to set up the equations for the next step is sought. We have

$$\begin{aligned}\bar{\delta}\,{}^{t+\Delta t}_{0}\mathbf{F} &= \bar{\delta}\left(\frac{\partial\,{}^{t+\Delta t}x}{\partial\,{}^{0}x}\right) = \bar{\delta}\left(\frac{\partial\,{}^{t+\Delta t}x}{\partial\,{}^{t}x}\frac{\partial\,{}^{t}x}{\partial\,{}^{0}x}\right)\\ &= \bar{\delta}\left({}^{t+\Delta t}_{t}\mathbf{F}\,{}^{t}_{0}\mathbf{F}\right) = \left(\bar{\delta}\,{}^{t+\Delta t}_{t}\mathbf{F}\right){}^{t}_{0}\mathbf{F} + {}^{t+\Delta t}_{t}\mathbf{F}\hat{\partial}\,{}^{t}_{0}\mathbf{F}\end{aligned} \tag{A.94}$$

which completes the derivation since it allows us by means of Eq. (A.94) to express the value of $\bar{\delta}\,{}_{0}\mathbf{F}$ at $t + \Delta t$ in terms of its previous value at t. We note

that since the variables ${}^{\tau}x_k$ (as opposed to ${}^{t}x_k$) are used as independent variables in the formulation, it is $\bar{\delta}\Delta u_{i,j}$, rather than $\bar{\delta}\Delta u_{i,j}$, which is solved for (according to the notation introduced in Eq. (A.57))—the equation [70]

$$\begin{aligned}\bar{\delta}(\Delta u_{i,j}) &= \bar{\delta}\left(\Delta u_{i;k}\,{}^{t}_{\tau}F^{-1}_{kj}\right)\\ &= \bar{\delta}\Delta u_{i;k}\,{}^{t}_{\tau}F^{-1}_{kj} - \Delta u_{i;k}\,{}^{t}_{\tau}F^{-1}_{kl}\bar{\delta}\,{}^{t}x_{l;m}\,{}^{t}_{\tau}F^{-1}_{mj}\\ &= \left(\bar{\delta}\Delta u_i\right)_{,j} - \Delta u_{i,k}\left(\bar{\delta}\,{}^{t}x_k\right)_{,j}\end{aligned} \tag{A.95}$$

has then to be employed to get the latter value as required by Eq. (A.93).

The values of $\partial\,{}^{t}_{\tau}J$ and $\partial\,{}^{t}_{\tau}J_{\vartheta}$ can be obtained using Eqs. (A.89).

Finally, let us consider the explicitly integrated constitutive equation (A.33) in the form

$$\Delta\tilde{\boldsymbol{\sigma}} = \tilde{\mathbf{C}}({}^{t}\boldsymbol{\sigma}(\mathbf{h}), {}^{t}\mathbf{p}(\mathbf{h}); \mathbf{h})\overline{\Delta\boldsymbol{\varepsilon}}(\mathbf{h}) + {}^{t}\tilde{\mathbf{H}}({}^{t}\boldsymbol{\sigma}(\mathbf{h}), {}^{t}\mathbf{p}(\mathbf{h}); \mathbf{h}) \tag{A.96}$$

Taking the design variation of the above equation gives

$$\bar{\delta}\Delta\tilde{\boldsymbol{\sigma}} = \underbrace{\left(\hat{\partial}\,{}^{t}\tilde{\mathbf{C}}\cdot\overline{\mathbf{A}} + {}^{t}\tilde{\mathbf{C}}\cdot\hat{\partial}\overline{\mathbf{A}}\right)\Delta\mathbf{u} + \hat{\partial}\,{}^{t}\tilde{\mathbf{H}}}_{\hat{\partial}\Delta\tilde{\boldsymbol{\sigma}}} + \underbrace{{}^{t}\tilde{\mathbf{C}}\overline{\mathbf{A}}\bar{\delta}\Delta\mathbf{u}}_{\bar{\delta}\Delta\tilde{\boldsymbol{\sigma}}} \tag{A.97}$$

which serves the purpose of finding $\bar{\delta}\Delta\tilde{\boldsymbol{\sigma}}$ once $\bar{\delta}\Delta\mathbf{u}$ has been solved for from the incremental sensitivity problem. The evolution equation for the internal variables can be employed in the same fashion to determine $\bar{\delta}\Delta\mathbf{p}$, cf. Eqs. (A.8)–(A.12). Both $\bar{\delta}\Delta\tilde{\boldsymbol{\sigma}}$ and $\bar{\delta}\Delta\mathbf{p}$ are then used to update the corresponding total values of sensitivity according to

$$\begin{aligned}\bar{\delta}\,{}^{t+\Delta t}\boldsymbol{\sigma} &= \hat{\partial}\,{}^{t}\boldsymbol{\sigma} + \bar{\delta}\Delta\tilde{\boldsymbol{\sigma}}\\ \bar{\delta}\,{}^{t+\Delta t}\mathbf{p} &= \hat{\partial}\,{}^{t}\mathbf{p} + \bar{\delta}\Delta\mathbf{p}\end{aligned} \tag{A.98}$$

To simplify the discussion, which by the very nature of the shape sensitivity problem is anyhow quite elaborate, we have so far based the considerations on the assumption that the explicit scheme was used to integrate the constitutive relationship while solving the incremental equilibrium problem. Because of this assumption, the problem was effectively linearized at the step considered, with the constitutive tensors evaluated at time t.

To obtain a more general formulation covering the use of more sophisticated, implicit time integration algorithms, we shall now use the weak form of the incremental equilibrium in the form of Eq. (A.69), in which the possible lack of equilibrium at the end of the previous step is accounted for by including on the right-hand side the appropriate residual, cf. Eq. (A.32).

We note that the incremental stress $\Delta\tilde{\sigma}_{ij}$ is assumed now to be computable from the finitely incremental constitutive equation (A.9) written in a more operator form as Eq. (A.11). It is easy to check that by assuming in Eq. (A.69) the constitutive law in the explicitly integrated form Eq. (A.33) we arrive at Eq. (A.70) considered above.

In accordance with the basic philosophy of the DDM we now perform the design variation on Eq. (A.70) and, after re-grouping terms, moving over to the right-hand side those that are known and suppressing the coefficients at $\partial(\delta\Delta\mathbf{u})$ representing the equilibrium condition, we obtain the following basic relationships written using the operator notation

$$\int_{\Omega^r} \Big[\overbrace{\hat{\mathbf{C}}\cdot(\bar{\mathbf{A}}\bar{\delta}\Delta\mathbf{u})}^{\bar{\delta}\Delta\bar{\boldsymbol{\sigma}}}\cdot(\bar{\mathbf{A}}\delta\Delta\mathbf{u}) + 2\,{}^t\boldsymbol{\sigma}\cdot\bar{\bar{\mathbf{A}}}(\bar{\delta}\Delta\mathbf{u},\delta\Delta\mathbf{u})\Big]\,{}^t_rJ\,\mathrm{d}\Omega^r$$
$$= \bar{\delta}\,{}^{t+\Delta t}\mathbf{R}\Big|_{\Delta\mathbf{u}\neq\Delta\mathbf{u}(\mathbf{h})}\circ\delta\Delta\mathbf{u}, \qquad \text{for any k.a. } \delta\Delta\mathbf{u} \tag{A.99}$$

Here the right-hand side stands for the following expression:

$$\bar{\delta}\,{}^{t+\Delta t}\mathbf{R}\Big|_{\Delta\mathbf{u}\neq\Delta\mathbf{u}(\mathbf{h})}\circ\delta\Delta\mathbf{u} = \hat{\partial}\,{}^{t+\Delta t}\mathbf{R}\circ\delta\Delta\mathbf{u} = \hat{\partial}\Big({}^{t+\Delta t}\mathbf{Q} - {}^{t+\Delta t}\mathbf{F}\Big)\circ\delta\Delta\mathbf{u} \tag{A.100}$$

in which

$$\partial\,{}^{t+\Delta t}\mathbf{Q}\circ\delta\Delta\mathbf{u} = \int_{\Omega^r}\partial\Big({}^{t+\Delta t}_r\hat{\mathbf{f}}\,{}^t_rJ\Big)\delta\Delta\mathbf{u}\,\mathrm{d}\Omega^r + \int_{\partial\Omega^r_\sigma}\partial\Big({}^{t+\Delta t}_r\hat{\mathbf{t}}\,{}^t_rJ_\partial\Big)\delta\Delta\mathbf{u}\,\mathrm{d}(\partial\Omega^r) \tag{A.101}$$

$$\begin{aligned}
\hat{\partial}\,{}^{t+\Delta t}\mathbf{F}\circ\delta\Delta\mathbf{u} &= \hat{\partial}\Big({}^t\mathbf{F}+\Delta\mathbf{F}\Big)\circ\delta\Delta\mathbf{u}\\
&= \int_{\Omega^r}\hat{\partial}\Big({}^t\boldsymbol{\sigma}\cdot\bar{\mathbf{A}}\,{}^t_rJ\Big)\delta\Delta\mathbf{u}\,\mathrm{d}\Omega^r\\
&\quad+\int_{\Omega^r}\Big[\Delta\tilde{\boldsymbol{\sigma}}\cdot\Big(\hat{\partial}\bar{\mathbf{A}}\delta\Delta\mathbf{u}\Big)+\partial\Delta\tilde{\boldsymbol{\sigma}}\cdot\Big(\bar{\mathbf{A}}\delta\Delta\mathbf{u}\Big)\Big]\,{}^t_rJ\,\mathrm{d}\Omega^r\\
&\quad+\int_{\Omega^r}\Delta\tilde{\boldsymbol{\sigma}}\cdot\bar{\mathbf{A}}\delta\Delta\mathbf{u}\hat{\partial}\,{}^t_rJ\,\mathrm{d}\Omega^r\\
&\quad+2\int_{\Omega^r}\Big\{\Big[\hat{\partial}\,{}^t\boldsymbol{\sigma}\cdot\bar{\bar{\mathbf{A}}}(\Delta\mathbf{u},\delta\Delta\mathbf{u})+{}^t\boldsymbol{\sigma}\cdot\hat{\partial}\bar{\bar{\mathbf{A}}}(\Delta\mathbf{u},\delta\Delta\mathbf{u})\Big]\,{}^t_rJ\\
&\quad+{}^t\boldsymbol{\sigma}\cdot\bar{\bar{\mathbf{A}}}(\Delta\mathbf{u},\delta\Delta\mathbf{u})\hat{\partial}\,{}^t_rJ\Big\}\,\mathrm{d}\Omega^r
\end{aligned} \tag{A.102}$$

The design variation of the constitutive equation, cf. Eqs. (A.8)–(A.12)

$$\Delta\tilde{\boldsymbol{\sigma}} = \Delta\tilde{\boldsymbol{\sigma}}\,({}^t\boldsymbol{\sigma},\,{}^t\mathbf{p},\mathbf{h};\overline{\Delta\boldsymbol{\varepsilon}}) \tag{A.103}$$

has been employed here to read

$$\bar{\delta}\Delta\tilde{\boldsymbol{\sigma}} = \underbrace{\frac{\partial\Delta\tilde{\boldsymbol{\sigma}}}{\partial\boldsymbol{\sigma}}\frac{\mathrm{d}\,{}^t\boldsymbol{\sigma}}{\mathrm{d}\mathbf{h}}+\frac{\partial\Delta\tilde{\boldsymbol{\sigma}}}{\partial\mathbf{p}}\frac{\mathrm{d}\,{}^t\mathbf{p}}{\mathrm{d}\mathbf{h}}+\frac{\partial\Delta\tilde{\boldsymbol{\sigma}}}{\partial\mathbf{h}}+\underbrace{\frac{\partial\Delta\tilde{\boldsymbol{\sigma}}}{\partial\overline{\Delta\boldsymbol{\varepsilon}}}}_{\hat{\mathbf{C}}}\partial\bar{\mathbf{A}}\Delta\mathbf{u}}_{\hat{\partial}\Delta\tilde{\boldsymbol{\sigma}}}+\underbrace{\underbrace{\frac{\partial\Delta\tilde{\boldsymbol{\sigma}}}{\partial\overline{\Delta\boldsymbol{\varepsilon}}}}_{\hat{\mathbf{C}}}\bar{\mathbf{A}}\bar{\delta}\Delta\mathbf{u}}_{\bar{\delta}\Delta\tilde{\boldsymbol{\sigma}}} \tag{A.104}$$

The complete correspondence of Eqs. (A.99) and the equation for the equilibrium problem can easily be observed. It goes without saying that Eq. (A.99) becomes identical to Eq. (A.90) if the constitutive law is integrated explicitly.

The right-hand-side vector $\hat{\partial}\,{}^{t+\Delta t}\mathbf{R}$ can easily be computed as it involves only the incremental solution vector $\Delta\mathbf{u}$ and the sensitivity coefficients defined at time instant t—all these are known at this stage by definition. Another crucial observation is that the left-hand side of Eq. (A.99) is precisely the same as that appearing in the virtual incremental work equation (A.69) specified to compute the last iterative correction to the solution $\Delta\mathbf{u}$ at the given step [70].

The spatial discretization of the sensitivity problem follows the standard route. It is important to recognize that the sensitivity problem discretization is entirely independent of the discretization employed for the equilibrium problem and can thus be entirely different in terms of the mesh, finite elements used, etc. The fundamental sensitivity equation (A.99) reads in the discretized form,

$$\hat{\mathbf{K}}^{(T)}_{N\times N}\tilde{\delta}\Delta\mathbf{q}_{N\times 1} = \hat{\partial}\left({}^{t+\Delta t}\mathbf{Q}_{N\times 1} - {}^{t+\Delta t}\mathbf{F}_{N\times 1}\right) \tag{A.105}$$

where

$$\hat{\mathbf{K}}^{(T)}_{N\times N} = \int_{\Omega^r}\left(\overline{\mathbf{B}}^{\mathrm{T}}\hat{\mathbf{C}}\,\overline{\mathbf{B}} + 2\,{}^{t}\boldsymbol{\sigma}\cdot\overline{\overline{\mathbf{B}}}\right){}^{t}_{r}J\;\mathrm{d}\Omega^r \tag{A.106}$$

while the right-hand-side vector results directly from the discretization of Eqs. (A.101) and (A.102), since, using Eq. (A.4),

$$\begin{aligned}
\overline{\Delta\varepsilon}_{ij} &= \overline{A}_{ijl}\,\Delta u_l(x_k) = \underbrace{\overline{A}_{ijl}\phi_{l\alpha}(x_k)}_{\overline{B}_{ij\alpha}(x_k)}\Delta q_\alpha \\
\overline{\overline{\Delta\varepsilon}}_{ij} &= \overline{\overline{A}}_{ij}(\Delta u_l(x_k), \Delta u_l(x_k)) = \underbrace{\overline{\overline{A}}_{ij}(\phi_{k\alpha}(x_k), \phi_{k\beta}(x_k))}_{\overline{\overline{B}}_{ij\alpha\beta}(x_k)}\Delta q_\alpha \Delta q_\beta
\end{aligned} \tag{A.107}$$

A.3 The material derivative approach

Having derived in the previous section the equations for shape sensitivity analysis within the DPA/DDM methodology, we will consider now the same problem in the context of the material derivative approach, MDA/DDM. Again, we consider the functional (A.1) and seek for its derivative with respect to the design variables grouped into the array $\mathbf{h} = \{h_d\}$, $d = 1, 2, \ldots, D$. Now, instead of conceiving design variations as different mappings from a reference, design-independent configuration to the actual configuration, as we did in DPA, here we evaluate the effect of design variations on the design functional (and hence on all the problem quantities it involves) in the actual configuration.

Within the UL strategy we can formulate the material derivative of $\mathcal{G}$ as

$$\begin{aligned}\frac{\mathrm{d}\mathcal{G}}{\mathrm{d}\mathbf{h}}(\mathbf{h}) &= \Big\{ \int_{\Omega^t} \Big[\Big(\frac{\partial^{t+\Delta t} g}{\partial \boldsymbol{\sigma}} \frac{\mathrm{d}^{t+\Delta t}\boldsymbol{\sigma}}{\mathrm{d}\mathbf{h}} + \frac{\partial^{t+\Delta t} g}{\partial \mathbf{u}} \frac{\mathrm{d}^{t+\Delta t}\mathbf{u}}{\mathrm{d}\mathbf{h}} + \frac{\partial^{t+\Delta t} g}{\partial \mathbf{h}} \Big) \mathrm{d}\Omega^t + {}^{t+\Delta t}g \frac{\mathrm{d}\,\mathrm{d}\Omega^t}{\mathrm{d}\mathbf{h}} \Big] \\ &+ \int_{\partial\Omega_\sigma^t} \Big[\Big(\frac{\partial^{t+\Delta t} g^{(\sigma)}}{\partial \mathbf{u}} \frac{\mathrm{d}^{t+\Delta t}\mathbf{u}}{\mathrm{d}\mathbf{h}} + \frac{\partial^{t+\Delta t} g^{(\sigma)}}{\partial \mathbf{h}} \Big) \mathrm{d}(\partial\Omega^t) + {}^{t+\Delta t}g^{(\sigma)} \frac{\mathrm{d}\,\mathrm{d}(\partial\Omega^t)}{\mathrm{d}\mathbf{h}} \Big] \\ &+ \int_{\partial\Omega_u^t} \Big[\Big(\frac{\partial^{t+\Delta t} g^{(u)}}{\partial \mathbf{t}} \frac{\mathrm{d}^{t+\Delta t}\mathbf{t}}{\mathrm{d}\mathbf{h}} + \frac{\partial^{t+\Delta t} g^{(u)}}{\partial \mathbf{h}} \Big) \mathrm{d}(\partial\Omega^t) + {}^{t+\Delta t}g^{(u)} \frac{\mathrm{d}\,\mathrm{d}(\partial\Omega^t)}{\mathrm{d}\mathbf{h}} \Big] \Big\} \end{aligned} \tag{A.108}$$

Again, the partial derivatives with respect to the design parameters can be routinely calculated from their respective explicit expressions. On the other hand, $\mathrm{d}^{t+\Delta t}\boldsymbol{\sigma}/\mathrm{d}\mathbf{h}$, $\mathrm{d}^{t+\Delta t}\mathbf{t}/\mathrm{d}\mathbf{h}$ and $\mathrm{d}^{t+\Delta t}\mathbf{u}/\mathrm{d}\mathbf{h}$ need prior evaluation of $\mathrm{d}\Delta\mathbf{u}/\mathrm{d}\mathbf{h}$ which, together with the accumulated values at time t, $\mathrm{d}^t\boldsymbol{\sigma}/\mathrm{d}\mathbf{h}$, $\mathrm{d}^t\mathbf{t}/\mathrm{d}\mathbf{h}$, $\mathrm{d}^t\mathbf{u}/\mathrm{d}\mathbf{h}$, and the solution increments $\Delta\tilde{\boldsymbol{\sigma}}$, $\Delta\mathbf{p}$, $\Delta\mathbf{t}$ and $\Delta\mathbf{u}$ allow us to evaluate the incremental sensitivities $\mathrm{d}\Delta\tilde{\boldsymbol{\sigma}}/\mathrm{d}\mathbf{h}$, $\mathrm{d}\Delta\mathbf{p}/\mathrm{d}\mathbf{h}$ and $\mathrm{d}\Delta\mathbf{t}/\mathrm{d}\mathbf{h}$.

In order to differentiate later on the equilibrium equation, as required by the DDM to obtain the sensitivity coefficients for $\Delta\mathbf{u}$, we must previously calculate the material derivatives of the involved variables. According to the definition, the material derivative of any quantity will result as the sum of a local (fixed to the reference domain) and a convective term

$$\frac{\mathrm{d}a(\mathbf{x})}{\mathrm{d}\mathbf{h}} = \frac{\mathrm{d}_l a(\mathbf{x})}{\mathrm{d}\mathbf{h}} + \frac{\partial a}{\partial \mathbf{x}} \frac{\partial \mathbf{x}}{\partial \mathbf{h}} = \frac{\mathrm{d}_l a(\mathbf{x})}{\mathrm{d}\mathbf{h}} + (\nabla a)^{\mathrm{T}} \mathbf{v}_{\mathrm{h}}(\mathbf{x}) \tag{A.109}$$

where the gradient ∇a is multiplied by the so-called design velocity $\mathbf{v}_{\mathrm{h}}(\mathbf{x}) = \mathrm{d}_l\mathbf{x}/\,\mathrm{d}\mathbf{h}$, which can be considered as the counterpart for this method to the mapping to the reference domain discussed in Section A.2. In fact, although the procedure for its calculation can be largely automatized, it can be said to be a problem dependent question the choice of a specific procedure in each particular case.

The methodology to be used upon deriving the sensitivity expressions within the DPA/DDM formalism consists in obtaining all the quantities that result from the application of the material derivative concept to our cost functional and to the equilibrium equations.

The basic variables are directly differentiated. However, the same definition of material derivative is not applicable to derived quantities since at least some of the terms cannot be evaluated. Instead, the material derivative of such quantities should be expressed in terms of that of the basic variables. In what follows these expressions will be derived, bearing in mind that in some cases we will have explicit functions of the basic variables. In addition, operators containing spatial derivatives may be involved and, finally, we may have also to deal with the material derivative of functionals containing integrals.

For an explicitly defined function $a = a(b, c; \mathbf{h})$ we make use of the chain rule to obtain

$$\frac{\mathrm{d}a}{\mathrm{d}\mathbf{h}} = \frac{\partial a}{\partial b}\frac{\mathrm{d}b}{\mathrm{d}\mathbf{h}} + \frac{\partial a}{\partial c}\frac{\mathrm{d}c}{\mathrm{d}\mathbf{h}} + \left.\frac{\mathrm{d}a}{\mathrm{d}\mathbf{h}}\right|_{b,c \text{ fixed}} \tag{A.110}$$

where the last term can be calculated explicitly.

Since the displacement increments constitute the independent variables at each increment, we can calculate their sensitivity directly as its material derivative with respect to the design variables. It reads

$$\frac{\mathrm{d}\Delta\mathbf{u}}{\mathrm{d}\mathbf{h}} = \frac{\mathrm{d}_t\Delta\mathbf{u}}{\mathrm{d}\mathbf{h}} + \frac{\partial\Delta\mathbf{u}}{\partial {}^t\mathbf{x}}\,{}^t\mathbf{v}_\mathbf{h} \tag{A.111}$$

which corresponds to the quantity $\tilde{\delta}\Delta\mathbf{u}$ as obtained in terms of variations within the DPA. As then, this will be our only unknown we have to solve for in each time step. Returning to the incremental methodology, we can accumulate the sensitivity of the displacement increments to have the sensitivity of the total displacements

$$\frac{\mathrm{d}^{t+\Delta t}\mathbf{u}}{\mathrm{d}\mathbf{h}} = \frac{\mathrm{d}^t\mathbf{u}}{\mathrm{d}\mathbf{h}} + \frac{\mathrm{d}\Delta\mathbf{u}}{\mathrm{d}\mathbf{h}} \tag{A.112}$$

and from the updated configuration

$${}^{t+\Delta t}\mathbf{x} = {}^t\mathbf{x} + \Delta\mathbf{u} \tag{A.113}$$

we may calculate the updated design velocity as

$${}^{t+\Delta t}\mathbf{v}_\mathbf{h} = \frac{\partial^{t+\Delta t}\mathbf{x}}{\partial\mathbf{h}} = \frac{\partial^t\mathbf{x}}{\partial\mathbf{h}} + \frac{\partial\Delta\mathbf{u}}{\partial\mathbf{h}} = {}^t\mathbf{v}_\mathbf{h} + \frac{\mathrm{d}\Delta\mathbf{u}}{\mathrm{d}\mathbf{h}} \tag{A.114}$$

The material derivative of the strain increment tensor results[1]

$$\frac{\mathrm{d}\overline{\Delta\boldsymbol{\varepsilon}}}{\mathrm{d}\mathbf{h}} = \frac{\mathrm{d}}{\mathrm{d}\mathbf{h}}\left(\frac{1}{2}\left(\frac{\partial\Delta u_i}{\partial x_j} + \frac{\partial\Delta u_j}{\partial x_i}\right)\right) = \frac{1}{2}\frac{\mathrm{d}}{\mathrm{d}\mathbf{h}}(\nabla\Delta\mathbf{u} + (\nabla\Delta\mathbf{u})^T) \tag{A.115}$$

where

$$\begin{aligned}
\frac{\mathrm{d}}{\mathrm{d}\mathbf{h}}(\nabla\Delta\mathbf{u}) &= \frac{\mathrm{d}}{\mathrm{d}\mathbf{h}}\left(\frac{\partial\Delta u_i}{\partial x_j}\right) = \frac{\mathrm{d}_t}{\mathrm{d}\mathbf{h}}\left(\frac{\partial\Delta u_i}{\partial x_j}\right) + \frac{\partial}{\partial x_k}\left(\frac{\partial\Delta u_i}{\partial x_j}\right)v_{hk} \\
&= \frac{\partial}{\partial x_j}\left(\frac{\mathrm{d}_t\Delta u_i}{\mathrm{d}\mathbf{h}}\right) + \frac{\partial}{\partial x_j}\left(\frac{\partial\Delta u_i}{\partial x_k}\right)v_{hk} \\
&= \frac{\partial}{\partial x_j}\left(\frac{\mathrm{d}\Delta u_i}{\mathrm{d}\mathbf{h}} - \frac{\partial\Delta u_i}{\partial x_k}v_{hk}\right) + \frac{\partial}{\partial x_k}\left(\frac{\partial\Delta u_i}{\partial x_j}\right)v_{hk} \\
&= \frac{\partial}{\partial x_j}\left(\frac{\mathrm{d}\Delta u_i}{\mathrm{d}\mathbf{h}}\right) - \frac{\partial\Delta u_i}{\partial x_k}\frac{\partial v_{hk}}{\partial x_j} = \nabla\left(\frac{\mathrm{d}\Delta\mathbf{u}}{\mathrm{d}\mathbf{h}}\right) - (\nabla\Delta\mathbf{u})(\nabla\mathbf{v}_\mathbf{h})
\end{aligned} \tag{A.116}$$

[1] in the following derivations the abbreviated notation $\mathbf{a} = a_{ij}$ has been used

from which, replacing into Eq. (A.115)

$$\begin{aligned}\frac{\mathrm{d}\overline{\Delta\boldsymbol{\varepsilon}}}{\mathrm{d}\mathbf{h}} &= \overline{\Delta\boldsymbol{\varepsilon}}\Big(\frac{\mathrm{d}\Delta\mathbf{u}}{\mathrm{d}\mathbf{h}}\Big) - \frac{1}{2}\Big((\nabla\Delta\mathbf{u}\nabla\mathbf{v}_{\mathrm{h}}) + (\nabla\Delta\mathbf{u}\nabla\mathbf{v}_{\mathrm{h}})^T\Big) \\ &= \overline{\Delta\boldsymbol{\varepsilon}}\Big(\frac{\mathrm{d}\Delta\mathbf{u}}{\mathrm{d}\mathbf{h}}\Big) - \hat{\mathbf{A}}(\Delta\mathbf{u}) \qquad \text{(A.117)} \\ \hat{A}_{ij}(\Delta\mathbf{u}) &= \frac{1}{2}\Big(\frac{\partial\Delta u_i}{\partial x_k}\frac{\partial v_{hk}}{\partial x_j} + \frac{\partial\Delta u_j}{\partial x_k}\frac{\partial v_{hk}}{\partial x_i}\Big)\end{aligned}$$

and for the non-linear increment, recalling the definition of the $\overline{\overline{A}}_{ij}$ operator from Eq. (A.5_2), (keeping in mind that $\overline{\overline{A}}_{ij}(\Delta\mathbf{u},\Delta\mathbf{w}) = \overline{\overline{A}}_{ij}(\Delta\mathbf{w},\Delta\mathbf{u})$)

$$\begin{aligned}\frac{\mathrm{d}\overline{\overline{\Delta\boldsymbol{\varepsilon}}}}{\mathrm{d}\mathbf{h}} &= \frac{\mathrm{d}}{\mathrm{d}\mathbf{h}}\Big(\frac{1}{2}\frac{\partial\Delta u_k}{\partial x_i}\frac{\partial\Delta u_k}{\partial x_j}\Big) \\ &= \frac{1}{2}\Big[\Big(\frac{\partial}{\partial x_i}\Big(\frac{\mathrm{d}\Delta u_k}{\mathrm{d}\mathbf{h}}\Big) - \frac{\partial\Delta u_k}{\partial x_l}\frac{\partial v_{hl}}{\partial x_i}\Big)\frac{\partial\Delta u_k}{\partial x_j} \\ &\quad + \frac{\partial\Delta u_k}{\partial x_i}\Big(\frac{\partial}{\partial x_j}\Big(\frac{\mathrm{d}\Delta u_k}{\mathrm{d}\mathbf{h}}\Big) - \frac{\partial\Delta u_k}{\partial x_l}\frac{\partial v_{hl}}{\partial x_j}\Big)\Big] \\ &= 2\overline{\overline{\mathbf{A}}}\Big(\frac{\mathrm{d}\Delta\mathbf{u}}{\mathrm{d}\mathbf{h}},\Delta\mathbf{u}\Big) - \hat{\hat{\mathbf{A}}}(\Delta\mathbf{u},\Delta\mathbf{u}) \qquad \text{(A.118)}\end{aligned}$$

where we have introduced the operator

$$\begin{aligned}\hat{\hat{\mathbf{A}}}(\Delta\mathbf{u},\Delta\mathbf{u}) &= \frac{1}{2}\Big(\frac{\partial\Delta u_k}{\partial x_l}\frac{\partial v_{hl}}{\partial x_i}\frac{\partial\Delta u_k}{\partial x_j} + \frac{\partial\Delta u_k}{\partial x_i}\frac{\partial\Delta u_k}{\partial x_l}\frac{\partial v_{hl}}{\partial x_j}\Big) \\ &= \frac{1}{2}[(\nabla\Delta\mathbf{u}\nabla\mathbf{v}_{\mathrm{h}})^T\nabla\Delta\mathbf{u} + (\nabla\Delta\mathbf{u})^T(\nabla\Delta\mathbf{u}\nabla\mathbf{v}_{\mathrm{h}})] \qquad \text{(A.119)}\end{aligned}$$

which can be extended for $\hat{\hat{\mathbf{A}}}(\Delta\mathbf{u},\Delta\mathbf{w})$ with $\Delta\mathbf{u} \neq \Delta\mathbf{w}$ by again requiring symmetry with respect to the arguments, as in Eq. (A.5_2)

$$\begin{aligned}\hat{\hat{\mathbf{A}}}(\Delta\mathbf{u},\Delta\mathbf{w}) &= \frac{1}{4}\Big[(\nabla\Delta\mathbf{u}\nabla\mathbf{v}_{\mathrm{h}})^T\nabla\Delta\mathbf{w} + (\nabla\Delta\mathbf{w}\nabla\mathbf{v}_{\mathrm{h}})^T\nabla\Delta\mathbf{u} \\ &\quad + (\nabla\Delta\mathbf{w})^T(\nabla\Delta\mathbf{u}\nabla\mathbf{v}_{\mathrm{h}}) + (\nabla\Delta\mathbf{u})^T(\nabla\Delta\mathbf{w}\nabla\mathbf{v}_{\mathrm{h}})\Big] \\ &= \frac{1}{4}\{\nabla^T\mathbf{v}_{\mathrm{h}}[(\nabla\Delta\mathbf{u})^T\nabla\Delta\mathbf{w} + (\nabla\Delta\mathbf{w})^T\nabla\Delta\mathbf{u}] \\ &\quad + [(\nabla\Delta\mathbf{w})^T\nabla\Delta\mathbf{u} + (\nabla\Delta\mathbf{u})^T\nabla\Delta\mathbf{w}]\nabla\mathbf{v}_{\mathrm{h}}\} \\ &= \nabla^T\mathbf{v}_{\mathrm{h}}\overline{\overline{\mathbf{A}}}^T(\Delta\mathbf{u},\Delta\mathbf{w}) + \overline{\overline{\mathbf{A}}}(\Delta\mathbf{u},\Delta\mathbf{w})\nabla\mathbf{v}_{\mathrm{h}} \qquad \text{(A.120)}\end{aligned}$$

so, replacing in Eq. (A.118) we get

$$\frac{\mathrm{d}\overline{\overline{\Delta\boldsymbol{\varepsilon}}}}{\mathrm{d}\mathbf{h}} = 2\overline{\overline{\mathbf{A}}}\Big(\frac{\mathrm{d}\Delta\mathbf{u}}{\mathrm{d}\mathbf{h}},\Delta\mathbf{u}\Big) - \Big(\nabla^T\mathbf{v}_{\mathrm{h}}\overline{\overline{\mathbf{A}}}^T(\Delta\mathbf{u},\Delta\mathbf{u}) + \overline{\overline{\mathbf{A}}}(\Delta\mathbf{u},\Delta\mathbf{u})\nabla\mathbf{v}_{\mathrm{h}}\Big) \qquad \text{(A.121)}$$

We can similarly develop the above expressions for $\mathrm{d}\overline{\Delta\boldsymbol{\varepsilon}}/\mathrm{d}\mathbf{h}$ and $\mathrm{d}\overline{\overline{\Delta\boldsymbol{\varepsilon}}}/\mathrm{d}\mathbf{h}$ by considering their operator form

$$\overline{\Delta\boldsymbol{\varepsilon}} = \overline{A}_{ijk}\Delta u_k \quad , \quad \overline{A}_{ijk} = \frac{1}{2}\Big(\frac{\partial}{\partial x_i}\delta_{jk} + \frac{\partial}{\partial x_j}\delta_{ik}\Big) \qquad \text{(A.122)}$$

$$\overline{\overline{\Delta\varepsilon}} = \overline{\overline{A}}_{ij}(\Delta u_k, \Delta u_k) \quad , \quad \overline{\overline{A}}_{ij}(a_k, b_l) = \frac{1}{4}\left(\frac{\partial a_k}{\partial x_i}\frac{\partial b_l}{\partial x_j} + \frac{\partial a_k}{\partial x_j}\frac{\partial b_l}{\partial x_i}\right) \tag{A.123}$$

which will be useful for further derivations. We then have, for the linear increment,

$$\frac{\mathrm{d}\overline{\Delta\varepsilon}}{\mathrm{dh}} = \frac{\mathrm{d}\overline{\mathbf{A}}}{\mathrm{dh}}\Delta\mathbf{u} + \overline{\mathbf{A}}\frac{\mathrm{d}\Delta\mathbf{u}}{\mathrm{dh}} \tag{A.124}$$

where

$$\frac{\mathrm{d}\overline{A}_{ijk}}{\mathrm{dh}}\Delta u_k = -\frac{1}{2}\left(\frac{\partial\Delta u_k}{\partial\, {}^t x_l}\frac{\partial\, {}^t v_{\mathrm{h}l}}{\partial\, {}^t x_i}\delta_{jk} + \frac{\partial\Delta u_k}{\partial\, {}^t x_l}\frac{\partial\, {}^t v_{\mathrm{h}l}}{\partial\, {}^t x_j}\delta_{ik}\right) = \widehat{A}_{ij}(\Delta\mathbf{u}) \tag{A.125}$$

and for the nonlinear increment

$$\frac{\mathrm{d}\overline{\overline{\Delta\varepsilon}}}{\mathrm{dh}} = \frac{\mathrm{d}\overline{\overline{\mathbf{A}}}}{\mathrm{dh}}(\Delta\mathbf{u}, \Delta\mathbf{u}) + 2\overline{\overline{\mathbf{A}}}(\frac{\mathrm{d}\Delta\mathbf{u}}{\mathrm{dh}}, \Delta\mathbf{u}) \tag{A.126}$$

where

$$\begin{aligned}
\frac{\mathrm{d}\overline{\overline{A}}_{ij}}{\mathrm{dh}}(a_k, b_l) &= \frac{1}{4}\frac{\mathrm{d}}{\mathrm{dh}}\left(\frac{\partial a_k}{\partial x_i}\frac{\partial b_l}{\partial x_j} + \frac{\partial a_k}{\partial x_j}\frac{\partial b_l}{\partial x_i}\right) \\
&= \frac{1}{4}\left[\frac{\mathrm{d}}{\mathrm{dh}}\left(\frac{\partial a_k}{\partial x_i}\right)\frac{\partial b_l}{\partial x_j} + \frac{\partial a_k}{\partial x_i}\frac{\mathrm{d}}{\mathrm{dh}}\left(\frac{\partial b_l}{\partial x_j}\right) + \frac{\mathrm{d}}{\mathrm{dh}}\left(\frac{\partial a_k}{\partial x_j}\right)\frac{\partial b_l}{\partial x_i} + \frac{\partial a_k}{\partial x_j}\frac{\mathrm{d}}{\mathrm{dh}}\left(\frac{\partial b_l}{\partial x_i}\right)\right] \\
&= -\frac{1}{4}\left(\frac{\partial a_k}{\partial x_m}\frac{\partial v_{\mathrm{h}m}}{\partial x_i}\frac{\partial b_l}{\partial x_j} + \frac{\partial a_k}{\partial x_i}\frac{\partial b_l}{\partial x_m}\frac{\partial v_{\mathrm{h}m}}{\partial x_j} + \frac{\partial a_k}{\partial x_m}\frac{\partial v_{\mathrm{h}m}}{\partial x_j}\frac{\partial b_l}{\partial x_i} + \frac{\partial a_k}{\partial x_j}\frac{\partial b_l}{\partial x_m}\frac{\partial v_{\mathrm{h}m}}{\partial x_i}\right) \\
&= -\frac{1}{4}\left[\frac{\partial v_{\mathrm{h}m}}{\partial x_i}\left(\frac{\partial a_k}{\partial x_m}\frac{\partial b_l}{\partial x_j} + \frac{\partial a_k}{\partial x_j}\frac{\partial b_l}{\partial x_m}\right) + \frac{\partial v_{\mathrm{h}m}}{\partial x_j}\left(\frac{\partial a_k}{\partial x_i}\frac{\partial b_l}{\partial x_m} + \frac{\partial a_k}{\partial x_m}\frac{\partial b_l}{\partial x_i}\right)\right] \\
&= -(\nabla\mathbf{v}_{\mathrm{h}}\cdot\overline{\overline{\mathbf{A}}} + (\nabla\mathbf{v}_{\mathrm{h}}\cdot\overline{\overline{\mathbf{A}}})^T) = \hat{\overline{\overline{\mathbf{A}}}}(\mathbf{a}, \mathbf{b})
\end{aligned} \tag{A.127}$$

The form of the material derivative of the stress increment will depend on whether the constitutive equation is integrated explicitly or implicitly. For the explicit case we obtain, using Eq. (A.33)

$$\frac{\mathrm{d}\Delta\tilde{\sigma}_{ij}}{\mathrm{dh}} = \frac{\mathrm{d}\, {}^t C_{ijkl}}{\mathrm{dh}}\overline{\Delta\varepsilon}_{kl} + {}^t C_{ijkl}\frac{\mathrm{d}\overline{\Delta\varepsilon}_{kl}}{\mathrm{dh}} + \Delta t\frac{\mathrm{d}\, {}^t H_{ij}}{\mathrm{dh}} \tag{A.128}$$

where, as defined in Eq. (A.9)

$$\begin{aligned}
C_{ijkl} &= C_{ijkl}(\sigma_{mn}, p_\zeta) \\
H_{ij} &= H_{ij}(\sigma_{mn}, p_\zeta)
\end{aligned} \tag{A.129}$$

where p_ζ is a set of internal parameters accounting for the material history. Then we have in turn their material derivatives

$$\begin{aligned}
\frac{\mathrm{d}C_{ijkl}}{\mathrm{dh}} &= \frac{\partial C_{ijkl}}{\partial\sigma_{mn}}\frac{\mathrm{d}\sigma_{mn}}{\mathrm{dh}} + \frac{\partial C_{ijkl}}{\partial p_\zeta}\frac{\mathrm{d}p_\zeta}{\mathrm{dh}} \\
\frac{\mathrm{d}H_{ij}}{\mathrm{dh}} &= \frac{\partial H_{ij}}{\partial\sigma_{mn}}\frac{\mathrm{d}\sigma_{mn}}{\mathrm{dh}} + \frac{\partial H_{ij}}{\partial p_\zeta}\frac{\mathrm{d}p_\zeta}{\mathrm{dh}}
\end{aligned} \tag{A.130}$$

Since in every step we calculate the sensitivities $\mathrm{d}\Delta\sigma_{ij}/\mathrm{d}\mathbf{h}$, we can accumulate them in order to obtain the sensitivities of the total stresses for their use in Eq. (A.130). In addition we find the sensitivity of the internal variables. Further specification of this term will depend on the law with which these internal variables $\mathbf{p}$ are calculated.

Meanwhile, for the case of implicit integration of the constitutive equation we have, more generally,

$$\Delta\tilde{\boldsymbol{\sigma}} = \Delta\tilde{\boldsymbol{\sigma}}({}^t\boldsymbol{\sigma}, {}^t\mathbf{p}, \mathbf{h}; \overline{\Delta\boldsymbol{\varepsilon}}) \tag{A.131}$$

for which the chain rule for differentiation yields an expression similar to A.104 with its terms having now the meaning of material derivatives of its variables. Again, by inspection of the particular quantities present we can recognize a series of terms known at time t, and only one resulting from the sensitivity of the present displacement increment

$$\frac{\mathrm{d}\Delta\tilde{\boldsymbol{\sigma}}}{\mathrm{d}\mathbf{h}} = \frac{\hat{\mathrm{d}}\Delta\tilde{\boldsymbol{\sigma}}}{\mathrm{d}\mathbf{h}} + \hat{\mathbf{C}}\overline{\mathbf{A}}\frac{\mathrm{d}\Delta\mathbf{u}}{\mathrm{d}\mathbf{h}} \tag{A.132}$$

where the effectively explicit derivative

$$\frac{\hat{\mathrm{d}}\Delta\tilde{\boldsymbol{\sigma}}}{\mathrm{d}\mathbf{h}} = \frac{\partial\Delta\tilde{\boldsymbol{\sigma}}}{\partial\boldsymbol{\sigma}}\frac{\mathrm{d}\,{}^t\boldsymbol{\sigma}}{\mathrm{d}\mathbf{h}} + \frac{\partial\Delta\tilde{\boldsymbol{\sigma}}}{\partial\mathbf{p}}\frac{\mathrm{d}\,{}^t\mathbf{p}}{\mathrm{d}\mathbf{h}} + \frac{\partial\Delta\tilde{\boldsymbol{\sigma}}}{\partial\mathbf{h}} + \underbrace{\frac{\partial\Delta\tilde{\boldsymbol{\sigma}}}{\partial\overline{\Delta\boldsymbol{\varepsilon}}}}_{{}^t\hat{\mathbf{C}}}\frac{\mathrm{d}\overline{\mathbf{A}}}{\mathrm{d}\mathbf{h}}\Delta\mathbf{u} \tag{A.133}$$

has been defined, in analogy to the effectively explicit variation of DPA previously introduced.

Finally, for the differential volume and surface we have

$$\frac{\mathrm{d}\,\mathrm{d}\Omega}{\mathrm{d}\mathbf{h}} = (\nabla\cdot\mathbf{v}_\mathbf{h})\,\mathrm{d}\Omega = v_{h\boldsymbol{k},\boldsymbol{k}}\,\mathrm{d}\Omega \tag{A.134}$$

$$\frac{\mathrm{d}\,\mathrm{d}(\partial\Omega)}{\mathrm{d}\mathbf{h}} = [\nabla\cdot\mathbf{v}_\mathbf{h} - (\nabla\mathbf{v}_\mathbf{h}\mathbf{n})\mathbf{n}]\,\mathrm{d}(\partial\Omega) = (\delta_{kl} - n_k n_l)v_{h\boldsymbol{k},l}\,\mathrm{d}(\partial\Omega) \tag{A.135}$$

It can be shown [15] that

$$(\nabla\mathbf{v}_\mathbf{h}\mathbf{n})\mathbf{n} = \nabla\cdot(\mathbf{n}v_n) - (\nabla\cdot\mathbf{n})\mathbf{v}_\mathbf{h}\mathbf{n} \tag{A.136}$$

where $v_n = \mathbf{v}_\mathbf{h}\cdot\mathbf{n}$ is the normal component of the design velocity field, and $\nabla\cdot\mathbf{n}$ is the curvature or twice the mean curvature of the surface $\partial\Omega$, in R^2 or R^3 respectively. Replacing in Eq. (A.135) we have

$$\frac{\mathrm{d}\,\mathrm{d}(\partial\Omega)}{\mathrm{d}\mathbf{h}} = [\nabla\cdot\mathbf{v}_\mathbf{h} - \nabla\cdot(\mathbf{n}v_n) + (\nabla\cdot\mathbf{n})\mathbf{v}_\mathbf{h}\mathbf{n}]\,\mathrm{d}(\partial\Omega) \tag{A.137}$$

which, after considering that only the normal components of the design velocity field affects the variation of the differential surface element (cf. [55]), reduces to

$$\frac{\mathrm{d}\,\mathrm{d}(\partial\Omega)}{\mathrm{d}\mathbf{h}} = (\nabla\cdot\mathbf{n})\mathbf{v}_\mathbf{h}\mathbf{n}\,\mathrm{d}(\partial\Omega) \tag{A.138}$$

Applying these results to generic volume and surface integrals we have

$$\frac{\mathrm{d}}{\mathrm{d}\mathbf{h}}\Big(\int_\Omega g_1\,\mathrm{d}\Omega\Big) = \int_\Omega \frac{\mathrm{d}g_1}{\mathrm{d}\mathbf{h}}\,\mathrm{d}\Omega + \int_\Omega g_1 \frac{\mathrm{d}\,\mathrm{d}\Omega}{\mathrm{d}\mathbf{h}}$$
$$= \int_\Omega \Big(\frac{\mathrm{d}g_1}{\mathrm{d}\mathbf{h}} + g_1 \nabla\cdot\mathbf{v}_\mathrm{h}\Big)\,\mathrm{d}\Omega \qquad \text{(A.139)}$$

$$\frac{\mathrm{d}}{\mathrm{d}\mathbf{h}}\Big(\int_{\partial\Omega} g_2\,\mathrm{d}(\partial\Omega)\Big) = \int_{\partial\Omega} \frac{\mathrm{d}g_2}{\mathrm{d}\mathbf{h}}\,\mathrm{d}(\partial\Omega) + \int_{\partial\Omega} g_2 \frac{\mathrm{d}\,\mathrm{d}(\partial\Omega)}{\mathrm{d}\mathbf{h}}$$
$$= \int_{\partial\Omega} \Big(\frac{\mathrm{d}g_2}{\mathrm{d}\mathbf{h}} + g_2(\nabla\cdot\mathbf{v}_\mathrm{h} - (\nabla\mathbf{v}_\mathrm{h}\mathbf{n})\cdot\mathbf{n})\Big)\,\mathrm{d}(\partial\Omega) \qquad \text{(A.140)}$$

Alternative forms may be obtained by application of the Cauchy theorem and Eq. (A.138) for the volume and surface integrals respectively

$$\frac{\mathrm{d}}{\mathrm{d}\mathbf{h}}\int_\Omega g_1\,\mathrm{d}\Omega = \int_\Omega \Big[\frac{\mathrm{d}_\mathrm{f} g_1}{\mathrm{d}\mathbf{h}} + (\nabla g_1)\mathbf{v}_\mathrm{h} + g_1\nabla\cdot\mathbf{v}_\mathrm{h}\Big]\,\mathrm{d}\Omega$$
$$= \int_\Omega \frac{\mathrm{d}_\mathrm{f} g_1}{\mathrm{d}\mathbf{h}}\,\mathrm{d}\Omega + \int_{\partial\Omega} g_1 v_n\,\mathrm{d}(\partial\Omega) \qquad \text{(A.141)}$$

$$\frac{\mathrm{d}}{\mathrm{d}\mathbf{h}}\int_{\partial\Omega} g_2\,\mathrm{d}(\partial\Omega) = \int_{\partial\Omega}\Big[\frac{\mathrm{d}g_2}{\mathrm{d}\mathbf{h}} + g_2(\nabla\cdot\mathbf{n})\mathbf{v}_\mathrm{h}\mathbf{n}\Big]\,\mathrm{d}(\partial\Omega)$$
$$= \int_{\partial\Omega}\Big[\frac{\mathrm{d}_\mathrm{f} g_2}{\mathrm{d}\mathbf{h}} + (\nabla g_2)\mathbf{v}_\mathrm{h} + g_2(\nabla\cdot\mathbf{v}_\mathrm{h})(\mathbf{v}_\mathrm{h}\cdot\mathbf{n})\Big]\,\mathrm{d}(\partial\Omega)$$
$$= \int_{\partial\Omega}\Big\{\frac{\mathrm{d}_\mathrm{f} g_2}{\mathrm{d}\mathbf{h}} + [(\nabla g_2)\mathbf{n} + g_2(\nabla\cdot\mathbf{n})]\mathbf{v}_\mathrm{h}\mathbf{n}\Big\}\,\mathrm{d}(\partial\Omega)$$
$$= \int_{\partial\Omega}\Big\{\frac{\mathrm{d}_\mathrm{f} g_2}{\mathrm{d}\mathbf{h}} + \Big[\frac{\partial g_2}{\partial n} + g_2(\nabla\cdot\mathbf{n})\Big] v_n\Big\}\,\mathrm{d}(\partial\Omega) \qquad \text{(A.142)}$$

These expressions contain partial derivatives with respect to the design parameters and whenever possible are formulated (in the case of the volume integral) in terms of surface integrals. The variety of expressions shows that different discretizations may arise from them.

We now proceed to derive the sensitivity expressions. Replacing the above expressions in Eq. (A.108) we have

$$\frac{\mathrm{d}\mathcal{G}}{\mathrm{d}\mathbf{h}}(\mathbf{h}) = \frac{\mathrm{d}G}{\mathrm{d}\mathbf{h}}(\sigma_{ij}, u_i; \mathbf{h})$$
$$= \frac{\mathrm{d}}{\mathrm{d}\mathbf{h}}\Big[\int_{\Omega^t} g(\sigma_{ij}, u_i; \mathbf{h})\,\mathrm{d}\Omega + \int_{\partial\Omega^t_\sigma} g^{(\sigma)}(u_i; \mathbf{h})\,\mathrm{d}(\partial\Omega) + \int_{\partial\Omega^t_u} g^{(u)}(t_i; \mathbf{h})\,\mathrm{d}(\partial\Omega)\Big]$$
$$= \int_{\Omega^t}\Big(\frac{\mathrm{d}g}{\mathrm{d}\mathbf{h}} + g\nabla\cdot\mathbf{v}_\mathrm{h}\Big) + \int_{\partial\Omega^t_\sigma}\Big(\frac{\mathrm{d}g^{(\sigma)}}{\mathrm{d}\mathbf{h}} + g^{(\sigma)}(\nabla\cdot\mathbf{v}_\mathrm{h} - (\nabla\mathbf{v}_\mathrm{h}\mathbf{n})\cdot\mathbf{n})\Big)\,\mathrm{d}(\partial\Omega)$$
$$+ \int_{\partial\Omega^t_u}\Big(\frac{\mathrm{d}g^{(u)}}{\mathrm{d}\mathbf{h}} + g^{(u)}(\nabla\cdot\mathbf{v}_\mathrm{h} - (\nabla\mathbf{v}_\mathrm{h}\mathbf{n})\cdot\mathbf{n})\Big)\,\mathrm{d}(\partial\Omega) \qquad \text{(A.143)}$$

where the left index $t+\Delta t$ for g, $g^{(\sigma)}$ and $g^{(u)}$ indicating that these quantities are evaluated in that time instant has been omitted for clearness of notation. The

expanded derivatives at fixed ${}^t\mathbf{x}$ read

$$\begin{aligned}
\frac{\mathrm{d}g}{\mathrm{d}\mathbf{h}} &= \frac{\mathrm{d}_t g}{\mathrm{d}\mathbf{h}} + \frac{\partial g}{\partial \sigma_{ij}}\frac{\mathrm{d}\sigma_{ij}}{\mathrm{d}\mathbf{h}} + \frac{\partial g}{\partial u_i}\frac{\mathrm{d}u_i}{\mathrm{d}\mathbf{h}} \\
\frac{\mathrm{d}g^{(\sigma)}}{\mathrm{d}\mathbf{h}} &= \frac{\mathrm{d}_t g^{(\sigma)}}{\mathrm{d}\mathbf{h}} + \frac{\partial g^{(\sigma)}}{\partial u_i}\frac{\mathrm{d}u_i}{\mathrm{d}\mathbf{h}} \\
\frac{\mathrm{d}g^{(u)}}{\mathrm{d}\mathbf{h}} &= \frac{\mathrm{d}_t g^{(u)}}{\mathrm{d}\mathbf{h}} + \frac{\partial g^{(u)}}{\partial t_i}\frac{\mathrm{d}t_i}{\mathrm{d}\mathbf{h}}
\end{aligned} \tag{A.144}$$

In the above expressions we can notice that all the material derivatives can be routinely obtained once $\dfrac{\mathrm{d}\mathbf{u}}{\mathrm{d}\mathbf{h}}$ is known. This is, in fact, the only unknown for which we have to solve the sensitivity problem.

We should now design-differentiate the equilibrium equations for both implicit and explicit integration of the constitutive law, Eqs. (A.36) and (A.37).

For the moment we assume that $\delta\Delta u_i$ depends arbitrarily on design, leaving for later discussion the form of this dependence. By application of the direct differentiation method to the explicit form Eq. (A.36) we have

$$\begin{aligned}
&\frac{\mathrm{d}}{\mathrm{d}\mathbf{h}}\left(\int_{\Omega^t}(\Delta\tilde{\sigma}_{ij}\overline{A}_{ijk}\delta\Delta u_k + 2\,{}^t\tilde{\sigma}_{ij}\overline{\overline{A}}_{ij}(\Delta u_k, \delta\Delta u_k))\,\mathrm{d}\Omega^t\right) \\
&\quad = \frac{\mathrm{d}}{\mathrm{d}\mathbf{h}}\left(\int_{\Omega^t} {}^{t+\Delta t}\hat{f}_i\delta\Delta u_i\,\mathrm{d}\Omega^t\right) + \frac{\mathrm{d}}{\mathrm{d}\mathbf{h}}\left(\int_{\partial\Omega_\sigma^t} {}^{t+\Delta t}\hat{t}_i\delta\Delta u_i\,\mathrm{d}(\partial\Omega^t)\right) \\
&\quad - \frac{\mathrm{d}}{\mathrm{d}\mathbf{h}}\left(\int_{\Omega^t} {}^t\sigma_{ij}\,\overline{A}_{ijk}\,\delta\Delta u_k\,\mathrm{d}\Omega^t\right)
\end{aligned} \tag{A.145}$$

or

$$\begin{aligned}
&\int_{\Omega^t}\Big\{\frac{\mathrm{d}\Delta\tilde{\sigma}_{ij}}{\mathrm{d}\mathbf{h}}\overline{A}_{ijk}\delta\Delta u_k + \Delta\tilde{\sigma}_{ij}\frac{\mathrm{d}\overline{A}_{ijk}}{\mathrm{d}\mathbf{h}}\delta\Delta u_k + \Delta\tilde{\sigma}_{ij}\overline{A}_{ijk}\frac{\mathrm{d}\delta\Delta u_k}{\mathrm{d}\mathbf{h}} \\
&\quad + \Delta\tilde{\sigma}_{ij}\overline{A}_{ijk}\delta\Delta u_k\nabla\cdot\mathbf{v}_\mathrm{h} + 2\frac{\mathrm{d}\,{}^t\sigma_{ij}}{\mathrm{d}\mathbf{h}}\overline{\overline{A}}_{ij}(\Delta\mathbf{u}, \delta\Delta\mathbf{u}) \\
&\quad + 2\,{}^t\sigma_{ij}\Big[\frac{\mathrm{d}\overline{\overline{A}}_{ij}}{\mathrm{d}\mathbf{h}}(\Delta\mathbf{u}, \delta\Delta\mathbf{u}) + \overline{\overline{A}}_{ij}(\frac{\mathrm{d}\Delta\mathbf{u}}{\mathrm{d}\mathbf{h}}, \delta\Delta\mathbf{u}) + \overline{\overline{A}}_{ij}(\Delta\mathbf{u}, \frac{\mathrm{d}\delta\Delta\mathbf{u}}{\mathrm{d}\mathbf{h}}) \\
&\qquad + \overline{\overline{A}}_{ij}(\Delta\mathbf{u}, \delta\Delta\mathbf{u})\nabla\cdot\mathbf{v}_\mathrm{h}\Big]\Big\}\,\mathrm{d}\Omega^t \\
&\quad = \int_{\Omega^t}\Big(\frac{\mathrm{d}\,{}^{t+\Delta t}\hat{f}_i}{\mathrm{d}\mathbf{h}}\delta\Delta u_i + {}^{t+\Delta t}\hat{f}_i\frac{\mathrm{d}\delta\Delta u_i}{\mathrm{d}\mathbf{h}} + {}^{t+\Delta t}\hat{f}_i\delta\Delta u_i\nabla\cdot\mathbf{v}_\mathrm{h}\Big)\,\mathrm{d}\Omega^t \\
&\quad + \int_{\partial\Omega_\sigma^t}\Big(\frac{\mathrm{d}\,{}^{t+\Delta t}\hat{t}_i}{\mathrm{d}\mathbf{h}}\delta\Delta u_i + {}^{t+\Delta t}\hat{t}_i\frac{\mathrm{d}\delta\Delta u_i}{\mathrm{d}\mathbf{h}} + {}^{t+\Delta t}\hat{t}_i\delta\Delta u_i(\nabla\cdot\mathbf{n})(\mathbf{v}_\mathrm{h}\cdot\mathbf{n})\Big)\,\mathrm{d}(\partial\Omega^t) \\
&\quad - \int_{\Omega^t}\Big(\frac{\mathrm{d}\,{}^t\sigma_{ij}}{\mathrm{d}\mathbf{h}}\overline{A}_{ijk}\delta\Delta u_k + {}^t\sigma_{ij}\frac{\mathrm{d}\overline{A}_{ijk}}{\mathrm{d}\mathbf{h}}\delta\Delta u_k + {}^t\sigma_{ij}\overline{A}_{ijk}\frac{\mathrm{d}\delta\Delta u_k}{\mathrm{d}\mathbf{h}} \\
&\qquad + {}^t\sigma_{ij}\overline{A}_{ijk}\delta\Delta u_k\nabla\cdot\mathbf{v}_\mathrm{h}\Big)\,\mathrm{d}\Omega^t
\end{aligned} \tag{A.146}$$

where the sum of the terms containing $\mathrm{d}(\delta\Delta\mathbf{u})/\mathrm{d}\mathbf{h}$ cancel each other since they form together the equilibrium equation, which is satisfied for the displacement

$\Delta\mathbf{u}$ (for which it has been solved), subject to an arbitrary perturbation $\delta\Delta\mathbf{u}$ which in this case amounts $\mathrm{d}(\delta\Delta\mathbf{u})/\mathrm{d}\mathbf{h}$. At the same time, recalling again the unsolved question about how the arbitrary variation $\delta\Delta\mathbf{u}$ depends on design, we see that the question is not relevant since there are no terms left containing its design derivatives $\mathrm{d}(\delta\Delta\mathbf{u})/\mathrm{d}\mathbf{h}$. Replacing $\mathrm{d}(\Delta\tilde{\boldsymbol{\sigma}})/\mathrm{d}\mathbf{h}$ from Eqs. (A.132) and (A.133) and reordering we obtain

$$\int_{\Omega^t} \Big[\underbrace{\hat{\mathbf{C}}\cdot(\bar{\mathbf{A}}\frac{\mathrm{d}\Delta\mathbf{u}}{\mathrm{d}\mathbf{h}})}_{\tilde{\delta}\Delta\tilde{\boldsymbol{\sigma}}}\cdot(\bar{\mathbf{A}}\delta\Delta\mathbf{u}) + 2\,{}^t\boldsymbol{\sigma}\cdot\bar{\bar{\mathbf{A}}}(\frac{\mathrm{d}\Delta\mathbf{u}}{\mathrm{d}\mathbf{h}},\delta\Delta\mathbf{u})\Big]\ \mathrm{d}\Omega^t$$
$$= \frac{\mathrm{d}\,{}^{t+\Delta t}\mathbf{R}}{\mathrm{d}\mathbf{h}}\bigg|_{\Delta\mathbf{u}\neq\Delta\mathbf{u}(\mathbf{h})} \circ \delta\Delta\mathbf{u}, \qquad \text{for any k.a. } \delta\Delta\mathbf{u} \tag{A.147}$$

with

$$\frac{\mathrm{d}\,{}^{t+\Delta t}\mathbf{R}}{\mathrm{d}\mathbf{h}}\bigg|_{\Delta\mathbf{u}\neq\Delta\mathbf{u}(\mathbf{h})} \circ \delta\Delta\mathbf{u} = \frac{\hat{\mathrm{d}}\,{}^{t+\Delta t}\mathbf{R}}{\mathrm{d}\mathbf{h}} \circ \delta\Delta\mathbf{u} = \frac{\hat{\mathrm{d}}}{\mathrm{d}\mathbf{h}}\left({}^{t+\Delta t}\mathbf{Q} - {}^{t+\Delta t}\mathbf{F}\right) \circ \delta\Delta\mathbf{u} \tag{A.148}$$

in which

$$\frac{\hat{\mathrm{d}}\,{}^{t+\Delta t}\mathbf{Q}}{\mathrm{d}\mathbf{h}} \circ \delta\Delta\mathbf{u} = \int_{\Omega^t}\Big(\frac{\mathrm{d}\,{}^{t+\Delta t}\hat{\mathbf{f}}}{\mathrm{d}\mathbf{h}} + {}^{t+\Delta t}\hat{\mathbf{f}}\nabla\cdot\mathbf{v}_\mathrm{h}\Big)\delta\Delta\mathbf{u}\ \mathrm{d}\Omega^t$$
$$+\int_{\partial\Omega^t_\sigma}\Big(\frac{\mathrm{d}\,{}^{t+\Delta t}\hat{\mathbf{t}}}{\mathrm{d}\mathbf{h}} + {}^{t+\Delta t}\hat{\mathbf{t}}(\nabla\cdot\mathbf{n})(\mathbf{v}_\mathrm{h}\cdot\mathbf{n})\Big)\delta\Delta\mathbf{u}\ \mathrm{d}(\partial\Omega^t) \tag{A.149}$$

$$\frac{\hat{\mathrm{d}}\,{}^{t+\Delta t}\mathbf{F}}{\mathrm{d}\mathbf{h}} \circ \delta\Delta\mathbf{u} = \frac{\mathrm{d}}{\mathrm{d}\mathbf{h}}\left({}^t\mathbf{F} + \Delta\mathbf{F}\right) \circ \delta\Delta\mathbf{u}$$
$$= \int_{\Omega^t}\Big\{\Big(\frac{\mathrm{d}\,{}^t\boldsymbol{\sigma}}{\mathrm{d}\mathbf{h}} + \frac{\hat{\mathrm{d}}\Delta\tilde{\boldsymbol{\sigma}}}{\mathrm{d}\mathbf{h}}\Big)\cdot\bar{\mathbf{A}}\delta\Delta\mathbf{u}$$
$$+ ({}^t\boldsymbol{\sigma} + \Delta\tilde{\boldsymbol{\sigma}})\cdot\Big(\frac{\mathrm{d}\bar{\mathbf{A}}}{\mathrm{d}\mathbf{h}}\delta\Delta\mathbf{u} + \bar{\mathbf{A}}\delta\Delta\mathbf{u}\nabla\cdot\mathbf{v}_\mathrm{h}\Big) + 2\frac{\mathrm{d}\,{}^t\boldsymbol{\sigma}}{\mathrm{d}\mathbf{h}}\cdot\bar{\bar{\mathbf{A}}}(\Delta\mathbf{u},\delta\Delta\mathbf{u}) +$$
$$+ 2\,{}^t\boldsymbol{\sigma}\cdot\Big[\frac{\mathrm{d}\bar{\bar{\mathbf{A}}}(\Delta\mathbf{u},\delta\Delta\mathbf{u})}{\mathrm{d}\mathbf{h}} + \bar{\bar{\mathbf{A}}}(\Delta\mathbf{u},\delta\Delta\mathbf{u})\nabla\cdot\mathbf{v}_\mathrm{h}\Big]\Big\}\ \mathrm{d}\Omega^t \tag{A.150}$$

In the above expressions we find the following quantities still not discussed

$$\frac{\mathrm{d}\bar{\mathbf{A}}}{\mathrm{d}\mathbf{h}}\delta\Delta\mathbf{u}\,, \quad \frac{\mathrm{d}\bar{\bar{\mathbf{A}}}}{\mathrm{d}\mathbf{h}}(\Delta\mathbf{u},\delta\Delta\mathbf{u})\,, \quad \frac{\mathrm{d}\,{}^{t+\Delta t}\hat{\mathbf{f}}}{\mathrm{d}\mathbf{h}}\,, \quad \frac{\mathrm{d}\,{}^{t+\Delta t}\hat{\mathbf{t}}}{\mathrm{d}\mathbf{h}} \tag{A.151}$$

By direct application of the expressions for operators $\hat{\mathbf{A}}$ and $\hat{\bar{\mathbf{A}}}$, from Eqs. (A.125) and (A.127) we have

$$\frac{\mathrm{d}\bar{\mathbf{A}}}{\mathrm{d}\mathbf{h}}\delta\Delta\mathbf{u} = -\frac{1}{2}[\nabla(\delta\Delta\mathbf{u})\cdot\nabla\mathbf{v}_\mathrm{h} + (\nabla(\delta\Delta\mathbf{u})\nabla\mathbf{v}_\mathrm{h})^T] \tag{A.152}$$

and

$$\frac{\mathrm{d}\overline{\overline{\mathbf{A}}}}{\mathrm{d}\mathbf{h}}(\Delta\mathbf{u},\delta\Delta\mathbf{u}) = -[\nabla\mathbf{v}_\mathrm{h}\cdot\overline{\overline{\mathbf{A}}}(\Delta\mathbf{u},\delta\Delta\mathbf{u}) + (\nabla\mathbf{v}_\mathrm{h}\cdot\overline{\overline{\mathbf{A}}}(\Delta\mathbf{u},\delta\Delta\mathbf{u})]^\mathrm{T} \tag{A.153}$$

For the body forces and surface traction we have in the general case

$$\begin{aligned}\frac{\mathrm{d}({}^{t+\Delta t}\hat{f}_i)}{\mathrm{d}\mathbf{h}} &= \frac{\mathrm{d}_t({}^{t+\Delta t}\hat{f}_i)}{\mathrm{d}\mathbf{h}} + \frac{\partial\,{}^{t+\Delta t}\hat{f}_i}{\partial\mathbf{x}}\mathbf{v}_\mathrm{h}\\ \frac{\mathrm{d}({}^{t+\Delta t}\hat{t}_i)}{\mathrm{d}\mathbf{h}} &= \frac{\mathrm{d}_t({}^{t+\Delta t}\hat{t}_i)}{\mathrm{d}\mathbf{h}} + \frac{\partial\,{}^{t+\Delta t}\hat{t}_i}{\partial\mathbf{x}}\mathbf{v}_\mathrm{h}\end{aligned} \tag{A.154}$$

and, if they are given in terms of the initial configuration, the mapping ${}^t_0\mathbf{F} = \partial\,{}^t x/\partial\,{}^0 x$ will still be used.

It can be observed that now, as usually in S.A., the equation system is linear with respect to the sensitivities. All the terms in the right hand side of Eq. (A.146) are known or may be calculated in terms of already available information. Upon discretization, the condition of arbitrariness of $\delta\Delta\mathbf{u}$ yields an element of the right hand side vector for each of its discrete components.

A.3.1 Comparison of both methods

We can try to find, for completeness, the relation between the material derivative and domain parametrization methods. It has been stated [107] that the material derivative method is a particular case of the domain parametrization method where the reference configuration coincides with the present configuration. In an updated Lagrangian approach as the one has been presented in this chapter, the choice of such reference configuration, even more than in a total Lagrangian approach makes the reference configuration to be design-dependent. This fact essentially affects the philosophy of the domain parametrization method. Many of the expressions which took advantage of the independence of the reference configuration on design will have to be reformulated, to such extent that we can speak rather of a general method of which both methods discussed are particular cases.

Nevertheless, we can try to show for a simple case the equivalence between both methods. This equivalence was shown [17], for linear problems.

If we consider a generic integral

$$A = \int_\Omega a({}^t x)\,\mathrm{d}\Omega = \int_{\Omega^r} a({}^r x)J\,\mathrm{d}\Omega^r \tag{A.155}$$

we have, by the DPA

$$\begin{aligned}\bar{\delta}A = \tilde{\delta}A + \partial A &= \int_{\Omega^r}[(\tilde{\delta}a + \partial a)J + a\partial J]\,\mathrm{d}\Omega^r\\ &= \int_{\Omega^r}(\tilde{\delta}aJ)\,\mathrm{d}\Omega^r + \int_{\Omega^r}\partial(aJ)\,\mathrm{d}\Omega^r\end{aligned} \tag{A.156}$$

while, by the MDA we calculate

$$\begin{aligned}\frac{\mathrm{d}A}{\mathrm{d}\mathbf{h}}\delta\mathbf{h} &= \left(\frac{\mathrm{d}_t A}{\mathrm{d}\mathbf{h}} + \frac{\partial A}{\partial x_i}v_i\right)\delta\mathbf{h} \\ &= \left(\int_{\Omega^r}\frac{\mathrm{d}_t a}{\mathrm{d}\mathbf{h}}J\,\mathrm{d}\Omega^r + \int_{\Omega^r}\left(\frac{\partial a}{\partial x_i}\frac{\partial x_i}{\partial \mathbf{h}}J + a\frac{\partial J}{\partial \mathbf{h}}\right)\mathrm{d}\Omega^r\right)\delta\mathbf{h} \\ &= \int_{\Omega^r}\frac{\mathrm{d}_t a}{\mathrm{d}\mathbf{h}}J\,\mathrm{d}\Omega^r\delta\mathbf{h} + \int_{\Omega^r}\underbrace{(\partial a J + a\partial J)}_{\partial(aJ)}\delta\mathbf{h} \end{aligned} \tag{A.157}$$

so that the design variation of a generic integral has the same expression for either of both methods. Now we will show that the variables entering in the integrand of the equilibrium equation have also equivalent expressions whether calculated by DPA or MDA. Moreover, we will show that the variations have two parts: the implicit part of DPA corresponds to the derivative calculated at fixed spatial coordinated of MDA, and the explicit part of DPA to the convective term of MDA. Finally, the design velocity shows to be equivalent to the variation of the mapping from the reference to the actual configurations.

We now consider the linear strain increment: we recall the expressions earlier obtained by DPA, cf. Eq. (A.82$_1$)

$$\begin{aligned}\bar{\delta}\overline{\Delta\boldsymbol{\varepsilon}}(\Delta\mathbf{u}) &= \overline{\Delta\boldsymbol{\varepsilon}}(\bar{\delta}\Delta\mathbf{u}) + \hat{\partial}\overline{\Delta\boldsymbol{\varepsilon}}(\Delta\mathbf{u}) \\ \hat{\partial}\overline{\Delta\boldsymbol{\varepsilon}}(\Delta\mathbf{u}) &= \frac{1}{2}\Big[\frac{\partial\Delta u_i}{\partial {}^r x_m}\bar{\delta}({}_0^r F_{mn}\,{}_t^0 F_{nj}) + \frac{\partial\Delta u_j}{\partial {}^r x_m}\bar{\delta}({}_0^r F_{mn}\,{}_t^0 F_{ni})\Big] \end{aligned} \tag{A.158}$$

whereas the MDA yields

$$\frac{\mathrm{d}\overline{\Delta\varepsilon}_{ij}}{\mathrm{d}\mathbf{h}} = \frac{\mathrm{d}_t\overline{\Delta\varepsilon}_{ij}}{\mathrm{d}\mathbf{h}} + \nu_k\frac{\partial}{\partial {}^t x_k}(\overline{\Delta\varepsilon}_{ij}) \quad ; \quad \nu_k = \frac{\partial {}^t x_k}{\partial \mathbf{h}} \tag{A.159}$$

where

$$\delta\mathbf{h}\frac{\mathrm{d}_t\overline{\Delta\varepsilon}_{ij}}{\mathrm{d}\mathbf{h}} = \overline{\Delta\varepsilon}_{ij}(\bar{\delta}\Delta\mathbf{u}) \tag{A.160}$$

$$\begin{aligned}\delta\mathbf{h}\frac{\partial\overline{\Delta\varepsilon}_{ij}}{\partial {}^t x_k}\frac{\mathrm{d}\,{}^t x_k}{\mathrm{d}\mathbf{h}} &= \frac{1}{2}\frac{\partial}{\partial {}^t x_k}\Big(\frac{\partial\Delta u_i}{\partial {}^r x_m}\,{}_0^r F_{mn}\,{}_t^0 F_{nj} + \frac{\partial\Delta u_j}{\partial {}^r x_m}\,{}_0^r F_{mn}\,{}_t^0 F_{ni}\Big)\frac{\mathrm{d}\,{}^t x_k}{\mathrm{d}\mathbf{h}}\delta\mathbf{h} \\ &= \frac{1}{2}\Big(\frac{\partial\Delta u_i}{\partial {}^r x_m}\frac{\partial\,{}_0^r F_{mn}}{\partial x_k^t}\,{}_t^0 F_{nj} + \frac{\partial\Delta u_j}{\partial {}^r x_m}\frac{\partial\,{}_0^r F_{mn}}{\partial x_k^t}\,{}_t^0 F_{ni}\Big)\frac{\mathrm{d}\,{}^t x_k}{\mathrm{d}\mathbf{h}}\delta\mathbf{h} \\ &\quad + \frac{1}{2}\Big(\frac{\partial\Delta u_i}{\partial {}^r x_m}\,{}_0^r F_{mn}\frac{\partial\,{}_t^0 F_{nj}}{\partial x_k^t} + \frac{\partial\Delta u_j}{\partial {}^r x_m}\,{}_0^r F_{mn}\frac{\partial\,{}_t^0 F_{ni}}{\partial x_k^t}\Big)\frac{\mathrm{d}\,{}^t x_k}{\mathrm{d}\mathbf{h}}\delta\mathbf{h} \\ &= \frac{1}{2}\Big(\frac{\partial\Delta u_i}{\partial {}^r x_m}\Big(\bar{\delta}\,{}_0^r F_{mn}\Big)\,{}_t^0 F_{nj} + \frac{\partial\Delta u_j}{\partial {}^r x_m}\Big(\bar{\delta}\,{}_0^r F_{mn}\Big)\,{}_t^0 F_{ni}\Big) \\ &\quad + \frac{1}{2}\Big(\frac{\partial\Delta u_i}{\partial {}^r x_m}\,{}_0^r F_{mn}\bar{\delta}\,{}_t^0 F_{nj} + \frac{\partial\Delta u_j}{\partial {}^r x_m}\,{}_0^r F_{mn}\bar{\delta}\,{}_t^0 F_{ni}\Big) \\ &= \hat{\partial}\overline{\Delta\varepsilon}_{ij} \end{aligned} \tag{A.161}$$

Similarly we can show that,cf. Eq. (A.82$_2$)

$$\frac{\mathrm{d}\overline{\overline{\mathbf{A}}}}{\mathbf{dh}} = \frac{\mathrm{d}_t\overline{\overline{\mathbf{A}}}}{\mathbf{dh}} + \frac{\partial\overline{\overline{\mathbf{A}}}}{\partial x_i}\frac{\partial x_i}{\partial \mathbf{x}} = \overline{\overline{\mathbf{A}}}(\bar{\delta}\Delta\mathbf{u}, \delta\Delta\mathbf{u}) + \hat{\partial}\overline{\overline{\mathbf{A}}}(\Delta\mathbf{u}, \delta\Delta\mathbf{u}) \tag{A.162}$$

while the term $\overline{\overline{\mathbf{A}}}(\Delta\mathbf{u}, \partial\delta\Delta\mathbf{u})$ will vanish by the arbitrariness of the $\delta\Delta\mathbf{u}$ variations. For the material derivative of the strain increment variation

$$\frac{\mathrm{d}\delta\overline{\Delta\varepsilon}_{ij}}{\mathbf{dh}} = \frac{\mathrm{d}_t\delta\overline{\Delta\varepsilon}_{ij}}{\mathbf{dh}} + \frac{\partial\delta\overline{\Delta\varepsilon}_{ij}}{\partial x_i}\frac{\partial x_i}{\partial \mathbf{h}} \tag{A.163}$$

where again the two terms correspond to the implicit and explicit parts of the DPA expression.

For the Jacobian variation we have

$$\begin{aligned} \bar{\delta}\,{}^t_\tau J &= \partial\,{}^t_\tau J \quad (\bar{\delta}\,{}^t_\tau J = 0) \\ \frac{\mathrm{d}\,{}^t_\tau J}{\mathbf{dh}} &= \frac{\partial x_i}{\partial \mathbf{h}}\frac{\partial\,{}^t_\tau J}{\partial x_i} \end{aligned} \tag{A.164}$$

Since there is a one to one equivalence between the implicit variations and the derivative at fixed x, on the one hand, and the explicit variations and the convective term of the material derivatives, we can check after eliminating respectively the terms involving the design variation of the displacement increment variation, $\partial\delta\Delta\mathbf{u}$, and those containing its material derivative, $\mathrm{d}\delta\Delta\mathbf{u}/\mathrm{d}h$, that we obtain the same equation for the sensitivities with any of both methods.

In the preceding discussion the quantity $\mathrm{d}\,{}^t x/\mathbf{dh}$ has been shown to be needed for every time step. Since its calculation requires manipulations of the deformation gradients and their sensitivities, this term may be regarded as an awkward point of the MDA. However, it can be noticed that this term is equivalent to the variations indicated by $\hat{\partial}$, where the same operators are involved. With this observation the equivalence between both approaches is reinforced.

A.4 Summary of the chapter

The objective of this chapter was to demonstrate that the appropriate theoretical treatment allows us to reduce shape sensitivity problems to a more intuitive formulation typical of non-shape sensitivity. The two basic techniques have been applied to derive shape sensitivity expressions for large deformation problems within an incremental formulation. Equivalence of the respective expressions obtained using either of the methods has been shown.

After combining any of the above techniques with the non-shape sensitivity techniques, the resulting combined methodologies can be classified as shown in Table A.1.

Table A.1 Methodologies for shape sensitivity analysis

Treatment of shape variations \ Basic sensitivity methodologies	DDM	ASM
DPA	DPA/DDM	DPA/ASM
MDA	MDA/DDM	MDA/ASM

Appendix B

Final conclusions and thesis' original elements

B.1 Physical and computational model

- Material model at low strain rates: the constitutive law has been modified to assure continuous derivatives with respect to the strain rate. This improves the numerical behaviour of the tangent stiffness matrix during the mechanical solution by the Newton Raphson method and the sensitivity solution.

- The previously developed technique [1] of pressure scaling to extend the range of applicability of the flow approach to lower strain rates has been widely applied and extended to the temperature solution. In this way, the so-called cutoff value when $\dot{\bar{\varepsilon}} \to 0$ can be reduced by several orders of magnitude.

- Contact-friction elements based on Coulomb's law are used to solve the friction problem within a velocity formulation. They generate the friction force and detect dead zones.

- Stabilization of the pressure solution: the stabilization method has been extended and applied to metal forming problems. The extension concerned the elimination of the assumption of constant viscosity.

- Transient semi-analytical model: for seamless tube rolling a semi-analytical formulation has been developed, including the required extension of the pseudo-concentration method to simulate transient processes.

- Numerical experiments on non-uniqueness for almost ideally plastic materials have been performed. They show that different initial guesses yield different final solutions in problems where the domain is to be determined as part of the solution.

- Bilinear and linear elements for metal forming: for both direct and incremental-explicit solutions, stabilization matrices have been introduced. This additionally allows to use such interpolations in spite of the Brezzi-Babuska condition, which is thus circumvented.

- The relation between time-step, design and velocity of sound when taken as numerical parameters for the explicit model (quasi-static processes) has been discussed.

B.2 Sensitivity analysis and tool shape optimization

- Sensitivity with respect to material, contact (friction), shape and numerical parameters, while addressing thermally coupled problems and transient processes, has been computed. The work presented is one of the first applications of the sensitivity methods (DDM, ASM) to metal forming.

- Iterative form of the sensitivity equations for almost ideally plastic materials: it has been developed for situations where the tangent stiffness matrix is almost singular and its inversion cannot be used to calculate the sensitivity coefficients due to numerical errors in the system solution.

- Formulation of shape sensitivity at large deformations for both MDA and DPA: the equations have been derived for a general displacement-based formulation, and in a particular form have been used within the flow approach.

- Bilinear and bispline interpolations have been introduced within design elements to define a general framework for shape sensitivity analysis. They have been further used in shape optimization. Bispline interpolation allows for the use of angles as design variables and it shows to be more efficient than its bilinear counterpart.

References

[1] H.J. Antúnez. *Análisis por elementos finitos del conformado de metales, con orientación a la laminación de tubos sin costura.* PhD thesis, Universidad Nacional de Córdoba, Argentina, 1990.

[2] H.J. Antúnez. Non-unique numerical solutions in visco-plasticity. *Eng. Trans.*, 40:525–536, 1992.

[3] H.J. Antúnez. Thermo-mechanical modelling and sensitivity analysis for metal-forming operations. *Comput. Meth. Appl. Mech. Engrg.*, 161:113–125, 1998.

[4] H.J. Antúnez. Linear elements for metal forming problems within the flow approach. *Comput. Meth. Appl. Mech. Engrg.*, 190(5-7):783–801, 2000.

[5] H.J. Antúnez. Sensitivity analysis of transient metal forming problems with incompressible linear elements. *Comput. Assisted Mech. Eng. Sci.*, 7(4):449–460, 2000.

[6] H.J. Antúnez and S. Idelsohn. Topics in numerical solution of isothermal and thermal-coupled forming processes. *Latin Am. Appl. Res.*, 20:69–83, 1990.

[7] H.J. Antúnez and S. Idelsohn. Using pseudo-concentrations in the analysis of transient metal forming processes. *Eng. Comput.*, 9(5):547–559, 1992.

[8] H.J. Antúnez and S. Idelsohn. Transient analysis of tube rolling processes by a semi-analytical formulation. *Int. j. numer. methods eng.*, 37:3621–3632, 1994.

[9] H.J. Antúnez, S. Idelsohn and N. Dvorkin. Metal forming analysis by fourier series expansion and further uses of pseudo-concentrations. *Comput. Struct.*, 44(1-2):435–451, 1992.

[10] H.J. Antúnez and M. Kleiber. Parameter sensitivity of metal forming processes. *Comput. Assisted Mech. Eng. Sci.*, 3:263–282, 1996.

[11] H.J. Antúnez and M. Kleiber. Sensitivity analysis of metal forming processes involving frictional contact in steady state. *J. Mater. Proc. Technology*, 60:485–491, 1996.

[12] H.J. Antúnez and M. Kleiber. Sensitivity of forming processes to shape parameters. *Comput. Meth. Appl. Mech. Engrg.*, 137:189–206, 1996.

[13] H.J. Antúnez, M. Kleiber and W. Sosnowski. Shape and non-shape sensitivity and optimization of metal forming processes. In E. Oñate, D.R.J. Owen and E. Hinton, editors, *Computational Plasticity, Proc. COMPLAS VI*, pages 783–791. Barcelona, Pineridge Press, 1997.

[14] H.J. Antúnez, O.C. Zienkiewicz, R.L. Taylor and J. Rojek. Explicit formulation and incompressible linear elements for metal forming problems. In S.R. Idelsohn, E. Oñate and E.N. Dvorkin, editors, *Computational Mechanics - New trends and applications, WCCM IV, Buenos Aires, 29 June–2July 1998*, Barcelona, 1988. CIMNE - IACM.

[15] J.S. Arora. An exposition of the material derivative approach for structural shape sensitivity analysis. *Comput. Meth. Appl. Mech. Engrg.*, 105:41–62, 1993.

[16] J.S. Arora and J.B. Cardoso. Variational principle for shape sensitivity analysis. *AIAA J.*, 30:538–547, 1992.

[17] J.S. Arora, T.H. Lee and J.B. Cardoso. Structural shape sensitivity analysis: relationship between material derivative and control volume approaches. *AIAA J.*, 30:1638–1648, 1992.

[18] J.S. Badrinaraganan and N.B. Zabaras. A sensitivity analysis for the optimal design for metal-forming processes. *Comput. Meth. Appl. Mech. Engrg.*, 129:319–348, 1996.

[19] T. Belytchko, D.P. Flanagan and J.M. Kennedy. Finite element methods with user controlled mesh for fluid structure interaction. *Comput. Meth. Appl. Mech. Engrg.*, 33:669–688, 1982.

[20] J.A. Bennett and M.E. Botkin. Shape optimization with geometric structural description and adaptive refinement. *AIAA J.*, 23:458–464, 1985.

[21] J.A. Bennett and M.E. Botkin, editors. *The optimum shape: automated structural design*. Plenum Press, New York, 1986.

[22] J. Bonet and A.J. Burton. A simple average nodal pressure tetrahedral element for incompressible and nearly incompressible dynamic explicit applications. *Communications in Numerical Methods in Engineering*, 14:437–449, 1998.

[23] V. Braibant and C. Fleury. Shape optimal design: a performing cad oriented formulation. In *AIAA Papers 84-0857*, 1984.

[24] A.N. Brooks and T.J.R. Hughes. Streamline upwind Petrov-Galerkin formulations for convection dominated flows with particular emphasis on the incompressible Navier-Stokes equations. *Comput. Meth. Appl. Mech. Engrg.*, 32:199–259, 1982.

[25] S.M. Byon and S.M. Hwang. Process optimal design in non-isothermal, steady-state metal forming by the finite element method. *Int. j. numer. methods eng.*, 46(7):1075–1100, 1999.

[26] A. Chandra and S. Mukherjee. A finite element analysis of metal-forming problems with an elastic-viscoplastic material. *Int. j. numer. methods eng.*, 20:1613–1628, 1984.

[27] J-H. Cheng and N. Kikuchi. An analysis of metal forming processes using large deformation elastic-plastic formulations. *Comput. Meth. Appl. Mech. Engrg.*, 49:71–108, 1985.

[28] J.L. Chenot and M. Bellet. The viscoplastic approach for the finite element modelling of metal forming processes. In P. Hartley, I. Pillinger and C.E.N. Sturges, editors, *Numerical modelling of material deformation processes*, pages 179–224, London-Berlin, 1992. Springer-Verlag.

[29] K.K. Choi. Shape design sensitivity analysis of displacement and stress constraints. *Struct. Mech.*, 13(1):27–41, 1985.

[30] K.K. Choi and E.J. Haug. Shape design sensitivity analysis of elastic structures. *J. Struc. Mech.*, 11:231–269, 1983.

[31] K.K. Choi and H.G. Seong. A domain method for shape design sensitivity analysis of built-up structures. *Comput. Meth. Appl. Mech. Engrg.*, 57:1–15, 1986.

[32] A.J. Chorin. A numerical method for solving incompressible viscous problems. *J. Comput. Phys.*, 2:12–26, 1967.

[33] A.J. Chorin. On the convergence of discrete approximation to the Navier-Stokes equations. *Math. Comput.*, 23, 1969.

[34] S.H. Chung and S.M. Hwang. Optimal process design in non-isothermal, non-steady metal forming by the finite element method. *Int. j. numer. methods eng.*, 42(8):1343–1390, 1998.

[35] G.C. Cornfield and R.H. Johnson. Theoretical prediction of plastic flow in hot rolling including the effect of various temperature distributions. *J. Iron and Steel Inst.*, 211:567–573, 1973.

[36] J.B. Dalin and J.L. Chenot. Finite element computation of bulging in continuously cast steel with a viscoplastic model. *Int. j. numer. methods eng.*, 25:147–163, 1988.

[37] P.R. Dawson and E.G. Thompson. Finite element analysis of steady state elasto-visco-plastic flow by the initial stress rate method. *Int. j. numer. methods eng.*, 12:47–57, 1978.

[38] K. Dems and R.T. Haftka. Two approaches to sensitivity analysis for shape variation of structures. *J. Mech. Struc. Machines*, 16:501–522, 1989.

[39] K. Dems and Z. Mróz. Variational approach by means of adjoint systems to structural optimization and sensitivity analysis. II. Structure shape variation. *Solids Struct.*, 20(6):527–552, 1984.

[40] K. Dems and Z. Mróz. Shape sensitivity analysis and optimal design of physically nonlinear plates. *Arch. Mech.*, 41:481–501, 1989.

[41] J. Van der Lugt and J. Huetink. Thermal mechanically coupled finite element analysis in metal forming processes. *Comput. Meth. Appl. Mech. Engrg.*, 54:154–160, 1986.

[42] J. Donea, S. Giuliani and J.I. Halleux. The arbitrary lagrangian eulerian finite element method for transient dynamic fluid structure interaction. *Comput. Meth. Appl. Mech. Engrg.*, 33, 1982.

[43] R. Fletcher and C.M. Reeves. Function minimization by conjugate gradients. *Computer Journal*, 7:149–154, 1964.

[44] L. Fourment, T. Balan and J. Chenot. Shape optimization for the forging process. In D.R.J. Owen, E. Oñate and E. Hinton, editors, *Computational Plasticity, Proc. COMPLAS IV*, pages 1369–1381. Barcelona, Pineridge Press, 1995.

[45] L. Fourment, T. Balan and J.L. Chenot. Optimal design for non-steady-state metal forming processes–ii. application of shape optimization in forging. *Int. j. numer. methods eng.*, 39(1):51–65, 1996.

[46] L. Fourment and J.L. Chenot. Optimal design for non-steady-state metal forming processes–i. shape optimization method. *Int. j. numer. methods eng.*, 39(1):33–50, 1996.

[47] L.P. Franca, T.J.R. Hughes and M. Ballestra. Two classes of mixed finite element methods. *Comput. Meth. Appl. Mech. Engrg.*, 69:89–129, 1988.

[48] M. Gadala, G. Oravas and M. Dokainish. A consistent eulerian formulation of large deformation problems in statics and dynamics. *Int. J. Non-Linear Mechanics*, 18(1):21–35, 1983.

[49] J.C. Gelin and B.V. Nguegang. Modelling of thermomechanical coupling during hot forming of viscoplastic materials. *J. Mater. Proc. Technology*, 60:441–446, 1996.

[50] V. Girault and P.A. Raviart. *Finite element approximation of the Navier-Stokes equations*. Springer Verlag, 1980.

[51] G.Y. Goon, P.I. Poluchin, W.P. Poluchin and B.A. Prudcowsky. The plastic deformation of metals. *Metallurgica (in Russian)*, 1968.

[52] A.M. Habraken and S. Cescotto. An automatic remeshing technique for finite element simulation of forming processes. *Int. j. numer. methods eng.*, 30:1503–1525, 1990.

[53] R.T. Haftka and R.K. Grandhi. Structural shape optimization – a survey. *Comput. Meth. Appl. Mech. Engrg.*, 57:91–106, 1986.

[54] C.S. Han, R.V. Grandhi and R. Srinivasan. Optimum design of forging die shapes using nonlinear finite element analysis. *AIAA J.*, 31:774–781, 1993.

[55] E.J. Haug, K.K. Choi and V. Komkov. *Design Sensitivity Analysis of Structural Systems*. Series in Math. Sci. Eng. Academic Press, Orlando, 1986.

[56] J.C. Heinrich, P.S. Huyakorn, A.R. Mitchell and O.C. Zienkiewicz. An 'upwind' finite element scheme for two-dimensional convective transport equation. *Int. j. numer. methods eng.*, 11:131–143, 1977.

[57] J.C. Heinrich and O.C. Zienkiewicz. Quadratic finite element schemes for two dimensional convective transport problems. *Int. j. numer. methods eng.*, 11:1831–1844, 1977.

[58] H.R. Hill. *The mathematical theory of plasticity*. Clarendon Press, Oxford, 1950.

[59] R. Hill. On the state of stress in a plastic–rigid body at the yield point. *Phil. Mag.*, 42:868–875, 1951.

[60] N.J. Hoff. Approximate analysis of structures in the presence of moderately large deformation. *Quart. Appl. Math.*, 2(1):49, 1954.

[61] J.W. Hou, J.L. Chen and J.S. Sheen. A computational method for shape optimization. In *AIAA Papers 85-0773*, 1985.

[62] J. Huetink. Analysis of metal forming processes based on a combined eulerian-lagrangian finite element formulation. In J.F. Pittman, R.D. Wood, J.M. Alexander and O.C. Zienkiewicz, editors, *Numerical Methods in Industrial Forming Processes*, pages 501–509. Pineridge Press, 1983.

[63] T.J.R. Hughes, L.P. Franca and M. Balestra. A new finite element formulation for computational fluid dynamic: V. Circumventing the Babuska-Brezzi condition: A stable Petrov-Galerkin formulation for the Stokes problems accommodating equal-order interpolations. *Comput. Meth. Appl. Mech. Engrg.*, 59:85–99, 1986.

[64] S. Idelsohn, M. Storti and N. Nigro. Stability analysis of mixed finite element formulations with special mention of equal order interpolations. *Int. J. Num. Methd. Fluids*, 20:1003–1022, 1985.

[65] B.M. Irons. A frontal solution program for finite elements. *Int. j. numer. methods eng.*, 2:5–32, 1970.

[66] M.S. Joun and S.M. Hwang. Die shape optimal design in three-dimensional shape metal extrusion by the finite element method. *Int. j. numer. methods eng.*, 41:311–335, 1998.

[67] A. Karagiannis and H. Mavridis. A finite element convergence study for shear-thinning flow problems. *Int. J. Num. Meth. Fluids*, 8:128–138, 1988.

[68] M. Kawahara and K. Ohmiya. Finite element analysis of density flow using the velocity correction method. *Int. J. Num. Methd. Fluids*, 5:981–993, 1985.

[69] P. Kelly, A. Nakazawa, O.C. Zienkiewicz and J.C. Heinrich. A note on upwinding and anisotropic balancing dissipation in finite elements approximations to convective diffusion problems. *Int. j. numer. methods eng.*, 15:1705–1711, 1980.

[70] M. Kleiber, H.J. Antúnez, T.D. Hien and P. Kowalczyk. *Parameter Sensitivity in Nonlinear Mechanics.* Wiley, Chichester, 1997.

[71] M. Kleiber and T.D. Hien. Nonlinear dynamics of complex axisymmetric structures under arbitrary loads. *Comput. Meth. Appl. Mech. Engrg.*, 37:93–107, 1983.

[72] M. Kleiber, T.D. Hien, H.J. Antúnez and P. Kowalczyk. Parameter sensitivity of elasto-plastic response. *Engng. Computations*, 12:263–280, 1995.

[73] M. Kleiber and W. Sosnowski. Parameter sensitivity analysis in frictional contact problems of sheet metal forming. *Comput. Mech.*, 16:297–306, 1995.

[74] S. Kobayashi, S. Oh and T. Altan. *Metal Forming and the Finite Element Method.* Oxford University Press, 1989.

[75] J. Kusiak. *Optimization techniques in computer simulation of metal forming processes (in polish).* Wydawdnictwo AGH, Krakow, 1995.

[76] J. Kusiak and E.G. Thompson. Optimization techniques for extrusion die shape design. In E.G. Thompson, R.D. Wood, O.C. Zienkiewicz and A. Samuelsson, editors, NUMIFORM'86, *Numerical Methods in Industrial Forming Processes*, pages 569–574. Balkema, 1989.

[77] K. Kuzman, E.Pfeifer, N. Bay and J. Hunding. Control of material flow in a combined backward can-forward rod extrusion. *J. Mater. Proc. Technology*, 60:141–147, 1996.

[78] J.Y. Lamant, M. Larrecq, J.P. Birat, J.L. Hengsen, J.D. Weber and J.C. Dhuyvetter. Study of slab bulging in a continuous caster. In *Metals Society Conference*, London, 1985.

[79] C.H. Lee and S. Kobayashi. New solutions to rigid plastic deformation problems using a matrix method. *J. Eng. for Ind., Trans. ASME*, 95:865–873, 1973.

[80] T.H. Lee, J.S. Arora and V. Kumar. Shape design sensitivity analysis of viscoplastic structures. *Comput. Meth. Appl. Mech. Engrg.*, 108:237–259, 1993.

[81] L. Malvern. *Introduction to the mechanics of a continuous medium.* Prentice Hall, Englewood Cliffs, 1969.

[82] T.D. Marusich and M. Ortiz. Modelling and simulation of high-speed machining. *Int. j. numer. methods eng.*, 38(21):3675–3694, 1995.

[83] Z. Mróz. Variational methods in sensitivity analysis and optimal design. *Eur. J. Mech. A/Solids*, 13:115–147, 1994.

[84] Z. Mróz, M.P. Kamat and R.H. Plant. Sensitivity analysis and optimal design of nonlinear beams and plates. *J. Struct. Mech.*, 13:245–266, 1985.

[85] T. De Mulder. The role of bulk viscosity in stabilized finite element formulations for incompressible flow: a review. *Comput. Meth. Appl. Mech. Engrg.*, 163:1–10, 1998.

[86] E. Oñate, M. Kleiber and C. Agelet de Saracibar. Plastic and viscoplastic flow of void containing metals: applications to axisymmetric sheet forming problems. *Int. j. numer. methods eng.*, 25:225–251, 1988.

[87] R. Michałowski and Z. Mróz. Associated and non-associated sliding rules in contact friction problems. *Arch. Mech.*, 30:259–276, 1978.

[88] P. Perzyna. The constitutive equation for rate-sensitive plastic materials. *Quart. Appl. Math.*, 20:321–332, 1963.

[89] P. Perzyna. *Fundamental problems in viscoplasticity*, chapter 9. Academic Press, New York, 1966.

[90] H. Petryk. Non-unique slip-line field solutions for the wedge indentation problem. *J. Mechanique Appliquée*, 4(3):255–282, 1980.

[91] H. Petryk. On the stability of non-uniquely defined processes of plastic deformations. *J. Mechanique théorique et appliquée*, spec. nr.:187–202, 1982.

[92] H. Petryk. Slip line field solutions for sliding contact. In *Proc.Inst.Mech.Engrs., Int. Conf. Tribology - Friction, Lubrication and Wear, Fifty Years On*, pages 987–994, London, 1987.

[93] H. Petryk and Z. Mróz. Time derivatives of integrals and functionals defined on varying volume and surface domains. *Arch. Mech.*, 38:697–724, 1986.

[94] P.G. Phelan, C.A. Vidal and R.B. Haber. Explicit sensitivity analysis of nonlinear elastic systems. In *Proc. 1st Int. Conf. Computer Aided Optimal Design of Structures, Southampton, U.K.*, 1989.

[95] K. Schittkowski. `NLPQL`: a fortran subroutine solving constrained nonlinear programming problems. *Annals of Operations Research*, 5:485–500, 1986.

[96] G.E. Schneider, G.D. Raithby and M.M. Yovanovich. Finite element analysis of incompressible fluid flow incorporating equal order pressure and velocity interpolation. In C. Taylor, K. Morgan and C.A. Brebbia, editors, *Numerical Methods in Laminar and Turbulent Flow*, Plymouth, 1978. Pentech Press.

[97] P.J. Schreurs, F.F. Veldpaus and W.A. Brakalmans. An eulerian and lagrangian finite element model for the simulation of geometrical non-linear hyper elastic and elasto-plastic deformation processes. In *Proc. Conf. on Industrial Forming Processes*, pages 491–500. Pineridge Press, 1983.

[98] G.S. Sekhon and J.L. Chenot. Numerical simulation of continuous chip formation during non-steady orthogonal cutting. *Engng. Computations*, 10:31–48, 1993.

[99] W. Sosnowski and M. Kleiber. A study on the influence of friction evolution on thickness changes in sheet metal forming. *J. Mater. Proc. Tech.*, 60:469–474, 1996.

[100] J.S. Strenkowski and J.T. Carroll. A finite element model of orthogonal metal cutting. *J. Engrg. Ind.*, 107:349–354, 1985.

[101] A.U. Sulijoadikusomo and O.W. Dillon. Temperature distribution of the asixymmetric extrusion of ti-6al-4v. *Univ. of Kentucky - Lexington, Int. rep.*, 1978.

[102] W. Szczepiński. *Introduction to the mechanics of plastic forming of metals.* Sijthoff-Noordhoff, Alphen aan den Rijn, 1979.

[103] E. Thompson. Use of pseudo-concentrations to follow creeping viscous flows during transient analysis. *Int. J. Num. Meth. Fluids*, 6:749–761, 1986.

[104] E. Thompson and R.E. Smelser. Transient analysis of forging operations by the pseudo-concentration method. *Int. j. numer. methods eng.*, 28:177–189, 1989.

[105] J.J.M. Too. On numerical modelling of hot rolling of metals. *Int. j. numer. methods eng.*, 30:1699–1718, 1990.

[106] D.A. Tortorelli, J.A. Tomasko, T.E. Morthland and J.A. Dantzig. Optimum design of nonlinear parabolic systems. Part II: Variable spatial domain with applications to casting optimization. *Comput. Meth. Appl. Mech. Engrg.*, 113:157–172, 1994.

[107] D.A. Tortorelli and Z. Wang. A systematic approach to shape sensitivity analysis. *Solids Struct.*, 30:1181–1212, 1993.

[108] L.A. Winnicki and O.C. Zienkiewicz. Plastic (or visco-plastic) behaviour of axisymmetric bodies subjected to non-symmetric loading—semi-analytical finite element solution. *Int. j. numer. methods eng.*, 14:1399–1412, 1979.

[109] R.J. Yang and K.K. Choi. Accuracy of finite element based shape design sensitivity analysis. *J. Struct. Mech.*, 13:223–239, 1985.

[110] P. Yu and J.C. Heinrich. Petrov-Galerkin method for the time dependent convective transport equation. *Int. j. numer. methods eng.*, 23:883–901, 1986.

[111] O.C. Zienkiewicz. Flow formulation for numerical solution of forming processes. In J.F.T. Pittman, O.C. Zienkiewicz, R.D. Wood and J.M. Alexander, editors, *Numerical Analysis of Forming Processes*, pages 1–44, Chichester, 1984. Wiley.

[112] O.C. Zienkiewicz and R. Codina. A general algorithm for compressible and incompressible flow - Part I. The split, characteristic-based scheme. *Int. j. numer. methods eng.*, 20:869–885, 1995.

[113] O.C. Zienkiewicz and I.C. Cormeau. Visco-plasticity—plasticity and creep in elastic solid — a unified approach. *Int. j. numer. methods eng.*, 8:821–845, 1974.

[114] O.C. Zienkiewicz and P.N. Godbole. Flow of plastic and viscoplastic solids with special reference to extrusion and forming processes. *Int. j. numer. methods eng.*, 8:3–16, 1974.

[115] O.C. Zienkiewicz and P.N. Godbole. Flow of plastic and viscoplastic solids with special reference to non-newtonian (plastic) fluids. In *Finite elements in fluids*, volume 1, pages 25–55, 1974.

[116] O.C. Zienkiewicz, P.C. Jain and E. Oñate. Flow of solids during forming and extrusion: some aspects of numerical solutions. *Solids Struct.*, 14:15–38, 1978.

[117] O.C. Zienkiewicz, Y.C. Liu and G.C. Huang. Error estimation and adaptivity in flow formulation for forming problems. *Int. j. numer. methods eng.*, 25:23–42, 1988.

[118] O.C. Zienkiewicz, K. Morgan, B.V. Satya Sai, R. Codina and M. Vasquez. A general algorithm for compressible and incompressible flow - Part II. Tests on the explicit form. *Int. j. numer. methods eng.*, 20:887–913, 1995.

[119] O.C. Zienkiewicz, E. Oñate and J.C. Heinrich. A general formulation for coupled thermal flow of metals using finite elements. *Int. j. numer. methods eng.*, 17:1497–1514, 1981.

[120] O.C. Zienkiewicz, J. Rojek, R.L. Taylor and M. Pastor. Triangles and tetrahedra in explicit dynamic codes for solids. *Int. j. numer. methods eng.*, 43:565–584, 1998.

[121] O.C. Zienkiewicz and J. Wu. Incompressibility without tears—how to avoid restrictions of mixed formulations. *Int. j. numer. methods eng.*, 32:1189–1209, 1991.

[122] O.C. Zienkiewicz and J.Z. Zhu. A simple error estimator and adaptive procedure for practical engineering analysis. *Int. j. numer. methods eng.*, 24:337–357, 1987.

[123] J.P. Zolesio. The material derivative (or speed) method for shape optimization. In E.J. Haug and J. Cea, editors, *Optimization of Distributed Parameter Structures*. Sijthoff & Noordhoff, 1981.